Uncovering the Predominant Factors Influencing the Transient Stability Margin in Power Systems with Increasing Renewable Generation using Interpretable Machine Learning

PhD Thesis

Robert I Hamilton

Institute for Energy and the Environment

Electronic and Electrical Engineering

University of Strathclyde, Glasgow

November 9, 2022

This thesis is the result of the author's original research. It has been composed by the author and has not been previously submitted for examination which has led to the award of a degree.

Signed: 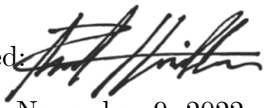

Date: November 9, 2022

Abstract

This thesis is centred around the impact of increasing penetrations of Renewable Energy Sources (RES)—which are often connected to power networks via Power Electronic Converters (PEC)—and disconnection of conventional Synchronous Generation (SG) on transient stability. The significantly different dynamic characteristics between these types of generation mean that the dynamic response of power systems to faults is changing. The increasingly large number of variables (and complex interactions between them) make understanding the factors that influence transient stability very difficult with existing tools. Without full knowledge of the factors and mechanisms responsible for impacting transient stability boundary, operational blind spots may exist, and effective transient stability enhancement measures are not easy to develop. Moreover, the intermittent nature of RES means that the transient stability boundary changes over very short timescales. This drives a need for more frequent Transient Stability Assessment (TSA) that can capture the full dynamic response of Converter Interfaced Generation (CIG).

However, existing TSA tools (namely Transient Energy Function (TEF) and Time Domain Simulations (TDS)) are limited in that they can either not capture the dynamic response of CIG or are computationally expensive to run and extraction of meaningful insights complicated. This increases the requirement for the design and development of new tools for TSA—the primary focus of this thesis.

Machine Learning (ML) can provide explicit mappings of complex functions and accelerate computationally heavy tasks and has been used for TSA in recent years. However, research has mainly focused on error reduction and the computational savings

that can be achieved—rather than obtaining detailed insights into the predominant factors influencing the transient stability boundary.

To gain such insights, this thesis proposes the use of Interpretable Machine Learning (IML)—an emerging area of research—to provide detailed explanations of complex ML models trained to predict the transient stability margin at each location on a power network. Insights can be used to understand better the main power system variables that impact transient stability, the interactions between them, and locational trends. Such tools can bolster existing knowledge of the transient stability boundary and/or infer new information that can be used to enhance situational awareness and develop stability enhancement measures.

Robert Hamilton is sponsored by Engineering and Physical Sciences Research Council (EPSRC) Centre for Doctoral Training (CDT) in Future Power Networks and Smart Grids (EPSRC reference EP/L015471/1). The project is supervised by Dr Panagiotis Papadopoulos and Professor Keith Bell.

Contents

List of Figures

List of Tables

List of Tables

Acknowledgements

I would like to express my deepest gratitude to Panagiotis Papadopoulos for his support, guidance and contributions throughout my PhD. This experience was a first for both of us, but without access to his wealth of expertise, this work would not have been possible. I would also like to extend my sincere thanks to Keith Bell for his valuable insights and advice over the years. In addition, I must recognise the assistance of countless individuals in the research group at the University of Strathclyde, whose depth of knowledge is limitless.

Thanks to all those involved with the EPSRC Centre for Doctoral Training in Future Power Networks and Smart Grids, particularly Shirley Kirk, for all her work in running the centre. The research environment cultivated in the centre has enabled numerous early-stage researchers to develop the necessary skills to begin to address some of the significant challenges facing power systems. Thanks also to Colin Foote and Cornel Brozio from Scottish Power Energy Networks, who I also had the great pleasure of working with, for taking an interest in and ensuring the industrial relevance of this research.

Last but never least, a profound thanks to my Mum and Dad, to whom I am eternally indebted for their steadfast support, to James and Stuart for their bond of brotherhood, to Isabelle for her endless encouragement, to Licky for his feline friendship, and to all my family and friends.

The impediment to action advances action. What stands in the way becomes the way.

—Marcus Aurelius

Acronyms

AC Alternating Current.

ANN Artificial Neural Network.

AVR Automatic Voltage Regulator.

BECCS Bioenergy with Carbon Capture Usage and Storage.

BES Battery Energy Storage.

CAES Compressed Air Energy Storage.

CART Classification and Regression Tree.

CBA Cost-Benefit Analysis.

CCT Critical Clearing Time.

$\mathbf{CCT_{min}}$ Minimum Critical Clearing Time.

CFL Critical Fault Location.

CIG Converter Interfaced Generator.

CSC Current Source Converter.

CSG Critical Synchronous Generator.

DC Direct Current.

DFIG Doubly-Fed Induction Generator.

DG Distributed Generator.

DSA Dynamic Security Assessment.

DT Decision Tree.

EAC Equal Area Criterion.

ECES Electrochemical Capacitor Energy Storage.

EDR Electrical Distance Ratio.

EEAC Extended Equal Area Criterion.

EES Electrical Energy Storage.

EFR Enhanced Frequency Response.

EMT Electromagnetic Transients.

EROI Energy Return on (energy) Investment.

ESS Energy Storage Systems.

FES Flywheel Energy Storage.

FRC Fully-Rated Converter.

FSIG Fixed Speed Induction Generator.

GB Great Britain.

GCR Grid Code Requirement.

GSC Grid-Side Converter.

HV High Voltage.

HVDC High-Voltage Direct Current.

IEC International Electrotechnical Commission.

IEEE Institute of Electrical and Electronics Engineers.

IML Interpretable Machine Learning.

KKT Karush Kuhn Tucker Multiplier.

LCC Line-Commutated Converter.

LIME Local Interpretable Model-agnostic Explanations.

LMP Locational Marginal Price.

LOS Loss of Synchronism.

LV Low Voltage.

LVRT Low-Voltage Ride Through.

MAPE Mean Absolute Percentage Error.

ML Machine Learning.

MOE Maximum Over-Estimate.

MSE Mean Squared Error.

MUE Maximum Under-Estimate.

NBP National Balancing Point.

NEA Net Energy Analysis.

NGESO National Grid Electricity System Operator.

OAT One-At-A-Time.

OPF Optimal Power Flow.

PCA Principle Component Analysis.

PCC Point of Common Coupling.

PEC Power Electronic Converter.

PFI Permutation Feature Importance.

PMSG Permanent Magnet Synchronous Generator.

PMU Phasor Measurement Unit.

PSS Power System Stabiliser.

PV Photovoltaic.

RES Renewable Energy Source.

RF Random Forest.

RFE-CV Recursive Feature Elimination with Cross Validation.

RMS Root Mean Square.

RMSE Root Mean Squared Error.

ROCORS Rate of Change of Rotor Speed.

RSC Rotor-Side Converter.

RSQ Coefficient of Determination.

SA Sensitivity Analysis.

SBR Series Braking Resistor.

SCIG Squirrel Cage Induction Generator.

SCIM Squirrel Cage Induction Machine.

SG Synchronous Generator.

SHAP SHapley Additive exPlanations.

SMES Superconducting Magnetic Energy Storage.

SMIB Single-Machine Infinite-Bus.

SO System Operator.

SSR Subsynchronous Resonance.

STATCOM Static Synchronous Compensator.

SVM Support Vector Machine.

TDS Time-Domain Simulation.

TEF Transient Energy Function.

TKE Total Kinetic Energy.

TO Transmission System Owner.

TPE Total Potential Energy.

TSA Transient Stability Assessment.

TSC-OPF Transient Stability Constrained Optimal Power Flow.

TSDb Transient Stability Database.

UK United Kingdom.

VOI Variable of Interest.

VSC Voltage-Source Converter.

WECC Western Electricity Coordinating Council.

WF Wind Farm.

WRIG Wound Rotor Induction Generator.

WRSG Wound Rotor Synchronous Generator.

WT Wind Turbine.

WTG Wind Turbine Generator.

XGBoost eXtreme Gradient Boosting.

Chapter 1

Introduction and Objective of Research

This Chapter introduces the problem area addressed within this thesis, which influences the motivation and, ultimately, the research questions that this work seeks to address. The contributions from this work are summarised, along with academic publications resulting from the work presented in this thesis. Finally, an overview of the Chapters contained within this thesis is given.

1.1 Introduction and Motivation for Research

The global decarbonisation agenda is leading to changes to the mix of generation connected to modern power systems. In particular, this has resulted in conventional thermal Synchronous Generators (SGs) such as coal and gas plant, being displaced by intermittent Renewable Energy Source (RES). These RES are often connected to the network via a Power Electronic Converter (PEC) and so are frequently referred to as Converter Interfaced Generator (CIG). In addition, the different dynamic characteristics and the uncertainty of renewable resources are increasing the requirement for Transient Stability Assessment (TSA).

Transient stability has historically been regarded as a complex and multidimensional problem due to the large number of power system variables and parameters that can

impact the transient stability boundary—and is defined as;

"*the ability of SGs of an interconnected system to remain in synchronism when subjected to a major disturbance*" [1].

The connection of increasing volumes of RES with complex non-linear dynamic response has further increased the complexity of the transient stability problem [2]—including the introduction of more parameters to the multidimensional problem. In particular, SG and CIG possess significantly different dynamic characteristics and therefore respond differently to network faults, increasing the system's complexity.

For decades, power systems have been built and operated around conventional thermal SG and the associated characteristics. SG have a direct electromagnetic coupling with the system, meaning that they provide synchronising torque and inertia to the system. SG also possess control systems that are beneficial for maintaining power system stability, such as Automatic Voltage Regulators (AVRs) and Power System Stabilisers (PSSs). As outlined above, RES are often connected to the power system through PEC, which decouples the rotational mass (if any) from the system. The synthetic responses from PEC are often non-linear and can be very fast since the response is generated through a series of power electronic switches. The change in the dynamic characteristics of the generation connected to power systems significantly impacts transient stability, leading to an increased requirement to perform TSA to ensure sufficient stability margin. The authors in [3] identify this and subsequently propose the use of a probabilistic approach.

Academic research has sought to reduce the complexity of the transient stability problem when studying the impact of RES on transient stability; by focusing on the impact of single/few parameters(s), often in simple networks. However, while such studies have provided insights into important parameters that impact transient stability, the findings may not directly translate into different systems (e.g., larger systems with an increased number of non-linear complexities and parameter interdependencies). Therefore, methodological approaches that can uncover the predominant factors that influence the transient stability boundary of any system are incredibly beneficial.

RES are often connected in different locations (typically remote from demand centres) and are intermittent, leading to significant changes to generator dispatch patterns and network power flows, impacting transient stability. Such changes are happening in longer-term planning timescales with governments seeking to decarbonise their generation portfolio, but also in operational timescales as System Operators (SOs) strive to make full use of the RES available in real-time, increasing the amount of time the system is operating in highly stressed conditions. Such conditions may include scenarios where there is particularly high demand, high loading of transmission corridors and/or high penetration of RES. In industry, knowledge of the system and so-called *'operational expertise'* are frequently relied upon when looking at the transient stability problem. However, the volume and intermittency of RES connecting in different locations of power systems, the retirement of conventional SG, and (more recently) emergency recommissioning of coal plant [4] patterns as a result of recent gas price volatility [5] may lead to irregular generator dispatch patterns and indeed changes to demand. Regardless of the reasons for changes to the generation connected to power systems, the number of operational scenarios that require TSA are only increasing. What is more, the output of RES may vary in relatively short timescales, meaning that performing online TSA for every potential operational scenario becomes impractical. These significant changes to power system dynamics may result in changes in the transient stability boundary such that the critical fault of a system may change in duration or even location—as demonstrated in this thesis. Moreover, a SO or planner may be unaware of this due to computational constraints preventing a detailed TSA from revealing the entire stability boundary, limiting studies to small portions of the boundary known to be of concern—leading to potential operational blind spots.

The above points are driving a need to perform TSA for large numbers of operational scenarios at multiple locations in a power system—to determine the duration and location of the critical fault, which may change over various timescales. Moreover, a need exists to better understand the parameters driving the system towards instability. However, existing tools are becoming increasingly outdated in this new environment—driving the need for the development of *new* tools and methodologies (the

evidence for which is detailed in Chapter 5). Such tools and methods should possess three desirable attributes, which are defined in this thesis and relate to; reduction of computational expense, enhancement of understanding of the stability boundary and accurate representation of the transient stability boundary.

One approach that can assist in uncovering the predominant factors that impact transient stability is Sensitivity Analysis (SA). Such tools can be used to identify the impact of uncertain input variables on the variation of a model output [6] enables the identification of the parameter (or set of parameters) that have the greatest influence on the model output. A notable application relating to power system dynamic performance (relating to transient response prediction) can be found in [7]. SA methods are classified into three main categories: (i) local, (ii) screening and (iii) global. Local SA relates to determining the impact of individual input variables on the model output, such as One-At-A-Time (OAT) [8] which involves changing only one variable whilst keeping others constant to assess the impact. Screening methods evaluates the input-output relationship of one input variable in a high dimensional space. One such approach is the Morris screening method [9], which can effectively identify the most influential parameters. Global SA (reviewed in detail in [10]) considers the impact of the variation in all inputs on the output. These methods are outlined in detail in [11] from a power systems small signal stability perspective. Notable methods that fall under this category are Pearson Correlation Coefficient (which determines the linear dependency between the inputs and output) [12] and Sobol [10, 13] (which determines the contribution the input variables and their interactions to the output variance).

However, such approaches are not designed to reduce the computational expense associated with TSA (which typically is conducted using Root Mean Square (RMS)-Time-Domain Simulation (TDS) for multiple fault locations and operational scenarios). Machine Learning (ML), however, has been used for TSA due to the inherent ability to accelerate computationally heavy tasks. This requires training an ML model to predict some transient stability index, using a range or credible operating conditions. This may either be from a database of measured system responses, but in practice is more likely to be from a database of simulated system responses (e.g., using RMS-TDS) using a

representative model of the power system.

Linear models are inherently *interpretable*, however in reality simple models such as this are unlikely to accurately capture the complex dynamic response of the system (particularly in systems with the nonlinear response from CIG)—therefore more complicated and, thus, less interpretable ML models are likely to be required. Interpretable Machine Learning (IML) (a relatively new umbrella term, that covers a suite of techniques) can be used to understand how the ML model reaches predictions, by gaining insights into black-box ML models. As such, different IML techniques may be required to understand these more complicated ML models. There exists a suite of methods (summarised in [14]), each with benefits and drawbacks that must be fully considered based on the specific application. In general, methods can be categorised as either *global* or *local* in nature that can either capture feature *importance* or *effects*. To this end, this thesis proposes using IML—a relatively new concept that focuses on providing explanations of ML models. An overview and an in-depth literature review relating to this topic is provided later in this thesis in Chapter 5.

Through the development of such tools and methodologies, targeted and effective transient stability enhancement measures can be designed and implemented to ensure the system continues to operate in a stable and secure manner—even in systems with high penetrations of CIG. These are the key motivating factors for the work presented in this thesis.

This Chapter looks at the drivers for decarbonisation from the (often overshadowed) *net energy* perspective. First, taking Great Britain (GB) as a representative example, recent trends in electricity generation are outlined—illustrating how increasing volumes of RES are connecting to power systems.

In this context, the research questions motivating the work contained within this thesis are outlined. Furthermore, the main contributions arising from this thesis work are summarised, including a list of academic publications. Finally, an overview of the Chapters contained within this thesis is provided.

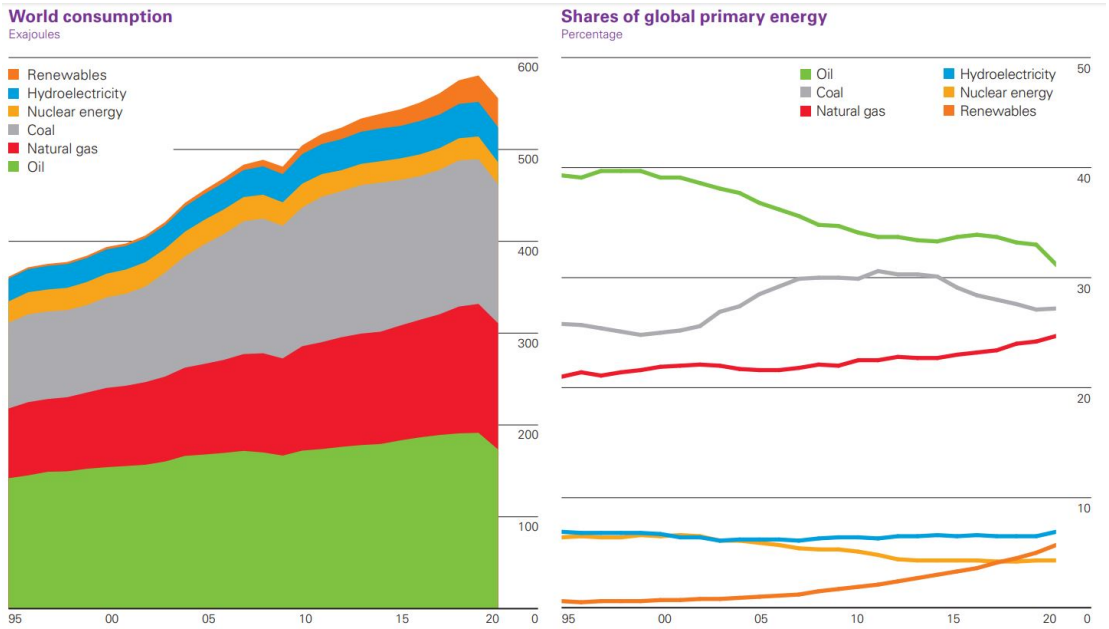

Figure 1.1: World energy consumption in exajoules by type (left) and percentage share of global primary energy by type (right) [15]

1.1.1 The Global Decarbonisation Agenda: A Net Energy Perspective

The motivation to decarbonise power systems is primarily driven by concerns around carbon emissions and the impact on climate change. However, another frequently overlooked aspect is the *finite* nature of fossil fuels (namely oil, gas and coal) upon which the world has been—and continues to be—extremely reliant (Figure 1.1).

Since the discovery of oil in the 19^{th} century, the liberation of large volumes of chemical energy stored in the form of fossil fuels has enabled human population expansion and economic growth. The link between energy, the economy and the environment is inescapable and drives everything we do—which has increasingly become apparent during the energy crisis in Europe in 2022. One means of looking at this problem is using the Net Energy Analysis (NEA) conceptual framework from the early 1970s. NEA, derives the value of energy surplus of a given system using Equation 1.1.

$$\text{Net energy} = \text{Gross energy} - \text{Energy required to deliver energy} \tag{1.1}$$

The energy required to deliver energy can be computed through net-energy indica-

tors, such as Energy Return on (energy) Investment (EROI) [16]—which is the ratio between usable energy acquired from an energy carrier and the amount of energy expended to obtain that energy (Equation 1.2) [17]. An EROI equal or less than 1 can be considered a *energy sink*, or when greater than 1 an *energy source*. Combining Equation 1.1 and 1.2 gives net energy (Equation 1.3).

$$\text{EROI} = \frac{\text{Energy delivered}}{\text{Energy required to deliver energy}} \tag{1.2}$$

$$\text{Net energy} = \text{Gross energy} \times \left(1 - \frac{1}{\text{EROI}}\right) \tag{1.3}$$

The high EROI of oil (and thus high net energy) enabled this population and economic expansion through a large surplus of energy (i.e., positive net energy). However, as these finite resources are gradually depleted, the harder-to-reach resources that require higher energy input to get the same output must be sought (i.e., there is a reduction in the EROI). This is illustrated in Figure 1.2, where the *energy required to produce energy* (uppermost yellow portion) grows historically and is projected to grow further in the coming decades—while supplies reduce. As the energy surplus shrinks over time, increasing pressures on the economic debt-based system that relies on an ever-increasing energy supply will intensify. Whilst wind and solar have relatively good EROI, is it unlikely that anything will exceed the EROI from the abundant oil of the 19^{th} and 20^{th} centuries.

In this context, the question becomes one of energy budgeting: optimising the available energy resources to establish a truly sustainable energy system. To build such a system, with large volumes of RES, the energy available today (predominantly from finite oil and gas resources) must be invested in the energy of tomorrow. The question should be framed as: 'how to best spend the energy surplus to achieve this goal whilst minimising environmental impacts?'. By focusing on climate targets alone (i.e., carbon emission targets such as net-zero by 2050)—which rely on large volumes of Bioenergy with Carbon Capture Usage and Storage (BECCS) to yield negative carbon emissions in GB [18] which may have ecological consequences—there is a danger that the larger

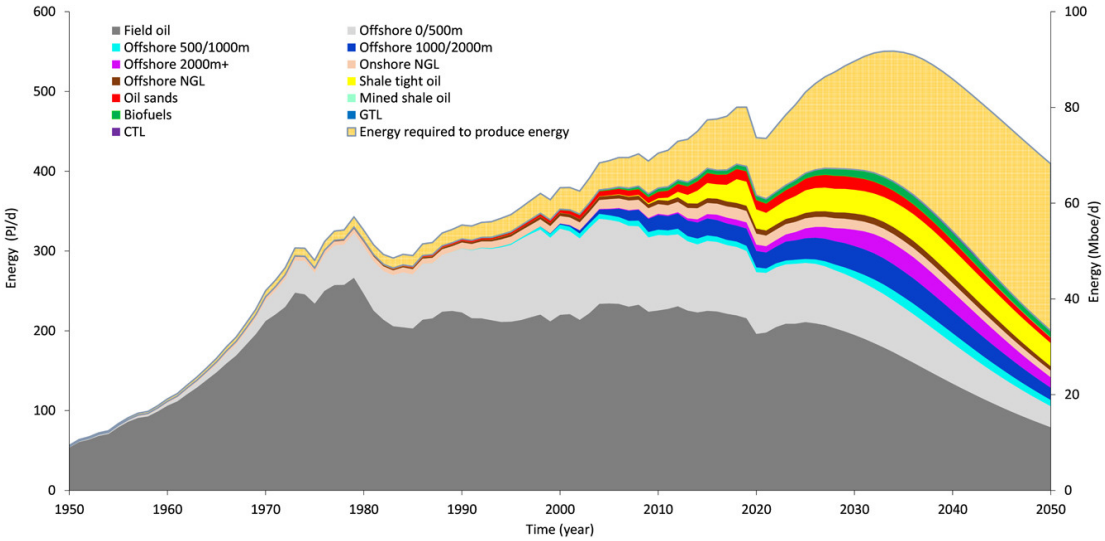

Figure 1.2: Average oil liquids net-energy production from 1950 to 2050, compared to the gross energy. [17].

net-energy perspective is missed and resources are poorly allocated.

In the context of depleting fossil fuel resources and a reducing energy surplus, the focus should be on building a truly sustainable system with the remaining limited natural resources available whilst respecting the environment and transitioning to a new economic model. From a power systems perspective, this will result in a considerable and rapid change to the generation connected to power systems. Furthermore, these new types of generation possess significantly different dynamic characteristics, which will impact the transient stability of power systems.

Regardless of the reasons and drivers for changes to the way that electrical energy is generated, the direction of travel is the same throughout the world (i.e., away from conventional fossil-fuelled often SG and towards RES, which are often CIG). This trend is outlined below using GB as a representative case study. From a transient stability perspective, this is a significant change due to the intermittency of renewable resources and the significantly different dynamic characteristics.

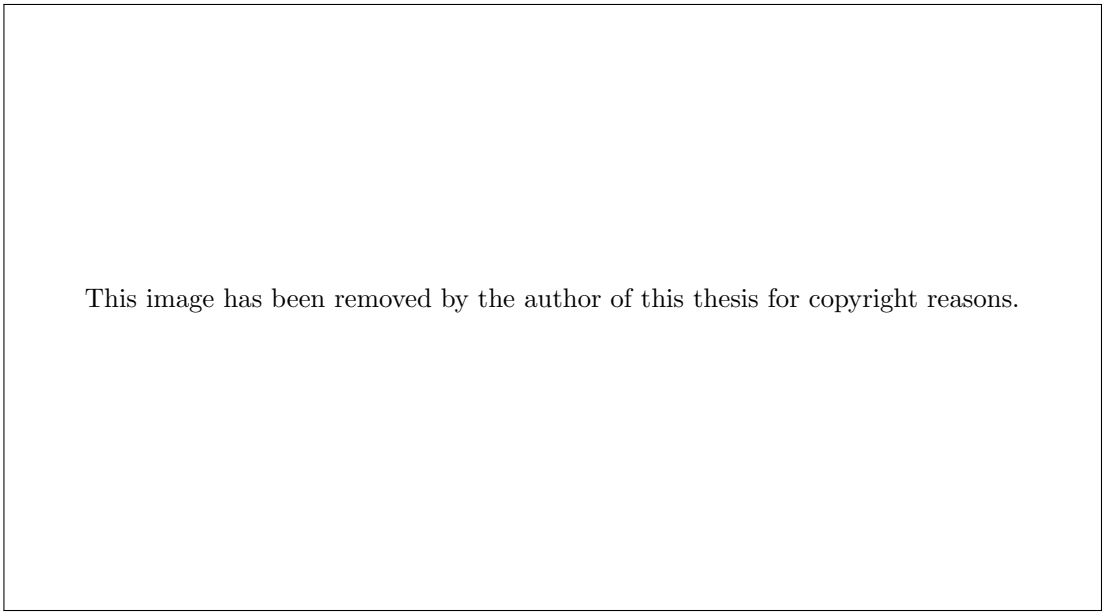

Figure 1.3: Great Britain (GB) annual end consumer (including residential, road transport and industrial commercial) energy demand in 2050 [18].

Evolving Electricity Generation Mix in Great Britain

Shifting energy demand away from fossil fuels and towards RES requires significant changes in both consumption and generation. This is a global movement, with 192 countries plus the European Union joining the legally binding Paris Agreement—with the primary goal of reducing emissions [19].

In GB, annual energy consumer demand in 2020 and 2050 across all four of National Grid Electricity System Operator (NGESO) Future Energy Scenarios [18] is given in Figure 1.3. Electricity demand is forecast to significantly increase across all scenarios as transport and heat move from internal combustion engines and heating systems using liquid fuels to electric transportation and heating systems. From the generation perspective, electricity generation in GB has made progress over recent decades with 43 % of electricity output in 2020 coming from RES (Figure 1.4).

However, the generation mix in GB must evolve to increase the installed capacity of intermittent RES whilst decreasing conventional (typically carbon intensive) SG capacity. The relatively low capacity factor of RES compared to traditional coal and gas plant means that a larger installed capacity relative to peak system demand is

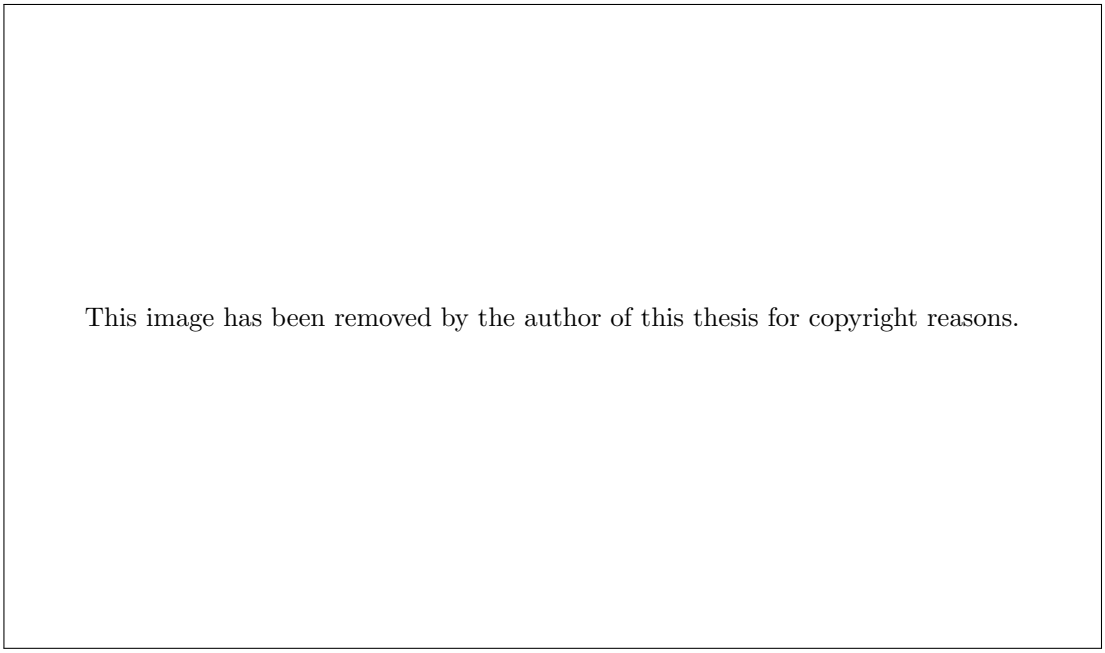

Figure 1.4: Great Britain (GB) electricity generation capacity and output in 2020 [18].

required to ensure supply by 2050. Indeed, in recent years GB has decommissioned a number of conventional plant including the 2.3 GW Longannet coal power station in Scotland in 2016 [20]) and 1 GW Hunterston B nuclear power station in 2022 [21]. The impact of reducing SG capacity on transient stability (defined in Chapter 2) is a key theme of this thesis. The swing equation (Equation 2.4 in Chapter 2), describes how a SG (or indeed a group of SGs electrically distant from another group of SGs) will accelerate or decelerate following a disturbance. The acceleration will be larger when the inertia constant of a machine is small. Decommissioning of SG in Scotland reduces the inertia (stored energy measured in MVA.s) of the region, which typically exports electrical power across a constrained transmission boundary (through long transmission lines) to Northern England.

This is a key concern highlighted by NGESO, with the transfer requirements set to double in the next decade with the connection of as much as 40 GW of installed offshore wind capacity (tripling Scottish wind connected by 2030) (Figure 1.5). Such an increase in Scottish wind would lead to increased volatility in North to South power flows due to the intermittent nature of wind [22], and will have implications for transient stability.

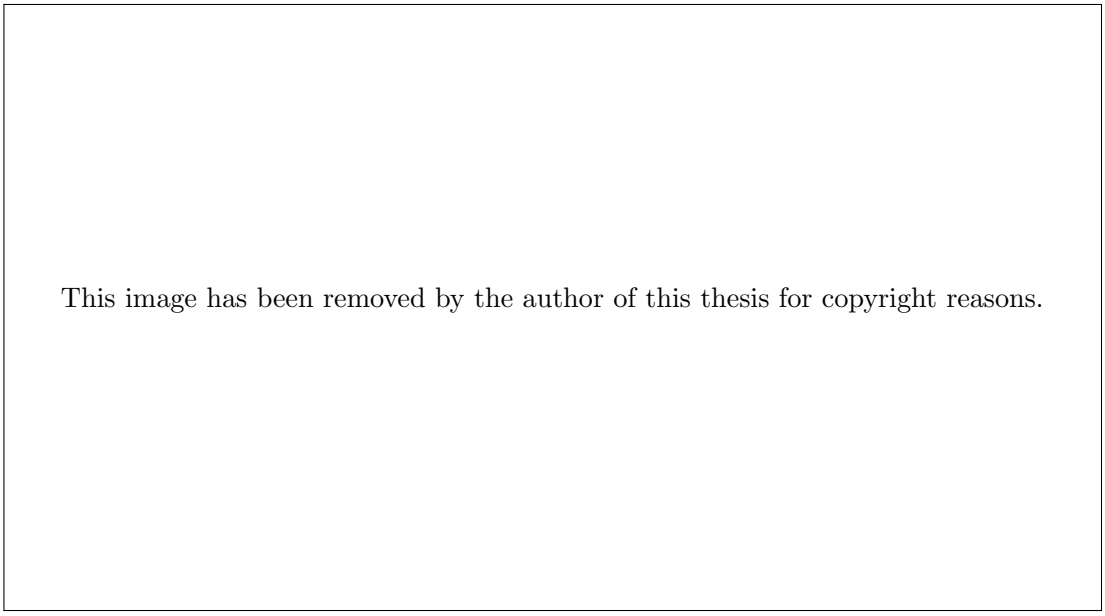

Figure 1.5: Great Britain (GB) forecast B6 boundary transfers (MW) between Scotland and England [22].

Efforts to increase the transfer limit have recently been taken through measures like the commissioning of the Western High-Voltage Direct Current (HVDC) link in 2017 and the upgrade of cables at Torness. However, this is unlikely to be sufficient to accommodate future power transfers.

Additional changes expected include the connection of 12 GW of transmission-connected low-carbon RES in East Anglia between 2020 and 2030, more interconnectors with Europe (e.g. North Sea Link from Norway to GB recently became operational [23]) connecting into the South-East meaning that the interconnector capacity in the region will exceed transmission connected generation [22].

This trend is not unique to GB, and the significant changes to the electrical power generation technologies connected in different locations on power systems throughout the world will impact the transient stability of systems. One contributing factor is the significantly different generator characteristics between SG and CIG, outlined below.

1.1.2 Research Questions

The research questions motivating the work presented in this thesis are as follows:

1. Does the connection of, often renewable, CIG and disconnection of conventional SG impact the transient stability boundary? If so, what are the main parameters/variables/mechanisms responsible, and are any factors missing from existing literature?

2. Are the current suite of TSA tools fit for purpose in modern power systems in the context of increasing CIG output? If not, what are the desirable attributes of such tools?

3. How can the computational burden of RMS-TDS be reduced, whilst enhancing understanding of the factors influencing the transient stability boundary when faced with a wide variety of hitherto unfamiliar system conditions, in addition to the changing dynamic behaviour due to RES connection?

4. How can the predominant factors (i.e., power system parameters and variables) that influence the transient stability boundary in the context of increasing CIG be identified in any power system? Is the impact of these factors consistent between operational scenarios, or does the impact vary and why?

5. From this enhanced understanding, can stability boundary trends be identified? This may be either a trend in power system parameters/variables (i.e., complex interactions between parameters) or between power system locations.

1.2 Contributions from this Thesis

The work within this thesis contributes to several areas of power systems research, particularly relating to the development of new IML-based TSA methodologies that are suitable for use in modern power systems. The methods developed can not only quickly perform TSA but also identify important power system variables and parameters that impact the transient stability boundary. These insights could inform the design and development of transient stability enhancement measures. The key novel contributions found within this thesis are as follows:

- Assessment of the impact of RES on the transient stability boundary and the mechanisms responsible. This is addressed in two key ways. First, a literature review to identify the key factors that impact transient stability. Secondly, the combined impact of economic dispatch (i.e. generator cost), as well as the location of RES on transient stability is systematically identified in the Institute of Electrical and Electronics Engineers (IEEE) 9-bus test network [J1]. Quantifying locational aspects is missing in current literature, so it is addressed by defining a new metric, the Electrical Distance Ratio (EDR). This is defined as the ratio between the transient reactance of an SG and the electrical impedance from the SG terminals to RES. Note that supplementary studies are included in Appendix A where a Single-Machine Infinite-Bus (SMIB) with a Wind Farm (WF) added is used to assess the impact wind control parameters, displacement of SG by wind, locational aspects and WF loading.

- Design and development of a TSA methodology that uses Permutation Feature Importance (PFI) to identify important variables to the prediction of Critical Clearing Time (CCT) in a series of location-specific Decision Tree (DT) models [J2]. The method leverages the transparent nature of DTs to extract key threshold values for important variables. The method can also rapidly predict the stability margin at each location in a network, providing computational savings online compared to RMS-TDS whilst maintaining accuracy. Indeed, the use of maximum and minimum errors is proposed to assess ML model error. This is

important in the context of TSA as a large error may result in an overly cautious dispatch or operation closer to the stability boundary than comfortable. The top-3 most important variables to the prediction of the stability margin at each location (ranked using PFI) and key threshold values (extracted from the DTs) are used to generate 3D transient stability boundary representations at each location. This enables previously unseen operational scenarios to be mapped onto the transient stability boundary representation to provide situational awareness. In the example provided, non-conventional features (such as OPF variables) are included to highlight how the feature selection can impact the types of insights available.

- Design and development of a IML-based TSA methodology that can use any ML model to predict the stability margin rapidly and SHapley Additive exPlanations (SHAP) framework to identify important variables impacting the stability boundary on a locational basis. The locational nature of the method enables insights into the critical fault (Minimum Critical Clearing Time (CCT_{min})) to be extracted. SHAP is particularly beneficial in this setting because it provides both feature importance and effects. Obtaining feature effects is advantageous since they quantify the impact of a variable in sec on a CCT prediction. SHAP provides local explanations (i.e. explanations of single operational scenarios) which, when viewed in a global frame, provide insights into the ML model behaviour as a whole—providing a global view of transient stability at each location. Extraction of rules from SHAP values for a particular power system variable of interest can be used to better understand the complex power system dynamics. This may either reinforce existing knowledge or infer new knowledge. Moreover, the locational nature of the methodology proposed is leveraged to provide locational stability boundary trends for a variable of interest. To do so, the covariance between a variable of interest and location-specific SHAP values for that variable is calculated. This provides a sense of the impact of a change in that variable on CCTs throughout the network. Such insights would be helpful for decision support in operational or planning settings.

1.2.1 Academic Publications

Lead-author publications resulting from the work undertaken in this thesis include:

[J1] R. I. Hamilton, P. N. Papadopoulos, K. Bell, "An investigation into spatial and temporal aspects of transient stability in power systems with increasing renewable generation," *International Journal of Electrical Power & Energy Systems*, vol 115, 2020.

The above publication was invited based on a conference paper and presentation delivered at the 11^{th} Mediterranean Conference on Power Generation, Transmission, Distribution and Energy Conversion 2018. Therefore, only the journal paper was eventually published.

[J2] R. I. Hamilton, P. N. Papadopoulos, W. Bukhsh and K. Bell, "Identification of Important Locational, Physical and Economic Dimensions in Power System Transient Stability Margin Estimation," *IEEE Transactions on Sustainable Energy*, vol. 13, no. 2, pp. 1135-1146, 2022.

Lead-author publications in *review* resulting from the work undertaken in this thesis include:

[J3] R. I. Hamilton and P. N. Papadopoulos, "Using SHAP Values and Machine Learning to Understand Trends in the Transient Stability Margin," *IEEE Transactions on Power Systems*, first round review submitted December 2022.

Lead-author *pending* publications resulting from the work undertaken in this thesis include:

[J4] R. I. Hamilton, et al., "Interpretable Machine Learning for Power Systems: Establishing Confidence in SHapley Additive exPlanations," *IEEE Power Engineering Letters*, August 2022. Preprint available: https://arxiv.org/abs/2209.05793.

[J5] R. I. Hamilton and P. N. Papadopoulos, "Using SHAP Values and Machine Learning to Understand the Impact of Wind Control Parameters and Location on Transient Stability Margin", journal t.b.c.

1.3 Overview of Chapters

Chapter 2: Power System Stability Phenomena

Chapter 2 first gives an overview of the characteristics of SG and CIG. The chapter goes on to provide a technical overview of power system stability in general, with a particular focus on *transient stability*. This background to transient stability is provided for readers who need an overview of the transient stability problem, which is required to understand the remainder of this thesis fully. A summary of the recently updated definition of power system stability [2] is discussed—where two new power system stability definitions were added to the traditional stability framework to reflect the faster dynamic response of RES. The main methods used for TSA of power networks are summarised (namely Transient Energy Function (TEF) and RMS-TDS). A key disadvantage of TEF based methods over RMS-TDS is the inability to capture detailed information due to the use of simplified models. Therefore, this thesis focuses on using RMS-TDS.

As such, the main indices used for RMS-TDS based TSA are given. These are broken down into *fixed* and *variable* fault-time metrics (the former requiring only a single RMS-TDS per operational scenario and the latter requiring multiple—which is computationally expensive). However, variable fault metrics such as the CCT—the upper bound on the fault duration such that the system will regain synchronism—quantify the proximity of an operational scenario to the stability boundary as opposed to the less informative binary stable/unstable quantification.

Chapter 3: Literature Review on the Impact of Converter Interfaced Generation on Transient Stability

In Chapter 3, a detailed literature review provides an overview of some of the factors that have been found to impact transient stability due to the changing generation mix—going some way to address research question 1. The different dynamic response of CIG compared to SG to a fault, changes to network power flow and loss of conventional SG attributes will change the dynamic response of the network. This will likely

have a significant impact on all aspects of power system stability—including transient stability—and must be properly understood to avoid potentially severe consequences.

The impact of increasing penetrations of RES and disconnection of SG is assessed through a detailed review of academic literature. The wide range of studies reviewed highlights that the dimensions of the transient stability problem increase as CIG connects and can have a widely varying impact on transient stability depending on many variables and parameters. Often findings presented are system-specific, which means that findings may not translate onto different networks—which is a key drawback of many of these studies. This points to the need for the development of new TSA methodologies that are also capable of identification of the power system variables that impact the transient stability margin in the context of increasing RES and decreasing SG capacity in any system.

This Chapter also points the reader towards some supplementary studies conducted as part of this PhD using a SMIB in Appendix A. These studies seek to understand some mechanisms that impact the transient stability boundary, in light of the complexity RES introduces—specifically relating to the impact of displacement of SG by RES, wind control parameters, WF location with respect to SG and RES loading—going further in addressing research question 1. Despite not being included in the main body of this thesis, the studies highlight some interesting trends that are built on in later Chapters.

Note that this literature review focuses on demonstrating the widely varying impact that CIG can have on transient stability. Therefore no literature relating to ML or IML is given at this point. This review is provided later in the thesis in Chapter 5.

Chapter 4: Investigation into Spatial and Temporal Aspects of Transient Stability

In Chapter 4, some of the additional dimensions to the transient stability problem missing from the academic literature in Chapter 3 are investigated (as per research question 1). In particular; the impact of generator cost (which has been varying significantly with European wholesale gas price volatility in 2021-22 [24]), along with locational

aspects of RES with respect to SG is assessed. Results using an adapted version of the IEEE 9-bus test network illustrate how (a) the location of RES with respect to SG matter, (b) generator cost (i.e., dispatch) has an impact on transient stability and the critical fault (that is, the short-circuit fault which results in the shortest CCT) can vary both in terms of duration and location as more RES connects in different locations.

Ultimately, this Chapter highlights that the way RES is connected to and dispatched on power systems can significantly impact transient stability. As such, credible contingency lists may no longer be up to date, potentially leading to 'blind spots' in credible contingency lists that could lead to severe consequences—such as blackouts. The number of these blind spots can be reduced using the exhaustive approach proposed in this Chapter by assessing stability at multiple locations—increasing computational requirements.

Chapter 5: Machine Learning and Interpretable Machine Learning for Transient Stability Assessment

Chapter 5 discussed the shortcomings of existing TSA tools and outlines three desirable attributes that TSA methodologies should possess for use in modern power systems—motivated by the drawbacks of current TSA methods (outlined in Chapter 2) and the changes to power system dynamics (Chapter 3, 4 and indeed Appendix A)—thus, addressing research question 2. These attributes are:

1. reduction of computational expense for obtaining the transient stability margin in operational timescales,
2. enhancement of understanding of the predominant factors influencing the transient stability boundary, and
3. accurate representation of the transient stability boundary.

The Chapter also addresses research question 3, outlining that the primary motivations for using ML is to provide explicit mappings of complex functions and accelerate computationally heavy tasks. This is advantageous for TSA, which is traditionally used computational expensive RMS-TDS to capture the full dynamic response of CIG.

However, as the accuracy of ML algorithms increases, they also become more black-box—leading to an accuracy vs interpretability tension. This limits the ability to understand how an ML model reaches predictions and, thus, limits the ability to understand predominant factors influencing transient stability. IML (an emerging area of research) can be used to provide detailed insights into black-box ML models. IML techniques could be extremely valuable for TSA, enabling the development of *fast*, *accurate* and *interpretable* methodologies. The potential to uncover important parameters that impact transient stability margin would be highly beneficial, providing a deeper understanding of the stability boundary (enhancing situational awareness) and assisting in the design of stability enhancement measures. Indeed, this is a key motivation for the work presented in the remaining Chapters of this thesis. Some fundamental ML concepts are introduced in Chapter 5 that are referred to throughout the remainder of this thesis.

Chapter 6: Identification of Important Power System Parameters using Decision Trees and Permutation Feature Importance

Chapter 6 proposes an IML-based methodology that possesses the three desirable attributes outlined above—directly addressing research question 4. In a similar manner as proposed in Chapter 4, the method proposed in this Chapter determines the stability margin at each bus in the network. This enables the rapid prediction of the transient stability margin (including tracking the critical fault) *and* an understanding of the important power system parameters that impact the transient stability margin on a locational basis. Such insights are then used to inform operational rules or design stability improvement measures.

This Chapter uses DTs to predict the locational stability margin. PFI—a model inspection technique—is subsequently used to identify the important variables of each locational DT model, revealing the main factors that influence the stability margin at each location. The white-box nature of DTs combined with PFI enables rule extraction of important variables from the DTs that can be used to form rules—going some way to address research question 5. The accuracy of the ML models is reported using widely used ML error metrics. However, for TSA, minimising the maximum absolute error

is particularly important. This is because a large error in a single prediction may either lead to overly cautious dispatch (with cost implications) or (conversely) provide a false sense of security. Therefore, this Chapter specifies using the maximum error to benchmark performance.

The proposed method is implemented on an adapted version of the IEEE 39-bus test network with Type-4 wind. It is observed that DTs achieve good accuracy in the prediction of the stability margin (the CCT). The efficacy of the method to identify important power system variables that impact the stability boundary is tested by using an important feature to inform a stability enhancement measure. An example of one such intervention is provided, demonstrating how effectively the method reduces the complexity and dimensionality of the transient stability boundary. In addition, a sensitivity analysis of the impact of feature selection, DT cost metric and ML algorithm is tested. Whilst DTs achieve good accuracy, other ML algorithms offer improved accuracy, which may further enhance confidence in the method. However, this increase in accuracy is at the expense of interpretability. Whilst PFI is capable of identifying important features for any ML model, rule extraction from black-box ML algorithms is extremely difficult compared to DTs. This problem forms the focus of the proceeding Chapters.

Chapter 7: Identification of Trends in the Transient Stability Margin Estimation using Feature Effects obtained from SHapley Additive exPlanations

Chapter 7 presents an alternative and *improved* method using the SHAP framework that addresses research questions 4 and 5 in a more comprehensive manner. The method proposed in Chapter 6 is limited in that DTs must be used, and in certain instances, DTs may not be accurate enough. Therefore this Chapter seeks to develop a methodology that can be implemented with any ML algorithm (i.e., model-agnostic). In addition, PFI is limited in that; (a) it is a *global* IML technique, that (b) offers feature *importance* (based on the decrease in model performance when a feature is permutated). This further limits the method since (a) explanations of single operational scenarios cannot be obtained and (b) feature *effects* are not captured.

The SHAP framework is centred around the use of Shapley values, which have a theoretical foundation in coalitional game theory. Rather than computing the contribution of a coalition of players in a game, SHAP computes feature contributions to the prediction of a ML model for a given instance. Therefore, the contribution of each feature to the model estimation can be derived. Since SHAP is model agnostic, complex black-box models can be implemented to enhance the prediction accuracy of the stability margin. Indeed, a framework for selecting an appropriate ML algorithm is proposed based on the desired accuracy. SHAP primarily provides *local* explanations but can be extended across multiple points to provide*global* interpretations of the model as a whole. What is more, SHAP gives feature *effects* (i.e., the impact of a feature on the outcome). This is particularly advantageous since the feature *effect* in this context quantifies the impact of each power system variable on the stability margin. The locational nature of the methodology proposed in this Chapter enables a comparison between feature effects per location. In doing so, any locational trends in the stability margin can be revealed. In addition, due to the foundations in cooperative game theory, interaction effects between features can also be analysed. Detailed insights into important parameters are revealed—providing a detailed understanding of the transient stability boundary.

A case study using an adapted version of the IEEE 39-bus network with Type-4A wind is provided where the SHAP framework is used to (a) identify locational trends in the transient stability boundary, (b) identify interdependencies between power system variables and (c) identify system-wide trends in the transient stability boundary (going further than the method proposed in Chapter 6). In doing so, the impact of transient stability margin enhancement measures can be assessed on the local stability margin—and the system-wide stability margin. In the case study provided, Artificial Neural Network (ANN) models are used to increase prediction accuracy, enhancing trust in the models' capability to represent the power system's dynamics and, in turn, enhancing trust in the important features identified. In addition, results from SHAP and PFI are compared, highlighting the advantages of using SHAP. Findings show that the method proposed in Chapter 7 is capable of significantly greater accuracy and

insights than that proposed in Chapter 6.

Chapter 8: The Impact of Wind Control Parameters and Location on Transient Stability using SHapley Additive exPlanations

In Chapter 8 the SHAP framework is again used, with a particular focus on assessing the impact of wind control parameters and location on the transient stability margin in analysis more suited to planning timescales. Research questions 1, 4 and 5 are addressed in doing so. Wind control parameters are found to change the dynamic response of the Wind Turbine Generator (WTG) and thus impact the dynamic response of the network in both the literature review presented in Chapter 3 and the supplementary studies using a SMIB in Appendix A. Locational aspects of wind were analysed in some detail in Chapter 4 and demonstrated how wind location with respect to SG could have a significant impact on the transient stability boundary in the IEEE 9-bus test network.

Previous academic studies have looked into specific wind controller settings in isolation (e.g., the post-fault active power recovery ramp rate [25]). However, there is a gap in the literature relating to developing a holistic methodology capable of assessing the impact of wind control parameters in any system. In this Chapter, SHAP is again used to identify important power system variables on the transient stability margin—with a particular focus on wind location and controller parameter settings. Using an adapted version of the IEEE 39-bus test network, the method is shown to be effective in enhancing understanding of how RES location and controller settings (among other factors) impact the transient stability margin. Whilst the case study provided reaches system-specific conclusions, the method can be applied to any system to gain similar detailed insights.

Chapter 9: Conclusions and Further Work

Chapter 9 provides a comprehensive summary of all the findings from this thesis, addressing how the research questions detailed in this Chapter have been addressed. In addition, potential avenues for future research are outlined.

Chapter 2

Power System Stability Phenomena

This Chapter outlines the fundamental concepts behind power system stability, focusing on *transient stability*. A summary of the two additional categories added to the power system stability framework in 2020 [2] to reflect the faster dynamics introduced by RES (converter-driven and resonance stability) is also provided. In particular, this Chapter presents much of the technical background relating to transient stability, which is the primary focus of this thesis.

A description of the traditional methods used for TSA, that is; TEF and TDS are given. Whilst more computationally intensive, the ability of TDS to capture the dynamic response of RES means that they are typically favoured over TEF methods. For this reason, TDS (specifically RMS-TDS) are used throughout this thesis. As such, the metrics used in TDS-based methods to describe transient stability are outlined (namely fixed and variable fault duration metrics) along with a description of the level of detail captured by each metric.

As mentioned in Chapter 1, the transition from fully synchronous power systems toward systems dominated by RES is likely to lead to significant changes to the transient stability phenomena. This means that the transient stability margin of systems will constantly vary as the mix of technologies connected changes. This could happen

in both operational (e.g., as wind speed varies) and planning timescales (e.g., commissioning or decommissioning SG that use certain fuel types). This leads to a requirement for the tools and methods traditionally used to assess transient stability to adapt.

2.1 Synchronous vs Converter Interfaced Generator Characteristics

Electrical power generators convert mechanical power to electrical power through interactions of magnetic fields of the stator and rotor and the airgap between the two. However, there exist differences between conventional thermal power plants and RES. In particular, SGs converts rotational mechanical energy from a prime mover to electrical energy in the form of three-phase Alternating Current (AC) electrical power while RES synthetically replicates three-phase AC electrical power via a a PEC. In [26], authors define SG as a device that embeds three functions: (i) energy source (namely the mechanical power coming from the turbine), (ii) energy conversion (from mechanical to electrical through the magnetic coupling between rotor and stator), and (iii) energy storage (the rotating mass of the rotor and turbine).

CIG provide energy conversion from Direct Current (DC) to AC, through power electronic switches. Consequently, the converter would require an energy source, energy storage, and control (e.g., grid forming) to fully resemble a SG. The injection of power to the network through PECs decouples the mechanical input (note. in the case of solar Photovoltaic (PV), for example, there is no mechanical input) and electrical output. Accordingly, the electrical torque component (discussed in Chapter 2) may be absent from power injected by CIG depending on the control scheme deployed. One difference between conventional SG and CIG frequently discussed is that the rotating parts of the SG inherently provide inertia to the system, unlike resources that are decoupled from the system by the PEC (Figure 2.1 compared to Figure 2.2). This inertia inherent in SG acts to slow down the natural reaction of the system during disturbances (as per the swing equation (Equation 2.4)). As the system inertia reduces (due to the abovementioned changes to electricity generation), these timescales also reduce [26].

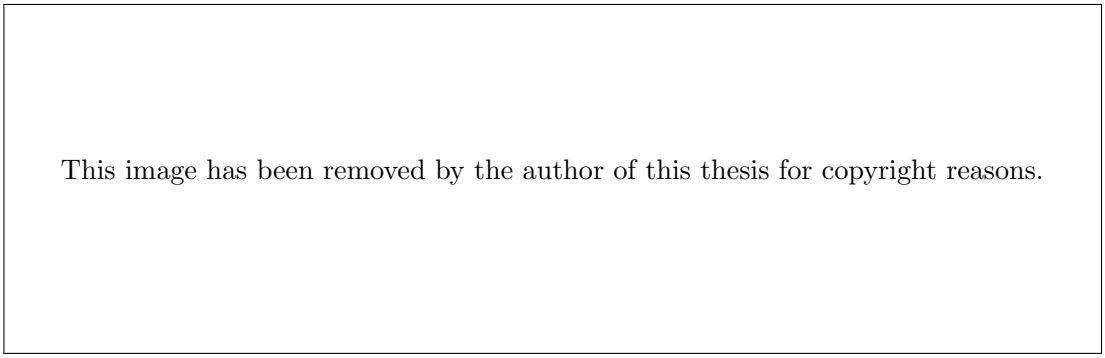

Figure 2.1: Synchronous Generator (SG) coupling with power system: synchronous coupling [28].

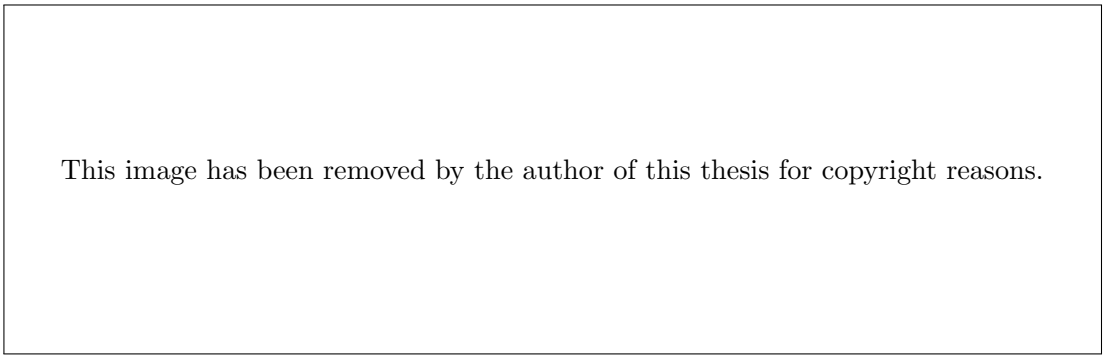

Figure 2.2: Converter Interfaced Generator (CIG) connection to power system: no synchronous coupling [28].

The reduction in the number of SGs connected to power systems will also reduce the normal short-circuit capacity current, which is necessary for protection devices (which aim to preserve stability) to successfully operate [27]. Along with this, the disconnection of SG results in the loss of AVRs and PSS that provide system control tasks such as voltage support and oscillation damping.

PEC interfaced RES introduce faster non-linear dynamics compared to conventional SG for active and reactive power support. In addition, the intermittency of renewable resources can mean that generators injecting power into the network vary in real-time in terms of technology type, capacity and location. For example, RES are typically connected to the system in different locations than conventional SG (i.e., in regions with renewable resource availability, which may be electrically distant from demand centres). In addition, CIG is often connected to lower voltage levels than conventional SG and

not directly to transmission levels. This has implications from a transient stability perspective as the system operator may not know what technologies are operating at a distribution level or the control modes selected by each individual generator.

Therefore as the renewable resource varies, there may be: (a) significant changes to the dynamic characteristics of the generation connected to the network and (b) significant changes to the power flows on a network that may not be designed to manage such power flows. These changes may happen in planning timescales (e.g., due to government policy decisions to decommission coal generators) and in operational timescales—as the resource availability varies along with the output of conventional SG.

Indeed, the consequent loss of aforementioned SG attributes (upon which power systems have been built and operated around for decades), intermittency of RES and complex highly non-linear dynamics associated with converter-interfaced RES is proving challenging for maintaining power system stability [29]. In recognition of this, an IEEE task force revised the power system stability definition to include converter-driven stability in 2020 [2] as outlined in Chapter 2. In addition to this, transient stability may also impacted—which is the principal focus of this thesis.

2.1.1 Conventional Synchronous Generation

SGs have traditionally formed the principal source of electric energy in power systems. Conventional thermal power plant use SGs to convert rotational mechanical energy from a prime mover to electrical energy in the form of three-phase AC electrical power. These machines typically use a constant rotating magnetic field—produced in the rotor through DC excitation of the rotor windings. This field is rotated by the prime mover at synchronous speed, or some fraction of synchronous speed, depending on the number of poles of the machine. Figure 2.3 shows the schematic of the cross-section of a three-phase SG with one pair of poles and consists of two key elements: the field and the armature. The relationship between rotor speed (ω_{msyn}), number of poles (P) and the electrical frequency of the grid voltage waveform (ω_{syn}) is given by:

$$\omega_{msyn} = \frac{2}{P}\omega_{syn} \tag{2.1}$$

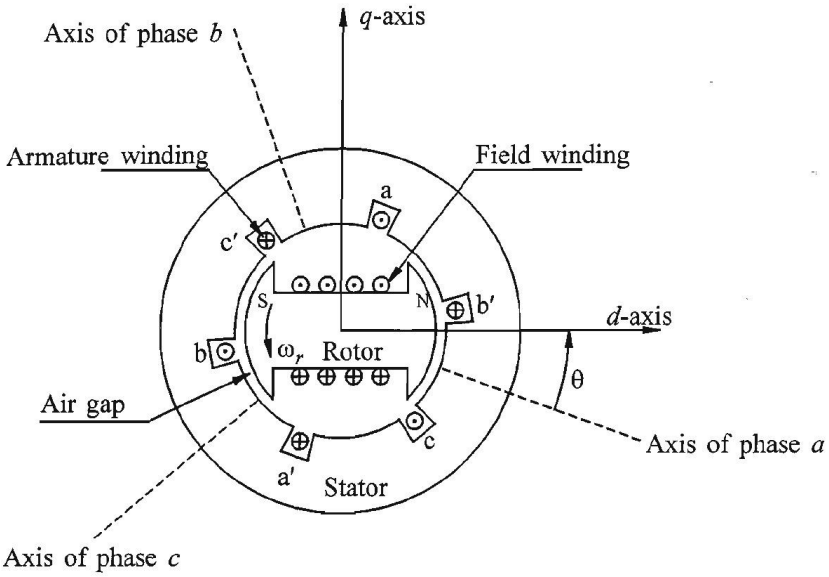

Figure 2.3: Schematic diagram of a three-phase Synchronous Generator (SG) [30].

AC voltages are induced in the three-phase stator (armature) windings and depend on the rotor rotational speed, the number of poles and the excitation current in the rotor windings (i.e., the magnetic field strength). Field excitation of a SG is important in maintaining a constant stable voltage at the generator terminals and responding rapidly to grid-side changes. An AVR may be used to control the voltage at the machine terminals by manipulating the field excitation current.

Automatic Voltage Regulator (AVR)

A SG must regulate the grid voltage of the transmission system to which the machine is connected. The field excitation of a SG is important as it must maintain a stable machine terminal voltage and respond quickly to any sudden grid-side load changes to maintain system stability. An AVR may be used in the control logic of the generator, which maintains the machine terminal voltage at the desired level through manipulating the field excitation current.

Power System Stabiliser (PSS)

The PSS seeks to improve the power system dynamic performance by controlling the generator excitation system using auxiliary stabilising signals. The tuned feedback system commonly takes inputs from the shaft speed, terminal frequency and power. The dynamic performance of the power system can be improved by damping system oscillations and can enhance small-signal stability performance.

2.1.2 Converter Interfaced Generation

A summary of prevalent RES that are dominating modern power systems is outlined below. A particular focus is given to wind generation due to the particularly high prevalence—for example, accounting for 29 % of GB electricity output in 2020 (Figure 1.4). In addition, HVDC and Electrical Energy Storage (EES) are discussed due to the likely increase in prevalence over the coming decades. Although HVDC and EES are not strictly RES, the PEC interface poses similar challenges as outlined above. Finally, an overview of Low-Voltage Ride Through (LVRT) behaviour is provided, which is a fundamental capability of RES in modern power systems.

Wind Turbine Generators

There are two main types of WTGs—fixed and variable speed [31]. The turbine rotor of a fixed speed WTGs is bound by the frequency of the grid to rotate at a *fixed* speed and typically uses a Squirrel Cage Induction Generator (SCIG). Modern variable speed WTGs can operate across a range of speeds due to a decoupling of mechanical and electrical frequencies through the use of PECs.

More specifically, there are four common WTG technologies (Figure 2.4). The Type-1 generator is a fixed-speed machine that uses a conventional SCIG, run at super-synchronous slip speed, and so the electrical model for the machine is a standard induction machine model. The Type-2 machine was the first step toward variable-speed operation, achieved through a Wound Rotor Induction Generator (WRIG) and an external resistor to vary the rotor resistance and thus the turbine speed. Type-3

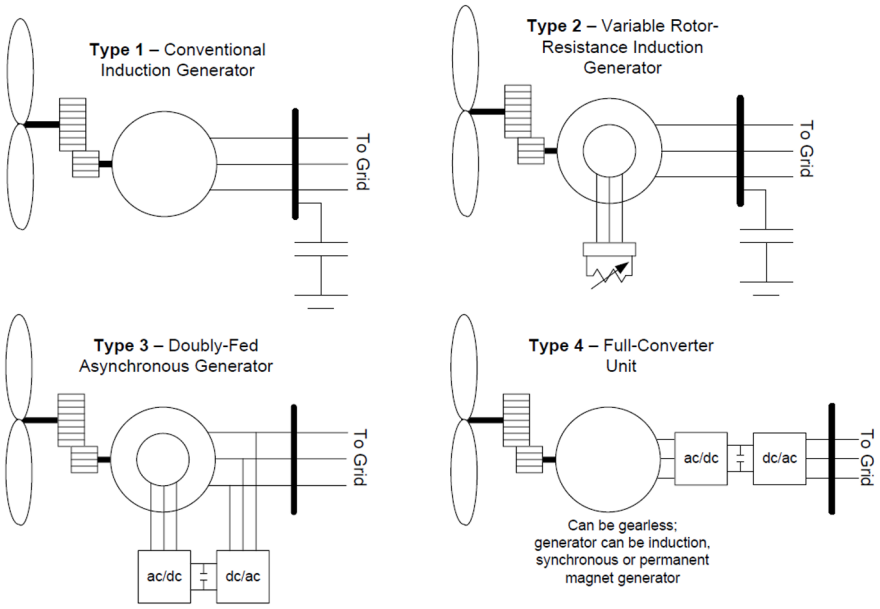

Figure 2.4: Generic Type-1, 2, 3 and 4 models Wind Turbine Generator (WTG) [33].

and 4 variable speed generators are now the predominant WTG technologies deployed on modern power systems. Both types achieve variable speed operation by decoupling mechanical and electrical frequencies through the use of PECs.

The Type-3 machine uses a Doubly-Fed Induction Generator (DFIG), where the stator is directly connected to the grid, and the rotor is connected through a partial-scale (rated at approximately 30 % of the nominal generator power) back-to-back power converter (typically through slip rings) [32]. Consequently, the electrical and mechanical rotor frequency is decoupled because the PEC compensates for the difference between mechanical and electrical frequency by injecting a rotor current with variable frequency, thus enabling variable speed operation. Moreover, the reactive power of the DFIG can also be controlled by the PEC.

Type-4 WTGs (often referred to as Fully-Rated Converter (FRC) turbines) are connected to the grid through a full-scale back-to-back power converter, enabling variable speed operation. This may be implemented with different generator types such as Wound Rotor Synchronous Generator (WRSG), WRIG or Permanent Magnet Synchronous Generator (PMSG). A low-speed multi-pole synchronous ring generator with the same rotational speed as the wind turbine rotor is used to convert mechanical en-

ergy into electricity. The generator can have a wound rotor or a rotor with permanent magnets. The stator is coupled to the grid through a PEC. This may consist of a back-to-back Voltage-Source Converter (VSC) or a diode rectifier with a single voltage source converter. Reactive power generation can be controlled by the grid side of the PEC. Type-4 is advantageous over Type-3 due to: improved efficiency, no slip rings, simple (or no) gearbox, full power and speed controllability, better grid support abilities and less complex LVRT capability. However, because the converter is rated to 100 % of rated power, Type-4 has a higher cost than Type-3 [32].

Solar Photovoltaic (PV)

Much of the solar PV capacity connecting in GB is at distribution level by residential rooftop PVs that are located closer to the load; in some cases, causing voltage issues, increased losses and sending transmission system demand to historic lows [34]. In addition to this, increasing volumes of solar PV are connecting at the transmission level, which causes significantly different problems than those on the distribution networks.

A key concern from a transient stability perspective is that it is connected through a PEC interface [35], which can control active and reactive power instantaneously. In addition, PV has typically been connected at a domestic level which may lead to reverse power flows from the distribution level to the transmission level. However, larger-scale transmission-connected solar parks, such as the 350 MW Cleve Hill in GB, are expected to come online. Moreover, a solar PV converter equipped with conventional proportional integer controllers is naturally insensitive to changes in grid frequency which may have consequences from a transient stability perspective.

High-Voltage Direct-Current

The two dominant forms of HVDC transmission are the Line-Commutated Converter (LCC) or Current Source Converter (CSC) and the VSC [36]. LCC-HVDC uses a thyristor-based technology, which relies on the line voltage of the AC system. The VSC-HVDC is s six-pulse converter which uses insulated gate bipolar transistor technology and is capable of creating AC voltages independently from the grid voltage.

Each technology has advantages and disadvantages, and the technology selected often depends on the needs of the specific application.

From the perspective of transient stability, concerns relating to the impacts of an increase in the number of *inter*connectors—or indeed *intra*connectors such as the Eastern Link in GB [37]—primarily relate to the resulting changes to network power flows that may potentially be rapid due to changes in price signals at either end of the connection. This may lead to a requirement for rapid TSA to ensure continued secure operation.

Energy Storage Systems (ESS)

To address some of the intermittency issues caused by RES, there has been an increased interest in Energy Storage Systems (ESS) to provide balancing and ancillary services. Technologies that currently have high levels of interest are: Battery Energy Storage (BES), Compressed Air Energy Storage (CAES), Superconducting Magnetic Energy Storage (SMES), Electrochemical Capacitor Energy Storage (ECES), and Flywheel Energy Storage (FES) [38]. An example of the rollout of BES was in the Enhanced Frequency Response (EFR) market in GB, where all of the 200 MW capacity available was awarded to BES technologies in 2016 [39]. Although not the primary reason that justifies the economic validity of ESS devices, the controllability of active and reactive power inherent with VSC technologies means that there is potential for ESS to be used to benefit the transient stability of power systems. Indeed, ScottishPower Renewables aims to install 1.5 GW of BES by 2030 [40].

Low-Voltage Ride Through (LVRT) Capability

LVRT is an imperative capability of CIG to ensure units are not erroneously disconnected and is increasingly important in systems with large volumes of RES. Grid Code Requirements (GCRs) specify that generators should remain connected to the grid during network faults to ensure system stability. More specifically, CIG must have the capability to provide reactive power during the faults and to supply active and reactive power post-fault (to support grid voltage and frequency).

GCRs define LVRT capability in terms of *voltage and time profiles*, which sets limits

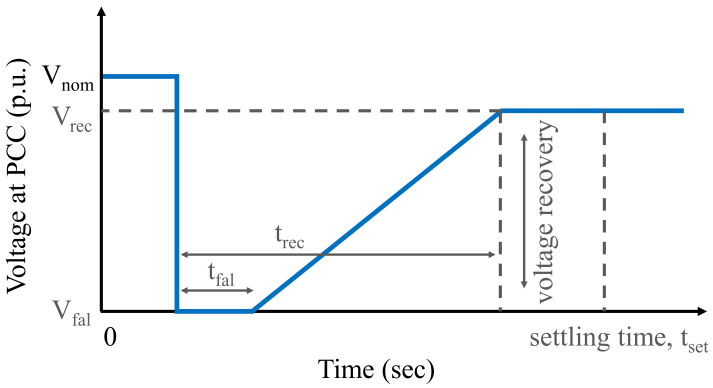

Figure 2.5: Generic Low-Voltage Ride Through (LVRT) capability voltage-time characteristic.

for which generators must ride through faults on the grid without disconnecting. In Figure 2.5, the blue line indicates a generic voltage-time characteristic, above which the generator must remain connected to the network. In an event where the generator terminal voltage drops below the voltage-time characteristic, disconnection from the network is permitted.

More specifically, GCR defines fault time (t_{fault}), fault voltage permitted (V_{fault}), recovery time (t_{rec}) and voltage to be recovered within recovery time (V_{rec}) and the prescribed sustaining period or settling time (t_{set}) as shown in Figure 2.5 (where all voltages are taken at the Point of Common Coupling (PCC)). After fault clearance, the voltage recovery to the pre-fault condition of nominal voltage (V_{nom}) is indicated by (t_{set}). Since the timescales associated with the LVRT response are during and immediately after a fault, there is an inherent interaction with the transient stability of the system. As such, LVRT behaviour may impact transient stability—a theme that is also explored at various points throughout this thesis.

2.2 Power System Stability Overview

Power system stability is defined as:

"*the ability of an electric power system, for a given initial operating condition, to regain a state of operating equilibrium after being subjected to a physical disturbance, with most system variables bounded so that practically the entire system remains intact*" [1],

and is an umbrella term that can, at times, mask the underlying detail and cause(s) for the instability. Traditionally, power system stability is further classified into rotor angle, frequency and voltage stability (outlined in Figure 2.6). This definition is useful in that it assists in the identification of the causes of instability, the application of suitable analysis tools and the development of prevention/corrective measures. In general terms, the three traditional stability classifications can be described as follows.

- **Rotor angle stability**: the ability of SGs of an interconnected system to remain in synchronism when subjected to a disturbance.
- **Voltage stability**: the ability of the power system to maintain steady voltages at all buses in the system after being subjected to a disturbance.
- **Frequency stability**: the ability of the power system to maintain a steady frequency following a severe disturbance resulting in a significant imbalance between generation and demand.

2.2.1 2020 Power System Stability Definition Update

The different dynamic behaviour of RES compared to that of conventional SGs may lead to new types of power system stability problems. Whilst the traditional definition of power system stability from [30] still applies, two new classifications of power system stability have recently been added to the traditional framework to reflect the faster dynamic response of RES (which ranges from a few μsec to several msec (i.e., wave and electromagnetic phenomena)). These new stability classes are outlined in Figure

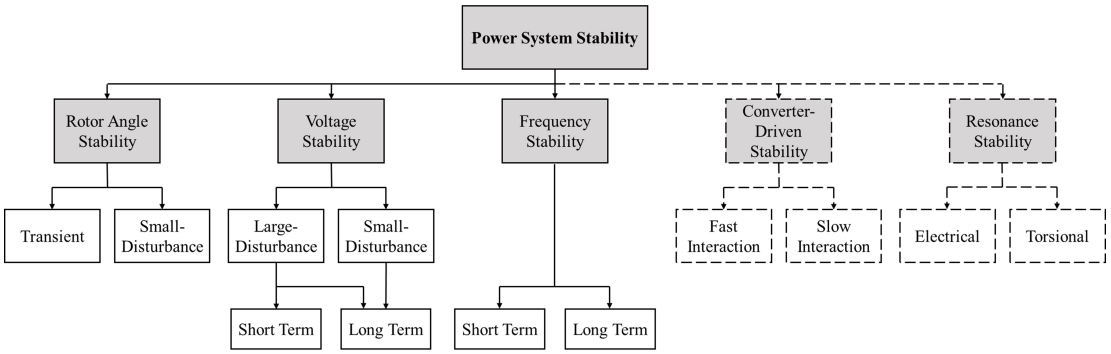

Figure 2.6: Traditional definition of power system stability, with the two new classes included as per the 2020 revisited and extended definition [2].

2.6) [2]. Converter-driven stability relates to both slow- and fast interactions caused by the fast response of RES control loops and algorithms, whilst resonance stability encompasses Subsynchronous Resonance (SSR) and is included due to power electronic dynamics in electromagnetic transient timescales.

The use of the term 'power system stability' to describe different forms of instability reflects that it is improbable that any one form of instability will occur independent of others, and the system's overall stability must always be considered. This is increasingly true as the speed of the dynamic behaviour increases. For example, the frequency of a power system is often treated as one single entity. However, system frequency is simply an aggregate of regional frequencies, which are an expression of the interaction of the rotor angles of synchronous machines in an area. As the inertia of different areas of the system varies at different rates (depending on SG connected in that area, renewable resource availability and so on), the frequency in different areas of the system will respond at different rates following a disturbance. As system frequency is increasingly considered to be a 'distributed' phenomenon (as it is in the Enhanced Frequency Control Capability project [41]), the frequency problem begins to increasingly look like a transient stability problem.

However, this thesis is primarily concerned with rotor angle stability (specifically transient stability); which refers to the ability of SGs of an interconnected system to remain in synchronism when subjected to a major disturbance.

2.3 Rotor Angle Stability

Rotor angle stability refers to the ability of SGs of an interconnected power system to remain in synchronism after being subjected to a disturbance, and the objective of transient stability studies is to determine whether or not the SGs will return to synchronous speed with new steady-state power angles. This depends on the ability to maintain or quickly restore equilibrium between electromagnetic torque and mechanical torque of each SG in the system. In steady-state conditions, an equilibrium exists between input mechanical torque and the output electromagnetic torque of each SG, so the rotor speed remains constant. When the system is subject to a disturbance, this torque equilibrium is perturbed, resulting in an acceleration or deceleration of SG rotors in accordance with the laws of motion of a rotating body. If one SG accelerates compared to another, its rotor angle (relative to the other slower machine) will advance. The resulting angular difference between the SGs has the effect of transferring part of the load from the slower SG to the faster one in accordance with the power-angle relationship (Figure 2.7). This effectively acts to reduce the speed of the faster SG, and so the angular separation between the machines decreases. However, beyond a point, an increase in angular separation between SGs results in a decrease in power transfer such that the angular separation is increased further. The system becomes *unstable* when the kinetic energy gained by the accelerated SGs cannot be absorbed by others to regain energy balance. The stability of the system depends on whether or not the deviations in angular positions of SG rotors result in sufficient restoring torques [30]. A SG loses synchronism with the system when its rotor runs at a faster or slower speed than required to generate voltages at system frequency.

The change in electrical torque of a SG following a disturbance can be resolved into two components; *synchronising* and *damping* torque components as outlined in Equation 2.2, both of which are essential for each SG in a network to have in order to maintain system stability. Active power injected by a SG maintains synchronism and damps mechanical oscillations through these components of electrical torque.

$$\Delta T_e = T_s \Delta\delta + T_d \Delta\omega \tag{2.2}$$

where ΔT_e is the change in electrical torque, $T_s \Delta\delta$ is the component of torque change in phase with the rotor angle perturbation (synchronising torque component) and $T_d \Delta\omega$ is the component of torque in phase with the speed deviation (damping torque component) of a SG.

It is common practice to categorise rotor angle stability into two subcategories: small disturbance stability (often referred to as *small signal* stability) and large disturbance stability (often referred to as *transient* stability—which includes both first-swing and multi-swing stability). Both forms of angular stability are considered to be short-term phenomena, where the time frame of interest is typically between 0 to 15 sec following a disturbance. The following sections describe the nature of these categories of rotor angle stability in more detail. An overview of small-signal stability is provided for completeness. For convenience, both torque and power are used since power is the product of angular velocity and torque.

2.3.1 Small-Signal Stability

Small-signal stability is concerned with the ability of the power system to maintain synchronism under small disturbances, such as changes in demand, generator set-points etc. The disturbances are considered to be sufficiently small that system differential algebraic equations may be linearised for purposes of analysis [42]. System dynamics tend to be analysed in the frequency domain using eigenvalue and/or eigenvector analysis. Small-signal stability issues may be either local or global in nature, with local modes (local plant modes) being associated with the swinging of units of a generator swinging with respect to the rest of the system, whilst global modes (inter-area modes) are caused by interactions between large groups of generators. What is more, small-signal stability is dependent on the initial operating condition of the system, and instability may be a result of:

i) increase in rotor angle through non-oscillatory mode due to lack of *synchronising*

torque, or

ii) rotor oscillations of increasing amplitude due to lack of sufficient *damping torque*.

2.3.2 Transient Stability

Transient rotor angle stability is concerned with the ability of the power system to maintain synchronism when subjected to a severe disturbance. The disturbance may be a short circuit on a transmission line or generator, disconnection of a line or a generator outage. The resulting system response involves large excursions of SG rotor angles from a pre-fault equilibrium and is influenced by the highly non-linear power-angle relationship (defined mathematically in Equation 2.3). Therefore, oscillations that follow the fault should be damped within the first few cycles post-fault. If this is not achieved, the transient behaviour of the network may dominate such that the system diverges from the pre-fault point of equilibrium, potentially resulting in a SG losing synchronism and leading to a cascading failure.

For example, a SG in Figure 2.7 is represented by the classical model where the voltage behind the transient reactance (X_T) is denoted by E, and the rotor angle δ represents the angle by which the SG voltage leads that of the system (V). This is defined algebraically in Equation 2.3.

$$P_e = \frac{EV}{X} sin\delta = P_{max} sin\delta \tag{2.3}$$

During steady-state operation, the mechanical power input (P_m) is in equilibrium with the machine's electrical power output (P_e). However, during a transient event, there is a mismatch in mechanical and electrical power. The resulting torque causes the rotor to accelerate (if $P_m > P_e$) or decelerate (if $P_m < P_e$) from the initial operating point, tracing the power-angle curve at a rate determined by the swing equation (Equation 2.4).

$$M\frac{d^2\delta}{dt^2} = P_m - P_e = P_a \tag{2.4}$$

where M is the inertia coefficient, δ is the rotor angle with respect to a synchronously

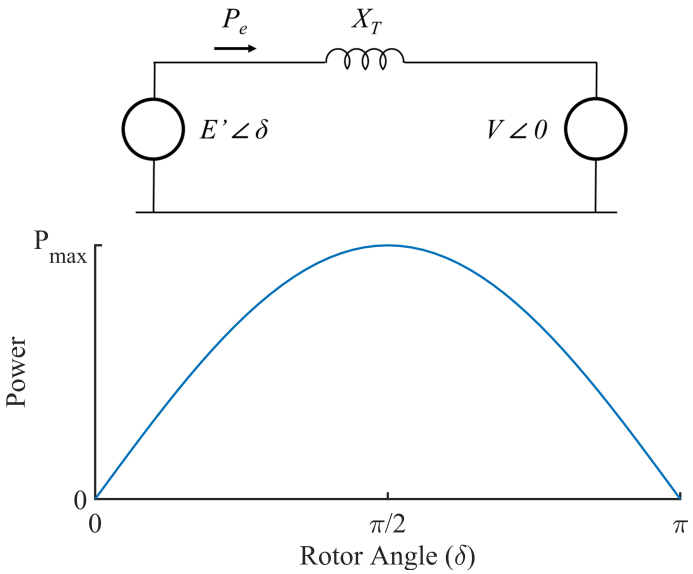

Figure 2.7: Power-angle relationship for a simple two-machine system [43].

rotating reference frame, P_m is the mechanical power, P_e is the electrical power and P_a is the accelerating power. The inertia coefficient (M) is a function of the inertia constant (H) and the machine rating (S_n) at synchronous speed (ω_s).

$$M = \frac{2HS_n}{\omega_s} \tag{2.5}$$

Since the time derivative of the rotor angle is the rotor speed deviation, the second-order differential equation (Equation 2.4) can be replaced by two first-order equations (Equation 2.6 and 2.7).

$$M\frac{d\Delta\omega}{dt} = P_m - P_e = P_{acc} \tag{2.6}$$

$$\frac{d\delta}{dt} = \Delta\omega = \omega - \omega_s \tag{2.7}$$

The swing equation ultimately describes how the changes in the SG power (or torque since power is the product of angular velocity and torque) balance are transferred to the rotor speed (ω) and ultimately represented in the angular position of the SG rotors (δ).

The transient stability of the system depends on both the initial operational scenario

(defined as a particular realisation of demand, wholesale electricity markets preference for generation dispatch, and a network state) in the network and the severity of the disturbance, with instability usually manifesting in first-swing instability caused by insufficient *synchronising* torque. However, note that transient instability may not always occur as a first-swing instability but could result from the superposition of a slow inter-area and local plant mode causing instability beyond the first swing.

The Equal Area Criterion (EAC) is the most basic method of analysing the impact of disturbances on transient stability and is ultimately formalised in *Lyapunov's direct method*. Using this method, one can assess power system stability without solving complex system differential equations. Although much research has gone into energy function based techniques, the most common approach for TSA is via TDS in which the non-linear differential equations are solved using numerical integration techniques.

2.4 Traditional Methods for Transient Stability Assessment

The objective of TSA methods is to determine whether or not the SGs will return to synchronous speed with new steady-state power angles following a disturbance. The details and the advantages of the most common TSA methods are discussed in this Chapter, with particular focus on the ability of the method to capture the fast dynamic behaviour of RES.

2.4.1 Transient Energy Function Analytical Methods

Direct methods determine stability without explicitly solving the system differential equations. TEF methods are derived from Lyapunov stability theory and provide an analytical expression for the stability boundary. In a SMIB system, the TEF analysis is equivalent to the EAC.

Figure 2.8 illustrates the EAC where in the steady-state the mechanical power P_m of a SG is equal to the electrical power P_e, with a rotor angle δ_0. A close-up fault at the SG terminals causes P_e to reduce to zero and the rotor accelerates until the fault

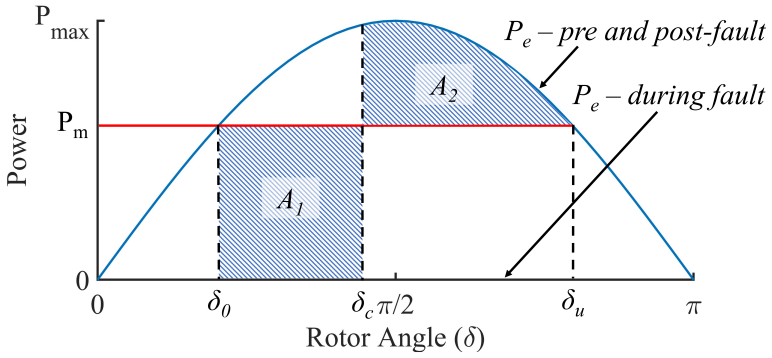

Figure 2.8: Illustration of Equal Area Criterion (EAC) for a self-clearing close-up fault on Single-Machine Infinite-Bus (SMIB) system. A1 and A2 are the accelerating and decelerating areas respectively.

is cleared, advancing the rotor angle to the critical clearing angle (δ_c). Once the fault is cleared (the post-fault network returns to the same configuration as pre-fault in this example), P_e exceeds P_m and the rotor begins to decelerate. δ_c is determined when the accelerating and decelerating energy areas are equal (A_1 and A_2 respectively). The kinetic energy gained during the fault-on period is added to the potential energy at the corresponding rotor angle, and the sum is compared to the critical potential energy to determine stability. If the energy at fault clearance is less than the critical energy then the system is stable. The magnitude of the difference between these two quantities represents the transient energy margin.

Whilst TEF are less time-consuming and computationally burdensome than TDS, they are unable to replicate the level of detailed information available in TDS due to the use of highly simplified models required in large systems (e.g., classical SG model, constant impedance loads and inadequate controller representation which are unable to capture controller saturation). This is a key disadvantage in systems with high volumes of RES.

2.4.2 Time-Domain Simulation-Based Methods

Unlike TEF methods, TDS methods are able to use significantly more detailed generator models. For example, typically SG models for RMS simulations use up to 6^{th} order models, whilst Electromagnetic Transients (EMT) simulations (which solve the differential equations) use higher order models (e.g., 8^{th} order) that considers very short stator transients [44]. The fast control systems used in PEC interfaced generation (the dynamics of which being in the order of several kHz) cannot be adequately represented by RMS dynamic models [45]. EMT dynamic models can overcome this limitation through the inclusion of higher level of detail that captures switching.

Root Mean Square (RMS) Simulations

The RMS-TDS approach models all the system dynamic components in detail with ordinary differential-algebraic equations (Equation 2.8) with known initial values and solves them iteratively in time (with a time-step typically in the order of msec).

$$\frac{dx}{dt} = f(x,t) \tag{2.8}$$

where x is the state vector of n dependent variables and t is the independent variable (time). The objective is to solve x as a function of t, with initial values of x and t equal to x_0 and t_0 respectively.

TDS approaches suffer because simulation time is long, particularly in analysing large power systems. This makes them computationally expensive to conduct, which is exacerbated by the inclusion of intermittent RES in different network locations, significantly increasing the number of operational scenarios and thus the computational burden.

Electromagnetic Transients (EMT) Simulations

An electromagnetic transient is defined as the response of the power system elements to a perturbation caused by external electromagnetic fields or to a change in the physical configuration of the network such as switching and loading. Applications such as

insulation coordination, design of protection schemes, and power electronic converter design require the computation of electromagnetic transients. EMT simulations must be done by considering all phases, over a wide range of frequencies, and with a time-step in the range of μsec.

RMS-TDS are unable to represent RES in the same level of detail as EMT simulations (especially during the fault-on period) [46]. Questions surrounding the suitability of RMS-type modelling for dynamic simulations in the context of high penetrations of RES have driven the development of EMT type models, capable of representing RES in more detail. However, the level of detail provided in EMT type models means that simulating an entire system can often be impractical. Often RMS models are used to identify critical scenarios which can subsequently be studied using EMT simulations, or indeed by co-simulation using both RMS and EMT models where additional detail is required.

In the future, EMT may indeed be required to capture the full dynamic response of all generators connected to the network. As such, methods capable of reducing the associated computational burden may also be required (as this thesis seeks to address for RMS in later Chapters).

2.5 Indices for Transient Stability Simulation-Based Methods

In this thesis, transient stability indices for time-domain simulation-based methods are considered explicitly. The analytical methods (e.g., TEF) are not included due to limited usefulness in large and complex power systems with increasing penetration of RES.

As detailed in Section 2.3.2, the transient stability behaviour of a power system is determined by the pre-fault steady state condition, the nature of the fault, and the post-contingency structure of the power system. Hence, transient stability is characterised entirely by the pre-fault conditions for a given fault in a given power system [47]. The use of transient stability indices in stability studies provides a means for com-

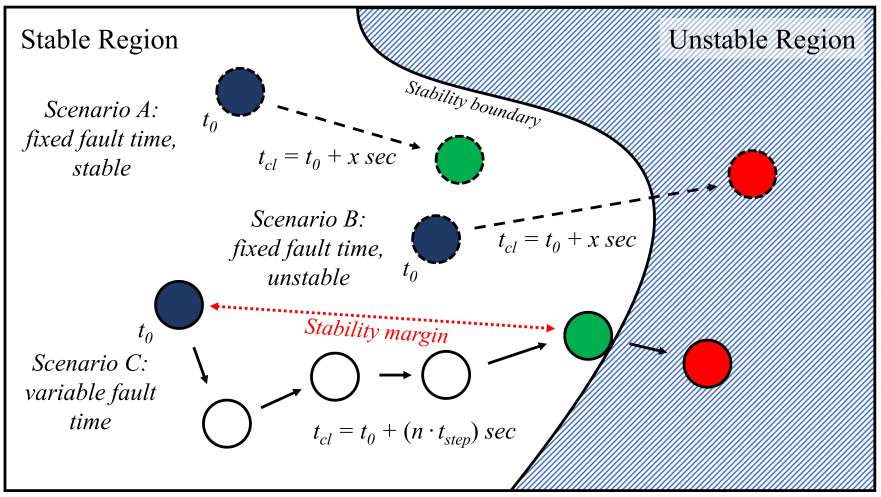

Figure 2.9: Transient stability metrics: an overview of the key differences between fixed and variable fault-time based indices for a simplified illustrative example of the stability boundary.

paring different operational scenarios and can provide useful information on how the transient stability of a network changes as network parameters change. For a given initial pre-contingency state, and a given fault, the corresponding transient stability index is typically obtained by solving a large number of coupled non-linear differential and algebraic equations. Common indices used in literature are based on two main methods; *fixed* fault-time (Section 2.5.1), and *variable* fault-time (Section 2.5.2)—the differences between which are summarised graphically in Figure 2.9. Although these indices provide useful indicators of system transient stability, more detail is often required to provide a full and comprehensive analysis since these indices cannot identify the underlying reasons for instability.

2.5.1 Fixed Fault-Time

Fixed fault-time metrics can be determined by running a single TDS, which is a key advantage compared to the variable fault-time approach (see below) due to the relatively low computational burden. However, in doing so, details relating to the exact *proximity* of an operational scenario to the stability boundary are not fully captured. Rather, the magnitude of fixed fault-time metrics can be compared between operational scenarios

to assess transient stability or an arbitrary value selected beyond which the system is considered to be unstable.

Indices calculated using a *fixed* fault-time include maximum rotor angle deviation (deg), fault-on Rate of Change of Rotor Speed (ROCORS) (deg/sec) [48], fault-on generator energy export (MW.sec), fault-on and post-fault SG net energy (MW.sec), rotor angle difference based (deg) [49], Total Kinetic Energy (TKE) (J) [30], Total Potential Energy (TPE) (J) [50] and oscillation duration [51] over the predefined fault period (sec). The suitability of some of these indices is discussed in [52].

Scenario A in Figure 2.9 provides an example of an operational scenario that remains in the stable region for a fault of a predefined duration, x sec. Scenario B provides an example of an operational scenario where the system does not remain stable after the same fault. In this scenario, the fault results in the system state crossing the boundary that partitions secure and insecure operating regions (i.e., the transient stability boundary). For Scenario A and B, the above-described transient stability indices are entirely appropriate and provide a means of assessing the relative stability of operational scenarios against each other. However, it should be noted that they cannot provide detailed information about the proximity of an operating condition to the stability boundary—which is where variable fault-time metrics are advantageous.

2.5.2 Variable Fault-Time

A *variable* fault-time metric is capable of identifying the upper bound on the duration of a fault on a power system before it is removed, such that the system will regain synchronism once the fault is cleared—known as the CCT. In other words, it indicates the power system transient stability *margin* of a given fault for a given operational scenario.

To calculate CCT using RMS-TDS, the fault duration must be increased iteratively until the Loss of Synchronism (LOS) condition is detected—leading to a requirement to run numerous TDS (which also depends on the time resolution required e.g., sec or msec). This is a computationally expensive, and therefore time-consuming process. Mathematically, CCT for a given fault for a given operational scenario on a given

network is calculated by:

$$CCT = t_{cl} - t_0 \tag{2.9}$$

where t_0 is the time at which the fault is instigated and t_{cl} is the time at which the fault is cleared. Although this makes it significantly more computationally burdensome to calculate than the aforementioned stability indices, CCT is regarded as a very informative means of assessing transient stability because it captures the full dynamic response of the system. This is described by Scenario C in Figure 2.9 where the fault duration, t_f, is increased by time-step, t_{step}, n times until the upper bound for the fault duration for a given operational scenario is found. In doing so the proximity of the operational scenario to the stability boundary for that particular fault is identified—i.e., the stability *margin*.

Of particular interest is the *duration* and *location* of the fault with the shortest CCT (i.e., the CCT_{min}), since this fault leaves the least amount of time for protection devices to activate to avoid instability. The location of the fault that results in the CCT_{min} is referred to as the Critical Fault Location (CFL) throughout this thesis.

Determining these indices significantly increases computational intensity since determination of CCT_{min} and corresponding CFL is contingent on calculating CCT at each of the possible fault locations, n. This is described mathematically in Equation 2.10.

$$CCT_{min} = min\left\{CCT_1, CCT_2, ..., CCT_n\right\} \tag{2.10}$$

Figure 2.10 shows a representation of the stability margin for two different faults, resulting in two different stability margins (A and B). It can be seen that stability margin A is significantly shorter, and therefore of greater importance, than stability margin B and would be reflected in the CCTs for these two faults (i.e., $\text{CCT}_B > \text{CCT}_A$).

In large power systems, every fault location is not typically considered since the possibilities are extremely large and computational power limited. Instead, engineering judgement must be applied to determine only the most severe fault locations and thus

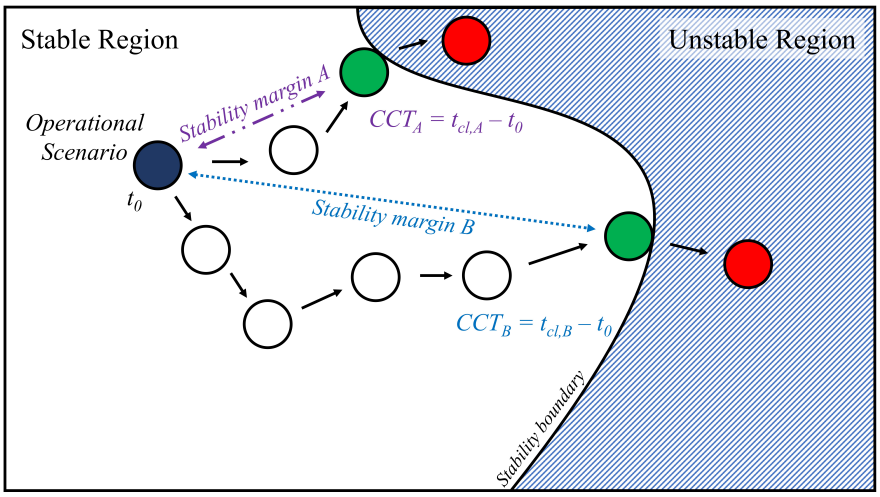

Figure 2.10: Impact of fault type on the transient stability margin for the same operational scenario, using a simplified illustrative example of the stability boundary.

reduce the number of faults studied. For example, it is appropriate to assume that the shortest CCT for a transmission line connecting bus A to bus B would be at either busbar. Ultimately, the time resolution required in the CCT and CCT_{min} depends on the application.

For transmission system faults, where the main protection can typically be expected to operate within approximately 100 ms [53], a SG stability margin approaching this threshold can be considered to be critical.

Synchronous Machine Loss of Synchronism Condition

A SG losing synchronism will accelerate with respect to its initial synchronous rotation at nominal speed, which will result in an advancement of the rotor angle from the initial steady-state angle [53]. The theory says that a SG has experienced a LOS once its rotor angle (δ) reaches π, although the reference point from which the rotor angle is to be taken is somewhat ambiguous in a multi-machine system. In the relevant literature, the angle limit used for stability analysis varies widely [54], with most studies using a heuristic limit on the rotor angle deviation between two SGs on the network.

In this thesis, if the difference between any two SG rotor angles is greater than π at an instance in time, then the system is considered unstable as outlined in Equation

2.11.

$$\Delta\delta_{ij} = \delta_i - \delta_j > \pi \tag{2.11}$$

where δ_i and δ_j are the rotor angles of SGs i and j. For example, if $\delta_i > \delta_j$ and SG_i has the greatest initial acceleration, then SG_i is the first SG to go unstable. The relative rotor angles of each SG are obtained from TDS and are considered with respect to the reference SG. Using relative rotor angles rather than absolute angles enables the relative motion of rotors between SGs to be observed. The SG that is first to experience a LOS from the others is referred to as the Critical Synchronous Generator (CSG) throughout this thesis.

2.6 Conclusion

As outlined above, existing methods for TSA all have benefits and drawbacks. For example, whilst TEF-based methods are computationally inexpensive, the use of simplified models limits their use in power systems with high volumes of RES. Conversely, RMS-TDS can capture the full dynamic response of RES but are computationally expensive—particularly when seeking to determine the transient stability *margin* for the critical contingency. What is more, when assessing numerous operational scenarios, the complexity of the transient stability problem increases due to a large number of problem dimensions. This makes understanding the factors influencing transient stability extremely difficult using these methods.

Chapter 3

Literature Review on the Impact of Converter Interfaced Generation on Transient Stability

As outlined in Chapter 1, the decarbonisation of power systems is resulting in carbon-intensive generators (typically conventional thermal SG) being replaced with often renewable CIG. The consequent loss of SG attributes, the complex non-linear dynamics associated with RES, and the changing generator dispatch patterns are proving challenging for maintaining system stability—particularly transient stability, which is a complex non-linear problem (detailed in Chapter 2).

In this context, a review of the existing academic literature relating to the impact of increased RES on transient stability is presented—primarily from the perspective of increased wind generation. Other PEC-interfaced technologies such as solar PV [55] and HVDC [56] will also impact transient stability, however these have not been considered in this literature review as in later Chapters only wind is analysed. Since the focus of this thesis is the development of methodologies that can be applied to any network, this has no implications for the methods presented. To assess the impact of other technologies of particular interest, the operational scenarios can be adjusted to reflect this.

Through a detailed review of this literature, this Chapter identifies key parameters and variables that have been shown to impact transient stability in the academic literature. The impact of increasing RES on transient stability is found to be wide-ranging in that it may improve or deteriorate depending on a wide range of parameters and variables (i.e., it is an increasingly complex and highly multidimensional problem). This Chapter concludes that the complexity of the problem limits the usefulness of many academic studies, which often seek to simplify the problem through the use of simple networks and case studies as, often, the conclusions are not transferable to other power systems.

Ultimately, the dimensions of the transient stability problem are likely to increase as new forms of generation connect to power systems. This complex non-linear, and therefore more unpredictable behaviour results in less confidence in so-called 'operational expertise', driving the need for new tools for TSA to ensure that the transient stability margin of a system is not only known but the factors influencing the transient stability boundary are also well understood. This is a crucial motivation for later Chapters of this thesis, where methodologies are developed to specifically address the issue of the complexity of the transient stability problem.

The following literature review is carried out on the basis of a survey of recently published representative papers on the impact of WTG on transient stability.

3.1 Impact of Wind Generation on Transient Stability

The focus of this review is on variable speed wind turbine technology rather than fixed speed wind technology because all new wind generators are usually either DFIG or FRC (i.e., Type-3 or 4 in Figure 2.4), and older Squirrel Cage Induction Machine (SCIM) (Type-1) machines are being replaced by these newer variable speed machines.

The approach adopted in academia to assess the impact of increasing levels of wind generation on transient stability has been to either model wind generation being *added* to the system (Figure 3.1) or wind generation *displacing* conventional SG (Figure 3.2). The difference is that in the case of conventional SG displacement by wind generation,

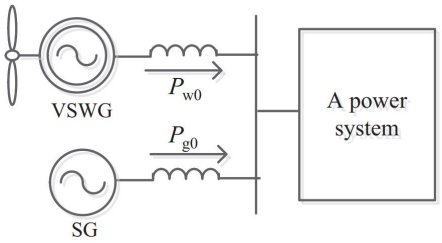

Figure 3.1: Wind Turbine Generators (WTG) connect to a power system resulting in changed power flows, but inertia and capabilities of Synchronous Generation (SG) unchanged [57].

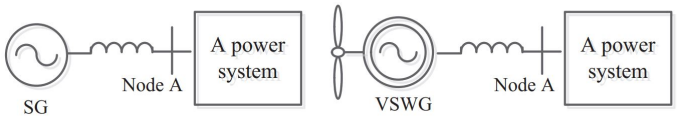

Figure 3.2: Wind Turbine Generators (WTG) displace conventional Synchronous Generation (SG), leading to a reduction in inertia and loss of SG capabilities. [57]

there is a reduction in system inertia, unlike when WTG is added to the system where system inertia is unchanged and none of the capabilities of SGs lost. The approach varies depending on the scenarios the authors are seeking to represent.

3.1.1 Impact of Adding Wind Generation

In [58], the impact of increased penetration of DFIG WFs on the transient stability of SG is examined using a SMIB network (Figure 3.3). Based on the power angle relationship, the transient stability of the system is analysed using both the EAC (Figure 2.8) and the CCT by treating pre- and post-fault WF as a constant power source and a negative impedance during a fault. The results show that the performance of SGs can either improve or deteriorate when DFIGs are added to the network. However, the paper also finds that transient stability deteriorates as more wind connects. The reliability of the EAC results are verified through TDS using GE_1.5MW_DFIG generators, producing similar findings.

Research to investigate the impact of adding SCIGs and DFIGs into the network in relatively low volumes and comparing the difference in behaviour on transient stability of the system was conducted a few years ago. For example, in [59] the authors illustrate

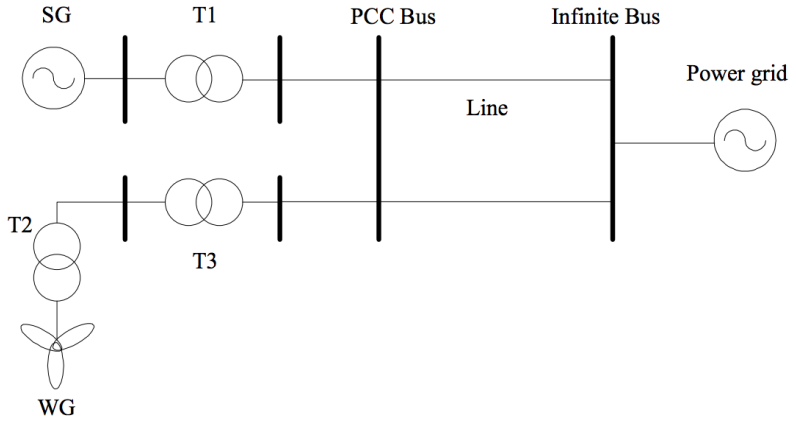

Figure 3.3: Single-Machine Infinite-bus (SMIB) network with connection of a Wind Farm (WF) [58]

that a DFIG and a four-quadrant ac-to-ac converter connected to the rotor windings can improve the overall transient stability performance, over cage rotor induction generator (fixed speed wind systems), due to its reduced reactive power demand during LVRT operation (see Section 2.1.2). The work highlights the poor transient stability performance of squirrel cage generators, with transient stability worsening with an increase in these generators electrically far from the SGs. Conversely, it was shown that the DFIG improves transient stability. This is attributed to the ability of the DFIG to maintain torque equilibrium during disturbances.

A study by Slootweg and Kling [51] concluded that transient stability depends on penetration level and Distributed Generator (DG) technology. In this paper, the impact of DG technology and penetration level on the dynamics of a test system is investigated by increasing system load and covering the load increase with different generation technologies. Technologies included the SCIG, uncontrolled SG, SG with grid voltage and frequency control, uncontrolled PEC and PEC with grid voltage and frequency control. The study finds that power system transient stability depends both on the penetration level and the technology of the DG. What is more, the authors state that "it can be concluded that it is difficult to derive an overall conclusion with respect to the impact of distributed generation technology and penetration level on power system stability, because the results are quite mixed".

In [60], transient stability simulations were conducted for three wind scenarios (Fixed Speed Induction Generator (FSIG) installed at Low Voltage (LV) side, FSIG windfarms installed at High Voltage (HV) and LV, equal penetration of FSIG and DFIG) based on WF integration and wind generator technology. The HV level integration of FSIG WFs provides comparatively high stability over LV level integration due to strong voltage support in the HV system. The installation of DFIG-based WFs has also significantly improved system stability due to their reduced reactive power consumption. Although these factors have improved the stability at low wind penetration levels, system stability is significantly degraded at high penetration levels (50 %) due to the high reactive power absorption of wind generators under transient disturbances.

The impact of connecting a SG compared to DFIG in an area with lots of large motor demand is assessed in [61]. In this paper, the authors attempt to compare the impact, in terms of transient stability, of adding a conventional generator and a variable speed (DFIG) WF into a weak area of the grid. The effects of various farm load factors (100, 60 and 25 % of nameplate rating) are investigated compared to a 100 MW conventional SG interconnected at the same location. The paper advocates that the DFIG equipped with PEC and LVRT capability will have no adverse effect on the stability of a weak grid and that DFIGs provide a good damping performance.

The methodology used in [62] is to design a network where wind power is consumed close to the point where it is generated to avoid issues of frequency and angular stability. It is highlighted that the integration of wind will alter system power flows, transmission line loading, network voltages and system losses, and this influence could be different according to the power system topology and generator distribution across the network. The paper suggests that WFs should be "relatively dispersed" throughout the network, and wind generation should be consumed at the point of generation where possible, to avoid having any significant impact on network power flows.

A hybrid system is examined in [63], where the transmission system is modelled with a significant penetration level of radial distribution feeders connected to a collection of small WFs. The control strategies at the distribution farms are varied and the impact of the reactive power control strategy employed by WF is observed. It aimed

to illustrate that the additional impedance of the distribution system will have unintended consequences on the transmission system and the application of voltage control is less critical. The paper finds that distributed wind can help transient stability for a transmission fault.

Meegahpola et al. find that network regions with high penetration of wind and SG are detrimental to transient stability, whilst when wind or SG is dominant, stability is improved [64]. This study examined the large disturbance stability issues in power networks with geographically distributed wind resources in the context of a number of dispatch scenarios based on profiles of historical wind generation for a real power network. The results of the study show that localised stability issues worsen when significant penetration of both conventional and wind generation is present. In contrast, network stability improves when either high penetration of wind and SG is present in the network. As a result of this, the authors suggest that network regions can be clustered into two distinct stability groups (superior and inferior stability regions). Moreover, it is highlighted that network stability improves when a voltage control strategy is implemented at WFs, however, both stability clusters remain unchanged irrespective of change in the control strategy. Finally, the authors highlight that an enhanced LVRT strategy for WFs can improve both voltage and transient stability locally, but only a marginal improvement is evident in neighbouring regions—highlighting a locational nature to the transient stability problem in the context of increasing RES output.

3.1.2 Impact of Wind Generation Displacing Synchronous Generation

Reference [65] studies the impacts of both FSIG and DFIG wind turbines on power system transient stability based on Extended Equal Area Criterion (EEAC). The study groups SGs into either a "critical cluster" (the SGs that accelerate away from the other units) or a "remaining cluster" and SGs in each of the clusters are replaced by either FSIG or DFIG wind turbines of equivalent capacity and static output. Transient stability is found to either improve or deteriorate regardless of which cluster wind replaces SG. What is more, transient stability varies depending on what SG is replaced, the wind technology, the fault location and fault clearing time. Based on the EEAC,

authors attribute changes to transient stability to electrical output power and the inertia of either cluster.

Authors in [66] used the Western Electricity Coordinating Council (WECC) 3-generator 9-bus test system and replaced different SGs independently with DFIG WFs of the same capacity and static output. The simulation results show that when a conventional SG is replaced with DFIGs, the stability of the network can be found to either improve or deteriorate depending on the location of the fault.

Gautam et al. in [67] and Elkington et al. in [68] indicate that transient stability can be either improved or reduced when some conventional SGs are replaced with DFIGs of the same capacity. As previously mentioned, in [67] authors develop an approach to analyse the impact of increased penetration of DFIG based wind turbines on transient and small signal stability of a large power system. Eigenvalue analysis is conducted to evaluate their sensitivity with respect to inertia and using the concept of participation factors, specific modes can be excited in time domain. The results obtained indicate that the proposed method effectively identifies both detrimental and beneficial impacts of increased DFIG penetration both for transient stability and small signal stability related performance by a change in inertia.

In [69], authors present a comparison of transient stability characteristics of DFIG WFs and conventional SG with the same capacity. The study uses a simple test network and conventional SG is replaced by DFIG wind turbines operating at 1.00 power factor (i.e., reactive power transfer is zero). The study indicates that, for the system studied, when the scale of WF connected is below 12.3 %, the transient stability is better than SG integrated with the identical capacity. When the capacity of the WF increases beyond this, the fault CCT is shorter. When the scale of WF exceeds 12.3 %, the terminal voltage of PCC is below 0.95 p.u., meaning that the grid is weaker. Unsurprisingly, this leads to a reduction in the transient stability of the network.

Studies have also assessed the impact that different wind technologies will have on stability. One such example is presented in [70] where it is revealed that the location and technology of wind generation have an impact on transient stability in the New Zealand power system. The paper demonstrates how wind generation using FSIG technology

tends to reduce power system transient stability, whilst DFIG or FRC technologies had a minor effect on power system performance in the cases studied. The paper highlights that transient stability must be considered on a case-by-case basis and that the displacement of conventional SG by wind generation may have a different impact on the stability boundary depending on the location of the disturbance.

The majority of wind generators connected to today's power systems are either DFIG or FRC wind turbines, and so more recent research has focused on the impact that these technologies have on transient stability. Authors in [71], investigate the impact on transient (and frequency) stability for a power system at high wind penetration, which was classed as 40 % in the study. Wind penetration is based on the DFIG, and a systematic approach was used for wind power integration. Four scenarios were formulated: (i) base case with all generation is SG, (ii) 40 % wind power penetration with an increase in local load to absorb wind generation without changing SG loading and network power flows, (iii) 40 % wind power penetration with synchronous generation output reduced by 40 % whilst keeping all SG online, and (iv) 40 % wind power penetration, while 40 % of the synchronous generation was kept offline. In scenarios (iii) and (iv), the steady-state rotor angles are affected by wind integration, since branch flows and steady-state bus voltages in the network will change. Various fault locations were studied for the stability analysis, based on the proximity to SG and WFs. It is found that stability is significantly improved for scenarios (iii) and (iv) for faults close to the terminals of SGs. This is because their steady-state rotor angles are improved compared to other cases and a significant proportion of branch flows come from wind generation, and hence the fault power contribution from SG is reduced. The analysis also highlights that transient stability is adversely affected when faults are initiated close to areas with high wind penetration, due to the significant reduction in active power generation and high reactive power absorption during crowbar operation. However, this may be largely alleviated when wind generators are partially loaded. Therefore, it is essential to avoid crowbar operation and deploy active LVRT strategies to improve transient stability performance.

A comprehensive study by Eping et al. [72] looked into a wide range of impacts

that increasing wind penetration may have on transient stability including the location of generation, generator technology, wind penetration and infeed voltage level. It was found that the location of wind generators can have a significant impact on transient stability, especially when wind resources are located in one particular area (leading to highly modified power flows). In addition to this the generator technology used was also found to have a significant impact on transient stability; with DFIGs improving stability margins when equipped with LVRT capabilities. Finally, the work finds that wind generation connecting to distribution networks has a negative impact on transient stability since the reactive contribution is highly limited due to the reactive power losses in the distribution networks. The paper concluded that there is no generalisation that can be made when it comes to the impact of wind generation on transient stability and that a wide range of factors influences transient stability which must be taken on a case-by-case basis.

Work conducted in [25], demonstrates the impact of displacement of conventional SG by WTG in the context of the power system of GB using a simplified network model. The work highlights that the replacement of conventional SG in an exporting area of the network by DFIG wind power plants acts to erode transient stability margins for faults on a critical corridor within the GB transmission system. However, when the newly introduced wind power plants consist of FRC wind turbines, these stability margins may be increased, depending on the penetration level. The work highlights the complex relationship between the location, penetration level, turbine type and voltage control method and the effect on transient stability margins in the power system.

The locational aspect of wind generation on transient stability is taken one step further in [73], where it is shown that the effect of displacement on power system transient stability is beneficial if the displacement makes the system more "symmetrical" and vice versa, which is related with the steady-state load flow conditions and distribution of inertia of SGs in the power system. The analysis summarises that applying the theory of the continuum model indicates that the effect of reduced inertia due to the wind displacing SGs is different as the locations of displacement change.

The importance of the control techniques adopted by wind generation has been

highlighted in many recent research efforts. One such example focuses on the operational mode of variable speed wind turbines that could enhance the transient stability of the nearby conventional SGs [74]. In this work, constant power factor operation, voltage control mode operation and transient stability enhancement mode of FRC wind turbines are analysed in the context of the Nordic network. It is found that if WFs operate in the constant power factor mode during network faults, the transient stability of the nearby grid is deteriorated compared to the case with no wind generation in that location. By incorporating the mode of operation in the control of several planned WFs in the Nordic grid, the transient stability of the nearby grid can be recovered or increased. It is concluded that care has to be taken when selecting the control mode of a WF in different scenarios when it is located close to a conventional SG (it was found that transient stability deteriorated when the WFs were sited closer to conventional SG).

Work done by the Eirgrid Group in Ireland [75] highlights the impact of some potential mitigation methods on transient stability for a number of faults on their network. Results demonstrate the importance of the reactive current capability of a generator during and after the fault for transient stability. The study found the most effective mitigation measure for transient stability issues to be voltage support by WFs according to current (2009) grid code requirements (maximisation of reactive current up to generator ratings while providing active power in proportion to retained voltage during faults).

In [63] authors suggest that when active power flows change minimally, the manner in which wind provides reactive power support is critical in maintaining rotor angle stability. It is shown that the rotor angle of SGs is directly influenced by the reactive power control strategy employed by the wind generation. It is concluded that the implementation of terminal voltage control helps mitigate large rotor angle swings and assists conventional SG in damping oscillatory signal following a loss of generation event, in line with [75]. The work suggests that this is primarily because of the reduction in reactive power requirements from conventional SGs. Ultimately, it highlights that by utilising the built-in capabilities of wind generation to provide the SG with reactive

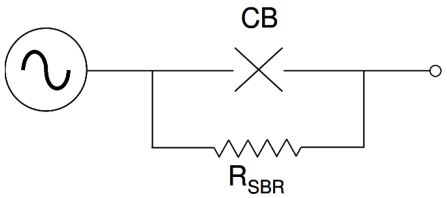

Figure 3.4: Series braking resistor configuration [77]

power support, the onus on SG can be eased and the stability margin improved. The paper warns that the displacement of conventional SG will have consequences beyond the loss of inertia and synchronising and damping torque, suggesting that the loss of AVRs, dynamic VAR support, and governor action will significantly impact stability.

The above papers highlight just some of the mechanisms that increasing CIG can impact transient stability. A key finding, and a primary motivation for the work conducted in this thesis, is the large number of variables and parameters that can impact the transient stability boundary.

3.1.3 Potential Transient Stability Enhancement Solutions

Edrah et al. highlight that replacing a large proportion of SGs with DFIGs can have a negative impact on stability, but control techniques can be used to improve it [76]. More specifically, the paper investigates the impact of DFIG control and operation on rotor angle stability, using a control strategy for both the Rotor-Side Converter (RSC) and Grid-Side Converter (GSC) of the DFIG. The DFIG-GSC is utilised to be controlled as Static Synchronous Compensator (STATCOM) to provide reactive power support during grid faults. This was found to be a cost-effective solution for maintaining local voltages at WFs without an external STATCOM. In addition to this, a PSS is implemented in the reactive power control loop of DFIG-RSC. This can influence the rotor angle of SG and thus dampens the power system oscillations effectively. What is more, as wind penetration increases, the benefit of such a control scheme is that the DFIG WFs are able to take over the SGs responsibility to support power system stability.

In [77], authors present simulation results that demonstrate the use of a Series Braking Resistor (SBR) to improve the transient stability of low inertia power systems. The basic primary system configuration for a SBR is shown in Figure 3.4 below where the device is effectively switched into a circuit between the SG terminals and the network by opening the circuit breaker. By opening the circuit breaker and bringing the SBR into the circuit during a fault, the SG is able to export more active power than before (without a SBR), resulting in a smaller acceleration of the rotor thus improving its angular stability (as per Equation 2.4). Note that LVRT has a similar impact on SG angular stability since active power output drops to zero during the fault, meaning that the SG can export more power (depending on the location of the SG and the wind generator).

Using a GB representative reduced test network, authors in [78] investigate the impact of altering the immediate post-fault active power recovery ramp-rate of WFs. The studies show that the replacement of conventional SG with DFIG wind power plants can act to erode or improve transient stability margins for faults on a critical corridor within the GB transmission system, depending on the location of the wind power plant. Further, it has been shown that the utilisation of reduced post-fault active power ramp rates from the wind turbines in the exporting area can provide a significant improvement in the transient stability margins. This highlights how RES controller parameter settings can significantly impact transient stability.

3.2 Conclusion

The transient stability problem is highly non-linear and multidimensional, which is exacerbated by the loss of SG attributes and the addition of complex highly non-linear dynamics associated with RES. This significantly increased complexity makes the transient stability problem more non-linear and thus difficult to understand.

This Chapter presents a review of the literature relating to the impact of CIG on transient stability, addressing research question 1. The literature shows how the different dynamic characteristics of CIG compared to conventional SG alters the dynamic

Influencing Factor		Reference(s)
Generation & Demand	Penetration Level	[79], [58], [80], [81], [82], [51], [60], [64], [69], [71], [72], [25], [83].
	Inertia Level	[65], [68], [84], [67], [59], [71].
	Demand Level	[67], [85].
	Dynamic Importance of SG	[57], [65], [66], [86], [87].
	Wind Technology	[82], [51], [60], [65], [70], [72], [25], [88].
Grid Configuration	Generator Locational Aspects	[57], [66], [86], [67], [89], [60], [62], [90], [64], [70], [71], [72], [25], [73], [74].
	Changes to Power Flows	[62], [71], [72], [85], [91].
	System Strength	[61], [69].
	Transmission Line Length	[90], [92].
Wind Operation	Mode of Operation	[74], [75], [79], [80], [89], [90], [91].
	LVRT Capabilities	[61], [64], [71], [72], [75].
Faults	Fault Location	[65], [66], [70], [71].
	Fault Clearing Time	[65].
	Fault Type	[65].
Control	Advanced Control Strategies	[93].

Table 3.1: Factors found to impact the transient stability boundary from existing academic literature.

response of power systems to faults in complex ways. More specifically, the literature review highlighted that there are a large number of factors that influence and shape the transient stability boundary, as summarised in Table 3.1. Over and over again, studies highlight that transient stability may improve in some cases and deteriorate in others. This discrepancy forms the motivation for later Chapters, where new TSA tools are developed to capture and understand these changes.

Similar studies and analysis (conducted as part of this PhD using a SMIB) are included as supplementary material in Appendix A. These studies seek to investigate the mechanisms that are impacted as a result of the complexities introduced by RES dynamics. In particular, the impact of displacement of SG by RES, wind control parameters, WF location with respect to SG and RES loading is assessed.

A reoccurring drawback with many academic studies is that the conclusions are

very specific to the operational scenarios considered and/or network used. This is a limitation in making more general conclusions about the impact of RES on the transient stability boundary since results for certain operational scenarios on a specific network are unlikely to transfer onto other systems directly. For example, many studies seek to assess the impact of a single parameter on transient stability to assess the impact on the stability boundary. However, in reality, many of these parameters will change simultaneously—making identifying their impact on transient stability an even more complicated task. In addition, papers often use simplified network models and case studies to reduce the complexity of the problem. This allows for a detailed analysis of the impact that RES has on transient stability and the mechanisms at play—without the additional complexity of a more complex multi-machine network.

Although such approaches can highlight general trends specific to the case studies and network used, the dynamic behaviour is likely to differ in larger networks. This limits the usefulness of these studies in other power systems, as findings may not be transferable between different systems. This limitation means that authors cannot provide specific planning and operational suggestions that can be generalised relating to how best to integrate CIG whilst ensuring a sufficiently large transient stability margin.

This makes the development of rules and recommendations from such studies difficult and any that are successfully developed are likely to be inappropriate—limiting the use of such studies outwith academia. Therefore, the development of methodological-based approaches that can be implemented to analyse the dynamics of any system and reach conclusions is favourable over the case-study-based approaches that were presented in this Chapter. Such methods should be able to reduce the complexity of the problem, by reducing the problem dimensions to only the most influential. In doing so, trends in the transient stability boundary can be identified and stability enhancement measures developed. This is a key motivation for the research presented in later Chapters of this thesis, where the remaining research questions are addressed. A literature review of techniques used (namely ML and indeed IML) is provided for the reader in Chapter 5.

Chapter 4

Investigation into Spatial and Temporal Aspects of Transient Stability

4.1 Introduction

This Chapter investigates the impact of generator dispatch (dictated by cost via economic dispatch) and locational aspects related to RES connection and consequent disconnection of SG on the transient stability margin. The impact of generator cost on transient stability is clear (indeed, this forms the basis of Transient Stability Constrained Optimal Power Flow (TSC-OPF)); however, the combined impact of economic dispatch and location of RES with respect to SG has not previously been studied. Particular focus is given to the impact of the LVRT behaviour of RES on nearby SG, and the loading of that SG.

The link between generator cost and dispatch (i.e., loading) is well-known and is based on fundamental economic principles. Moreover, it is widely acknowledged that SG loading significantly impacts that generator's susceptibility to losing synchronism following a transient event [30]. There is, therefore, a link between generator cost and transient stability, motivating studies whereby transient stability is included as a

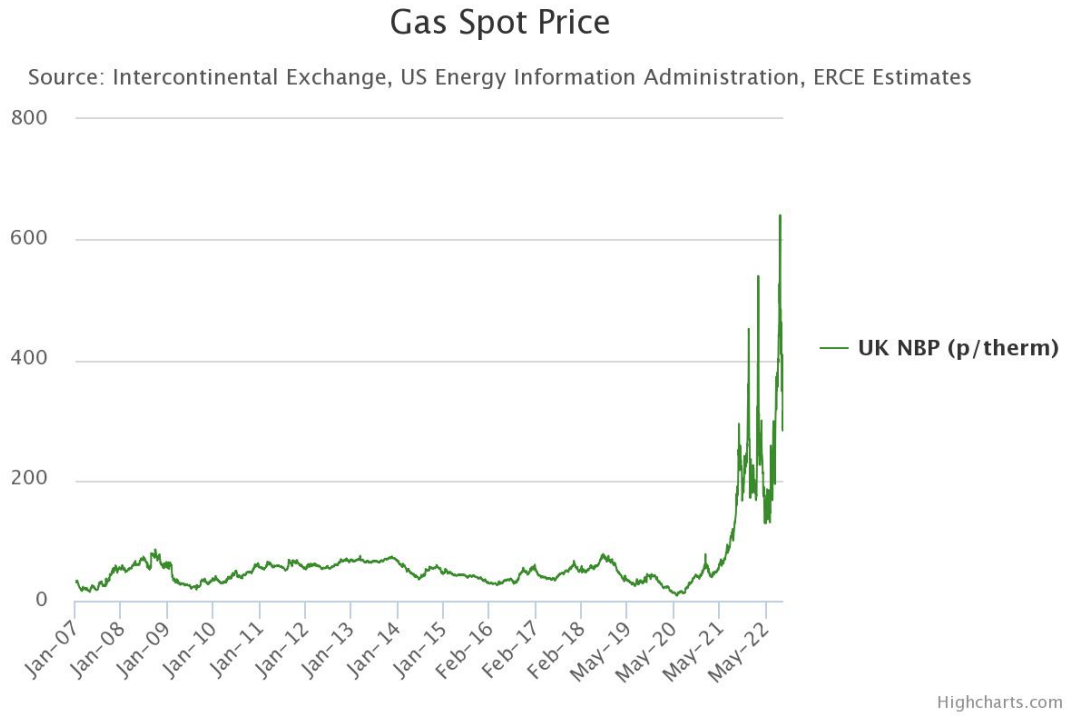

Figure 4.1: United Kingdom (UK) natural gas National Balancing Point (National Balancing Point (NBP)) spot price (p/therm) [96].

constraint in the Optimal Power Flow (OPF). For example, [94] highlights the conflict between transient stability and the economic objective and proposes a risk-averse multi-objective generation dispatch model to balance this. In [95], transient stability is included in the economic dispatch problem, minimising the risk of transient instability. What is more, recent unprecedented European gas price volatility [5] may lead to significant changes to the merit order of generation, resulting in unusual generator dispatches (e.g., higher output from coal generation and lower output from gas mixed with intermittent wind, as observed in Germany in 2022 [4]). In the United Kingdom (UK), the Gas Spot Price has climbed significantly since March 2021 and 2022 (Figure 4.1). Trends like these may test 'operational expertise' and potentially lead to blind spots without detailed and frequent TSA.

Numerous studies (some of which are summarised in Chapter 3) suggest that as SG is displaced by RES, there is a significant impact on transient stability in power systems. It can be hard to predict to what extent different parameters influence the stability

boundary—be it an improvement or deterioration [26,67]—due to the complexity of the dynamic behaviour of power systems. The uncertain nature of renewable generation means that the pre-disturbance operating conditions and the number of connected SGs tend to vary more, reshaping the stability boundary in operational time [97]. For example, the authors in [51] find that the volume of RES connected is an important factor in determining the transient stability of the network. Qi et al. find that the influence of uncertainties in RES become influential when penetration exceeds 30 % [98].

Locational aspects have been explored in various papers. For example, in [99], authors propose a voltage sensitivity-based index to identify network locations where the connection of RES would have a beneficial and detrimental impact on transient stability. [100] demonstrates how the SG that is displaced and the fault location are crucial in shaping the stability boundary. Locational aspects are further considered in [73], where it is found that "symmetrical" displacement of SG by RES (i.e., evenly distributed throughout the network) has a beneficial impact on transient stability. Fault location with respect to RES location is considered in [87], where transient stability is found to either improve or deteriorate based on the proximity of the fault to RES. However, no effort is made to quantify what is meant by "near", or "far". Findings are supported by [101], where it is concluded that stability depends on the relative position of the RES (in this case, energy storage) with respect to both the fault and SG. What is more, the post-fault active power recovery rate of RES is also found to have a significant impact on the stability boundary in [78], depending on whether RES is located in an exporting or importing network area. This is further analysed in more general terms in [102].

This Chapter presents initial results considering the impact on transient stability from the displacement of SG (with different costs) by RES in different network locations (i.e., disconnection in high vs low-cost areas). An AC-OPF is used to determine the dispatch of generators on a IEEE 9-bus test network, and transient stability is assessed using RMS-TDS to determine the stability margin at each busbar in the network for each operational scenario (i.e., a particular realisation of demand, wholesale electricity markets preference for generation dispatch, and a network state). This locational

approach in calculating the stability margin provides an understanding of the entire stability boundary and enables the identification of changes in the critical fault.

These initial studies aim at identifying patterns arising from the combined impact of varying fault location, volume and location of SG, RES penetration and RES location on transient stability within the context of economic dispatch. Furthermore, locational parameters relating to changes in transient stability are quantified using the network admittance matrix, the electrical distance ratio (EDR—a metric defined in this Chapter to capture the combined effect of SG disconnection and the electrical distance between a SG and a RES unit) and short-circuit capacity. Special attention is given to the identification of cases when there is a change in critical area (i.e., area with the lowest CCT and consequent switch in the CSG) due to the aforementioned variation of parameters related to generator cost and locational aspects under increasing penetrations of RES.

Locational trends in the stability boundary are uncovered, stemming from the loss of attributes associated with SG and dynamic characteristics of RES. The transient stability of SGs in close electrical proximity to RES is observed to improve, whilst the stability of SGs electrically further from RES decreases. Depending on the cost of the SG that is displaced, this may improve the duration of the critical fault (i.e., for the CCT to increase) and, in some instances, can cause the critical fault to shift location. This is an important observation and highlights how significant changes to the stability boundary can occur in operational timescales—highlighting the need for detailed and frequent TSA.

Whilst the results presented may be network-specific, this Chapter presents a systematic way to investigate the impact of generator cost and locational aspects related to RES on the transient stability of a power system. Moreover, the methodology developed and the metrics used can be applied to any network to extract results and draw conclusions.

4.1.1 Contribution

The methodology and results presented in this Chapter were published in Elsevier International Journal of Electrical Power and Energy Systems [J1]. The key contributions

from this Chapter are as follows:

- Systematic identification of the combined impact of economic dispatch (i.e., generator cost) and location of RES in the context of power systems with increasing penetrations of RES on transient stability using detailed RMS models and TDS.
- Quantifying locational aspects relating to the impact of RES location on transient stability, which is missing in the existing literature. This is achieved by defining a new metric, the EDR. This is defined as the ratio between the transient reactance of a SG and the electrical impedance from the SG terminals to RES.

4.2 Methodology

Studies are performed using a small but detailed RMS power system model. The primary aim is to identify key parameters that impact transient stability in power systems with increasing penetrations of RES in different areas of the network (high vs low cost). Generator dispatch is established using an AC-OPF, with simple linear cost curves (with high, medium or low incremental cost) that are swapped between the machines systematically to determine different generator dispatches (effectively changing the merit order). These changes to generator dispatch will, in turn, impact transient stability. The impact on the stability boundary of generator cost is discussed in Section 4.3.1, locational aspects in Section 4.3.2 and the sensitivity of SGs to changes in active power output in Section 4.3.3. An overview of the methodology is outlined in Figure 4.2 and the remainder of this Chapter details the methodology used to obtain results.

4.2.1 IEEE 9-Bus Test Network Overview

This Chapter uses a modified version of the IEEE (Anderson-Fouad) 9-bus model (Figure 4.3) implemented in DIgSILENT PowerFactory [43]. The network nominal voltage is 230 kV, and the nominal frequency is 60 Hz. The total active power demand of the network is 315 MW, modelled as balanced three-phase constant impedance loads in the dynamic simulation.

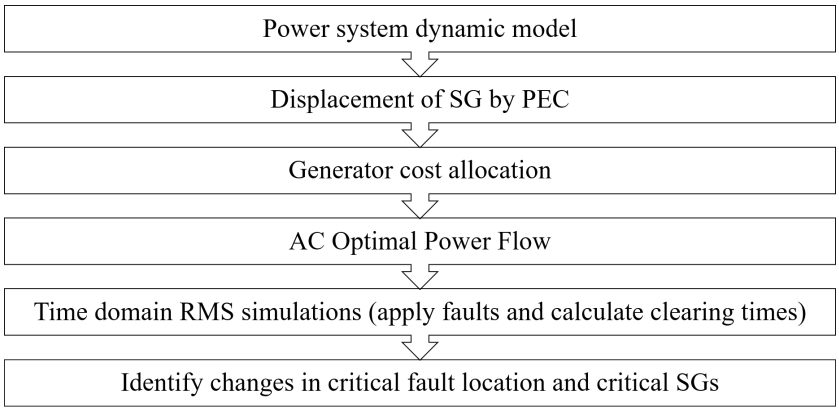

Figure 4.2: Procedure used to generate credible operational scenarios and assess network stability.

There are three SGs in the network, represented by full detail four winding models (6^{th} order). SG2 and SG3 are assumed to represent four equal-sized units (to simplify SG displacement in Section 4.2.2). Additional details regarding the parameters of the network and machines can be found in [43]. The reference machine is SG1 which is rated at 247.5 MVA with an inertia constant of 9.55 sec. SG2 is a 192 MVA machine with an inertia constant of 3.92 sec (representing four 48 MVA machines), equipped with an IEEE DC1C AVR and a PSS. SG3 is the smallest machine on the network at 128 MVA with an inertia constant of 2.77 sec (representing four 32 MVA machines). All generators have an operating region from 0.35 to 1 p.u. active power loading and -0.25 to 0.5 p.u. reactive power loading. No protection devices are modelled.

IEC Type-4A wind turbines [103] are used to model wind generation in these studies. Note that Type-4A neglects the aerodynamic and mechanical parts and therefore does not simulate any power oscillations, however, the Type-4B model includes a 2-mass mechanical model to replicate the power oscillations by assuming constant aerodynamic torque [104]. Using the assumption that RES is not required by grid code to provide voltage control, the controller operates at unity power factor (i.e., no MVAr are injected into the system [91]). It should be noted that this capability may vary from system to system and will impact reactive power dispatch and therefore transient stability. However, the investigation of this capability remains out of the scope of this Chapter (and indeed thesis) so is left for future work, with analysis here focusing primarily on

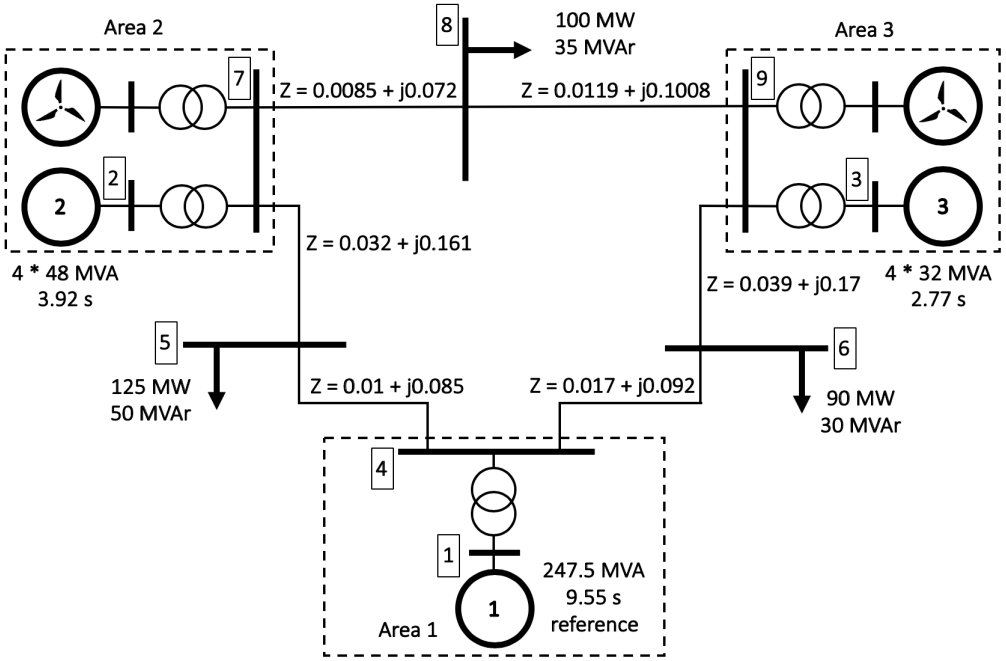

Figure 4.3: Adapted version of the IEEE 9-bus test network with International Electrotechnical Commission (IEC) Type-4A wind turbines connected in different areas.

active power dispatch changes due to different generator costs. The WTGs used has LVRT capability and reactive power support. Reactive power injection is controlled as the pre-fault value plus an additional voltage-dependent reactive current injection during the fault, and as the pre-fault value plus an additional constant reactive current injection post-fault. A WF is treated as an aggregate of individual 1 MW turbines, each with its own transformer, where the total output of the WF is the summation of each individual WTGs active power output. The volume of wind and its location on the network depends on the particular displacement scenario, defined in Section 4.2.2 below.

To simplify the analysis of the network, three generating areas have been defined and are referred to as areas 1, 2 and 3 throughout this Chapter. The three load busbars are not part of any area in particular so are referred to by their bus number.

Network Area	1	2	3
Original Load Flow (MW)	71.6	163.0	85.0

Table 4.1: IEEE 9-bus test network active power dispatch from original load flow solution [43].

Case	Dispalcement Case	Area 1	Area 2		Area 3	
		SG1	SG2	RES2	SG3	RES3
Base	0 %	247.5	192.0	0.0	128.0	0.0
1	25 % A2	247.5	144.0	40.0	128.0	0.0
2	50 % A2	247.5	96.0	81.0	128.0	0.0
3	75 % A2	247.5	48.0	122.0	128.0	0.0
4	25 % A3	247.5	192.0	0.0	96.0	21.0
5	50 % A3	247.5	192.0	0.0	64.0	42.0
6	75 % A3	247.5	192.0	0.0	32.0	63.0

Table 4.2: Displacement cases used in studies showing Synchronous Generator (SG) machine rating (MVA) and volume of wind generation (MVA).

4.2.2 Operational Scenarios

To simplify the studies RES connecting in one area of the network displaces the SG in the same area, and displacement only occurs in one area at a time. No displacement in area 1 is studied because SG1 is the reference machine with the largest rating and inertia. As a starting point when defining the scenarios explained in detail below, the volume of RES connecting in areas 2 and 3 is based on the active power export from each area from the original load flow solution, with no wind generation (Table 4.1).

The seven displacement scenarios are defined by a displacement percentage and displacement area and outlined in Table 4.2. For example; case 1 illustrates 25 % displacement of SG by wind in area 2. This means 25 % penetration of wind generation from the original load flow solution (25 % of 163 MVA, equating to 40 MVA when rounded down to the nearest MVA) and the disconnection of 25 % of SG2 (one of the four 48 MVA units which it represents, leaving three units connected with a combined rating of 144 MVA). The active and reactive power operating points of all SGs are obtained from the OPF solution. The base case has no displacement in any area.

4.2.3 Generator Dispatch via AC Optimal Power Flow

An AC-OPF [105] is used to determine the dispatch of the SGs on the test network using the inbuilt AC-OPF solver in DIgSILENT PowerFactory. Whilst real market operations might lead to different generator dispatches, in this Chapter it is assumed that the OPF solution is a reasonable representation to generate credible generator dispatches.

AC Optimal Power Flow

The objective function for an AC-OPF [106] is to find a steady state operating point that minimises the cost of generation while satisfying operating constraints and meeting demand, described mathematically:

$$f(x) = min \sum_{i=1}^{i} C_i(P_{gi}) \tag{4.1}$$

$$g(x) = 0 \tag{4.2}$$

$$h(x) \leq 0 \tag{4.3}$$

$$x_{min} \leq x \leq x_{max} \tag{4.4}$$

where Equation 4.1 is the objective function, Equation 4.2 define the equality constraints (e.g., power balance and power flow constraints), Equation 4.3 model the inequality constraints (e.g., apparent power line ratings) and Equation 4.4 model the bounds on state and control variables (e.g., min/max generation). Each generator is subjected to the standard polynomial cost function:

$$Cost(\$/hr) = c_0 + c_1 P_e + c_2 P_e^2 \tag{4.5}$$

where P_e is the electrical power output and c_0, c_1 and c_2 are cost coefficient values. Locational Marginal Price (LMP) of electricity at a location (bus), λ_n, is defined as the least cost to service the next increment of demand at that location. Diverging LMPs between busbars are indicative of active constraint(s), reflected in the associated

	HML	HLM	MHL	MLH	LHM	LMH
SG1	1.47	1.47	0.73	0.73	0.07	0.07
SG2	0.95	0.09	1.89	0.09	1.89	0.95
SG3	0.14	1.42	0.14	2.84	1.42	2.84

Table 4.3: Incremental cost of each Synchronous Generator (SG) for each cost allocation (£/MW).

Karush Kuhn Tucker Multipliers (KKTs). Since a KKT only becomes non-zero once a constraint is active, they can offer additional information about constraints [107].

Each generator on the network is allocated either a high (H), medium (M) or low (L) incremental cost to establish a merit order between the SGs. Each incremental cost (H, M or L) is only ever allocated to one generator at a time, meaning that there are six cost combinations for the three SGs. Wind has no fuel cost [108], and thus no associated cost in the OPF, so operates at 100 % of rated power when connected to the network. The exact dispatch of generation is determined by the OPF, with the objective of minimising cost (Equation 4.1) whilst respecting constraints—as detailed above. This results in RES operating at full active power output, cheaper SG running at a high active power loading, and the more expensive SG running at lower active power loading.

Generator cost allocations are referred to using a three-letter code, with the first letter referring to the cost of SG1, the second SG2 and the third for SG3. For example, an 'HML' cost code means that SG1 is the most expensive, followed by SG2 and SG3 is the cheapest. The incremental costs for each cost allocation are given Table 4.3. Incremental costs here are designed only to determine a credible dispatch of generation (i.e., the cost of the dispatch is not important for these studies). As a generator is displaced (as outlined in Section 4.2.2), the operating range (i.e., the minimum and maximum absolute active power limits (which corresponds to an operating range of 30 - 85 % of S_{rated})) of the SG reduces, however, the incremental cost stays the same.

The approach used in this Chapter on changing generator costs is to establish a wide range of possible operating scenarios that could be observed in different systems. For example, these systems may have different generation mixes in different locations due

to variations in generator availability or decommissioning of certain types of generation. Moreover, changes to the relative fuel cost of generators due to global market forces may also lead to significant changes in dispatches. However, this is likely to vary in relatively long timescales (i.e., weeks, months and years and not in operational timescales). For example, the impact of a low-cost SG being displaced by RES may result in different changes to the dynamic behaviour of the system than if a high or medium-cost SG is displaced.

4.2.4 Transient Stability and the Critical Clearing Time

For each displacement case (Table 4.2), a series of separate RMS-TDS (introduced in Chapter 2) are performed in DIgSILENT PowerFactory to determine the CCT for each case. The process for doing so is automated in Python using the process shown in Figure B.1 in Appendix B. This is repeated for each of the six possible cost combinations (Section 4.2.3), resulting in 42 different operational scenarios. Since IEC Type-4 wind models are used, the impact of the dynamic characteristics of wind generation—including the LVRT behaviour—impact the dynamic response of the network and so are captured in the CCT metric for each operational scenario.

As outlined in Chapter 2, in transient stability studies, CCT is frequently used as an indicator of the severity of a fault. For transmission system faults, the main protection may generally be expected to operate within 100 msec [53], so a CCT approaching this threshold can be considered critical. Conversely, CCTs greater than 500 msec are considered to be non-critical in this Chapter. CCT is therefore used in this Chapter as a metric for transient stability. Note that as Chapter 2 highlighted, determining the CCT for a fault is a computationally expensive iterative process.

Since the location of the fault with respect to each SG is important for transient stability, the CCT is determined at each bus on the network for each displacement scenario and cost allocation. This is a key aspect of the methodology that enables the identification of locational trends. This principle is used later in Chapter 6 and 7 of this thesis. To do so, a balanced three-phase-to-ground fault is applied at each bus on the network in turn, and the CCT is determined iteratively, increasing the fault duration

(as outlined in Section 2.5.2). After the fault is cleared, the network returns to the pre-fault network topology with no generators or lines tripping (i.e., three-phase self-clearing faults). In order to do so, the criteria for instability must first be defined—the details of which are defined in Section 2.5.2.

In terms of describing changes to the transient stability boundary between scenarios, the following stability terms are used; bus with the shortest CCT ($\mathrm{CCT}_{\mathrm{min}}$) for a particular operational scenario is referred to as the CFL, and the SG that experiences a LOS first for the critical fault is referred to as the CSG (formally defined in Section 2.5.2). The CCT for a particular bus fault may be abbreviated to $\mathrm{CCT}_{bus,no}$ (for example; CCT_6 denotes the CCT at bus 6).

4.2.5 Locational Aspects

To assess locational aspects; the pre-fault network admittance matrix (a measure of electrical distance between key network locations), electrical distance ratio (EDR, defined below), and short-circuit capacity (a measure of network strength) at different network locations are used. Important locational aspects include fault location, SG location, RES location and the location of displacement—all with respect to each other. Moreover, the location of the CSG with respect to the aforementioned aspects is likely to be important, since the CSG dictates $\mathrm{CCT}_{\mathrm{min}}$ (for example, the location of the CSG with respect to RES may be of interest).

Network Admittance Matrix

The admittance between busbars in a network can be obtained from the network admittance matrix [109], mathematically described for a network with n busbars as;

$$Y_{bus} = \begin{bmatrix} Y_{11} & Y_{12} & \cdots & Y_{1n} \\ Y_{21} & Y_{22} & \cdots & Y_{2n} \\ \vdots & \vdots & \ddots & \vdots \\ Y_{n1} & Y_{n2} & \cdots & Y_{nn} \end{bmatrix} \tag{4.6}$$

where Y is the n x n network admittance matrix. Diagonal elements (Y_{kk}) are determined by summing the admittances connected to that bus, whilst off-diagonal elements (Y_{kn}) are the inverse of the sum of admittances between the two buses in question.

The base case network 9 by 9 pre-fault admittance matrix is formed following the process described in [43], with appropriate values of transient reactance (x'_d) included. For cases 1 - 6, six separate 10 by 10 admittance matrices are formulated since varying volumes of RES are connected in different areas of the network. RES is connected to the network through transformers in parallel, resulting in an increased admittance between RES and the point of connection with the grid as RES penetration increases (and consequently the number of connected wind turbines). Since this Chapter is interested in the location of power system components (connected at different bus) with respect to each other, the electrical distance between said busbars is of interest (i.e., the non-diagonal elements of the admittance matrix).

Electrical Distance Ratio (EDR)

The relationship between SG transient reactance (x'_d), the impedance between RES and the network (impedance from RES terminals to the high-voltage side of the grid transformer), and the overall network impedance are important—since the impact on the net electrical distance between SG and RES is dependent on the magnitude of each parameter. These values can be derived from the network admittance matrix for different displacement scenarios. In this Chapter, the EDR is defined as the ratio between the transient reactance of a SG (x'_d), and the electrical impedance from the terminals of that same SG to the terminals of RES (denoted as x_{grid} in Equation 2, comprising of the impedance of the SG transformers ($x_{SG,trnf}$), RES transformers ($x_{PEC,trnf}$) and network impedance between the generators ($x_{network}$)).

$$EDR = \frac{x'_d}{x_{SG,trnf} + x_{PEC,trnf} + x_{network}} = \frac{x'_d}{x_{grid}} \tag{4.7}$$

The EDR therefore accounts for the changes to electrical distance between SGs and RES as a result of SG disconnection, providing a metric that describes the proximity of

RES to SG on the network. This is done through a comparison of the effective electrical distance between the transient reactance of SG (i.e., how large or small the rating of the SG is) with respect to the electrical distance from the SG terminals to the RES unit (including the network impedance). For example, an EDR below 1 indicates that the transient reactance of the SG is smaller than the impedance between the SG terminals and RES, whilst a EDR above 1 indicates that the transient reactance is larger. As a result, it is useful in highlighting the extent to which LVRT capability (related to the reduction in active power output and increase in reactive power) from RES can positively impact SG.

Short-Circuit Capacity

The short-circuit capacity is used here as a measure of system strength. Short-circuit calculations are performed according to IEC 60909 [110] in DIgSILENT PowerFactory for each displacement scenario, with RES disconnected from the network. The reason for this choice is to quantify only the effect of reducing synchronous generation, neglecting the dynamic behaviour of RES in this metric, which is considered in detail in RMS-TDS performed when calculating the CCTs. Therefore in these studies, this metric reduces with increasing penetrations of RES and consequent disconnection of SG.

4.3 Results

Three important factors that significantly impact the stability boundary are analysed in this Chapter. The first is generator cost (which ultimately dictates active power loading) with no displacement of SG by RES. The second is locational aspects that influence the stability boundary (interrogated through the network admittance matrix). Finally, the impact of SG sensitivity to changes in active power output (dependent upon generator incremental cost, SG MVA-rating, RES penetration, and demand level). This Chapter presents several case studies to highlight the impact of these factors and subsequent changes to the shape of the stability boundary. These factors should not

Cost Allocation	CCT_{min} (msec)	CFL (bus)	CSG (SG no.)	SG1	SG2	SG3
				Active power loading (%)		
LMH	540	1	SG1	100	43	35
LHM	420	3	SG3	100	35	46
MLH	210	2	SG2	56	100	35
HLM	210	2	SG2	38	100	71
MHL	170	3	SG3	72	35	100
HML	170	3	SG3	35	83	100

Table 4.4: CCT_{min}, CFL, CSG and % of maximum Synchronous Generator (SG) active power loading in the base case for all cost allocations.

be considered in isolation as numerous factors impact the transient stability boundary in complex and non-linear ways. As such, it is often difficult to decouple the impact of each factor on the transient stability boundary—a challenge addressed in later Chapters of this thesis.

4.3.1 Impact of Generator Cost and Non-Operational Parameters

It is widely known that generator cost (i.e., active power loading of SG) impacts transient stability—with highly-priced generators operating far from the stability boundary and cheaper generators operating much closer to it [30]. In addition, non-operational parameters (such as SG MVA-rating and inertia) also play an important role. The objective of this Chapter is to (a) illustrate how the marginal costs determine generator dispatch, (b) illustrate the extent of the impact that generator cost can have on transient stability and (c) highlight the impact that the aforementioned non-operational parameters have on transient stability in the network used.

In Table 4.4, the base case for all cost allocations are compared (i.e., there is no displacement of SG by RES, and since the size of each SG remains the same, total system inertia remains constant). The only parameter changed is the generator cost which primarily alters the active power dispatch of SGs. It should be noted that reactive power flow changes also occur, affecting system stability.

The active power loading of SGs (Table 4.4), shows how each cost allocation establishes a clear merit order between SGs using the incremental costs outlined in Chapter

4.2.3, resulting in the lower priced SGs having higher active power loading. Consequently, CCT_{min} varies significantly from a minimum 170 msec to a maximum of 540 msec. More importantly, the CSG and CFL changes between different cost allocations—highlighting the significance of generator cost in the transient stability problem.

Apart from the impact of generator cost, the impact of SG non-operational parameters (i.e., MVA-rating and inertia) are also observed in Table 4.4. In general terms, CCT_{min} can be seen to reduce with the MVA-rating and inertia of the generator with the low-cost. The longest times are observed when SG1 is the low-cost generator (which has the largest MVA-rating and inertia) and the shortest when SG3 is the low-cost generator (smallest MVA-rating and inertia). What is more, the large MVA-rating and inertia of SG1 compared to the other SGs means that even when SG1 is the low-cost SG (with 100 % active power loading), SG3 (medium-cost) is the CSG in the LHM cost allocation. This is because a machine with smaller inertia requires less energy (and so less time) to advance the rotor angle beyond the stability limit, highlighting that transient stability also depends on the aforementioned non-operational parameters.

The results that follow illustrate how locational aspects and generator sensitivity to active power loading (determined by cost) in the context of displacement of SG by RES impact stability from the base case presented above.

4.3.2 Impact of Locational Aspects with an Increased Penetration of Wind Generation

As the displacement of SG by RES increases, there is a distinct impact on transient stability depending on the location of the RES with respect to SG. In general terms, the displacement of a SG by RES in the same area has a beneficial impact on the stability of that SG (reflected by an increase in CCTs for faults where that SG is the first to go unstable). Contrarily, the stability of more distant SGs deteriorate (reflected in a decrease in CCTs for faults where that SG is the first to go unstable). It is highlighted below that in certain scenarios, this locational improvement or deterioration in the stability boundary can result in a switch in the CFL and CSG. These reasons for an improvement or deterioration in the stability of SG between displacement cases can be

analysed using locational parameters defined in Section 4.2.5. These include admittance between various network locations (Table 4.5), the EDR (Table 4.6), and short circuit capacity (Table 4.7).

from	SG2				SG3				RES	
to	bus 2	bus 5	bus 6	bus 8	bus 3	bus 5	bus 6	bus 8	bus 2	bus 3
Base	5.5	3.3	2.8	4.1	4.2	2.4	2.7	3.1	-	-
1	4.5	2.9	2.5	3.5	4.2	2.4	2.7	3.1	16.7	2.3
2	3.3	2.3	2.1	2.7	4.2	2.4	2.7	3.1	33.8	2.5
3	1.8	1.5	1.4	1.6	4.2	2.4	2.7	3.1	50.7	2.6
4	5.5	3.3	2.8	4.1	3.3	2.1	2.3	2.6	2.4	8.8
5	5.5	3.3	2.8	4.1	2.4	1.7	1.8	2.0	2.7	17.5
6	5.5	3.3	2.8	4.1	1.3	1.0	1.1	1.1	2.9	26.2

Table 4.5: Admittance (in p.u.) from the generation source to given network locations in each displacement case.

Case	SG2 x'_d / x_{grid}	SG3 x'_d / x_{grid}
Base	-	-
1	1.30	0.73
2	2.60	0.83
3	5.83	0.87
4	0.39	1.41
5	0.48	3.13
6	0.52	7.50

Table 4.6: Electrical Distance Ratio (Electrical Distance Ratio EDR) for SG2 and SG3 in each displacement case.

Case	bus 2	bus 3	bus 5	bus 6	bus 8
base	1379.78	1080.44	879.38	837.3	933.26
1	-17 %	-1 %	-3 %	-1 %	-5 %
2	-35 %	-4 %	-7 %	-4 %	-12 %
3	-52 %	-7 %	-13 %	-7 %	-21 %
4	-1 %	-15 %	-1 %	-3 %	-4 %
5	-3 %	-30 %	-3 %	-6 %	-9 %
6	-5 %	-44 %	-6 %	-12 %	-16 %

Table 4.7: Synchronous short-circuit capacity (MVA) at different network locations for all displacement cases.

Three case studies are used to illustrate these locational aspects, looking at the CCTs at key fault locations for the MLH, MHL and HLM cost allocations (Figure

4.4, Figure 4.5 and Figure 4.6 respectively). Although not explicitly analysed in this Chapter, the following analysis holds for all cost allocations, including HML (Figure 4.7), which is presented in subsequent Chapters.

Firstly, the difference in the CFL between the MLH and MHL cost allocations is analysed (Figure 4.4 and Figure 4.5). In line with Section 4.3.1, the low-cost SG is the CSG. For example, in Figure 4.4 SG2 is low-cost and is the CSG with the CFL being at bus 2 in all displacement cases. In Figure 4.5, SG3 is the low-cost SG and is also the CSG with the CFL at bus 3 in all displacement cases. This is the case despite significant variations in CCTs throughout the network between displacement cases. For example, CCT_2 in Figure 4.4 (the CFL) varies by up to 80 msec and CCT_3 in Figure 4.5 (the CFL) varies by up to 50 msec. This results in large variations in $CCT_{\min}$, along with variations in CCTs throughout the network in both cases. Whether there is an improvement or deterioration depends on the fault location with respect to the location of displacement—CCTs improving for faults where the first SG to go unstable is displaced by RES, and deteriorating for faults where the first SG to go unstable is not displaced (i.e., displacement of an SG by RES improves the stability of that SG). In Figure 4.6 (HLM), the combined effect of an increase in CCT_2 and decrease in CCT_3 results in a switch in CSG and CFL between displacement cases 1 and 2. Additionally, the CSG switches from being the low-cost SG2 and, to being the medium-cost SG3 (blue box in Figure 4.6). Using the locational parameters defined in Section 4.2.5, the reasons for improvements and deteriorations in the stability margin are analysed below.

Locational Aspects of Transient Stability Enhancement (green arrows)

For the cases where there is an improvement in transient stability (green arrows), the locational metrics used (electrical distance and system strength) tend to show a consistent behaviour, as described below. As an SG is displaced, the admittance between this displaced SG and all network locations decreases (due to a decrease in the machine rating and consequent increase in x'_d of the machine), causing the fault to be seen electrically further from the generator internal voltage. In addition to this; as displacement increases, RES becomes electrically closer to the network (since an

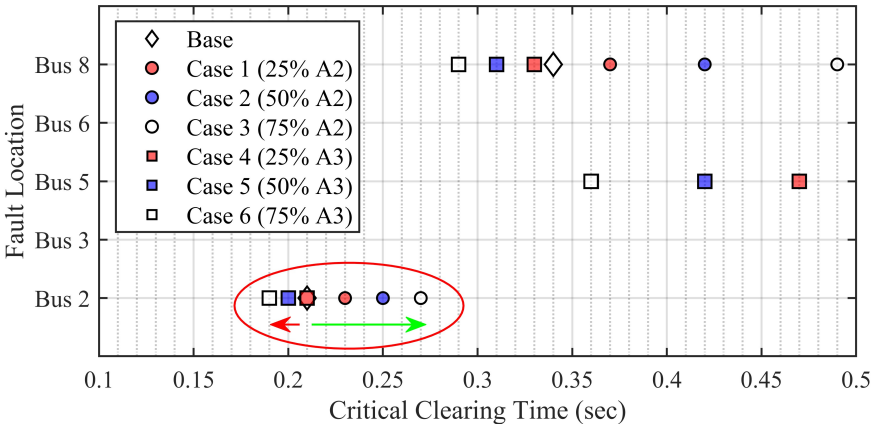

Figure 4.4: Medium-Low-High (MLH) generator cost allocation—CCTs at key fault locations for all displacement cases. CFL at bus 2 in every case.

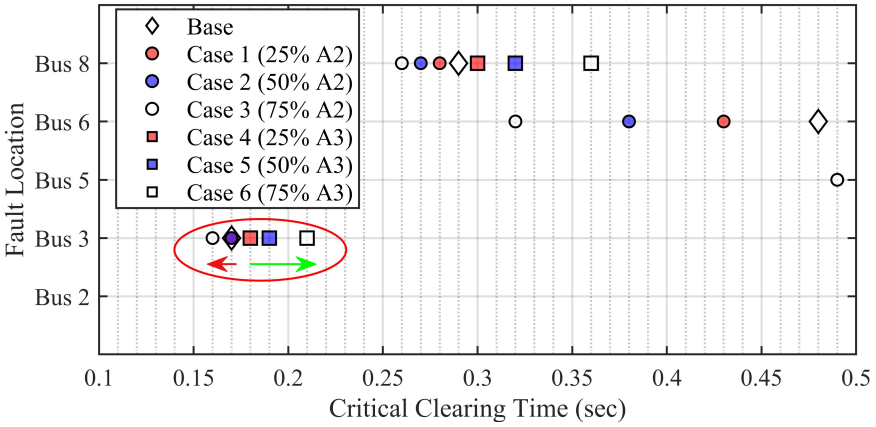

Figure 4.5: Medium-High-Low (MHL) generator cost allocation—CCTs at key fault locations for all displacement cases. CFL at bus 3 in every case.

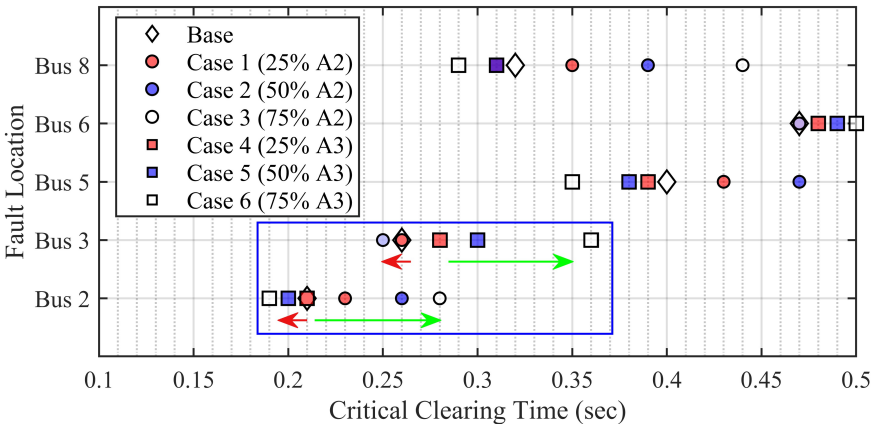

Figure 4.6: High-Low-Medium (HLM) generator cost allocation—CCTs at key fault locations for all displacement cases. Switch in CFL and CSG.

increase in the volume of RES connecting to the network in parallel results in an increase in admittance between RES and the grid). In the cases studied in this Chapter, this also results in RES becoming electrically closer to SG. This means that the LVRT capabilities of RES (a rapid reduction in active power output and injection of reactive power during and right after the fault) can support local SGs to a greater extent. This is consistent with findings in [64].

Table 4.5 shows that between displacement case 1 to case 3, the admittance between RES and bus 2 increases (from 16.7 p.u. to 50.7 p.u.), whilst the admittance between SG2 and bus 2 decreases (from 4.5 p.u. to 1.8 p.u.). The net result is that SG2 becomes electrically closer to RES. Therefore, any improvements to stability brought about by the LVRT capabilities of RES can be realised by SG2 to a greater extent. For example; in Figure 4.4 and Figure 4.6, an improvement in CCT_2, CCT_5 and CCT_8 is observed between case 1 and 3 (i.e., fault locations where SG2 is the first SG to go unstable). Similarly, in Figure 4.5 (MHL cost allocation), there is a significant improvement in the stability of SG3 when it is displaced (reflected in an improvement in CCT_3 from 0.17 sec in the base case through to 0.21 sec in case 6). Table 4.5 shows the network admittance between RES and bus 3 increasing from 8.8 p.u. in case 4 to 26.2 p.u. in case 6.

Therefore as displacement increases, the electrical distance between RES and the SG that is not displaced also decreases. However, the magnitude of the electrical distance between the RES and SGs that are not displaced is found to be too large for any benefits brought about by the LVRT capabilities of RES. For example, although the admittance between bus 2 and RES increases slightly from 2.4 to 2.9 p.u. from case 4 to 6 in Table 4.5, their overall electrical distance is higher compared to the admittance from RES to bus 3 (8.8 to 26.2 p.u.). In cases where there is a large electrical distance between any given SG and RES, the stability of that SG is found to deteriorate. Reasons for this deterioration in transient stability are discussed in more detail below.

Table 4.6 shows the EDR for SG2 and SG3 with respect to RES across all displacement cases. In cases 1 - 3, SG2 gets electrically further from the grid and RES2 gets electrically closer to the grid—but the extent to which SG2 gets further from the

grid is smaller than the extent to which RES gets closer to SG2—resulting in the EDR increasing from 1.30 in case 1 to 5.83 in case 3 (Table 4.6). In cases 1 - 3 for SG3, the EDR is below 1, indicating that the distance between SG and RES is larger. In addition to this, RES gets electrically closer to SG3 as between cases 1 - 3—resulting in an increase in the EDR. However, the increase in the EDR is much smaller than in the previous case since the grid impedance is larger between RES2 and SG3 compared to RES2 and SG2. Since the EDR represents the proximity of RES to SG (and therefore the ability of RES to support SG), a large value (above 1) in Table 4.6 corresponds to an improvement in stability of that SG and subsequent improvement in CCTs at locations where that SG is the first to go unstable.

Table 4.7 shows the short-circuit capacity at different network locations for each displacement scenario. As SG2 is displaced (cases 1 - 3), the short-circuit capacity decreases throughout the network—but most significantly at bus 2 (up to a 52 % reduction in short-circuit capacity between the base case and case 3 in Table 4.7). It would be expected that this significant reduction in short-circuit capacity at bus 2 would be reflected in a reduction in CCT_2. However the opposite is true, with CCT_2 increasing from the base case through to cases 1 - 3 (Figure 4.4 and Figure 4.6). Similar trends are observable for the displacement of SG3 (with up to a 44 % reduction in short-circuit capacity at bus 3 between the base case and case 6) and an improvement in CCT_3 from the base case and cases 4 - 6 in Figure 4.5. This suggests that the benefits to transient stability brought about by RES being connected close to SG can overcome a significant reduction in network strength.

In general terms, displacement of a SG by RES in the same area has been shown to have a beneficial impact on the stability of that SG since; (a) the electrical distance between the SG and the grid increases (due to the reduction in MVA-rating of the displaced SG), (b) the electrical distance between RES and the displaced SG decreases, (c) the LVRT capabilities of RES can support local SG (through the rapid reduction in active power output and injection of reactive power), and (d) as the proportion of displacement increases, the increasing volume of RES (MW) is increasingly able to support the increasingly smaller local SG (in terms of MVA rating) via the aforementioned

LVRT capabilities of RES. This is despite a significant reduction in network strength (coming only from SG disconnection) in the displacement area.

Locational Aspects of Transient Stability Deterioration (red arrows)

This section examines locational reasons for the deterioration in the stability of the SG that is not displaced by RES (indicated by red arrows in Figure 4.4 and Figure 4.5 and Figure 4.6). In cases where the EDR is small (Table 4.6 values below 1), a deterioration in the transient stability of the SG is observed.

For example, in Figure 4.4 CCT_2 reduces in cases 4 - 6. Similarly, in Figure 4.5, CCT_3 reduces between the base case and case 3. In addition to this, as the volume of RES connected increases, the electrical distance between RES and the SG that is not displaced reduces. This is reflected in a slight increase in the EDR as displacement increases (e.g., for SG2, the EDR increases from 0.39 in case 4 to 0.52 in case 6 (Table 4.6)). Despite this reduction in electrical distance, the CCTs for faults where that SG is the first to go unstable reduce (e.g., in Figure 4.4, CCT_2 reduces from 0.21 sec in case 4 to 0.19 sec in case 6). It is therefore likely that the large electrical distance between the SG and RES means that the beneficial impact from the LVRT capabilities of RES are unable to enhance the stability of the distant SG.

An additional reason for the reduction in transient stability margin relates to a reduction in network strength (i.e., short-circuit capacity) from the perspective of the SG that is not displaced. Between the base case and cases 1 - 3 (where SG2 is progressively displaced), there is a reduction in short-circuit capacity throughout the network. Although the largest reduction in short-circuit capacity is observed at bus 2, there is also a reduction (although smaller) in short-circuit capacity at bus 3—meaning that the network appears weaker from the perspective of SG3. This is observable in Figure 4.5, where the reduction in short-circuit capacity by 7 % at bus 3 between the base case and case 3 (Table 4.7) contributes towards the deterioration in CCT_3 (along with larger reductions CCT_5, CCT_6 and CCT_8, where larger decreases in short-circuit capacity are observed). Similarly in Figure 4.4; CCT_2, CCT_5 and CCT_8 reduce (suggesting a reduction in the stability of SG2) in cases 4 - 6 as a result of the reduction in short-circuit

capacity is observed at bus 2 (Table 4.7).

In summary, the stability of the SG that is not displaced deteriorates in these studies due to two key factors. Firstly, the point of connection of RES is too far away for the benefits of LVRT capabilities to be realised by the SG that is not displaced. Secondly, the strength of the network (i.e., the short-circuit capacity) reduces from the perspective of that SGs. If the SG that is not displaced happens to also be the CSG, then the CCT for the system (i.e., CCT_{min}) can reduce, since the stability of that SG has been found to deteriorate.

4.3.3 Impact of Sensitivity to Changes in Active Power Output of Synchronous Generators

Along with the locational aspects previously discussed, the sensitivity of the active power output of an SG as a result of the changes in wind generation active power output has also been found to significantly impact the stability boundary. This section provides three illustrative examples. Example A highlights a case where the active power output of a SG has a high sensitivity to changes in active power output of CIG between displacement cases. In the example presented, the large variations in active power loading results in significant changes to the stability boundary, such that a new CFL and CSG appear in one case. Example B highlights an additional case where the active power output of a SG has a high sensitivity to changes in active power output of CIG but with a limited impact on the transient stability boundary. Finally, Example C showcases a case where SG has low sensitivity to changes in active power output. As a result, the reasons for changes to the stability boundary between displacement cases are found to be purely locational (Section 4.3.2). The sensitivity of a SG to variations in active power output and subsequent variation in transient stability could occur in real-time, as regional wind speeds fluctuate and the system operator modifies the generator dispatch.

As SG is displaced by RES in operational or planning timescales, the dispatch of generation—dictated by the OPF—will vary. This means that the active power loading of SG could significantly vary in real-time (with some SGs being more sensitive

Displacement area	SG#	MLH	MHL	HML	HLM
2	SG1	-0.7 %	50.8 %	0.0 %	-0.2 %
2	SG2	0.0 %	0.0 %	57.0 %	0.0 %
2	SG3	0.0 %	0.0 %	0.0 %	-0.7 %
3	SG1	28.5 %	-4.1 %	0.0 %	0.5 %
3	SG2	0.0 %	0.0 %	-4.6 %	0.0 %
3	SG3	0.0 %	0.1 %	0.1 %	23.3 %

Table 4.8: Active power % output variation of Synchronous Generators (SGs) for displacement in area 2 and 3 for key cost allocations.

bus_{no}	MLH	MHL	HML	HLM
bus 1	-49.1 %	-66.7 %	-21.9 %	-22.9 %
bus 2	-28.6 %	28.6 %	151.9 %	33.3 %
bus 3	-7.0 %	23.5 %	17.6 %	38.5 %

Table 4.9: Maximum Critical Clearing Time (CCT) % deviation from the base case at busbars near Synchronous Generators (SG) terminals.

to changes in active power output than others), which could impact the transient stability of the network. The extent to which an SG is sensitive to changes in active power output depends on SG size (MVA-rating), volume of RES (MW), generator cost, demand level (MW) and network constraints—all of which are considered in the OPF formulation. More specifically, when generator costs and MVA-rating result in the low-cost SG being at maximum active power output and the high-cost SG is at its minimum—the medium-cost generator covers any active power mismatches. Therefore, the medium-cost generator is highly sensitive to changes in active power output. This is dependent on demand level and displacement scenario. This Chapter does not consider changes to the overall demand level to highlight the impact on the sensitivity of SG active power loading coming only from changes in generator cost and RES displacement.

Table 4.8 shows the maximum variation in active power output for each SG between the base case and cases 1 - 3 (displacement in area 2), and for cases 4 - 6 (displacement in area 3). The SG with the highest sensitivity to changes in active power output (and the extent to which it varies) changes depending on the displacement case and cost allocation.

Table 4.9 shows the maximum variation in CCT_1, CCT_2 and CCT_3 from the base case (expressed as a percentage difference from the base case CCTs given in Table 4.4) at busbars near SG terminals for all displacement cases and key cost allocations. A correlation between a large variation in active power output of a SG and a large variation in CCTs (Table 4.8) at the bus local to that generator can be observed. However, it should be noted that this is not the only factor that impacts transient stability. As discussed previously in Section 4.3.1, multiple factors (such as generator cost, RES dynamics, locational aspects and sensitivity to changes in active power) combine to influence the shape of the transient stability boundary—highlighting the complexity of the problem. Because of this, in this particular network; the high sensitivity of SG1 to changes in active power output is not as critical since either SG2 or SG3 are always the CSG. Therefore cases where SG2 or SG3 have a high sensitivity to changes in active power output result in a greater impact on transient stability. This is evident in the HML cost allocation where SG2 varies by up to 57.0 % (Table 4.8) and CCT_2 varies by 151.9 % (Table 4.9).

***Example A*: Significant impact on transient stability of SG having high sensitivity to changes in active power output (HML cost allocation)**

In the example presented, the CFL and CSG change. This is attributed to the combined effect of SG2 having a high sensitivity to changes in active power loading, locational aspects (discussed in Section 4.3.2), non-operational parameters and the dynamics of Type-4 wind. Being the low-cost generator, SG3 is the CSG in the base case for this cost allocation. However, the high sensitivity of SG2 (originally not the CSG) to changes in active power output between different displacement scenarios results in significant changes to the stability boundary. In case 6, CCT_2 and CCT_3 become equal (for the resolution used), meaning that both bus 2 and 3 are CFLs and SG2 and SG3 CSGs, respectively. This change in CFL and CSG can be largely attributed to an increase in SG2 active power loading between case 4 and 6 which results in a reduction in CCT_2. At the same time, an enhancement in the stability of SG3 (brought about by the locational aspects outlined in detail previously) results in an increase in CCT_3).

This results in two CFLs and CSGs in case 6 (highlighted by a red box in Figure 4.7).

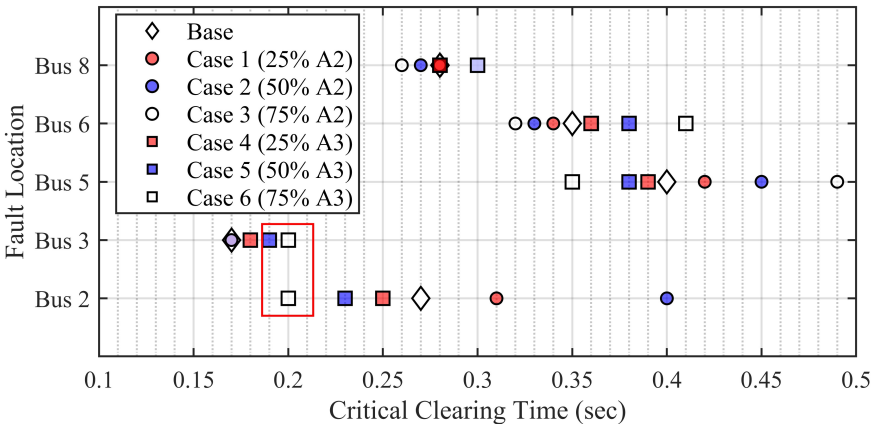

Figure 4.7: High-Medium-Low (HML) generator cost allocation—CCTs at key fault locations for all displacement cases. Additional CFL and CSG in case 6.

Figure 4.8 shows the active power loading of each SG in the HML case for each displacement case. The minimum and maximum active power limits (in MW) of each SG are shown by black upper and lower bounds and the MW dispatch given block colour. The active power loading (in %) of each SG is shown by a coloured dashed line. Crucially, it can be seen that the active power output of SG2 (the medium-cost SG) varies significantly between displacement cases (up to 59 %). This indicates that the active power output of SG2 has a high sensitivity to changes in CIG active power output compared to the other SGs on the network (which operate at maximum (100 %) or minimum (35 %) active power output depending on the generator cost).

Between the base case and cases 1 - 3, the volume of RES2 connecting in area 2 is greater than the reduction in the size of SG2. This reduces the active power loading of SG2 (despite the reduction in MVA-rating). What is more, SG1 (the high-cost SG) is dispatched to the minimum stable export and SG3 (the low-costSG) to the maximum stable export. Between the base case and cases 4 - 6, the volume of RES connecting is less than the reduction in the size of SG3, resulting in a reduction in the net export from area 3. This is because the MW increase from RES is not proportional to the reduction in the maximum stable MW export of SG in displacement cases (Table 4.2). The power deficit is taken up by SG2, once again resulting in a large variation in its

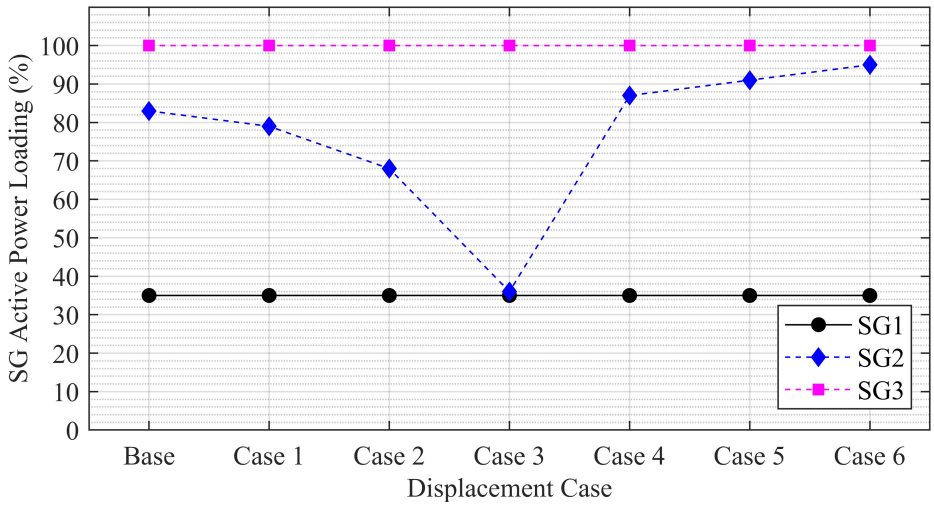

Figure 4.8: High-Medium-Low (HML) generator cost allocation—active power dispatch and loading of SGs. High sensitivity to changes in active power loading of SG2.

active power output compared to other SGs.

The large variation in SG2 active power loading is reflected in the significant variation in CCTs at the generator terminal bus (bus 2 in Figure 4.7). There appears to be a strong correlation between a reduction/increase in SG2 loading and an improvement/deterioration in CCT_2. This suggests that the high sensitivity of an SG to changes in active power loading can significantly influence the transient stability of the network. More specifically, between the base case and displacement case 3, the active power loading of SG2 reduces by 47 %. This reduction in active power loading is reflected in a significant improvement in CCT_2 (from 270 to 680 msec (not visible on scale used in Figure 4.7)). Similarly, the active power loading of SG2 increases by 12 % between the base case and case 6, resulting in CCT_2 reducing by 70 msec. The trend in CCT_5 between displacement cases mirrors that of CCT_2 despite SG3 being the CSG in all cases other than case 6 where the CSG switches to SG2. This highlights the impact of SG2 active power loading on the dynamic response for faults throughout the network.

There is no change to the active power loading of SG3 from case 1 - 3 (Figure 4.8), and no change in CCT_3 (Figure 4.7) since it is the low cost SG and therefore dispatched

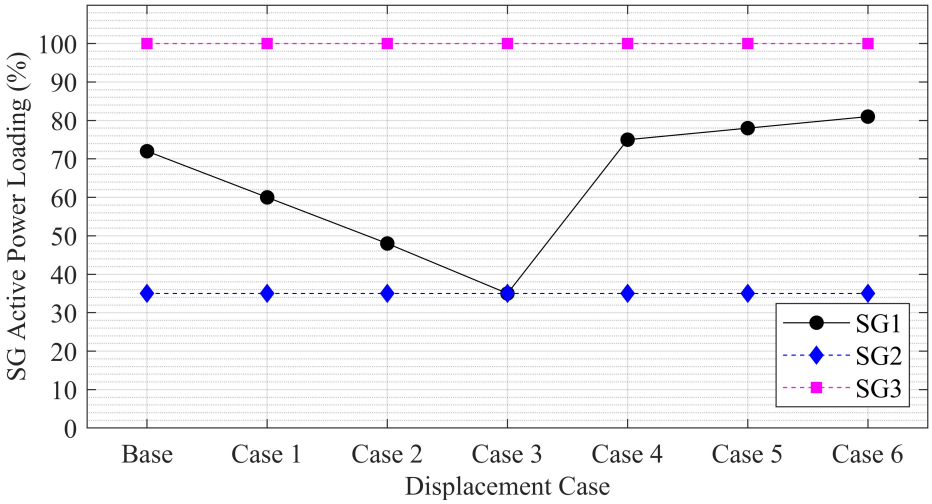

Figure 4.9: Medium-High-Low (MHL) generator cost allocation—active power dispatch and loading of SGs. SG1 high sensitivity to changes in active power loading.

at maximum stable MW export. Between cases 4 - 6, there is an improvement in CCT_3, despite there being no change to the active power loading of SG3. This disparity between SG3 loading and CCT_3 indicates that the reason for changes in transient stability is likely to be because of other factors (such as locational aspects, discussed in Section 4.3.2) and not as strongly related to active power loading.

***Example B*: Minimal impact on transient stability of SG having a high sensitivity to changes in active power output (MHL cost allocation)**

A SG can have a high sensitivity to changes in active power output, but the impact on the stability boundary may be minimal. For example in the MHL cost allocation SG1 active power output has a high sensitivity to changes in CIG active power output (Figure 4.9), but there is a limited impact on the CSG (SG3 in Figure 4.5), CCT and CFL (bus 3 in Figure 4.5). This is because the high active power loading and small size (inertia/ MVA rating) of SG3 results in it being very unstable compared to SG1, meaning that the SG3 plays the main role in determining overall network stability.

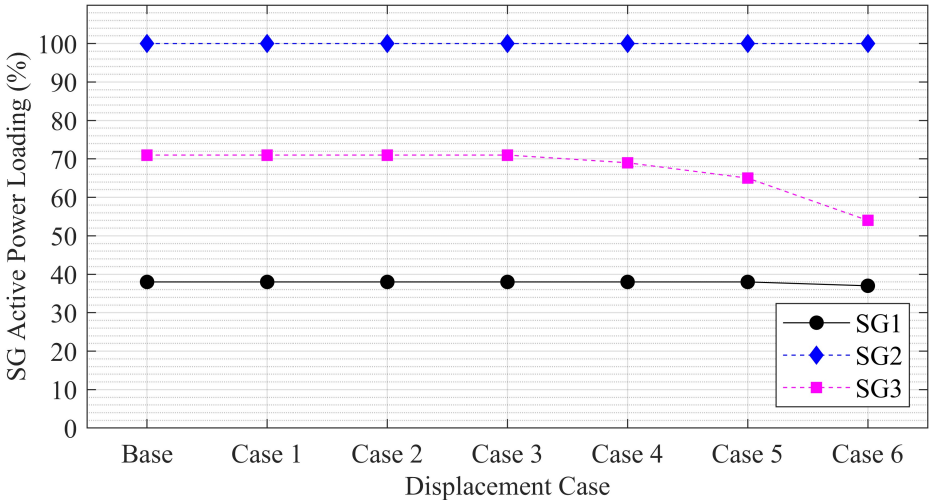

Figure 4.10: High-Low-Medium (HLM) generator cost allocation—active power dispatch and loading of SGs. Small variations in active power loading.

***Example C*: SG with a low sensitivity to changes in active power output (HLM cost allocation)**

In contrast to the high sensitivity cases above, the HLM cost allocation reveals SGs as having low sensitivity to changes in active power output, as shown in Figure 4.10. Between cases 1 - 3, there is no change to the total active power coming from each area, as the active power increase from RES2 is countered by the reduction in the size of SG2 (which operates at maximum output since it is the cheapest SG). In cases 4 - 6, as RES3 increases output, there is a slight reduction in active power loading of SG1 since it is the high-cost machine. Since SG1 is already operating close to its minimum stable output, the active power loading of SG3 is also reduced by the OPF. This is because the incremental costs of SG1 and SG3 are very similar in this cost allocation (Table 4.3). Compared to the high sensitivity case presented in Section 4.3.3, generators in this example have a relatively low sensitivity to changes in active power output. Despite this, there is still a significant variation in CCTs throughout the network between the different displacement cases (Figure 4.6), due to aspects discussed in Section 4.3.2.

In general terms, when the difference between the incremental costs of generators is substantial—such that the high-cost SG is dispatched at its minimum stable export

and the low-cost SG at its maximum stable export—any changes in RES output or demand level (changes to demand are not studied in this Chapter) are taken up by the medium-cost SG. For example, incremental costs in the HML cost allocation for SG1, SG2 and SG3 are 1.47, 0.95 and 0.14 £/MW respectively (Table 4.3). This results in a high sensitivity to changes in active power export of SG2 in Figure 4.8 (the medium-cost SG). However, when generator incremental costs are comparable, any such changes to RES output or demand are taken up by multiple generators. For example, in the HLM cost allocation active power loading of both SG1 and SG3 varies (Figure 4.10), since their incremental costs are similar (1.47 and 1.42 £/MW Table 4.3).

4.4 Discussion

Results presented in this Chapter highlight that as the generation mix varies, the 'most critical' fault on a network could change in terms of CCT_{min}, CFL and CSG. These changes to the transient stability boundary may result from long-term planning decisions to decommission specific types of power plants and operational decisions driven by cost, the variability of wind generation and the dynamic behaviour of RES. More specifically, the studies have shown that:

- generator cost dictates the general shape of the stability boundary (low-cost SGs dispatched with high active power loading, resulting in shorter CCTs for nearby faults);
- locational aspects result in either improvement or deterioration of the stability margin, depending on the location of connection of RES with respect to the CSG (near to versus far from) and;
- SGs with high sensitivity to changes in active power loading can also significantly impact the stability boundary in various displacement cases.

In planning timescales, connecting WFs close to SGs could lead to improvements in the transient stability of that group of generators, whilst the stability of more distant generators may deteriorate. Therefore, connecting WFs closer to the critical generators

on the network may lead to an overall improvement in the transient stability boundary. In operational timescales, the uncertain nature of wind may result in changes to generator dispatch. As a result of changes to the dispatch and the dynamics of RES, the CFL and CSG vary in operational time, thus changing the understanding of typical lists of critical contingencies. This Chapter has illustrated the trade-off between the most cost-effective dispatch and transient stability. Dispatch could be altered—through new ancillary services—to provide a more stable (but also more costly) dispatch.

It is important to note that these factors cannot be considered in isolation since they all ultimately affect the stability boundary. It is difficult to decouple the impact of any one parameter to determine the extent to which it impacts the stability boundary due to the complexity and non-linearity of the problem. Moreover, the extent to which each factor influences the shape of the stability boundary changes depending on the case. In some instances, this can result in significant changes to the stability boundary such that the CCT_{min}, CFL and CSG can move around the network.

4.5 Conclusion

This Chapter highlights changes to the stability boundary caused by the displacement of SG by RES interfaced generation as a result of operational and/or planning decisions. A framework to identify and investigate such changes is presented in this Chapter. Using RMS models and TDS, changes to the stability boundary have been attributed to two main factors; (a) locational aspects and (b) generator cost aspects. Locational aspects are investigated by analysing the electrical distance between key network locations via the network admittance matrix and the EDR (defined in this Chapter). Generator cost aspects are analysed through marginal costs, the difference between various generator costs and the subsequent impact on generator dispatch.

Results presented in this Chapter consistently highlight that—in the test network used—the displacement of SG by RES in a given area improves the CCTs in that area whilst reducing the CCTs in other generating areas. This can either result in an improvement or deterioration in CCT_{min}, depending on the displaced generator's cost.

In some instances, this can even result in a switch in both CFL and CSG. Locational aspects defined in this Chapter can explain these trends; with improvements to the stability boundary being explained through the beneficial impact of LVRT capability from RES being able to support nearby SG (quantified through the EDR). Conversely, deteriorations in transient stability can be partially attributed to a reduction in short circuit capacity in this case.

Moreover, the significance of the sensitivity of the CSG to changes in its active power output (dictated by generator marginal costs and the OPF solution) has been demonstrated by highlighting changes in CFL and CSG of the network. It is demonstrated that when there is a significant difference in SG marginal costs, displacement of SG by RES can result in a high sensitivity of changes to the active power output of SGs. In some cases, this can lead to significant changes to the transient stability boundary. This is because any changes in active power loading are taken up by a single SG. Conversely, there is a limited impact on the stability boundary when generator costs are closer since SGs share any changes in active power loading between them.

Overall, the results highlight the importance of generator cost, along with spatial and temporal aspects in changes to system dynamics that must be considered in both planning and operational timescales to ensure the secure operation of the network. In particular, the studies presented in this Chapter highlight two key aspects. First, connecting WFs close to SGs that frequently run at full output could lead to improvements in transient stability for local generators whilst deteriorations in the stability of more distant generators. Second, the intermittency of wind can vary the loading of conventional generation such that the CFL and CSG could change.

This Chapter has highlighted additional important dimensions to the transient stability boundary that must be considered in the context of increasing generation from RES. In doing so, the complexity of the problem is further increased beyond the dimensions introduced in Chapter 3 and in the supplementary studies in Appendix A. This demonstrates the need to establish a method capable of reducing the problem complexity (i.e., reducing the dimensions) and directing focus toward the most influential factors influencing the stability boundary.

The locational approach of the method—through calculation of the CCT at each busbar—enables locational trends to be observed (built on in later Chapters). While this Chapter has been successful in identifying locational trends in the transient stability margin using RMS-TDS to determine CCT and CCT_{min}, the network analysed was extremely small. This means that the computational burden of calculating the stability margin at each busbar is significantly smaller than a larger network, limiting the usefulness of such a method. Moreover, the simple network structure and careful case study design made stability trend identification straightforward. Such simplicity is not typically a possibility; therefore, the usefulness of these findings is limited outwith the academic domain.

Therefore, whilst the studies presented in this Chapter are informative and interesting—the remainder of this thesis focuses on reducing the aforementioned computational burden and formal methods for uncovering important parameters impacting the transient stability boundary and trend identification.

Chapter 5

Machine Learning and Interpretable Machine Learning for Transient Stability Assessment

5.1 Introduction and the *Three Desirable Attributes* for Modern Transient Stability Assessment

Throughout this thesis, the loss of SG attributes, non-linear dynamics of CIG and the intermittent nature of RES connecting at different locations to the network have demonstrated the increased requirement to perform TSA. However, existing methods for TSA have various limitations in modern power systems, leading to a need for the development of new methodologies capable of the identification of trends and patterns in the transient stability boundary—a nontrivial problem.

Chapter 2 outlined that the key drawback of TEF methods relates to an inability to capture the level of detail required due to the use of highly simplified models. While accurate, the key disadvantage of TDS approaches is the relatively slow computational speed. This is particularly the case when calculating the transient stability margin (i.e.,

CCT) and the critical fault (i.e., CCT_{min}, which is contingent on knowing the CCTs throughout the network).

However, when faced with a wide variety of hitherto unfamiliar system conditions in addition to the changing dynamic behaviour due to RES connection, it becomes crucial to rapidly perform TSA for a much larger number of fault locations (as demonstrated in Chapter 4) and form contingency lists appropriately. However, the ability to perform more frequent and detailed TSA in timescales much shorter than currently used is constrained by the relatively slow computational speed of TDS.

Understanding the predominant factors influencing the transient stability boundary is also extremely difficult when assessing larger numbers of operational scenarios, and trends observed across many operational scenarios may not be consistent with individual operating scenarios. So-called *'operational expertise'* may be able to offer some degree of insight into more apparent trends in system stability. However, this becomes less reliable in the context of increased connection of RES and associated fast dynamic response of their controllers (as demonstrated in Chapter 3, 4, and indeed Appendix A). Without understanding the predominant factors influencing the transient stability boundary, the effectiveness of any transient stability enhancement measures designed is likely to be limited.

Therefore, new methods suitable for TSA in modern power systems should possess *three desirable attributes*:

1. reduction of computational expense for obtaining the transient stability margin in operational timescales,
2. enhancement of understanding of the predominant factors influencing the transient stability boundary, and
3. accurate representation of the transient stability boundary.

ML can provide explicit mappings of complex functions and accelerate computationally heavy tasks. Research has therefore been increasingly deploying ML to overcome the limitations mentioned above of traditional TSA approaches. In particular, ML-based approaches have shown to be an effective way of overcoming the limitations of

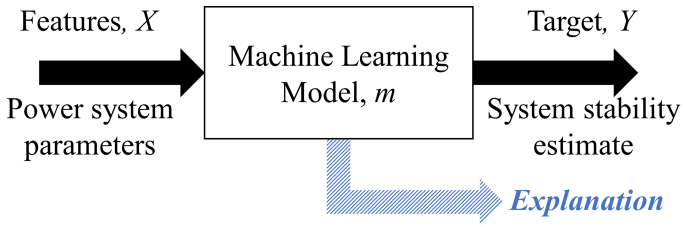

Figure 5.1: Machine Learning (ML) overview for Transient Stability Assessment (TSA) overview with explanation dimension.

RMS-TDS by reducing the computational burden online through the use of pre-trained ML models, as detailed extensively in [111–115]. In such approaches, the TDS and ML model training are conducted offline when time is inexpensive.

The premise of IML—an emerging area of research, that has gained some initial traction in power systems [116]—is to provide detailed explanations of ML model predictions in order to enhance trust and confidence in the model predictions. Insights can also be used to understand better the data upon which the ML model is trained to identify complex relationships. IML techniques can help overcome the tension between accuracy and interpretability that exists in ML (i.e., the ability of the ML model to *make correct predictions* vs the degree to which a human can *understand the model*). Such insights into the stability boundary may bolster existing knowledge and/or infer new information about the transient stability of a system. Therefore, development of a IML-based methodology for TSA means that an *explanation* dimension can be added to the traditional ML framework for TSA (Figure 5.1).

The three desirable attributes can therefore be successfully adhered to through the development of a methodology that (a) leverages the ability of ML to provide mappings between complex functions and accelerates the computationally heavy task of TDS, and (b) provides detailed insights into a ML model trained to predict the transient stability margin using IML techniques. Such a method could be used offline in planning timescales or to direct computational effort in an online setting (i.e., reduce the number of TDS required online). Furthermore, if enough confidence in such a method can be established, such IML-based methods could eventually be used for online TSA and enhancing situational awareness.

Section 5.4 summarises the current state-of-the-art in ML and IML for TSA. Then the fundamental concepts of ML and IML in the context of TSA. Specifically, Section 5.2 sets out the process for development of a ML-based methodology for TSA. This requires training a ML model from a database of operational scenarios that are representative of the types of operating conditions likely to be encountered. The database should be comprised of power system parameters and variables (known as *features*) and the corresponding transient stability index selected (known as the *target*) based on user requirements (see Section 5.2.1). A ML algorithm (Section 5.2.2) can then be selected, which seeks to learn the complex relationship between the features and target (as summarised in Figure 5.1). The ability of the ML model to find a mapping between the features and target can then be assessed using a wide range of error metrics (Section 5.2.3). Section 5.3 provides an overview of the drivers for development of IML techniques. In addition, an overview of the types of insights that are available from different techniques is provided. In short, techniques may be local or global (providing interpretations of single model predictions or the entire model) and offer feature importance or feature effects (ranking features or providing information regarding the impact of a feature on the target).

The concepts introduced in this Chapter are important to consider when developing an IML-based TSA methodology. Indeed, these concepts are used in Chapter 6, 7 and 8 of this thesis, where various methods are developed that adhere to the three desirable attributes.

5.2 Overview of Machine Learning for Transient Stability Assessment

The fundamental concept behind ML methods for TSA development of a model, m, capable of identifying the relationship between some power system variables and parameters (features, X) and the transient stability of a system (target, Y), using a number of simulated responses (Figure 5.1). The features and target for a number of operational scenarios are included in a database (here referred to as the Transient

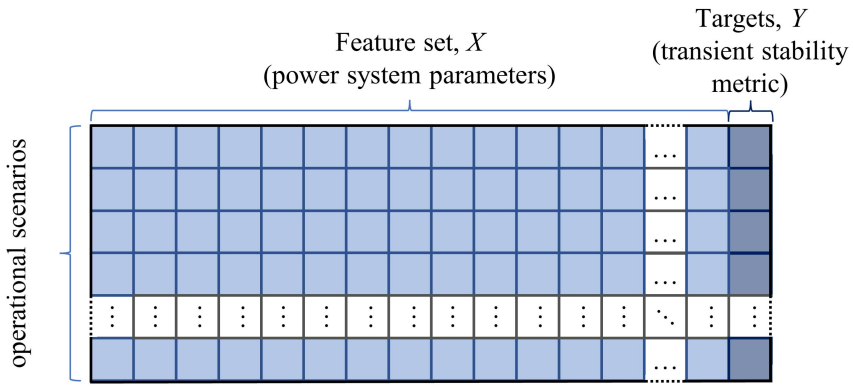

Figure 5.2: Generic training and testing database structure for Machine Learning (ML).

Stability Database (TSDb)), which is constructed using RMS-TDS offline. From this TSDb, a ML model can be trained offline, providing explicit mappings of complex functions. Once the relationship between the features and the target is established, previously unseen scenarios can be quickly and accurately approximated with reduced computational effort online since the computationally burdensome TSDb construction and model training are conducted offline.

There is an inherent link between the features selected for the TSDb, the choice of target, the ML algorithm selection and the overall accuracy of the model. Therefore, careful and considered design choices must be made to ensure the developed method is suitable for the intended application. These choices also impact the quality of insights available from the model at the IML stage.

5.2.1 Transient Stability Database

A TSDb is a database that contains the features and target for a number of operational scenarios (Figure 5.2). The operational scenarios should be a realistic and representative set of the system conditions likely to be encountered on the system of study.

Feature Selection

Features are the power system variables and parameters used to describe each operational scenario and act as the input to the ML model. Therefore, a feature is one column in the TSDb (Figure 5.2). Feature selection is very important and has consequences for model accuracy and the types of insights available at the IML stage and thus should be informative, discriminating and independent. Feature selection is subjective but should be informed by engineering knowledge of the transient stability problem.

ML for TSA should be not only able to accurately determine the stability of an operational scenario but also capable of identifying driving factors behind the outcome such that decisions on preventive or corrective control measures can be informed *sufficiently quickly* for them to be implemented without incurring undue risk in system operation. Indeed, the features selected ML algorithm significantly impacts this. It is common for authors in academic literature to use information collected after a fault happens to improve model accuracy [117–121]. However, this is at the expense of controllability since it allows only corrective control actions as a last resort with very short activation times. Consequently, the use of pre-fault data in the transient stability estimation problem is advantageous in this regard [122].

Target Selection

The target variable is the aspect of a dataset about which a deeper understanding is required, and in the context of TSA is the transient stability index. Many frequently used indices are summarised in Section 2.5, along with key advantages and disadvantages. In particular, the distinction between seeking to predict the stability status of a system (i.e., *stable* or *unstable*) or quantify the stability *margin* is significant. This design choice will depend on the application and consequently will impact the choice of ML algorithm and the accuracy of the model.

5.2.2 Machine Learning Algorithms

A ML *algorithm* is a procedure that is run on data, which results in the creation of a ML *model*. Many different ML algorithms exist that can perform both *classification* (predicts a discrete class label) or *regression* (predicts a continuous quantity). As such, *classification* methods can provide stability status predictions but no information regarding the proximity of the operational scenario to the stability boundary. On the other hand, *Regression* methods can predict the stability of *margin*—which is regarded as favourable and is the key focus of this thesis.

Due to the significant number of ML algorithms that exist, the details are excluded from this thesis. However, if details relating to the inner workings of the algorithms are used, mathematical details are provided at that point.

5.2.3 Error Metrics for Evaluation for Regression Algorithms

Both the features selected, the target used and ML algorithm used have a significant impact on model error. In the context of TSA, model error—that is, on average how closely model predictions are to their true values—fosters confidence in the ability of a model to represent the ground truth (i.e., the true stability of the system).

Whilst low morel error rates are important for planning-type applications; it is particularly important for online TSA—where operational decisions are taken based on model estimates, and the consequence of an erroneous estimate may be severe.

In the context of TSA, the model error relates to the ability of the ML model to predict the transient stability margin compared to the ground truth (typically determined via RMS-TDS). There exist several metrics that can be used to benchmark this, which are outlined in this Chapter. The metric used to benchmark ML algorithms largely depends on the application and the desired properties of the model. Typical metrics that are widely implemented include Mean Absolute Percentage Error (MAPE), Coefficient of Determination (RSQ) and Root Mean Squared Error (RMSE).

Mathematically, MAPE is described in Equation 6.5 where y_i is the actual value, $\bar{y}_i$ is the estimated value, n is the sample number and ϵ is an arbitrary small positive number (to avoid undefined results). The output will be between 0 and 1, where a

score closer to 0 indicates a more accurate model.

$$MAPE(x, \hat{x}) = \frac{1}{n} \sum_{i=1}^{n} \frac{|y_i - \hat{y}_i|}{max(\epsilon, |y_i|)} \tag{5.1}$$

The RSQ (Equation 5.2) describes the total variance between the dependent and independent variables. The RMSE is the standard deviation of the residuals (Equation 5.3). In both equations, n is the number of data points, i is the observation, y_i is the actual value, $\hat{y}_i$ is the estimate and $\bar{y}_i$ the mean of all observations.

$$RSQ = 1 - \frac{\sum_i^n (y_i - \hat{y}_i)^2}{\sum_i^n (y_i - \bar{y_i})^2} \tag{5.2}$$

$$RMSE = \sqrt{\sum_{n=1}^{N} \frac{(y_i - \hat{y}_i)^2}{n}} \tag{5.3}$$

5.3 Overview of Interpretable Machine Learning for Transient Stability Assessment

In order to achieve the low model error required in complex problems (and thus confidence in the ability of the ML algorithm in representing the ground truth), increasingly complex ML algorithms are required. However, these highly accurate algorithms are typically black-box and, thus, difficult to understand how predictions are made. In recent years, many ML applications to predict the behaviour of various aspects of power systems have been developed—some of which are summarised in [123]. While these black-box ML algorithms have shown good accuracy and computational savings, their applicability to mission-critical infrastructure (such as power systems stability applications) is limited due to the absence of trustworthy explanations—thus leading to a tension between two highly beneficial properties; *accuracy* and *interpretability*.

1. *Accuracy.* The ability of the ML model to predict the transient stability margin compared to the ground truth (typically determined via RMS-TDS). This is important in establishing confidence in the ability of the ML to capture the complex

power system dynamic behaviour.

2. *Interpretability.* The ability to understand how a ML model reaches predictions with respect to features (power system variables). This primarily enhances trust in the ML model (when comparing insights with power system engineering principles) but can also be used to increase knowledge of the transient stability of a network.

ML algorithm 'complexity' is difficult to define as it can be implementation dependent, and may depend on the data used. However, algorithm complexity can be better understood by appreciating how different algorithms work. For example, for linear regression a linear relationship is assumed and aim is to determine the predicted weights that result in the smallest residuals. However, ANNs (which comprise of an input layer, hidden layer(s) and an output layer) perform nonlinear transformations of the inputs in order to tune the weights and biases of the network. It is generally (but not always) the case that as algorithm complexity increases, the accuracy of the model will also increase—but the interpretability deteriorates. The term 'interpretability' is an umbrella term—the definition of which may vary depending on the application and type of insights required. However, it can be seen from the linear regression vs. ANN example given above that interpreting the predicted weights of a linear model (in the case of linear regression) is significantly easier than understanding the nonlinear transforms, weights and biases of multiple neurons (in the case of an ANN). As a result, an representation of the accuracy-interpretability tension is given in Figure 5.3. This accuracy-interpretability tension often forces methodological trade-offs [124]. For example, linear regression and DT [125, 126] are straightforward to interpret but may not achieve the desired accuracy in some instances. Conversely, black-box models such as eXtreme Gradient Boosting (XGBoost) and ANN [127, 128] tend to achieve higher accuracy but are difficult to interpret.

The premise of IML—an umbrella term that covers a range of techniques and is an emerging area of research—is to provide detailed explanations of complex ML models. The field has been gaining increasing attention in recent years due to the powerful

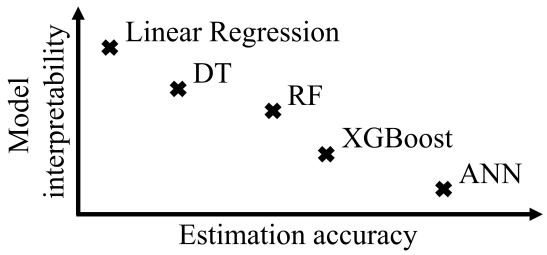

Figure 5.3: Tension between accuracy and interpretability in popular Machine Learning ML algorithms.

insights that can be obtained [116, 129]. Whilst ML can offer powerful predictive capabilities (i.e., *what* is the prediction?), IML methods offer insights into how the model came to the prediction (i.e., *why* was the prediction made?). To build confidence in ML and foster widespread use in the risk-averse power system domain, understanding how a ML model reaches predictions is important. IML techniques could be used to not only build confidence in ML but also bolster existing knowledge of the transient stability boundary of a system (i.e., do the findings relate to domain expertise?) and/or infer new information/knowledge.

Each IML technique possesses different benefits and drawbacks that must be fully considered based on the specific application. In general, methods can be categorised as either *local* or *global* in nature, and can either capture feature *importance* or *effects* (key techniques are categorised based on this in Table 5.1).

Local explanation methods (e.g., SHAP as per Table 5.1) explain individual predictions, whilst global methods (e.g., PFI as per Table 5.1) generate explanations that relate to the expected behaviour of an entire model with respect to the whole training database. In a TSA setting, local methods could be used to explain single operational scenarios which may be particularly well suited to an online environment (for example in a SO control room to design emergency control actions for the current operational scenario). Global methods could provide explanations across a representative set of operational scenarios, which may be better suited to operational planning and planning settings (e.g., to develop general operational rules and/or inform planning decisions).

The distinction between feature importance and effects is also important. Feature importance methods quantify the contribution of a feature to the model performance

	Local	**Global**
Feature Effects	ICE LIME Counterfactuals Shapley Values SHAP	PDP ALE
Feature Importance	ICI	PI PFI SAGE

Table 5.1: Selection of common Interpertable Machine Learning (IML) techniques, classified as either local or global and as feature effect or importance [130].

(e.g., PFI as per Table 5.1), whilst a feature effect indicates the direction and magnitude of a change in predicted outcome due to changes in the values of features (e.g., SHAP as per Table 5.1). For TSA, understanding the impact of changes in the value of a feature on the predicated outcome may be particularly beneficial—since a quantification of the impact of a variable may be useful in understanding the actual impact on the chosen stability index. Whilst IML can be a powerful tool, authors in [130] highlight many of the pitfalls, urging caution when using IML to avoid drawing incorrect conclusions.

5.4 Literature Review on the Current State-of-the-Art

5.4.1 Machine Learning for Transient Stability Assessment

Some of the earliest examples of ML in dealing with the transient stability problem can be found in [131] and [132]. Since then, extensive research has gone into applying various supervised ML techniques on transient stability in recent years, often driven by the need for rapid TSA. Recent detailed reviews of existing academic literature are presented in [111–115]. Popular ML algorithms used in these studies include DT [125, 126], Support Vector Machine (SVM) [117, 133] and ANN [127, 128]. Trade-offs exist regarding data pre-processing requirements, training time, accuracy, and interpretability.

A key consideration for the development of ML methods for TSA relates to what quantity the method seeks to predict, namely stability status (i.e., stable/unstable) or

stability margin (i.e., proximity to stability margin)—an important distinction. Stability status prediction can be made using binary classification methods [134–139]. Such methods offer insights into whether the operating point is stable or not; however, no details relating to the proximity of the operating point to the stability boundary are provided. Multiclass classification can improve on this. For example, authors in [140] use a four-level CCT-based stability index to provide information on the degree to which the system is stable. However, the definition of these levels is subjective and is not a widely adopted approach. Identification of unstable groups of machines can be used to group SGs based on the order in which they lose synchronism [125, 126, 141–147].

Transient stability indices have also been predicted through regression, with the transient stability metric estimated varying depending on the study. Metrics used in the literature range from kinetic energy gained and rotor angle deviation [148], [149]. Such metrics only require a single RMS-TDS to calculate—reducing the computational effort of constructing the training database. However, an improvement is through the use of the CCT [30, 150], which offers additional information relating to the proximity of the operating point to the stability boundary. As outlined in Section 2.5.2, the calculation of CCT is contingent on running a series of TDS, making CCT significantly more computationally burdensome to calculate than the aforementioned metrics—indeed, some poignant examples can be found in [47, 151–153]. Indeed, authors frequently cite this as a reason for not using CCT [112, 138].

The power system parameters and variables (known as features in ML) used to train the ML algorithm selected for a given method may significantly influence the usefulness, accuracy and interpretability of a model. Different features may be used depending on the study. For example, authors in [117–121] opt to use fault-on trajectories to improve prediction accuracy. However, using post-fault data means the method's usefulness is limited since the window to take a corrective control action is narrow, making activation times and communication delays or losses more significant. In [154], the authors seek to improve this by developing a method to balance the trade-off between assessment accuracy and response time. The results show that high assessment accuracy (classification in this case) can be achieved shortly after the fault clearance. A further

improvement is through the use of pre-fault data [122], expanding the time window in which corrective action can be taken in an online setting.

5.4.2 Interpretable Machine Learning for Transient Stability Assessment

Numerous post-hoc IML methods exist, which are presented concisely in [14]. However, there have been limited numbers of IML-based approaches in the context of power systems, and even fewer explicitly address the transient stability problem.

Whilst not strictly IML, Principle Component Analysis (PCA) (a method for dimensionality reduction in pattern recognition problems) is used in [155] to collapse the dimensions of the transient stability problem and is therefore highly relevant. Operating points are mapped in principal component space, enabling clusters of operational scenarios based on CCT to be defined. New operating points can then be mapped into the 3D space using the shortest Euclidean distance. Similarly, the authors of [156] determine the degree of influence features have on the splitting property and estimation accuracy of the DT. Whilst the method considers increased output from RES, it seeks to predict SG rotor angle deviation and does not include features relating to displacement of SG by RES. In [157], authors propose a method that combines deep learning and DTs (by regularising the deep learning model with the average DT path length during model training) to enhance interpretability of the ML model. Whilst the approach demonstrates how DTs can be used for rule extraction, the approach is limited in that it only seeks to predict the stability status of the system.

Local Interpretable Model-agnostic Explanations (LIME) is a local technique capable of providing feature effects for individual points that can be extrapolated to form global explanations (although global explanations may not be a good approximation) [158]. The technique was implemented to deal with the TSA (classification) problem in [159], demonstrating how LIME can produce local explanations of a XGBoost model. In addition, LIME was also used in [160] for TSA *and* transient stability preventative control. To do so, the authors propose the construction of two separate ML models and use LIME to understand factors influencing local predictions of stabil-

ity status (i.e., classification). A key limitation with LIME is that defining the correct neighbourhood around the local instance for explanation is complex and, therefore, can lead to errors [130].

Although not addressing the transient stability problem, authors in [161] use Shapley values to identify generators with a high contribution to the damping prediction in a global context in order to rank generators for rescheduling in the small-signal stability problem. Results indicate that the predicted damping of an inter-area mode is improved after performing generation rescheduling informed by Shapley values.

The SHAP framework [162] (with foundations in Shapley values mentioned above) has been very recently applied in the power systems domain, however not in the context of understanding the complexities of the transient stability margin. SHAP is a model-agnostic local IML technique that can be extended to form global explanations. The SHAP framework often uses *approximate* Shapley values from cooperative game theory, which are defined as the average marginal contribution of a feature to all feature coalitions with that feature [163]. The SHAP framework is of the class of additive feature attribution methods, meaning that for a given model prediction, an effect is attributed to each feature. This means the feature effects on the model outcome are provided for a single point (i.e., local explanations)—in the units of the target (a key advantage that is explained later in this Chapter)—along with global feature importance across multiple points (i.e., global interpretations). The local explanations are "atomic units" of global interpretations, making them consistent [162].

For example, in [164] SHAP is used in the frequency stability problem. In [165], authors use SHAP values to determine the relationship between small-signal stability and topological graph metrics relating to connection of RES. SHAP is demonstrated to effectively determine the relationships between small signal stability and metrics of interest using a Random Forest (RF) regressor. Authors in [166] integrate SHAP with Dynamic Security Assessment (DSA) for critical unit detection using classification. However, the authors seek to gain insights into a classifier and do not consider the impact of RES; which is a key driver of nonlinear changes in the dynamic response in power systems [2] that must be better understood. In [167], RES is considered and

SHAP used to understand a ML model trained to predict stability status of the system.

5.5 Conclusion

Existing TSA methods are no longer suitable as a result of the loss of SG attributes, non-linear dynamics introduced by CIG and the intermittent nature of RES connecting at different locations to the network. Specifically, they do not adhere to the three desirable attributes for TSA methodologies that are set out in Section 5.1. Therefore, this Chapter introduced ML and IML for TSA, which can be used to identify explicit mappings of the complex transient stability problem, accelerate computationally heavy TDS and provide stability boundary insights.

The development of a ML-based methodology for TSA using a database of power system responses obtained via RMS-TDS (which capture the full dynamic response of CIG) can reduce online computational burden and enable rapid and accurate TSA. This addresses desirable attributes 1 and 3 (defined in Section 5.1). Initially, such methods could be used to direct computational effort of near real-time RMS-TDS until sufficient confidence is established for ML-based approaches to become standardised.

IML techniques can help overcome the accuracy-interpretability tension, which often limits the usefulness of ML in real-world applications due to a lack of transparency into how models reach predictions. Addressing accuracy and interpretability concerns is the first step towards real-world implementation of ML-based methods for TSA—and is a particular focus of this thesis. Insights into the transient stability boundary are advantageous for building confidence in ML for TSA, but also bolster existing knowledge of the transient stability boundary of a system (i.e., do the findings relate to domain expertise?), and/or infer new information/knowledge. Indeed, such insights enhance situational awareness and could be used to design transient stability enhancement measures for operational and/or planning timescales. Therefore, IML-based techniques can help address desirable attribute 2.

Having set out the three desirable attributes of TSA methods for modern power systems and outlined how IML-based methodologies would possess these attributes,

the remaining Chapters of this thesis focus explicitly on the design and development of such methods. More specifically, two key approaches are investigated in detail (the first being PFI; which is a global importance method, and the second being SHAP [162]). PFI provides a global feature importance measure that accounts for feature interactions that does not require retraining of the ML model, which is advantageous. SHAP is a technique that has very recently emerged, which has foundations in Shapley values from coalitional game theory which has certain guarantees around fairly allocating a pay-out. SHAP is primarily a local explanation method that provides feature effects. However, these local explanations can be aggregated to form global interpretations which are consistent. In addition, the feature effects can be used to derive feature importance. For this reason, research into the usefulness or otherwise of SHAP deal with the high dimensionality of the TSA problem is required.

Chapter 6

Identification of Important Power System Variables using Decision Trees and Permutation Feature Importance

6.1 Introduction

TSA of power systems is challenging due to the complexity of system dynamics and high dimensionality—this is exacerbated with the connection of CIG. In addition, Chapter 3 and 4 highlighted that the transient stability boundary of a given power system depends on a large number of factors, many of which vary over time (the supplementary studies in Appendix A also demonstrate this). Furthermore, the intermittency of RES also increases the number of operational scenarios that require TSA. In addition, transient stability is location-dependent, meaning that the stability margin may increase at one location and decrease at another. This can lead to spatial changes in the critical contingency, highlighting the importance of methods that consider the effect of contingencies at various locations—as highlighted in Chapter 4.

As a result of the changing system dynamics and increase in operational scenarios

requiring TSA, it becomes important to assess a much larger number of fault locations and form contingency lists appropriately. The formation of correct critical contingency lists is an important aspect, but equally as important is understanding the factors that influence the transient stability boundary. Indeed, such knowledge may be used to design stability enhancement measures. Therefore, the objective of TSA methodologies suitable for modern power systems should be to not only accurately determine the stability of an operational scenario but also identify the driving factors behind the outcome. Furthermore, this should be done sufficiently ahead of time to allow for preventive or corrective control measures (as outlined in the three desirable attributes set out in Section 5.1).

Traditional TSA methods such as TDS have limitations with respect to computational requirements, some of which can be overcome using ML. However, for ML-based methods to be widely adopted for TSA, the method should be both accurate and interpretable to increase confidence and understanding of underlying prediction mechanisms. Unfortunately, ML algorithms with higher accuracy tend to be opaque, inhibiting user trust and usefulness for designing transient stability enhancement measures. As outlined in Chapter 5, IML may be able to help overcome this challenge.

To address this, a system-wide location-based IML-based methodology is developed in this Chapter to (a) predict the transient margin and (b) provide details of the important power system variables that influence the stability boundary. More specifically, a series of location-specific DT regressors are trained to predict CCT on a locational basis. Since an error of the same magnitude for a short CCT is more significant than for a long CCT, MAPE is used as the cost metric for the DTs. Subsequently, important power variables and parameters for CCT prediction at each location are identified using PFI (which is selected in this case because it is a simple to implement means of obtaining global feature importance—see Table 5.1). In doing so, prediction of the stability margin for previously unseen operational scenarios can be obtained without the need to run computationally intensive TDS online, along with details of the power system variables and parameters involved in shaping the stability boundary. In addition, two approaches for predicting the minimum CCT and corresponding location are proposed.

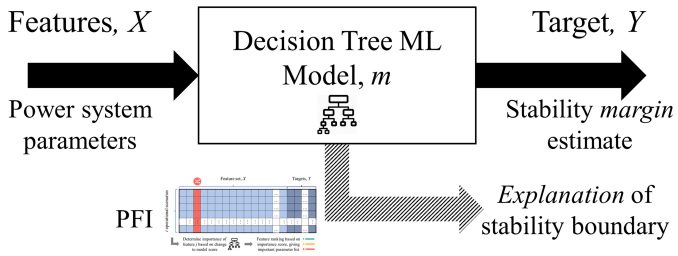

Figure 6.1: Generic Machine Learning (ML) block diagram illustrating proposed Decision Tree (DT) methodology overview with Permutation Feature Importance (PFI) explanation dimension.

Therefore, the proposed methodology is capable of (a) quantifying the transient stability margin on a locational basis (specifically, the CCT at each bus), (b) predicting the critical fault (both CCT_{min} and CFL) and (c) detailed insights into features impacting the stability boundary on a locational basis through interrogation of the locational DT models using PFI. In addition, feature threshold values can be extracted from the locational DT models. As a result, the original IML overview first given in Figure 5.1 can be updated to reflect DTs as the ML algorithm and PFI for model interpretability (Figure 6.1).

This Chapter seeks to demonstrate the effectiveness of the methodology outlined in Chapter 6 on an adapted version of the IEEE 39-bus test network (Figure 6.8); however, this method may be applied to any system. The network is selected because its dynamic behaviour has been extensively studied in the literature and therefore provides a good reference point.

An illustrative case study is provided demonstrating the ability of the method to track CCT_{min} in feature space as the operational scenario changes, as well as monitoring any locational shift in CFL. In doing so, an understanding of the underlying important power system features responsible for changes to the stability margin is provided. Furthermore, an example is provided where an important feature is used to target a stability enhancement measure, resulting in improvements in the stability boundary at that location.

In addition, a sensitivity analysis of the accuracy and interpretability of the method using different feature sets is conducted. Moreover, the efficacy of important feature

lists in designing targeted stability margin enhancement measures is demonstrated using two examples. Finally, potential options for reducing prediction errors are discussed. This includes changes to the DT cost metric used and changing the ML algorithm to an ensemble method. Changing the algorithm has some performance benefits; however, this is at the loss of detailed feature threshold values, which are available through the white-box DT algorithm. This trade-off must be considered when selecting the appropriate algorithm for use.

6.1.1 Contribution

The work presented in this Chapter has been published in the peer-reviewed journal IEEE Transactions on Sustainable Energy (see [J2]). A key contribution of the methodology proposed by this Chapter is the ability to identify important power system features on a locational basis, providing a system-wide perspective of features influencing the stability boundary, including the impact of RES. Whilst neither DT rule extraction nor ML model interpretation are novel in and of themselves, the extraction of important features and threshold values in the power system domain for stability margin prediction is a new contribution. More specifically, the key novel contributions from this Chapter include:

- a DT-based methodology capable of rapid transient stability margin prediction (specifically the CCT determined using RMS-TDS) and identifying the most important power system variables that impact it using PFI. This is done on a locational basis throughout the network, without the need to perform TDS online,
- including features related to physical system characteristics and economic dispatch (which dictates generator dispatch) enables the identification of complex trends impacting transient stability at different network locations. This approach can assist SOs and system planners in the design of targeted interventions,
- the use of maximum and minimum errors to assess ML model error in the context of TSA. This is important as a large error may result in an overly cautious dispatch or operation closer to the stability boundary than comfortable, and

- a method for generating location-specific 3D representations of the stability boundary in parameter space. The locational and graphical nature of the proposed method enables the identification of changes to the critical fault duration and location. Results can inform updates to credible contingency lists by being used as a fast-screening tool and inform the generation of rules for operational and planning decisions.

6.2 Methodology

The methodological details are given in Figure 6.2, where the off and online processes can be seen (black shaded and red unshaded respectively). A TSDb (outlined in Section 6.2.2) consisting of power system parameters and CCTs for each of the n fault locations across i operational scenarios is generated in the offline phase using RMS-TDS. The TSDb is then used to train n DT regressor models (outlined in Section 6.2.3) for local CCT prediction. PFI is subsequently applied to each location-specific DT model to identify the most important parameters for CCT prediction (outlined in Section 6.2.6).

A simplified illustration of this is represented on a fictitious network in Figure 6.3. It can be seen that a series of locational DTs are trained to predict CCT at each bus on the network. Locational important parameters are subsequently identified using PFI to interrogate each locational DT model. The extraction of locational important parameters enables a *system-wide parameter-space* representation of the stability boundary. In addition, threshold values for the locational important parameters from decision nodes in the DT models can also be extracted, adding an additional layer of information to the stability boundary representation. Since this method requires the extraction of rules from the DT models, the method is restricted to the use of DTs.

The prediction of CCT at each busbar means that an predict of the CCT_{min} and CFL can be derived (using locational CCT predicts in Equation 2.10, to determine the CCT_{min} and CFL predict). Whilst this is an effective means of determining the duration and location of the critical fault, no additional information about the important parameters that impact CCT_{min} explicitly can be derived. An additional method

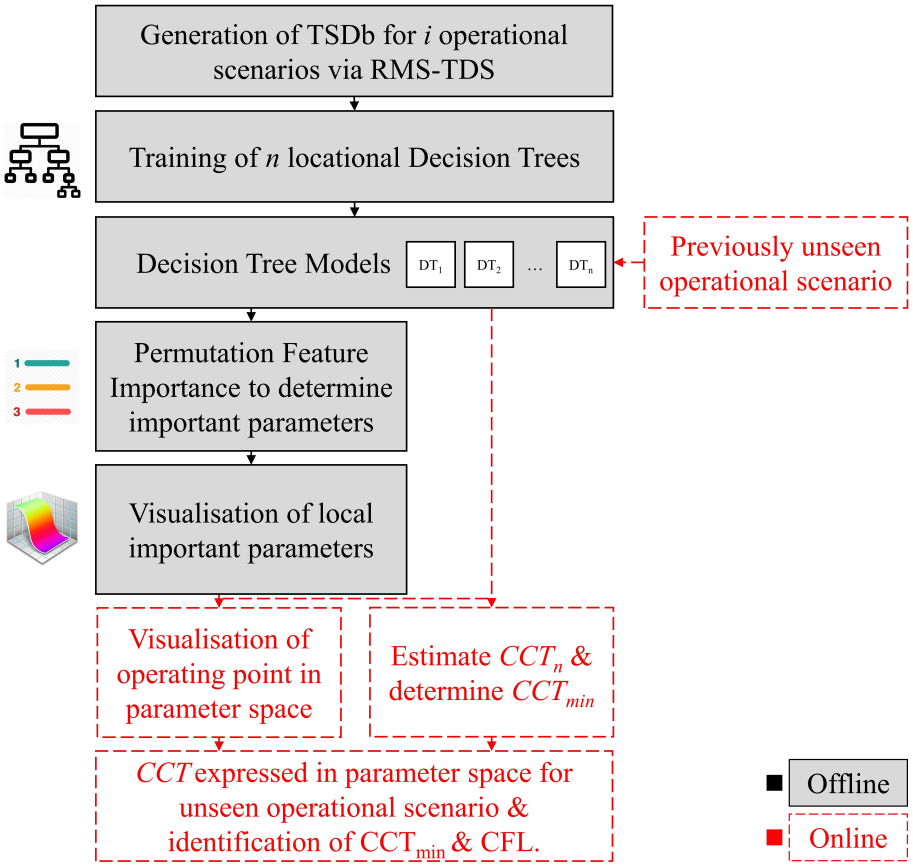

Figure 6.2: Proposed methodology flowchart for stability margin prediction and explanation.

for predicting the critical fault is proposed to overcome this. To do so, two additional columns are added as targets to the TSDb—CCT_{min} and CFL, which are both obtained via RMS-TDS. These two methods for critical fault prediction are highlighted in Figure 6.3 and summarised below.

- **Method *A***: *Derivation of the critical fault prediction from locational CCT predictions.* CCT_{min} is predictd by identifying the minimum CCT from each of the n locational DT model predicts and the CFL is taken as that location,
- **Method *B***: *Explicit prediction of the critical fault using additional DT models.* An additional DT regression model is trained specifically to predict CCT_{min}. In addition, a DT classifier is trained to predict CFL.

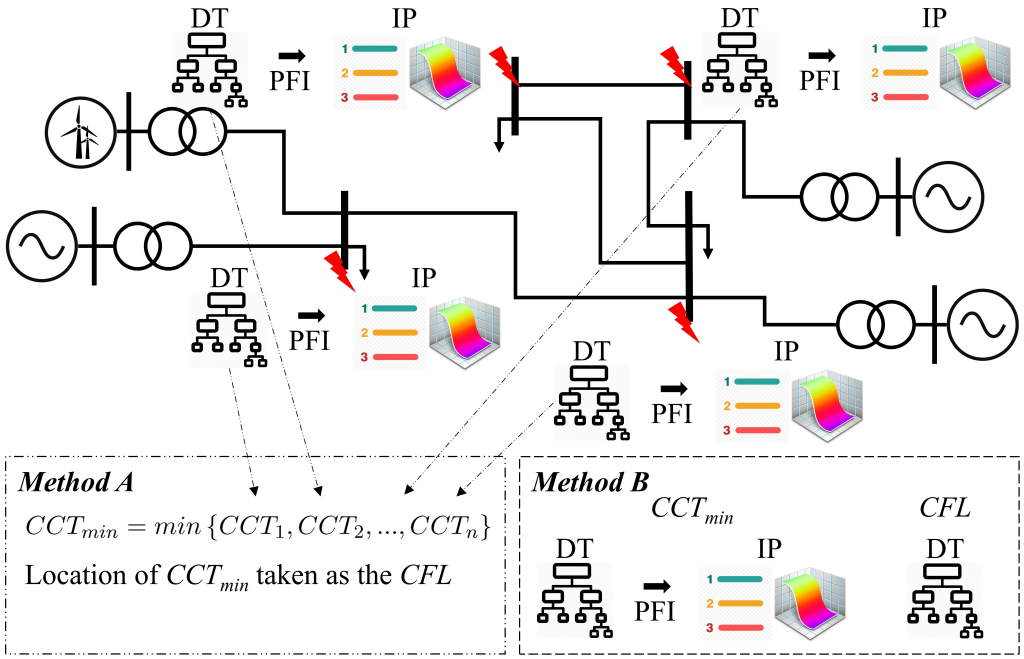

Figure 6.3: Illustrative four-bus network with locational DT models trained at each bus. PFI is applied to each DT model, revealing important parameters on a locational basis that can be visualised. Methods A and B for critical fault prediction summarised.

Both method A and B require the same computational effort for RMS-TDS, however method B explicitly trains trees to predict CCT_{min} and CFL. Consequently, method B offers additional details relating to the important features to CCT_{min} specifically compared to method A. Therefore, method B supplements method A by providing these additional details.

Although locational insights are provided in both methods, Method B is not contingent on the calculation of all CCTs and can also identify important parameters that impact CCT_{min}. The motivation for including both methods is to determine if there are significant differences in model error and illustrate the usefulness (or otherwise) of obtaining important parameters for predicting CCT_{min}.

In the online phase, previously unseen operational scenarios can be evaluated using the locational stability boundary representation (based on important features and threshold values extracted from DT models). This provides an informative and intuitive means of assessing the factors responsible for shaping the stability boundary.

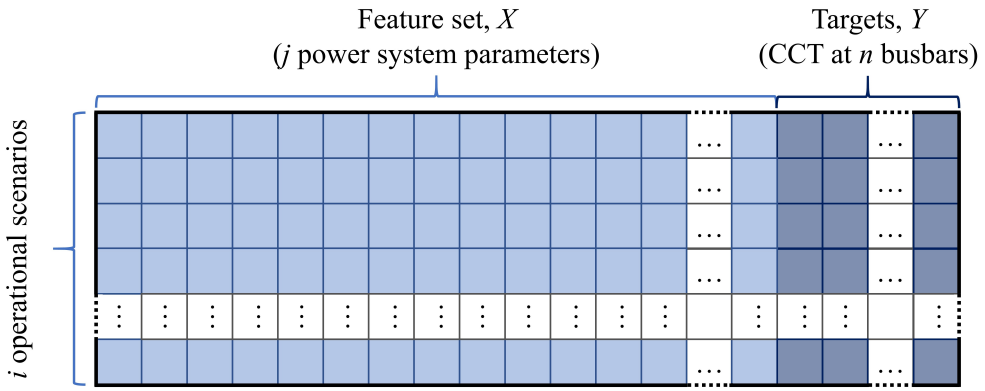

Figure 6.4: Transient stability database (TSDb) representation proposed by methodology—highlighting feature set (power system parameters) and targets (CCT at each bus for all operational scenarios).

6.2.1 Operational Scenarios and the AC Optimal Power Flow

Section 4.2.3 outlines the mathematical formulation. In this Chapter, the AC-OPF problem is used as a proxy to model the preference of a wholesale electricity system for dispatching generation that satisfies operational constraints. As a result, the OPF determines the setpoints of generators and, thus, significantly impacts transient stability. The AC-OPF is conducted in MATPOWER [106].

6.2.2 Transient Stability Database

As outlined in detail in Chapter 5, the fundamental concept behind ML methods for TSA is to train a model offline, capable of identifying the relationship between power system variables (features, X) and the transient stability of a system (target, Y), using a number of simulated responses that are representative of typical system conditions (i.e., credible operational scenarios).

In this case, the features are a set of power system variables and parameters. The target is the transient stability index of the system—specifically the CCT at a bus in the network. A TSDb consists of the features and target for each operational scenario. Since the locational trends in the stability boundary are of particular interest (for monitoring the critical fault), a separate TSDb is constructed for each bus on the network. The operational scenarios and features used in the TSDb remain unchanged

regardless of location, but the target changes based on location (i.e., the CCT at each bus). This is illustrated with various targets indicated in Figure 6.4.

Feature Selection

As outlined in Section 5.2.1—the features used may significantly impact the accuracy, interpretability, and ultimately the usefulness of the results. For this reason, the proposed methodology deliberately does not define which parameters to include to not limit the criteria above. Feature selection will depend on the network and operational scenarios considered. However, insights can be gained into the reasoning and motivations for feature selection in the case study in Section 6.3. Indeed, this is demonstrated in Section 6.5.1 where the impact of changing the feature set (from those defined in the case study presented in Section 6.3) on accuracy and interpretability is analysed in detail.

Target Selection

The target specified for use in this method is the CCT due to the ability of CCT (determined iteratively via RMS-TDS) to capture the full dynamic response of the system (including all control behaviour of generators). Since a locational approach is proposed—with a DT being trained to predict CCT at each bus on a network—the target varies depending on location.

To determine the CCT at every location on the network is computationally intensive, which increases with the physical size of the power system being analysed. One key advantage of the proposed method is that the computationally intensive processes can be conducted ahead of time (i.e., offline), where time is less expensive.

6.2.3 Decision Tree Regression

The proposed method uses DTs, which in the context of the impact of increasing RES output on transient stability is beneficial in three main ways. Firstly, DT models provide a means to interpret large numbers of operational scenarios, which tend to increase as more RES is added into the system. Secondly, DT regression is capable of

accurately making predictions of the target—in this case, locational CCT—even with complex non-linear relationships in the data. This reduces the need to run computationally intensive TDS close to real-time to determine the stability margin. Thirdly, DT models can deal with data sets containing large numbers of features and provide an intuitive representation of how these features influence the outcome. For example the threshold value—t_m for feature j in Equation 6.1 below—for the uppermost candidate split of an important parameter can be extracted from DT models, providing numerical limits for important parameters (which are identified using PFI) at the point of turning-points in the local stability margin.

The TSDb is partitioned using an 80:20% train:test split. The training portion of the data is used to train the locational DT models and determine feature importance. The testing portion of the data is reserved for analysis, representing previously unseen operational scenarios.

Decision Tree Algorithm Overview

The Classification and Regression Tree (CART) algorithm from scikit-learn package in Python [168] is used. The usefulness of the algorithm for regression in power systems is demonstrated in [149]. An overview of the mathematics behind the DT algorithm is provided below since later Chapters require this understanding to extract the threshold values for key parameters and variables.

DT models are a widely implemented ML approach that operates on the principle of recursively splitting training samples into smaller subsets (with similar target variables) in a top-down manner until a stopping criterion is met [169]. They are beneficial when there are complex non-linear relationships between features and the target—which is the case in the transient stability problem, especially as the penetration of RES increases.

DT models consist of a root node, branches, internal nodes and leaves. The root node is the starting point of a DT, which has no incoming branch. A branch is a connection between an upper (parent) and a lower (child) node. Internal nodes are those with incoming and outgoing branches. Each internal node (decision node) splits its sample set into two or more sub-classes following the defined splitting criterion.

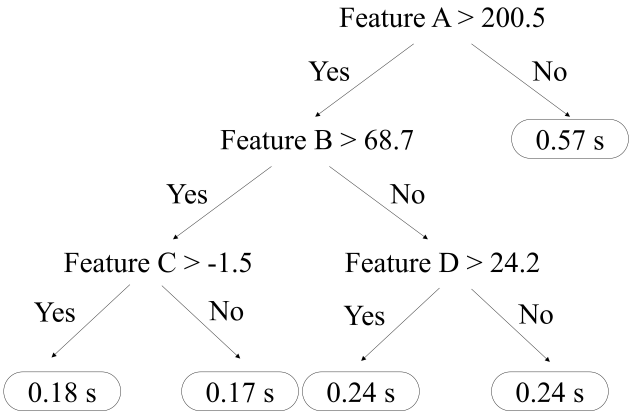

Figure 6.5: Illustrative example of a Decision Tree (DT) for Critical Clearing Time CCT prediction.

Nodes with incoming branches but no outgoing branches are leaf nodes (result nodes), which contain the terminal output decision. The DT is essentially formed on a series of if-then rules, which makes the internal process behind a DT model straightforward to interpret since each leaf node has an associated formula (Figure 6.5).

Specifically, for training vectors $x_j \in X$, with p where $j = 1, ..., p$ features and target vector Y, the DT recursively partitions the feature space, grouping data with similar target values. Let Q_m represent the data at node m be represented by with N_m samples. For each candidate split $\theta = (j,\ t_m)$ consisting of a feature j and threshold value t_m, data is partitioned into left and right subsets (Equation 6.1 and 6.2 respectively) [168].

The quality of the candidate split of the node is computed using the impurity cost function, where the goal is to minimise the impurity (Equation 6.4) recursively until the maximum depth is reached ($N_m < min_{samples}$). This can be varied depending on user requirements, but in this Chapter MAPE (Equation 6.5) is used. This is appropriate for CCT prediction since it accounts for the relative size of errors. This means that an error of the same magnitude for a short CCT is more significant than for a long CCT.

$$Q_m^{left}(\theta) = \{(x, y)|x_j \leq t_m\} \tag{6.1}$$

$$Q_m^{right}(\theta) = \frac{Q_m}{Q_m^{left}(\theta)} \tag{6.2}$$

$$G(Q_m, \theta) = \frac{N_m^{left}}{N_m} H(Q_m^{left}(\theta)) + \frac{N_m^{right}}{N_m} H(Q_m^{right}(\theta)) \tag{6.3}$$

$$\theta^* = argmin_\theta(G(Q_m, \theta)) \tag{6.4}$$

$$MAPE(x, \hat{x}) = \frac{1}{n} \sum_{i=1}^{n} \frac{|y_i - \hat{y}_i|}{max(\epsilon, |y_i|)} \tag{6.5}$$

DTs are sensitive to the data upon which they are trained. If the training data changes, the resulting DT can significantly change, changing the model predictions. In addition, DTs are computationally expensive to train, have a tendency for overfitting and tend to find local optima because they can not go back after they have made a split. Other (more complex) algorithms can overcome some of these limitations; however, these cannot be used in this method due to their black-box nature, limiting the ability to extract threshold values.

6.2.4 Recursive Feature Elimination with Cross-Validation Wrapper and k-fold Cross-Validation Model Scoring

Pruning redundant features results in removing features that have little predictive power, avoiding overfitting and improving model accuracy. Recursive Feature Elimination with Cross Validation (RFE-CV) is used on the training portion of the TSDb to do so. The wrapper-type algorithm selects the optimal number of features for a model by recursively removing features until the set of features that results in the best model score is identified (starting with the full feature set from the TSDb).

The model is then scored using repeated stratified k-fold cross-validation. The scoring approach splits the training data into k-folds (k = 10 in these studies) and is repeated n times ($n = 3$) with different randomisation in each repetition. The algorithm is trained on k – 1 folds, reserving the remaining fold as a test set. The performance model score is determined across each k-fold and n repeats. An average model score (using MAPE (Equation 6.5)) and standard deviation are determined (assuming a

Gaussian distribution of performance), resulting in a more accurate representation of the model performance. This provides a means of estimating the performance of a ML algorithm with less variance than a train:test split approach.

6.2.5 Additional Error Evaluation Metrics

During the training stages, the DT models are bench-marked using MAPE (Equation 6.5). For the final stage of analysis using the testing portion of the TSDb, two additional performance metrics are used in addition to the metrics detailed in Section 5.2.3.

Specifically, metrics relating to the maximum errors are also defined since an under-estimate of the CCT may result in an overly cautious dispatch. This may be good from a system security perspective but may result in increased costs. Conversely, an over-estimate may provide a false sense of security, potentially resulting in a higher risk of instability. For this reason, the Maximum Over-Estimate (MOE) (Equation 6.6) and Maximum Under-Estimate (MUE) (Equation 6.7) are determined. In addition, the MOE and MUE for the most critical faults (defined here as short-circuit faults, where the actual CCT < 0.30 sec) are also determined since a large error in a more critical fault may have more significant consequences.

$$MOE = max\left\{y_i - \hat{y}_i\right\} \tag{6.6}$$

$$MUE = min\left\{y_i - y_i\right\} \tag{6.7}$$

6.2.6 Model Interpretability: Permutation Feature Importance

In this Chapter, PFI (first introduced in [170]) is used to rank feature importance for DTs trained to predict the transient stability margin from a set of power system variables. Determining the most influential features (i.e., power system variables) on CCT estimation is important when seeking not only to ensure sufficient stability margin and enhance situational awareness but also in the design of transient stability enhancement measures.

PFI evaluates the change in the model score when individual features are permu-

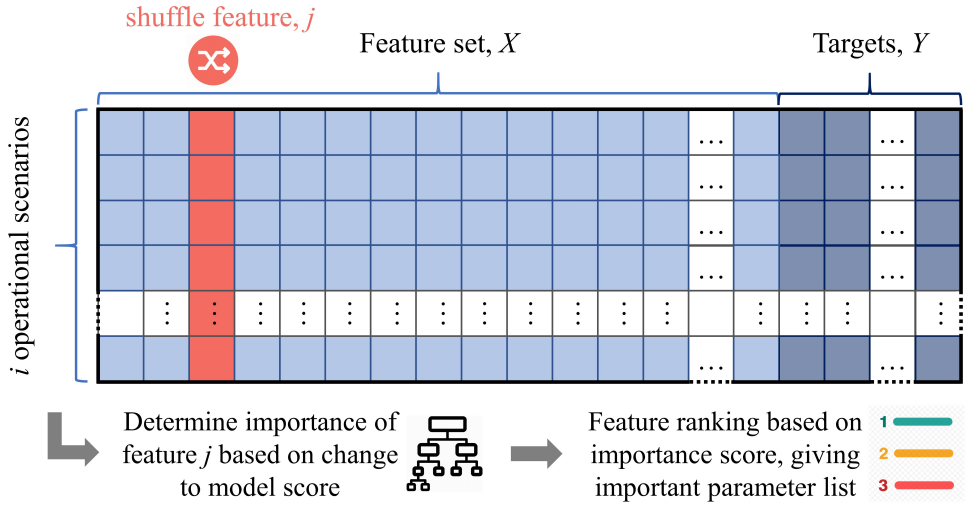

Figure 6.6: Illustration of Permutation Feature Importance PFI using the Transient Stability Database (TSDb) representation.

tated, breaking the relationship between the feature and the true outcome [170], thus determining the importance of that feature. This also means that any feature interactions are broken, meaning that both the main feature effect and interaction effects are captured. The reference score s of the model M for the dataset X with target vector Y is computed. For n repeats in $n = 1, ..., N$, each feature $j = 1, ..., p$ in the dataset is randomly permutated to generate a corrupted version of the data $\tilde{X}_{n,j}$. The score $s_{n,j}$ j of model M on the corrupted data is then computed, and the importance i_j of each feature is determined by Equation 6.8. The method only requires permutating each feature to determine its importance; therefore, computationally expensive model retraining is not required.

$$i_j = s - \frac{1}{n}\sum_{n=1}^{N} s_{n,j} \tag{6.8}$$

In the proposed method, PFI is applied to each location-specific DT model to rank features based on their importance for locational CCT prediction. The process is illustrated in Figure 6.6 and results in a location-specific ranking of features based on parameter importance for local CCT prediction. Extracting threshold values t_m from Equation 6.1 of important features is used to enhance the information about the

features. This provides a list of important values and thresholds, enabling a better understanding of parameters impacting the stability boundary. In the examples presented in this thesis, the threshold value of the uppermost candidate split is taken (since a decision node close to the root node is involved in a higher proportion of decisions than a decision node further away). Note that other threshold values can be extracted in the same way. The three top-ranked important parameters for each DT model are of particular interest for visualising the stability boundary. Note that the method gives an importance-ranked list of all parameters for each DT model that can also be referred to if required.

6.2.7 Feature-Space Stability Boundary Representation

A visual representation of the stability boundary at each location can be generated by combining the relevant important feature list (Section 6.2.6) and corresponding threshold values (Section 6.2.3). This is possible due to the white-box nature of DTs. Previously unseen operational scenarios can be superimposed onto the stability boundary representation, offering operational context with respect to the stability margin on a locational basis (relative to important features and key threshold values). The three top-ranked important features at each location are of interest for stability boundary visualisation on a cartesian coordinate system. The CCT at each location can be added as a fourth dimension to the colour axis. Threshold values t_m (Equation 6.1) for each important feature are extracted from the corresponding DT model and added as flat planes to the plot, highlighting key stability turning points in the feature space. In this thesis, only the uppermost candidate split is taken. Note that additional threshold values could be extracted from subsequent candidate splits in the DT depending on the level of detail required.

6.3 Feature Selection

Feature selection for use in a ML model may impact the accuracy and interpretability of the output of the model, both of which are crucial when considering the transient sta-

bility problem as described in Section 5.3. As previously outlined, the objective for ML methods dealing with the transient stability problem is to accurately determine the stability margin and identify the most important features behind the outcome—sufficiently ahead of time to allow for preventive or corrective control measures to be taken.

In Section 6.2.2, the feature selection is deliberately not specified to ensure that accuracy and interpretability can be optimised by the user for the specific network and operational scenarios of particular interest. The inclusion of too many parameters is dealt with by RFE-CV, which eliminates features with no predictive power (Section 6.2.4). Therefore parameters that may influence transient stability should be included in the TSDb. As such, a wide range of features is included for assessment.

	Standard	Physical	OPF
SG	$\mathrm{P}_{set}, Q_{set}, V_{set}$	MVA, H, $\mathrm{x}'_d, P_{min}, P_{max}$	
RES		$\mathrm{P}_{set}, Q_{set}$	
Network	$\mathrm{V}_{bus}, \delta_{bus}, P_{line}, Q_{line}$	$\mathrm{P}_d, Q_d, P_g, Q_g, P_{loss}, Y_{bus,key}$	
Other		*various other derived*	\$/MW/hr , LMP, KKT

Table 6.1: Details of variables included in each feature set for case studies using IEEE 39-bus test network.

For the case study presented here, three categories of feature sets defined are outlined below, along with a brief summary of the motivation behind including each set. An overview of the features is provided in Table 6.1, and a more detailed breakdown and explanations for including various parameters follow below.

- **Standard (Std)**: Parameters typically available form Phasor Measurement Units (PMUs) situated in a network. These parameters are the most frequently used in the literature for transient stability estimation.

- **Physical (Phy)**: Parameters relating to physical characteristics of network components, such as generator nameplate ratings and elements of the network admittance matrix. Motivation for testing the impact of this group of features stems from the impact on transient stability from the displacement of conventional SG

by RES. Insights into the impact of disconnection patterns on transient stability may be able to be obtained through the inclusion of such parameters.

- **Optimal Power Flow (OPF)**: Parameters obtained through solving the AC-OPF problem. Since the OPF problem is used as a proxy to model the preference of a wholesale electricity system for dispatching generation that satisfies operational constraints, the OPF problem has direct consequences for network stability.

6.3.1 Standard Features

In this context, '*standard*' features refer to features widely used in similar studies in the literature, which are often obtainable from PMUs. These parameters include the SG set-points (active power, reactive power and voltage set-point), system voltages (busbar voltage magnitudes and voltage angles), and line power flows (active power and reactive power). The relevance of these parameters is explored in Chapter 2, and numerous studies have showcased the use of parameters such as these in similar ML approaches.

6.3.2 Physical Features

The size and type of generators in a network and how they are connected together (i.e. the network layout) have a significant impact on transient stability [30], forming the motivation for including the '*physical*' feature set. Parameters included in this category relate to physical SG, RES and network parameters and can be further categorised into capacity and locational.

Generation and Demand

More specifically SG size (MVA rating), inertia (MVA.s), transient reactance (x'_d) minimum and maximum power capability, RES size (MVA rating) and demand at each bus. Including such parameters offers insights into the impact of displacement patterns on the stability boundary. The total active power generation, total reactive power generation, and total active power losses are also included.

Location-based

Several additional parameters are derived from the above based on generator location. These are the inertia level per area (e.g., total system and the total per area), non-synchronous penetration (ratio of RES to SG MVA), RES penetration (ratio of RES to total active power demand).

The proximity of RES to SG in the network was demonstrated to impact the dynamic response of the network due to LVRT capability of RES in Chapter 4. Since the pre-fault network topology (and thus network impedance) remains unchanged for all operational scenarios, the ratio between SG transient reactance (x'_d) and impedance from RES to the PCC in the same area is used (Figure 6.9). The admittance between busbars in a network can be obtained from the network admittance matrix [109], given in Equation 4.6. From the network admittance matrix (Y_{bus}), the impedance between RES and the network is used. In addition, the impedance between RES and the network is expressed as a ratio to the transient reactance (x'_d) of SGs in the same area.

6.3.3 Optimal Power Flow Features

Generator dispatch is determined using AC-OPF as a proxy (see Equation 4.1-4.4). Therefore, the dispatch is the consequence of the physical constraints (generator size, line capacity etc.) and the preference of a wholesale electricity system for dispatching generation that satisfies operational constraints.

The link between generator dispatch (via AC-OPF) and transient stability is the starting point of the TSC-OPF problem. A particular output of the OPF solution that is of interest is LMP of electricity at a location (bus), denoted by λ_n, and KKTs. Since LMPs account for the physical limitations of generators, the network, demand and cost Equation 4.1 - 4.4, they may provide some predictive power. Moreover, LMPs are traditionally used to identify areas with insufficient generation. Generation in such areas may run at high active power output due to a constraint, pushing these machines closer to the stability boundary. Finally, since KKTs only become non-zero once the constraint is active, KKTs can provide additional insight and a systematic means of identifying the active constraint. Therefore they could be used to inform

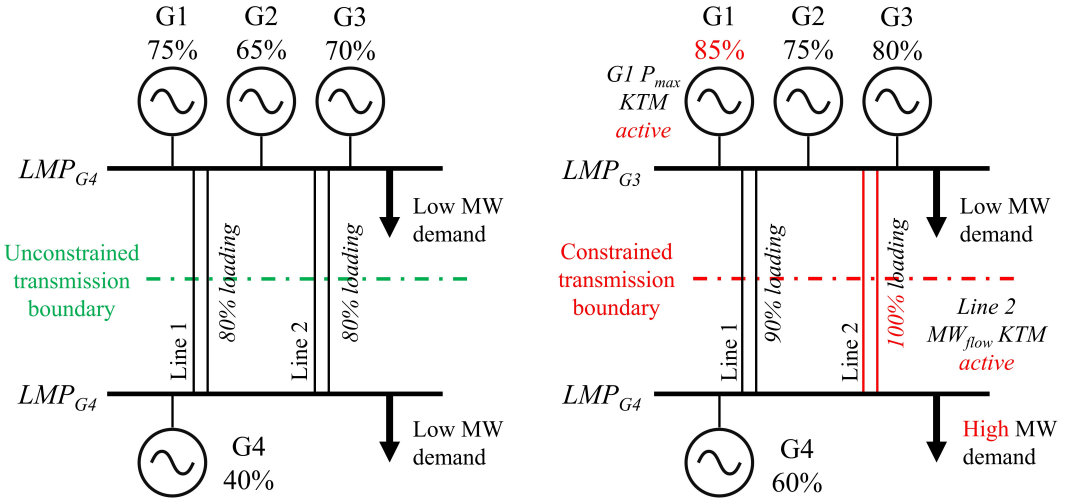

Figure 6.7: Illustrative example showing the impact on Optimal Power Flow (OPF) variables in an unconstrained vs constrained network.

planning decisions, e.g., identification of bottlenecks/constraints that frequently impact the stability boundary, which could be used to identify areas where reinforcements may be required. The cost of these reinforcements can be compared to the cost of re-dispatching to form the basis of a Cost-Benefit Analysis (CBA).

Figure 6.7 shows two different dispatches (one for *low* demand and one for *high* demand) on a fictitious network with some key OPF parameters displayed. In the *low* demand case, there are no active constraints in the network, so the LMPs are equal (set by the price of G4). In the *high* demand case, power flow on line 2 reaches its capacity, and G1 reaches its maximum active power output (i.e., there are constraints on the OPF problem). The constraint on line 2 means that G1-3 cannot service the higher demand on the other side of the constrained line. This causes the output of G4 to be increased, potentially deteriorating the transient stability in this area of the network.

6.4 Test Network and Case Study Design

6.4.1 IEEE 39-Bus Test Network Overview

The test network used (Figure 6.8) has a nominal voltage of 345 kV and frequency of 60 Hz. The total active power demand of the network is 6097.1 MW, modelled as

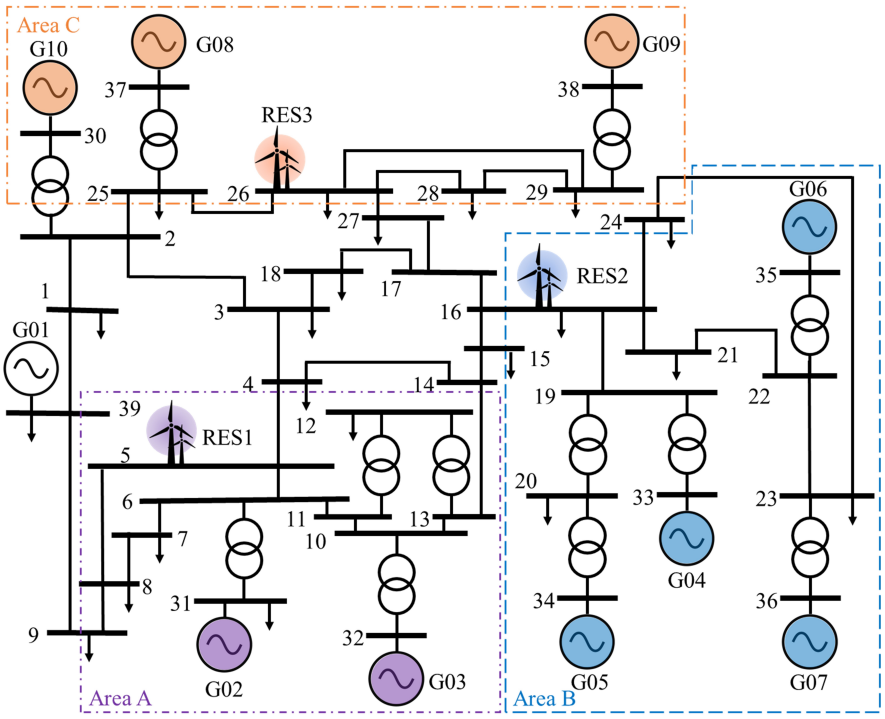

Figure 6.8: Adapted version of IEEE 39-bus test network to include a Type-4 Wind Farm (WF) at various locations.

balanced three-phase constant impedance loads in the dynamic simulations. SGs (G01-G10) are represented by full-detail four-winding 6^{th} order models. The slack generator is taken to be G01 without an AVR or PSS and represents the '*rest-of-system*', remaining unchanged throughout. G02-G10 are each equipped with an IEEE Type 1 AVR. The PSS is modelled based on [171]. Governors are IEEE Type G1 (steam turbine) for G02-G09 and IEEE Type G3 (hydro turbine) for G10 (full details in [172]). These machines are assumed to represent four equal-sized units to simplify disconnection stages in case studies. The network topology remains unchanged throughout the studies (i.e., no line tripping or network reconfigurations are studied).

IEC Type-4A wind turbines [103] are used to model wind generation in these studies. This means the dynamic characteristics of wind—including LVRT capabilities—on the dynamic response of the system is reflected in the CCT. Under the assumption that RES is not required by grid code to provide voltage control, the controller operates at a unity power factor, i.e., no reactive power is injected into the system. It should be

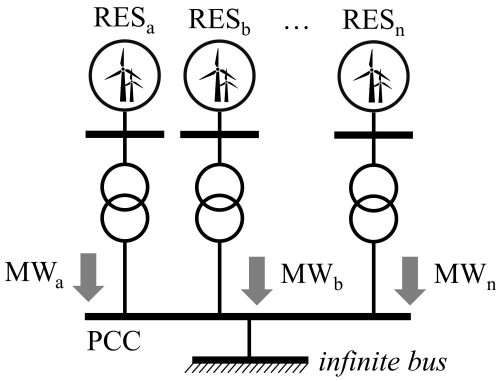

Figure 6.9: Method used for connection of Wind Turbine Generators (WTG) to a Point of Common Coupling (PCC).

noted that this capability may vary from system to system and will impact reactive power dispatch and, thus, transient stability. The WTGs have LVRT-capability and reactive power support. Reactive power injection is controlled as the pre-fault value plus an additional voltage-dependent reactive current injection during the fault and as the pre-fault value plus an additional constant reactive current injection post-fault. A WF is treated as an aggregate of individual 2 MW turbines connected in parallel. Each turbine has a separate transformer (Figure 6.9), where the total active power output of the WF at the PCC is the summation of each individual turbine's active power output. The volume of wind and its location on the network depends on the case study. Three generation areas (A, B and C) are defined (Figure 6.8).

6.4.2 Generator Dispatch via AC Optimal Power Flow

A full AC-OPF is implemented in MATPOWER [106] is used to establish generator dispatch, where cost coefficient values are allocated to generators as detailed in in Table 6.2 and subjected to the standard polynomial cost function (Equation 4.5). This resulting in cost-curves given in Figure 6.10 for SGs before any disconnection has taken place. As a SG is disconnected, the minimum and maximum active power capability change, thus changing the portion of the cost curve used. RES are considered to have zero marginal cost and therefore dispatched at full active power output.

	G02	G03	G04	G05	G06	G07	G08	G09	G10
c_0	0	0	0	0	0	0	0	0	0
c_1	2.8	4.7	2.8	3.6	2.5	3.7	4.8	3.7	3.9
c_2	0.0104	0.0088	0.0128	0.0113	0.0019	0.0094	0.0099	0.0111	0.0090

Table 6.2: Synchronous Generator (SG) cost curve coefficient values for polynomial cost-function.

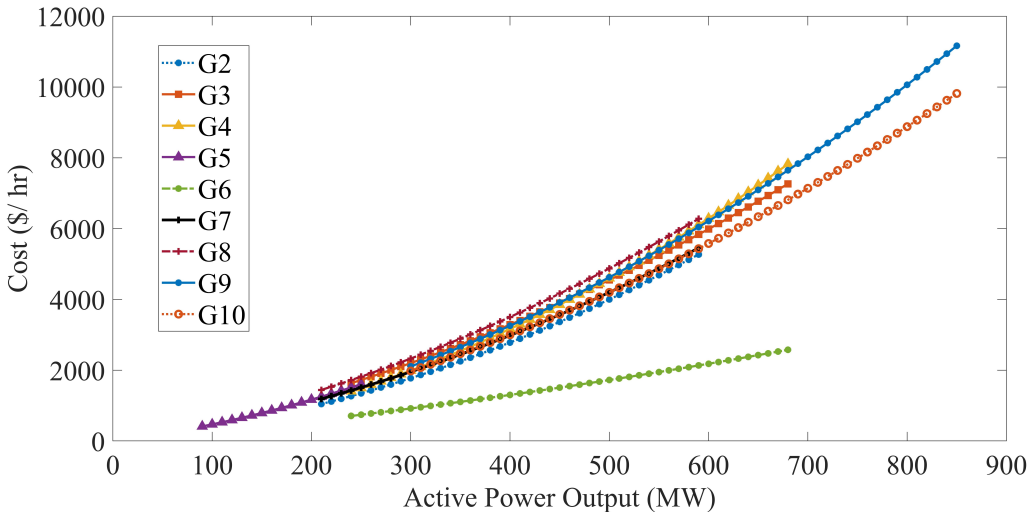

Figure 6.10: Cost curve functions allocated to Synchronous Generators (SG) in the IEEE 39-bus network.

6.4.3 Operational Scenarios

The range of case studies considered is designed to represent the various operational scenarios that may arise due to the displacement of conventional SG by RES (e.g., as WFs are constructed). Three parameters are varied to generate operational scenarios: SG level, RES penetration and system demand.

One SG is displaced at a time by RES connecting in the same network area. Each SG is taken to represent four equal-sized units, therefore each SG is disconnected in four stages (Equation 6.9). The new MVA rating of $SG_{MVA,new}$ is based the number of remaining generating units, u (where $u = 1, 2, 3, 4$ and is rated to $SG_{MVA,old}$). Should the network conditions or operational scenarios of interest change over time, it may be necessary to retrain the ML models with an updated set of scenarios.

$$SG_{MVA,new} = u\left(\frac{SG_{MVA,new}}{4}\right) \tag{6.9}$$

$$RES_{MVA} = r\left((5-u)\left(\frac{SG_{MVA,new}}{4}\right) + s(SG_{MVA,old})\right) \tag{6.10}$$

The capacity of RES connecting to the network is scaled in a similar, but inverse, manner (Equation 6.10). An additional penetration scaling factor, s (where $s = 0, -0.05, 0.05$), is included to decouple any proportional relationship between the decreasing SG MVA rating (and subsequent reduction in inertia) and increasing RES MVA rating. In addition, a RES scaling factor, r (where $r = 1$, 1.4), is applied to account for high-RES output scenarios. RES is rounded up to the nearest even value since each RES unit is rated at 2 MVA. Scenarios with no displacement are also considered. In addition, total system demand is varied uniformly throughout the network from 0.6 to 1.025 p.u. in 0.025 p.u. increments.

3906 operational scenarios are designed based on 18 demand levels, 36 SG disconnection stages (9 SGs, each disconnected in 4 stages) and 6 RES levels (summarised in Figure 6.11). The RES penetration in relation to SG capacity for generating areas A, B and C ranges from 0% to 131%, 59% and 54% respectively. This results in 3888 displacement scenarios, plus 18 scenarios with no displacement. From these 3906 operational scenarios, 144 (that is 3.7%) do not result in a successful convergence of the OPF solution. For the successfully converged scenarios (3762, that is 96.3%) RMS-TDS are executed using DIgSILENT PowerFactory, for all fault locations. Fault locations considered in this case study are three-phase-to-ground busbar faults excluding both the LV terminal busbars for all SGs (9 busbars) and all RES points of common coupling (3 busbars), resulting in a total of 27 fault locations.

If a single RMS-TDS was run for each operational scenario at each fault location (to calculate a fixed fault-time metric, such as those outlined in Section 2.5.1), a minimum of 101 601 simulations would be required. The iterative process required to determine CCT, means that the number of simulations required significantly exceeds this (by at least one order of magnitude), illustrating the usefulness of taking this process offline.

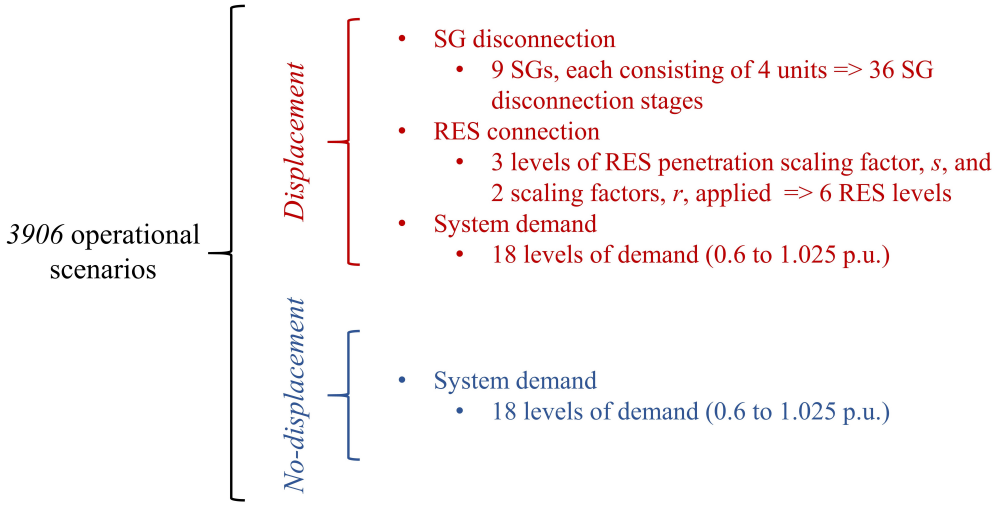

Figure 6.11: Breakdown of case studies used in the IEEE 39-bus network.

It takes in the region of 10-40 sec per operational scenario to calculate the CCT for a given fault using a Python script developed, meaning that the database creation takes in the region of 500 hours to obtain. This can be accelerated using high performance computers, running tasks in parallel and optimising the Python search script (e.g., improving the algorithm used in Figure B.1 in Appendix B by implementing golden-section search).

6.5 Results

6.5.1 Impact of Feature Selection on Accuracy

This section outlines the impact of feature selection (detailed above in Section 6.3) on accuracy (i.e., model error) and interpretability of the output of the method outlined in Section 6.2. Figure 6.12 illustrates how the feature set used for training the models impacts the average model estimation accuracy. In addition, the MOE and MUE also vary depending on the feature set (Figure 6.13).

Poorer performance is observed when 'OPF' or 'standard' parameters are used alone or together, and the inclusion of 'physical' parameters improves the performance. The performance improves when 'OPF & physical', 'physical & standard' and 'all' features

are used; however, no notable performance differences between these categories are observable. This demonstrates how feature selection can significantly impact the performance of—and, thus, confidence in—ML models for TSA. This is important for making accurate stability margin predictions and understanding the important variables and parameters influencing the stability boundary. This was outlined in Chapter 5, where it was noted that the inclusion/exclusion of features can not only impact accuracy—but also offer different insights into the stability boundary at the IML stage.

6.5.2 Accuracy and Interpretability using all Features

Since Figure 6.12 and 6.13 show that there is an insignificant difference between the performance of the method between 'OPF & physical', 'physical & standard' and 'all' feature sets—a full analysis using 'all' features is provided to open up interesting model interpretations at the PFI stage. The following section details key results and findings from implementing the proposed methodology on the IEEE 39-bus test network for the case studies previously described. Analysis of faults at bus 1 (B01) and bus 9 (B09) are excluded from the results since they rarely result in first swing instability.

Locational Critical Clearing Time (CCT) Estimation

The performance for each locational DT model is reported in full in Table 6.3 and graphically in Figure 6.14 for the 753 test cases (the testing portion (20 %) of the TSDb). Results show a high degree of accuracy for all trained DT models, with MAPE averaging 0.0127 % (ranging 0.0034–0.0245 % at B19 and B27 respectively). As previously described MAPE (Equation 6.5) is used as the cost metric during DT model building since it accounts for the relative size of errors, which is particularly important when estimating CCT. In addition, the results show strong performance in RSQ values averaging 0.9756 (ranging 0.9403–0.9975 at B10 and B21) and RMSE averaging 0.0279 sec (ranging 0.0037–0.0689 sec at B19 and B27). B12 achieves the highest accuracy across all metrics in general; however, results for B12 are impacted because B12 is connected to the transmission network via two step-down transformers (Figure 6.8). This results in only 1.20 % of cases resulting in first swing instability (as the maximum CCT

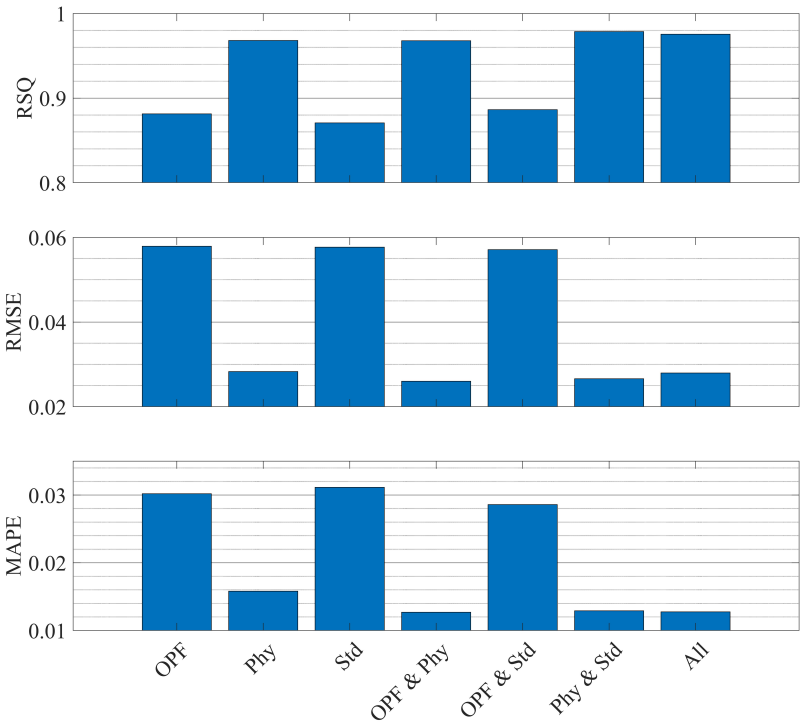

Figure 6.12: Average score (RSQ, RMSE and MAPE) across all locational Decision Tree (DT) models for each feature set tested.

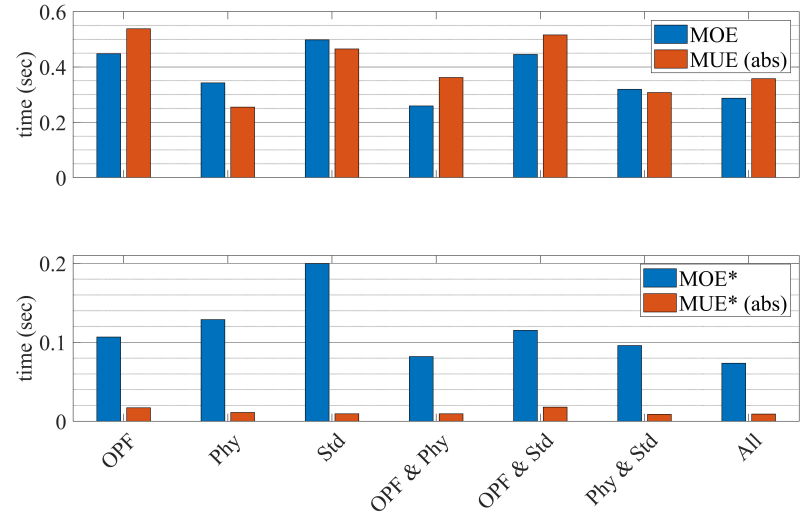

Figure 6.13: Top: maximum error (MOE and absolute MUE) across all locational Decision Tree (DT) models for each feature set tested. Bottom: average maximum error (MOE and absolute MUE) across all locational DT models for each feature set tested.

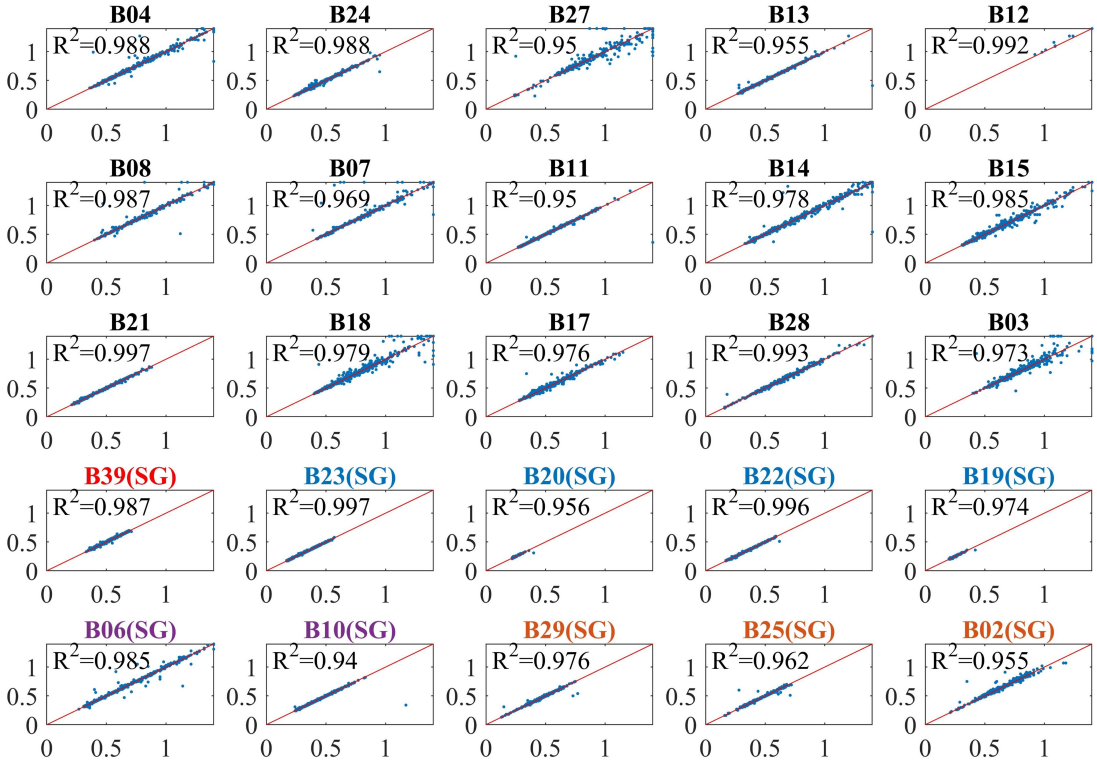

Figure 6.14: Locational Critical Clearing Time (CCT) estimation accuracy—actual vs predicted CCT in sec with RSQ for each bus.

of 1.4 sec is reached, which is the limit set in these studies). Results at this location should be taken in this context.

As previously outlined, MOE and MUE are calculated. This is because an under-estimate of the CCT may result in an overly cautious dispatch which may be good from a system security perspective, but may result in increased costs. Conversely, an over-estimate may provide a false sense of security, potentially resulting in a higher risk of instability. In many cases the MUE is significant, averaging 0.36 sec across all DT models (ranging 0.03–1.04 sec). However, large errors in the prediction of short CCTs is of even greater significance. For these most critical faults (taken as < 0.30 sec), the average MUE reduces to 0.01 sec (ranging 0.00–0.03 sec). Clearly, MOE and MUE metrics are capturing outliers that are significantly reduced when considering only short CCTs. This highlights the efficacy of using MAPE as the cost metric that the DT models seek to minimise during building when estimating CCT. The variation

Busbar	**B04**	**B24**	**B27**	**B13**	**B12**
MAPE (%)	0.0146	0.0138	0.0245	0.0105	0.0003
RSQ (sec)	0.9880	0.9880	0.9496	0.9547	0.9923
RMSE (sec)	0.0410	0.0164	0.0689	0.0378	0.0041
MOE (sec)	0.60	0.11	0.67	0.14	0.08
MUE (sec)	-0.57	-0.30	-0.47	-0.99	0.00
MOE<0.3 sec (sec)	n/a	0.01	0.67	0.14	n/a
MUE<0.3 sec (sec)	n/a	-0.02	-0.02	-0.01	n/a
Busbar	**B08**	**B07**	**B11**	**B14**	**B15**
MAPE (%)	0.0113	0.0159	0.0087	0.0186	0.0219
RSQ (sec)	0.9868	0.9690	0.9500	0.9776	0.9850
RMSE (sec)	0.0420	0.0648	0.0390	0.0504	0.0303
MOE (sec)	0.58	0.78	0.11	0.64	0.23
MUE (sec)	-0.61	-0.56	-1.04	-0.86	-0.22
MOE<0.3 sec (sec)	n/a	n/a	0.01	n/a	n/a
MUE<0.3 sec (sec)	n/a	n/a	-0.01	n/a	n/a
Busbar	**B21**	**B18**	**B17**	**B28**	**B03**
MAPE (%)	0.0092	0.0234	0.0196	0.0117	0.0220
RSQ (sec)	0.9975	0.9792	0.9765	0.9928	0.9732
RMSE (sec)	0.0077	0.0524	0.0245	0.0149	0.0554
MOE (sec)	0.04	0.47	0.41	0.21	0.67
MUE (sec)	-0.05	-0.49	-0.08	-0.08	-0.43
MOE<0.3 sec (sec)	0.04	n/a	0.01	0.21	n/a
MUE<0.3 sec (sec)	-0.03	n/a	0.00	-0.01	n/a
Busbar	**B39**	**B23**	**B20**	**B22**	**B19**
MAPE (%)	0.0081	0.0069	0.0041	0.0079	0.0034
RSQ (sec)	0.9868	0.9974	0.9560	0.9961	0.9740
RMSE (sec)	0.0081	0.0050	0.0045	0.0067	0.0037
MOE (sec)	0.05	0.03	0.02	0.03	0.02
MUE (sec)	-0.07	-0.03	-0.09	-0.11	-0.06
MOE<0.3 sec (sec)	n/a	0.03	0.02	0.03	0.02
MUE<0.3 sec (sec)	n/a	-0.01	-0.01	-0.03	-0.02
Busbar	**B06**	**B10**	**B29**	**B25**	**B02**
MAPE (%)	0.0146	0.0090	0.0098	0.0121	0.0166
RSQ (sec)	0.9854	0.9403	0.9759	0.9621	0.9553
RMSE (sec)	0.0340	0.0310	0.0150	0.0168	0.0243
MOE (sec)	0.34	0.07	0.16	0.32	0.40
MUE (sec)	-0.47	-0.83	-0.23	-0.20	-0.11
MOE<0.3 sec (sec)	0.00	0.07	0.16	0.32	0.10
MUE<0.3 sec (sec)	0.00	-0.02	-0.01	-0.02	-0.01

Table 6.3: Summary of all accuracy metrics for each location (bus).

Busbar	Area A (B06, B10)	Area B (B19, B20, B33, B23)	Area C (B02, B25, B29)
MAPE (%)	0.0118	0.0056	0.0128
RSQ	0.9629	0.9809	0.9644
RMSE (sec)	0.0325	0.0050	0.0187
MOE (sec)	0.21	0.03	0.29
MUE (sec)	-0.65	-0.07	-0.18
MOE <0.3 sec (sec)	0.04	0.03	0.19
MUE <0.3 sec (sec)	-0.01	-0.02	-0.01

Table 6.4: Summary of the average of all accuracy metrics for each generating area.

in model performance can be somewhat explained by the variation in the number of displacement cases considered for each area in the TSDb. For example, Area B has more displacement scenarios than the other areas since it comprises of four SGs. This means that the TSDb is populated with more cases with displacement in Area B than in the other two areas, resulting in an improvement in the accuracy of DT models in Area B (Table 6.4). This indicates that expansion of the TSDb over time would likely improve the overall estimation accuracy further.

Identification of the Duration and Location of the Critical Fault

A key highlight of the proposed method is the ability to identify both the CCT_{min} and CFL for a previously unseen operational scenario. The performance and advantages of the two proposed methods for CCT_{min} and CFL in Section 6.2 are compared. The actual versus predicted CCT_{min} for each method is given in Figure 6.15 and the performance metrics are given in Table 6.5. Both methods achieve a similar degree of accuracy in estimation of both CCT_{min} and CFL, however Method *B* reduces the size of the maximum error (notably the MOE improves from 0.16 to 0.09 sec). In terms of CFL estimation, Method *A* correctly locates the CFL in 96.5 % of test cases (727/753). For Method *B*—where a new classification DT is built with CFL as the target—CFL is correctly located in 96.1 % of test cases (724/753). The performance difference for CCT_{min} estimation between method *A* and *B* can be considered insignificant. However, the key advantage of Method *B* over *A* is that important parameters for CCT_{min}

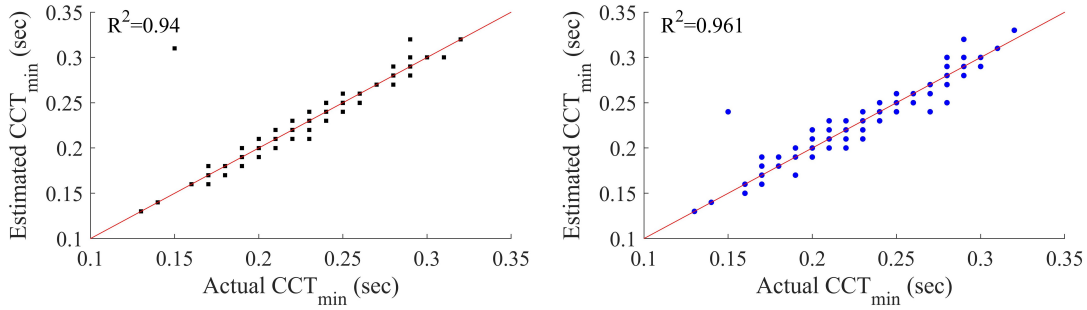

Figure 6.15: Comparison between the accuracy for estimation of the critical fault duration: method *A* (left) vs *B* (right). Actual vs predicted minimum Critical Clearing Time (CCT) (sec).

Busbar	Method *A* CCT_{min}	Method *B* CCT_{min}
MAPE	0.0057	0.0073
RSQ	0.9399	0.9605
RMSE	0.0068	0.0055
MOE (sec)	0.16	0.09
MUE (sec)	-0.02	-0.03
MOE <0.3 sec (sec)	0.16	0.09
MUE <0.3 sec (sec)	-0.02	-0.03

Table 6.5: Comparison between the accuracy for estimation of the critical fault duration across all accuracy metrics.

estimation can be determined (discussed below).

Identification of Changes in the Critical Fault

The efficacy of the method to identify variations in local CCTs that ultimately result in a variation in CCT_{min} and switch in CFL in the context of increased RES is illustrated using two example operational scenarios. Both scenarios have the same level of demand (0.9 p.u.). Scenario A has 280 MVA of RES3 connected to bus 26 and no disconnection of SG. In scenario B, three of the four generating units that make up G08 are disconnected, and RES3 is rated at 932 MVA.

Between scenario A and B, the CCT at B23 improves from 0.21 to 0.24 sec but CCT at B25 deteriorates significantly from 0.42 to 0.19 sec, as shown in Table 6.6. These two opposing locational trends ultimately lead to a deterioration in CCT_{min} from 0.21 to 0.19 sec and a switch in CFL from B23 (Area B) to B25 (Area A)—i.e., the CFL shifts

from one side of the network to the other. This example shows good accuracy, with each locational CCT being accurately predicted. In addition to this, CCT_{min} and CFL are correctly identified by and B (method *A* correctly predicts CCT and the CFL for scenario A, but incorrectly for scenario B in this instance). The method's capability to identify instances where the critical fault unpredictably changes (in both duration and location) due to displacement is of value to system planners and operators. Identifying such behaviours could inform the definition of credible contingency lists.

Operational Scenario details			Method *A* predictions				Method *B* predictions		Actual RMS-TDS results			
Scenario	RES3	G08	CCT B23	CCT B25	CCT_{min}	CFL	CCT_{min}	CFL	CCT B23	CCT B25	CCT_{min}	CFL
A (red circle)	280	700	0.21	0.42	0.21	23	0.21	23	0.21	0.42	0.21	23
B (red square)	932	175	0.24	0.19	0.19	25	0.19	23	0.24	0.19	0.19	25

Table 6.6: Exemplar operational scenarios demonstrating method efficacy in the identification of changes to the critical fault as a result of increased displacement.

Scenario	B23			B25			CCT_{min}		
	B14 LMP	G06 + G07 MVA	G07 MVA	G08 MVA	B01 LMP	Line 2-25 MVAr	B03 LMP	G08+G09 MVA	Line 20-34 MW flow
A	14.01	1500	700	700	9.35	-142.64	15.24	1700	255
B	13.16	1500	700	175	8.27	-73.96	14.50	1175	255
t_m	10.81	1225	525	437.5	8.56	-140.33	14.93	1187.5	236.34

Table 6.7: Parameter values for important parameters and uppermost threshold values (t_m).

Parameter Space Stability Boundary Representation

The application of PFI (outlined in Section 6.2.6) to gain global interpretations of each locational DT model, results in a location-specific ranking of parameters based on their importance for CCT estimation. The parameter space representation for B23 and B25 is given in Figure 6.16 and Figure 6.17 respectively, with scenario A (large red circle) and B (large red square) from Table 6.6 superimposed. Note that such plots are more interpretable when viewed in an interactive context, which is recommended when implementing the method. In addition, Figure 6.18 shows the parameter-space stability boundary representation for CCT_{min} estimation, using method *B*. The values of the important parameters at each location and for CCT_{min} are given in Table 6.7. A similar representation of the stability boundary can also be generated for all other locations. Since the example below demonstrates the method's capabilities well, important parameters for each location are provided in Table 6.8—rather than visualising the entire stability boundary.

A system planner or operator may reasonably conclude—through inspection of B23 stability boundary representation (Figure 6.16) that—to avoid such a significant reduction in the CCT at B23, disconnection of G06 or G07 should be avoided. Similarly, G08 should remain connected as far as possible should the stability of the system following a B25 fault be of concern. Whilst this is informative of locational trends, the overall stability boundary can be assessed through analysis of Figure 6.18. These are identified as B03 LMP, displacement of G08 and G09 and the dispatch of G05. The parameter space is partitioned using the uppermost threshold value of each important parameter from the DT, giving an indication of critical values for each important parameter where CCT_{min} worsens. For example, when B03 LMP > 14.93 \$/MWh (red surface in Figure 6.18), CCT_{min} is on average 23 % higher than if LMP < 14.93 \$/MWh. Similarly, if G08 and G09 combined MVA rating > 1187.5 MVA, CCT_{min} is 25 % higher than if less than this threshold. Finally, if line 20-34 active power flow < 236.34 MW, the average CCT_{min} is 15 % higher. When all three parameter thresholds are crossed, CCT_{min} is on average 29 % lower, providing situational awareness of CCT_{min} with respect to these important parameters. Combining this with the locational stability boundary

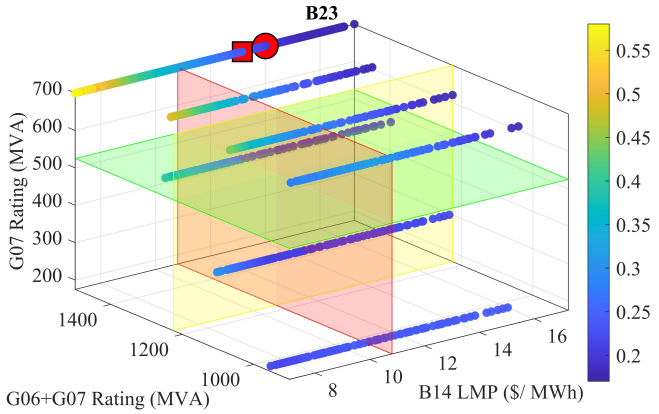

Figure 6.16: Important parameter space representation of B23 stability boundary showing scenario A (large red circle) and scenario B (large red square).

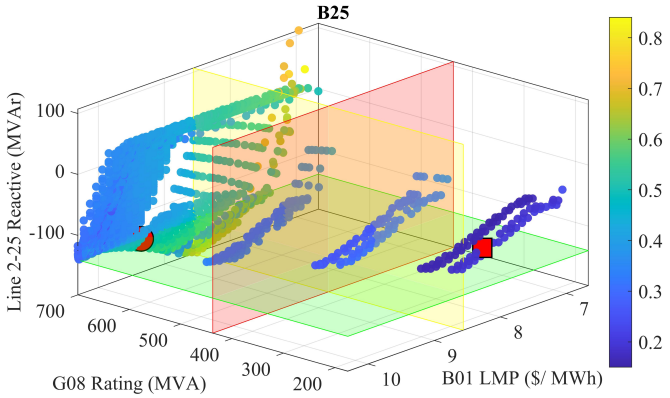

Figure 6.17: Important parameter space representation of B25 stability boundary showing scenario A (large red circle) and scenario B (large red square).

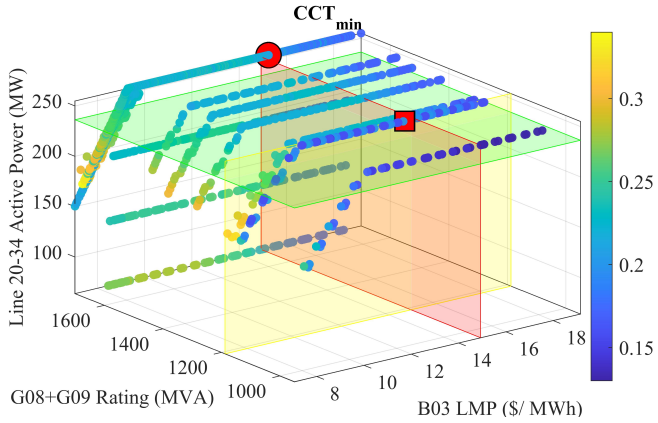

Figure 6.18: Minimum Critical Clearing Time (CCT_{min}) (colour axis) expressed with respect to the three top-ranked parameters. Uppermost Decision Tree (DT) threshold values (t_m) are included as flat surfaces, partitioning parameter space and highlighting operational zones that result in longer or shorter CCT_{min}.

	B04	**B24**	**B27**	**B13**	**B12**
IP1	B04 LMP	Line 12-11 MVAr	B03 LMP	B04 LMP	B14 LMP
IP2	G03 x'_d	Area B MVAs	G09 x'_d	G03 x'_d	B19 LMP
IP3	B13 LMP	B14 LMP	Line 5-6 MW	B11 LMP	B32 LMP
	B08	**B07**	**B11**	**B14**	**B15**
IP1	B16 LMP	B08 Q_LMP	B04 LMP	B04 LMP	Line 12-11 MVAr
IP2	G03 x'_d	B16 LMP	G03 MVA	G03 x'_d	B36 Vang
IP3	KKT Line 2-3	Line 1-39 MW	B11 LMP	G03 MW set	B03 LMP
	B21	**B18**	**B17**	**B28**	**B03**
IP1	B14 LMP	B03 LMP	KKT Line 2-3	G09 x'_d	B16 LMP
IP2	G06+G07 MVA	Line 6-31 MW	Line 19-20 MVAr	B26 LMP	G08 MVA
IP3	B03 LMP	Line 23-24 MW	B03 LMP	B27 LMP	Line 23-24 MW
	B39	**B23**	**B20**	**B22**	**B19**
IP1	Line 1-39 MW	B14 LMP	G05 MW set	B14 LMP	Line 20-34 MW
IP2	B01 LMP	G06+G07 MVA	B20 LMP	G06+G07 MVA	RES2-G04
IP3	Line 2-25 MW	G07 MVA	B14 Vang	Line 23-36 MW	G04+G06 MVAs
	B06	**B10**	**B29**	**B25**	**B02**
IP1	B20 LMP	G02 x'_d	G09 x'_d	G08 MVA	G08+G10 MVA
IP2	G03 MVA	B04 LMP	B27 LMP	B01 LMP	RES3-G09
IP3	KKT V B01	B11 LMP	Total Cost	Line 2-25 MVAr	B25 LMP

Table 6.8: Three top-ranked important parameters at each location (bus).

information provided by the DT models distributed throughout the network provides a network-wide view of the stability boundary. For example, one could suggest that dis-

connection of G06 and G07 worsens the stability for B23 faults but may be preferable in terms of overall stability to disconnection of G08. Interpretations such as this should come with a caveat (particularly if seeking to take control action based on results) since there may be correlations in the features, and the true cause of the stability boundary trend may be due to some other variable.

6.5.3 Location-Targeted Stability Boundary Intervention

Identifying important parameters on a locational basis enables the manipulation of important parameters to improve the stability margin at that location. The efficacy of changing an important parameter at a given location is tested by changing the parameter and re-running the RMS-TDS to determine the new stability margin, described in Figure 6.19.

Figure 6.19: Procedure for important parameter manipulation for stability margin improvement.

Stability Margin Improvement at B17 using OPF Parameters

The potential usefulness of including OPF parameters in the TSDb was discussed in Section 6.3.3. In particular, a divergence in LMPs in the network and the use of KKTs to identify active constraints.

The most important feature for CCT estimation at B17 is identified as the KKT for line 2-3 power flow (Table 6.8), which coincides with a divergence of LMP at B03. The KKT for line 2-3 power flow only becomes active once the constraint is active (i.e., remains zero until the power transfer on the line is equal to or greater than the line capacity). As such, this bottleneck in the network and the extent to which it impacts the final OPF solution is only identified because OPF parameters were included in the TSDb and would not be identified through the line power flows alone. The efficacy of the proposed method in identifying parameters that do indeed impact the stability

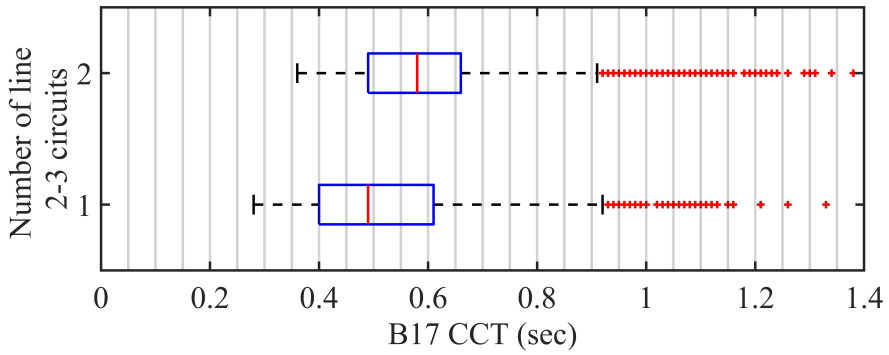

Figure 6.20: Important parameter manipulation for stability margin improvement at B17.

boundary (and can therefore be manipulated to improve the stability margin) is tested by increasing the capacity of line 2-3 (Figure 6.8). This is achieved by adding an additional identical circuit, re-running the OPF and running RMS-TDS to determine CCT at B17 across all operational scenarios.

Figure 6.20 shows the impact on B17 CCT when the capacity of line 2-3 is doubled. The lower extreme CCT for a B17 fault increases from 0.28 to 0.39 sec (39% improvement) and the median CCT increases from 0.49 to 0.58 sec (18% improvement). The upper extreme CCT does not change significantly, however, it decreases slightly from 0.92 to 0.91 sec (1% deterioration). This is sufficiently long to not be of concern since other fault locations are likely to be more critical in such an instance.

Improving the stability boundary at B17 reduces the likelihood of CCT_{min} occurring at this location. However, other locations may be adversely impacted by unintended consequences of the proposed network reinforcement. For example, removing the line 2-3 bottleneck means that G08 and G10 can export more active power, potentially reducing the CCT for short circuits near their terminals. Therefore, once a solution has been proposed, the entire method (including reconstruction of the TSDb) must be repeated to establish the shape of the new stability boundary and the new location-based important parameters. Note that any significant changes (e.g., changes to network topology, or operational strategies) requires periodic updates of the TSDb and thus, model retraining. Table 6.9 illustrates the extent of the change to the important parameter list at B17 after the above-described reinforcement after rerunning the

method for this location.

	Number of Line 2-3 circuits	
	1	2
IP1	KKT Line 2-3	Line 11-12 MVAr flow
IP2	Line 19-20 MVAr flow	total cost
IP3	B03 LMP	Area 2 total MVA rating

Table 6.9: Three top-ranked important parameters at B17 before and after line 2-3 reinforcement.

In this instance, the capital cost to build another circuit for Line 2-3 can be compared with other mitigating actions such as; manipulation of dispatch over a given time period or installation of braking resistors nearby SGs prone to instability.

6.6 Computational Details

The training time for the ML algorithm is conducted offline when time is not expensive; as such, the time required to train is not that important. The RMS-TDS and ML training were conducted on an Intel® Core™ i7-6700 CPU @3.40GHz with 16 GB installed RAM. A single DT can be trained using this PC specification in approximately 130 minutes using the TSDb that was generated offline ahead of this stage. The time-critical stage is the estimation of the stability margin, which can be achieved in approximately 0.2 sec, using the pre-trained ML algorithms. This is significantly shorter than calculating CCT using automated RMS-TDS which is an iterative process that may exceed 10 sec in some instances.

6.7 Discussion: On the Merits of Including Optimal Power Flow Features

Parameters included in the TSDb for the case study presented above included both pre-fault operational and physical parameters to assist in the identification of how operational decisions and displacement patterns impact stability. The inclusion of OPF parameters in the method is only of value if (a) they enhance prediction accuracy or (b)

they offer additional insight into the stability boundary. Upon repeating the method above for the same operational scenarios—but excluding the OPF parameters—no material difference in performance was observed. Since there is no performance benefit from including OPF parameters, a discussion around the potential benefits in terms of interpretability is given below.

OPF parameters such as LMP encapsulate multiple parameters in a single value, as described in Equation 4.1-4.4. Moreover, KKT can identify constraints/ bottlenecks, offering additional insights. The LMP at a busbar represents the cost associated with meeting that bus's next unit of demand. In a system with comparatively priced generation (as in this Chapter), a high LMP is associated with a lack of generation in an area and is often used as a signal to indicate where there is insufficient generation capacity. Conversely, a low LMP is a signal for demand to connect. It follows that LMP in the context of transient stability is an indicator for the loading of nearby SGs with respect to RESs output and demand level. This indicates that highly loaded SGs in an area results in poor transient stability. As such, LMPs could be an indicator for requiring some preventative measure. These may include (but are not limited to) operationally limiting the output of SGs in that area to maintain lower local LMPs or technological solutions such as braking resistor installations in areas with consistently high LMPs. KKTs give the cost associated with an active constraint. A divergence of LMPs at different locations indicates an active constraint in the system, meaning that the least-cost dispatch cannot be achieved due to some constraint. Such a constraint can be identified through the other KKTs (e.g., KKT for the maximum power output of a generator)—where a non-zero value for a KKT indicates an active constraint. This points towards the root causes of divergence of LMPs and may assist in the design of transient stability enhancement measures (e.g., corrective control actions or network reinforcement). Candidate measures can be validated using full RMS-TDS to assess their impact before implementation.

In addition, the OPF solution provides a means of assessing the cost implications of moving to a new—more transiently stable—operating point. For example, the cost of moving from scenario B to A would be 6,858 \$/hr for a 0.02 sec improvement in $\mathrm{CCT}_{\mathrm{min}}$.

Similarly, the cost of a network reinforcement can be compared. This could form the basis of a cost-benefit analysis for assessing technological vs operational transient stability improvement methods.

A focus for future work could also build on this, developing a new optimisation problem seeking to maximise CCT_{min} and minimising cost with respect to the important system parameters.

6.8 Machine Learning Model Performance Improvement Options

Despite the high degree of accuracy for the method previously described, changing the cost metric for the DT algorithm or, indeed, changing the ML algorithm itself could offer additional performance gains. Therefore, these aspects are investigated below using the same case studies outlined previously to assess whether there is a meaningful benefit.

6.8.1 Impact of Changing the Decision Tree Cost Metric

As previously described MAPE (Equation 6.5) is used as the cost metric during DT model building since it accounts for the relative size of errors, which is particularly important when estimating CCT. However, should the outliers described above (captured by the MOE and MUE metrics) be of concern, the cost metric for the models can be modified to include a square in the error term (e.g., Mean Squared Error (MSE) in Equation 6.11). In changing from MAPE to MSE outliers can be reduced, as detailed in Table 6.10. In addition, the performance for estimating the critical fault via both methods A and B are given in Table 6.11.

$$MSE = \frac{1}{n}\sum_{i=1}^{n}(Y_i - \hat{Y}_i)^2 \tag{6.11}$$

	DT MAPE	DT MSE	Change (%)
MSE (sec^2)	0.0009	0.0006	-30.3
MAPE (%)	1.19	1.12	-5.82
RSQ	0.9756	0.9790	0.35
RMSE (sec)	0.0223	0.0191	-14.3
MOE (sec)	0.24	0.18	-24.1
MUE (sec)	-0.18	-0.17	-4.07
MOE<0.3 sec (sec)	0.0331	0.0206	-37.7
MUE<0.3 sec (sec)	-0.0144	-0.0063	-56.5

Table 6.10: Decision Tree (DT) performance comparison between using MAPE or MSE as cost metric (average over all locations).

	Method *A*	Method *B*
MSE (sec^2)	0.000018	0.000019
MAPE (%)	0.70	0.69
RSQ	0.9761	0.9744
RMSE (sec)	0.0043	0.0044
MOE (sec)	0.03	0.02
MUE (sec)	-0.02	-0.03
MOE<0.3 sec (sec)	0.00	0.01
MUE<0.3 sec (sec)	-0.01	-0.01

Table 6.11: Decision Tree (DT) performance comparison: method *A* vs *B* using MSE cost metric.

6.8.2 Impact of Changing the Machine Learning Algorithm

In general terms, as the complexity of the algorithm increases (i.e., moves towards more of a black-box) accuracy tends to improve (as outlined in Figure 5.3). This is ultimately a design choice and will depend on both the application and what is deemed to be an acceptable degree of accuracy. This section is intended to demonstrate this principle by comparing the DT algorithm with the RF algorithm.

DTs are a simple algorithm constructed using the principle of recursively splitting training samples into smaller subsets (with similar target variables) in a top-down manner until a stopping criterion is met. RF is an ensemble method where multiple DT models are trained, generating a '*forest*'. In doing so, several weak homogeneous learners, trained in different ways, are generated—improving the performance compared

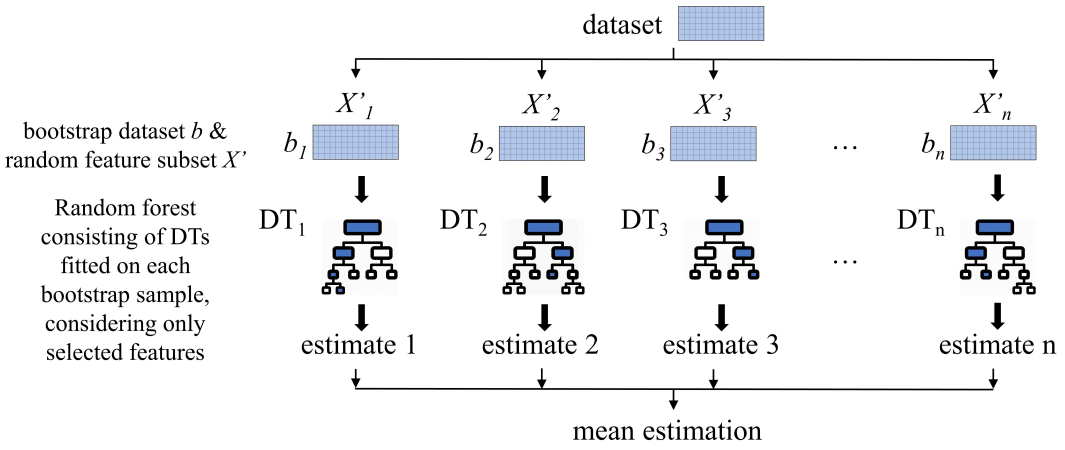

Figure 6.21: Random Forest (RF) algorithm structure.

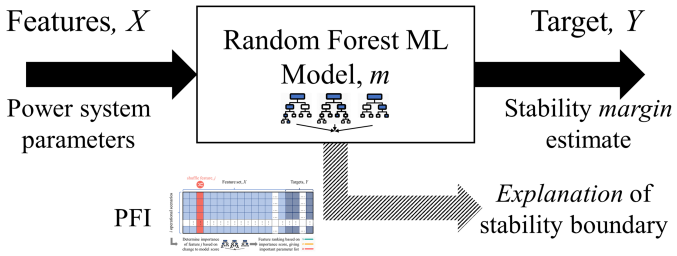

Figure 6.22: Generic Machine Learning (ML) block diagram illustrating proposed Random Forest (RF) methodology overview with Permutation Feature Importance (PFI) explanation dimension.

to a single model. The RF algorithm [173] is a bagging method where an ensemble of DTs, fitted on bootstrap samples, are combined to produce an output with lower variance. In addition to using bootstrap samples, features used to train each tree are also sampled (retaining a random subset of features for each tree). Figure 6.21 provides a graphical overview of RF. Whilst DTs offer some advantages over RFs, relating to interpretability and simplicity, the ability of RFs to leverage the power of multiple DTs means a higher accuracy is typically achievable. Although RF can determine feature importance, impurity-based feature importances can be misleading for high cardinality features—as is the case in [166]. Since RF randomly selects features during training, one specific set of features is not relied upon, meaning that RFs can generalise over the data more effectively than DTs.

The accuracy-interpretability tension, also introduced in Chapter 5, is therefore

revealed. For the particular application proposed in this Chapter, sufficient detail around parameter thresholds cannot be extracted from the RF algorithm due to the opaque nature of the algorithm. The IML framework first introduced in Figure 5.1 is updated to reflect the change in ML algorithm (Figure 6.22).

Improvement in Estimation Accuracy

The steps outlined in Section 6.2 are repeated, only the algorithm is changed from locational DT models to locational RF models. The performance achieved at each busbar is reported in Table 6.12 and the actual versus predicted CCT at six locations for both the DT and RF models are given in Figure 6.23 (where DT and RF predictions are represented by blue circles and black squares respectively). Note that all locations are given in Figure B.2 in Appendix B. While Table 6.12 can be compared directly to Table 6.3, a summary of the average performance change is given in Table 6.13. Here it can be observed that the RF algorithm performs better than the DT over most performance metrics. The one metric where DT outperforms RF in this case is MAPE. This is because the DT seeks to minimise MAPE, whilst the RF seeks to minimise MSE. However, RF outperforms DT across all other performance metrics (RSQ, RMSE, MOE and MUE).

Most locational RF models perform better than DT models, a performance deterioration is observed at B20 and B19 in terms of MAPE, RSQ, MSE and RMSE. However, the performance achieved is still very good, and the MOE and MUE metrics remain unchanged.

Critical Fault Estimation Accuracy

Along with the locational improvements in estimation accuracy, the accuracy for estimation of CCT_{min} using both method A and B remains comparable between the DT and RF algorithms (Figure 6.24 and 6.25). This suggests that in this instance, the DT models are stable, and the benefits of using the ensemble RF algorithm are thus limited in this example.

Busbar	**B04**	**B24**	**B27**	**B13**	**B12**
MAPE (%)	1.31	1.71	1.77	1.34	0.02
RSQ	0.9966	0.9946	0.9744	0.9980	0.9926
RMSE (sec)	0.0222	0.0115	0.0487	0.0091	0.0034
MOE (sec)	0.32	0.11	0.44	0.06	0.05
MUE (sec)	-0.16	-0.08	-0.37	-0.05	-0.05
MOE<0.3 sec (sec)	n/a	0.02	0.02	0.06	n/a
MUE<0.3 sec (sec)	n/a	-0.01	0.00	-0.01	n/a
Busbar	**B08**	**B07**	**B11**	**B14**	**B15**
MAPE (%)	1.31	1.31	1.28	1.63	1.87
RSQ	0.9924	0.9918	0.9977	0.9955	0.9934
RMSE (sec)	0.0320	0.0332	0.0095	0.0229	0.0204
MOE (sec)	0.35	0.32	0.05	0.25	0.10
MUE (sec)	-0.21	-0.28	-0.06	-0.18	-0.11
MUE<0.3 sec (sec)	n/a	n/a	-0.01	n/a	n/a
Busbar	**B21**	**B18**	**B17**	**B28**	**B03**
MAPE (%)	1.55	1.58	1.69	1.46	1.67
RSQ	0.9978	0.9943	0.9925	0.9887	0.9857
RMSE (sec)	0.0087	0.0276	0.0145	0.0108	0.0405
MOE (sec)	0.03	0.13	0.08	0.04	0.28
MUE (sec)	-0.04	-0.28	-0.11	-0.18	-0.34
MOE<0.3 sec (sec)	0.02	n/a	0.00	0.01	n/a
MUE<0.3 sec (sec)	-0.02	n/a	-0.01	-0.01	n/a
Busbar	**B39**	**B23**	**B20**	**B22**	**B19**
MAPE (%)	1.14	1.66	1.14	1.75	1.10
RSQ	0.9908	0.9963	0.9503	0.9970	0.9565
RMSE (sec)	0.0079	0.0073	0.0054	0.0075	0.0054
MOE (sec)	0.02	0.04	0.02	0.02	0.02
MUE (sec)	-0.04	-0.02	-0.02	-0.02	-0.02
MOE<0.3 sec (sec)	n/a	0.04	0.02	0.02	0.02
MUE<0.3 sec (sec)	n/a	-0.02	-0.01	-0.02	-0.02
Busbar	**B06**	**B10**	**B29**	**B25**	**B02**
MAPE (%)	1.56	1.36	1.17	1.71	1.19
RSQ	0.9962	0.9955	0.9903	0.9946	0.9914
RMSE (sec)	0.0180	0.0092	0.0107	0.0115	0.0117
MOE (sec)	0.09	0.13	0.05	0.11	0.08
MUE (sec)	-0.18	-0.04	-0.16	-0.08	-0.06
MOE<0.3 sec (sec)	0.00	0.13	0.00	0.02	0.05
MUE<0.3 sec (sec)	0.00	-0.02	-0.01	-0.01	-0.04

Table 6.12: Summary of the Random Forest (RF) accuracy metrics for each location (bus).

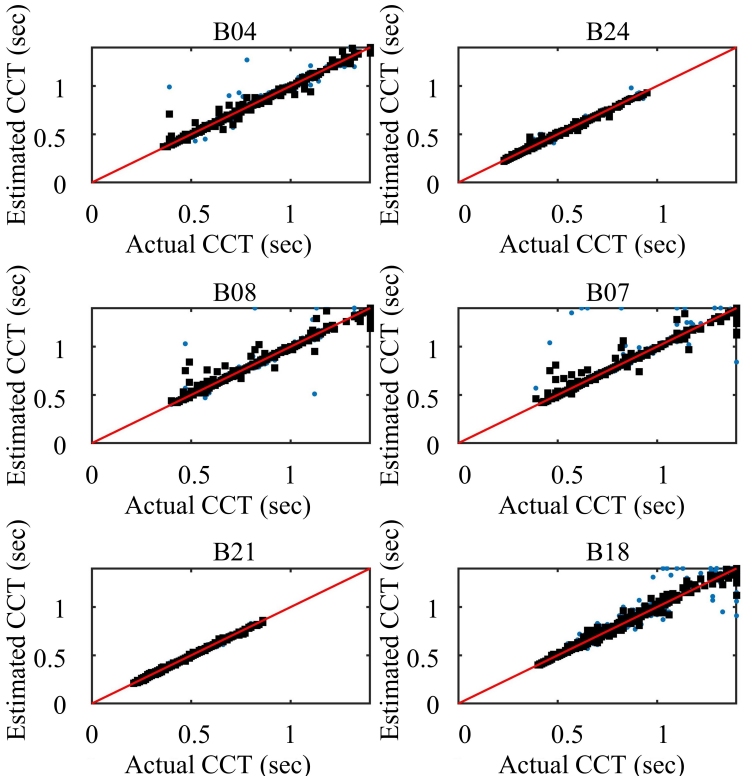

Figure 6.23: Comparison between Decision Tree (DT) (blue circles) and Random Forest (RF) (black squares) locational Critical Clearing Time (CCT) estimation accuracy in sec for six examples.

Impact on Important Parameter Lists

In addition to changes to estimation accuracy, changing the algorithm also impacts the important parameters obtained via PFI. The three top-ranked important parameters for each locational RF are given in Table 6.14. The features given in red ink represent a feature that is different to the features obtained using DT (full details in Table 6.8). There are significant changes to this, with 31 out of 75 features changing (41 % of important features change). This may have implications for the corrective measures the user decides to implement. Since two different ML algorithms are used, each mapping the input features to the target in a different way—such differences are expected. However, since the accuracy of each algorithm is comparable, the cause of differences is likely to be a result of the IML technique. To address this, a more robust means of identifying feature importance should be tested—this is a focus of Chapter 7.

	Decision Tree	Random Forrest	Change (%)
MSE (sec^2)	0.0009	0.0004	-53.1
MAPE (%)	1.19	1.41	18.3
RSQ	0.9756	0.9898	1.46
RMSE (sec)	0.0223	0.0164	-26.5
MOE (sec)	0.24	0.13	-45.7
MUE (sec)	-0.18	-0.13	-29.0
MOE<0.3 sec (sec)	0.0331	0.0300	-9.43
MUE<0.3 sec (sec)	-0.0144	-0.0138	-4.35

Table 6.13: Performance Comparison between Decision Tree (DT) and Random Forest (RF) algorithms (average over all locations).

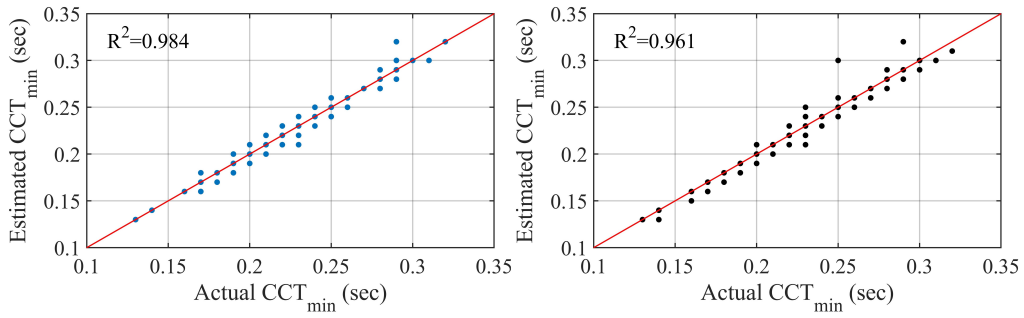

Figure 6.24: Comparison between Decision Tree (DT) (left) and Random Forest (RF) (right) for minimum Critical Clearing Time (CCT_{min}) estimation accuracy in sec (method *A*).

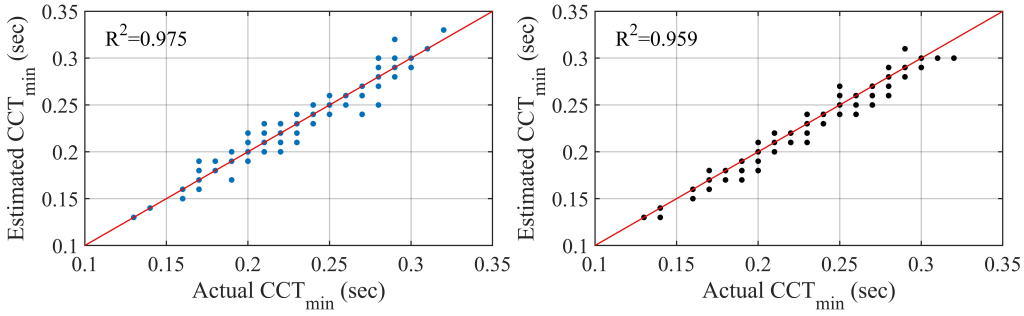

Figure 6.25: Comparison between Decision Tree (DT) (left) and Random Forest (RF) (right) for minimum Critical Clearing Time (CCT_{min}) estimation accuracy in sec (method *B*)

A clear benefit in terms of estimation accuracy has been demonstrated from changing ML algorithm. However, the loss of detailed information around important parameter threshold values (first discussed in Section 6.2.3) must be balanced against this when selecting the ML algorithm using this method.

6.9 Conclusions

There exists a need to assess the transient stability of new operational scenarios quickly and accurately—with a sufficient locational resolution to identify variations in the critical fault. Furthermore, identifying the underlying power system features that significantly influence the stability boundary is crucial for developing a detailed understanding of the stability boundary in a complex multidimensional space.

To address this, a novel ML-based methodology is proposed in this Chapter. In the proposed method, a series of location-based DT regressors are trained using pre-fault features to predict the CCT at each network location. This overcomes the need to run computationally intensive TDS online. The method can also identify features important to the prediction of CCT at each location through the application of PFI to each locational-DT model. Threshold values for the uppermost split in the DT for important features can be extracted from DT models, providing additional numerical feature limits with respect to the stability boundary. In addition, two methods for estimation of the duration and location of the critical fault (CCT_{min} and CFL) are also proposed. The performance difference and benefits of each are compared.

The proposed method is demonstrated using the IEEE 39-bus test network, where CCT is accurately predicted for a three-phase-to-ground fault at each bus. In the case study provided, both operational and power system variables and parameters are used as features, enabling the impact of generator dispatch and displacement patterns on the transient stability boundary to be assessed. As such, the method is well suited to assist in both planning and operational decisions. Results show high accuracy for all DT models, with some variation. Specifically, MAPE averages 1.27 % across all DTs (ranging 0.34–2.45 % at B19 and B27 respectively). In addition, the RSQ averages 0.9756 across all DTs (ranging 0.9403–0.9975 at B10 and B21) and the average RMSE is 0.0279 sec (ranging 0.0037–0.0689 sec at B19 and B27). Estimation of CCT_{min} is also found to be highly accurate for both CCT_{min} estimation methods proposed. Method *A*—which seeks to predict CCT_{min} from all locational DT models—achieves a MAPE of 0.57 %, RSQ of 0.9399 and RMSE is 0.0068 sec . The CFL is also correctly identified

in 96.5 % of cases. Method *B*—which builds additional DT models—achieves a MAPE of 0.73 %, RSQ of 0.9605 and RMSE is 0.0055 sec. The CFL is also correctly identified in 96.1 % of cases.

An illustrative case study highlights the ability of the method to track $\mathrm{CCT}_{\mathrm{min}}$ in feature space as the operational scenario changes, as well as monitoring any locational shift in CFL. What is more, the locational nature of the proposed method means that an understanding of the underlying important power system features responsible for changes to the entire stability margin is provided. This goes some way in reducing the dimensionality inherent in the transient stability problem. Indeed, an example provided demonstrates how an important feature can be used to target an enhancement measure, resulting in improvements in the stability margin at that location. This highlights how the method adheres to the three desirable attributes defined in Section 5.1.

However, the method is constrained to the use of DTs for extracting key parameter threshold values. Whilst this was not an issue in this Chapter (since the accuracy achieved by the DTs for the case studies considered was considered to be adequate), this may not be the case in different networks or other operational scenarios. Threshold values offer a sense of where the DT parses the data, giving a sense of significant turning points in the data, but are not a continuous measure of the impact of a feature on the model outcome. In addition, any interactions between features cannot be captured using such an approach. Moreover, the use of PFI limits the methodology because it only provides global feature importance and not feature effects [130]. Finally, this feature importance measure is based on the decrease in model performance when permutating a feature (i.e., it is linked to the error of the model).

Some performance improvement options were outlined in this Chapter. In particular, the impact of changing the ML algorithm to RF to improve performance is tested. While it is shown that performance can be enhanced with more complex models, the algorithm's complexity means rule extraction becomes increasingly difficult using this method. Therefore to increase accuracy and still obtain detailed insights into the ML models, more advanced IML techniques are required—the focus of the remaining Chapters.

	B04	**B24**	**B27**	**B13**	**B12**
IP1	B03 LMP	Line 11-12 MVAr	B03 LMP	B04 LMP	B18 LMP
IP2	B04 LMP	B03 LMP	G09 MVA	G03 xd'	KKT B37 Vmin
IP3	G03 MVA	B14 LMP	G09 xd'	G03 MVA	B14 LMP
	B08	**B07**	**B11**	**B14**	**B15**
IP1	B08 Q LMP	G03 xd'	B04 LMP	B04 LMP	Line 11-12 MVAr
IP2	G03 MVA	B08 Q LMP	G03 MVA	G03 xd'	B03 LMP
IP3	G03 xd'	G03 MVA	G03 xd'	G03 MVA	B36 Vang
	B21	**B18**	**B17**	**B28**	**B03**
IP1	B14 LMP	B03 LMP	KKT Line 2-3 MVA	G09 xd'	B16 LMP
IP2	G06+G07 MVA	Line 19-20 MVAr	Line 19-20 MVAr	G09 MVA	Line 23-24 MW
IP3	G06+G07 H	SG MW capacity	Line 11-12 MVAr	B27 LMP	G08 xd'
	B39	**B23**	**B20**	**B22**	**B19**
IP1	Line 1-39 MW	B14 LMP	Line 20-34 MW	B14 LMP	RES2-G04
IP2	B01 LMP	G06+G07 MVA	G05 MW set	G06+G07 MVA	Line 10-13 MW
IP3	Line 1-2 MW	G06+G07 H	B15 LMP	G06+G07 H	G05 MW set
	B06	**B10**	**B29**	**B25**	**B02**
IP1	B11 Q LMP	B04 LMP	G09 MVA	G08 MVA	G08+G10 MVA
IP2	G03 xd'	G03 MVA	G09 xd'	G08 xd'	RES3-G09
IP3	G03 MVA	G03 xd'	B04 LMP	Line 2-25 MVAr	G09 MVA

Table 6.14: Three top-ranked important parameters at each location using Random Forest (RF).

Chapter 7

Identification of Trends in the Transient Stability Margin Estimation using Feature Effects obtained from SHapley Additive exPlanations

7.1 Introduction

Chapter 6 outlined a methodology capable of fast and accurate TSA for large numbers of operational scenarios, with enough spatial granularity to capture any potential changes in the CFL. In addition, the features influencing the stability boundary at each location were identified along with key threshold values for these features. However, the method is constrained to the use of DTs and can only provide feature *importance* (via PFI)—rather than more informative feature *effects*. Whilst DT threshold values offer a sense of where the DT parses the data, it is not a continuous measure, and feature interactions are not captured. Moreover, the method offers no means of locational trend identification (i.e., identification of locations with similar (or dissimilar) stability

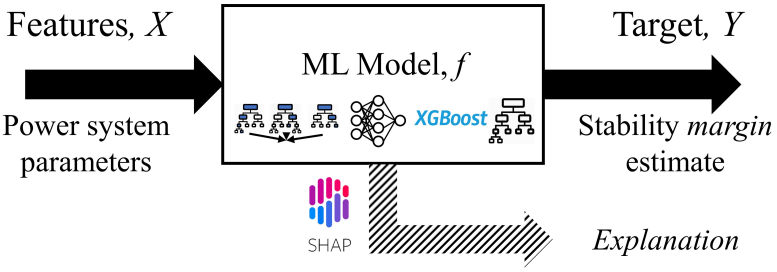

Figure 7.1: Explanation of Machine Learning (ML) model using SHAP.

boundary characteristics).

This Chapter seeks to address these shortcomings by developing a method capable of detailed interpretations of *any* ML model. The method also provides detailed model insights (i.e., both feature importance *and* effects). In addition, the method can capture locational trends in the stability boundary. To achieve this, the use of the SHAP framework [162] is proposed (Figure 7.1). Specifically, this Chapter proposes using SHAP values to identify the effect of power system variables on the transient stability margin on a locational basis. The model-agnostic nature of SHAP provides freedom regarding ML algorithm selection, unlocking more powerful predictors to enhance accuracy—whilst still providing detailed insights into the stability margin. A series of location-specific ML models are trained to predict the CCT at each bus in a network. The locational nature of the proposed method enables insights into the entire stability boundary, rather than just for a single contingency—in a similar manner proposed in Chapter 6.

The method proposed in this Chapter builds on and improves the method presented in Chapter 6. Whilst the locational framework remains unchanged (separate ML models are trained per location to predict the stability margin), SHAP is used for two key reasons. Firstly, the use of the SHAP framework removes the ML algorithm selection constraint (enabling prioritisation of accuracy). Secondly, to provide detailed insights into the locational stability boundary (i.e., local explanations of single operational scenarios and global interpretations of numerous credible operational scenarios). These global interpretations are then compared between the location-specific models to reveal locational trends in the stability boundary. In this Chapter, a power system Variable of

Interest (VOI) is defined as a variable known to be important to stability, controllable, likely to vary and/or be of interest to the user (e.g., an easily controllable variable). To identify the aforementioned locational trends, the covariance between a VOI and the SHAP values for that VOI from each location-specific ML model are calculated. In doing so, the impact of a change in a VOI on the entire stability margin behaviour can be assessed.

7.1.1 Contributions

The work presented in this paper has been submitted to the IEEE Transactions on Power Systems. The key novel contributions from this Chapter include:

- development of a methodology capable of identifying the effects (i.e., not just the importance, but also the impact in sec on CCT predictions) of power system variables on ML models trained to predict transient stability margin (specifically the CCT) at each bus in a system along with the critical fault (the CCT_{min}) using the SHAP framework,
- extraction of rules from SHAP values for particular power system variables or parameters that can lead to a new detailed understanding (or reinforcement of existing knowledge) of the complex power system dynamic characteristics, and
- identification of locational trends in the stability boundary using covariance between a VOI and location-specific SHAP values for that variable.

7.2 Methodology

This Chapter proposes the use of SHAP to identify important power system variables that impact the transient stability margin in the context of increasing volumes of RES (Figure 7.2 and 7.3). A ML algorithm is trained to predict CCT at each bus n on the network. The location-specific model is trained from a location-specific TSDb which contains power system variables and CCT at that location (calculated using RMS-TDS) for a number of operational scenarios that represent system conditions of interest (i.e.,

generation mix, demand level etc.). An additional model is trained to predict the duration of CCT_{min}, resulting in a total of $n + 1$ ML models. Whilst location-specific CCT provides important locational information, CCT_{min} is also important since it offers a sense of the proximity of the system as a whole to the stability boundary.

The ML algorithm used can be defined by the user but should be selected to achieve a high degree of accuracy. In doing so, confidence can be increased in the model since the dynamics of the system are likely to be better represented. The SHAP method is subsequently applied to each of the $n + 1$ ML models to identify the important variables impacting the stability margin and the extent to which they influence the CCT prediction. The nature of SHAP is such that both local explanations (i.e., for individual operational scenarios) and global interpretations (i.e., for the model as a whole) can be extracted.

Finally, locational trends in the transient stability boundary are revealed through analysis of the covariance between a power system VOI and the location-specific SHAP values of that VOI. Similar trends can be revealed for CCT_{min}. A VOI can be any feature in the TSDb. Typically, a VOI may be selected because it is identified as important, controllable, or likely to change. Thus, understanding its impact on the stability margin is beneficial.

The precise methodological steps are outlined in detail in the preceding sections. Operational scenarios depend on the case study and can be selected by the user based on current or likely future system conditions that require analysis and understanding. AC-OPF is used to determine the generator dispatch (Section 7.2.1). For each operational scenario, RMS-TDS are conducted to determine the CCT for a short circuit fault at each bus on the network (of which there are n). From this, the CCT_{min} is also determined, resulting in the calculation of $n+1$ sets of fault clearing times. Power system variables form a total of $n+1$ TSDbs; each with the same features but a different CCT (Section 7.2.2). Each TSDb is split into training and testing portions, and $n + 1$ ML models are trained using the training portion of the corresponding TSDb to predict CCT. The accuracy of the $n + 1$ ML models are then assessed using the testing portion of the corresponding TSDb (Section 7.2.3). The ML algorithm can be changed depending on

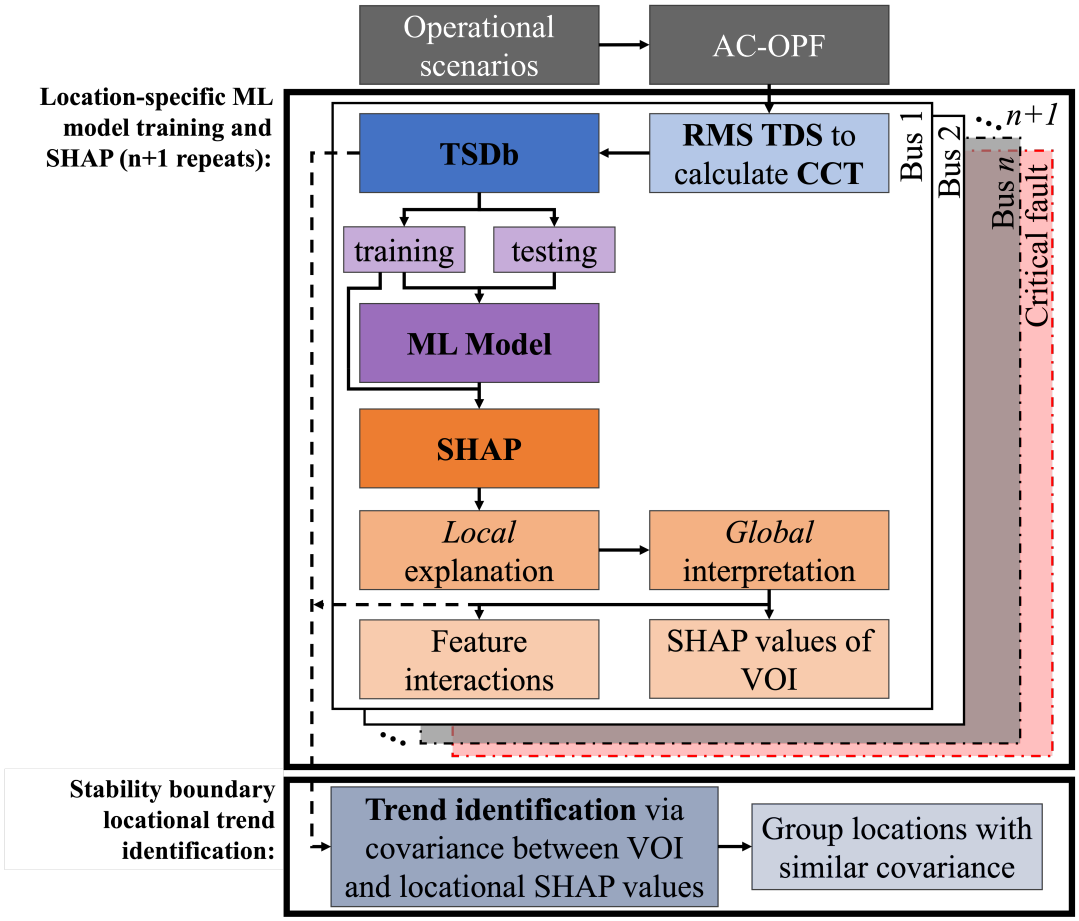

Figure 7.2: Methodology overview: illustrating how enhanced stability boundary insights can be extracted from location-specific machine learning (ML) models using SHAP.

the desired accuracy.

SHAP is used to determine impact of power system variables on CCT prediction for each of the $n+1$ ML models. Since n represents the number of busbars in the system, a system-wide stability understanding of the boundary is formed. Locational trends in transient stability are determined by taking a VOI and determining the covariance with SHAP values of the $n+1$ ML models. The impact on CCT at locations with a similar covariance (i.e., both either positive or negative) between the VOI and SHAP value will be similar (i.e., improve or deteriorate together). Locations with opposing covariance (i.e., one positive and the other negative) will have inverse trends (Chapter

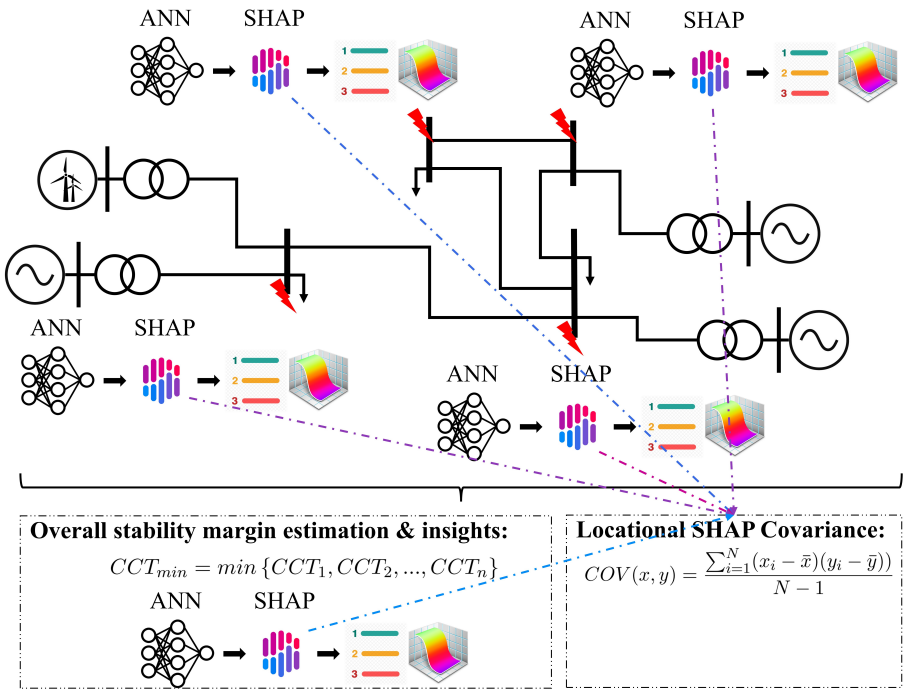

Figure 7.3: SHAP methodology overview on simple example network.

7.2.6). Since a model representing the CCT_{min} is also trained, locational trends with respect to CCT_{min} are also revealed.

7.2.1 Generator Dispatch via AC Optimal Power Flow

The definition of an operational scenario and overview of the AC-OPF is identical to that described in Section 6.2.1. The resulting dispatch is used to initialise the dynamic studies to capture how the market would dispatch generation. In doing so, the impact of the market forces is inherently included in the operational scenarios and, thus, the stability margin.

7.2.2 Transient Stability Database

In this Chapter, individual ML models are trained to predict the CCT for each of the $n+1$ faults considered (one for each of the n bus faults considered and another for CCT_{min}). As such, an individual TSDb for each fault is generated, from which the $n+1$

SG	RES	System
$\mathrm{SG}_{P,v}, SG_{Q,v}, SG_{MVA,v}$, $\mathrm{SG}_{MVA,k,total}, SG_{MVA,total}$, $\mathrm{SG}_{H,v}, SG_{H,k,total}, SG_{H,total}$, $\mathrm{SG}_{P,max,v}, SG_{P,min,v}, SG_{Q,max,v}$, $\mathrm{SG}_{Q,min,v}, SG_{Ploading,v}$.	$\mathrm{RES}_{P,w}, RES_{Q,w}$, $\mathrm{RES}_{MVA,w}$, $\mathrm{RES}_{MVA,total}$, $\mathrm{RES}_{MVA,total}/SG_{MVA,total}$, $\mathrm{RES}_{MVA,k,total}/SG_{MVA,k,total}$, $\mathrm{RES}_{MVA,total}/SG_{P,total}$.	$\mathrm{P}_{d,l}, Q_{d,l}$, $\mathrm{v}_{bus,n}, v_{bus,\delta,n}$, $\mathrm{P}_{from,n}, P_{to,n}$, $\mathrm{Q}_{from,n}, Q_{to,n}$.

Table 7.1: Power system features used for model training.

ML models will be trained. The operational scenarios and features remain unchanged between the databases, with only the target column varying.

The TSDb creation process is similar to that described in Section 6.2.2. In particular, the features selected are a set of power system parameters, and the target is the transient stability of the system—specifically the CCT at every bus in the network (see Figure 6.4).

Feature Selection

Section 6.2.2 highlights the importance of feature selection and how changes to this may impact the accuracy, interpretability and ultimately the usefulness of the results from the methodology.

Since the proposed method is intended to illustrate the importance of interpretability of the ML model for TSA, the inclusion of features that the SO has some degree of control over are proposed. This includes parameters relating to SG, RES and the system. SG parameters relate to P, Q and V setpoints as well as machine size (MVA rating, inertia, and generator limits). RES parameters include P, Q and V setpoints along with parameters relating to the MVA rating. System parameters include total P and Q demand, network voltages, angles and the power flow in lines. The full details are provided in Table 7.1 for a network with k generating areas, v SG units, w RES units, l loads and n buss, resulting in M features in the TSDb.

Target Selection

As outlined in Figure 2.9 (Chapter 2), the stability margin is the most informative means of assessing the stability of an operational scenario since it includes the full dynamic response of the system.

Since a locational approach is again proposed, with a ML model being trained to predict CCT at each bus on a network—the target varies depending on the location. Therefore, the target for the ML model is the CCT for a zero impedance three-phase to ground self-clearing fault at that location.

7.2.3 Machine Learning Algorithm Selection Procedure

Accuracy is fundamental in building confidence in a model/method since a more accurate model can represent the simulated dynamic response of the power system (obtained via RMS-TDS of a representative model) and thus the actual system dynamics. Therefore, in this context, accuracy is very important. However, authors in [130] suggest that avoiding the use of unnecessarily complex models is advisable—particularly when the performance of a more interpretable model is only "negligibly" worse. The authors suggest that the best practice is to define a desired level of accuracy (metrics defined in Section 5.2.3). Various ML algorithms can then be tested—starting with simple algorithms and gradually increasing the model complexity until the desired level of accuracy is reached.

Therefore this Chapter specifies that ML algorithm complexity should be increased from a simple algorithm until a predefined accuracy threshold is reached, following the process in Figure 7.4. Note that ML algorithm complexity is difficult to define explicitly, therefore using engineering judgement such as the description provided alongside Figure 5.3 is advised. The desired accuracy depends on the application and is therefore left to the user to define. The widely used accuracy evaluation metrics for regression are detailed in Section 5.2.3.

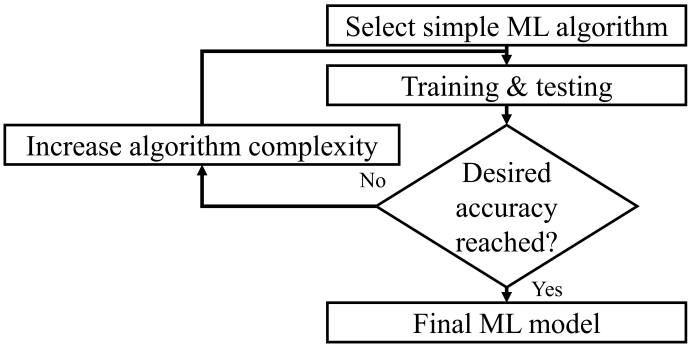

Figure 7.4: Interpretable Machine Learning (IML) algorithm selection process.

7.2.4 Desired Accuracy

For this application, the accuracy threshold is MOE or MUE <0.02 sec due to the importance of minimum/maximum errors in TSA (which is set out in Section 5.2.3). Note: this can be varied depending on user requirements.

7.2.5 SHapley Additive exPlanations

The SHAP framework [162] is model agnostic and is of the class of additive feature attribution methods, meaning that an effect is attributed to each feature based on the influence on the model prediction. Feature effects are based on Shapley values [163], which stem from game theory and describe the average marginal contribution of a player to all coalitions in which the player contributes. SHAP is primarily a local explanation technique (i.e., provides feature effects for a single model outcome) that can be extended to provide global interpretation. These global interpretations are composed of multiple local explanations (e.g., across an entire training database) and provide overall feature importance (e.g., ranked based on average feature effect). Since local explanations are the "atomic units" of global explanations, they are consistent. Therefore, analysis of SHAP values in the global frame assists in understanding the global model structure.

In the context of this Chapter, the SHAP framework is used to attribute an effect of each feature (i.e., each power system variable included in the TSDb) on the transient stability margin at a particular bus (i.e., the CCT) for a given operational scenario. In addition, general stability boundary trends can be obtained through analysis in the

global frame (i.e., by looking at feature effects for multiple operational scenarios).

Since SHAP is used to obtain such insights into each location-specific ML model, insights are obtained into the entire stability boundary rather than just a single contingency. Global interpretations from each location-specific model are compared to reveal locational trends in the stability boundary.

Such insights may inform the design and development of transient stability enhancement measures with the capability to extract turning points for important power system variables. Since SHAP can be applied to any black-box ML model, the ML algorithm can be as complex as required to achieve the desired accuracy and therefore increase trust in feature importance results. The accuracy is likely to vary with different operational scenarios, feature selection etc. This capability of SHAP to provide a detailed understanding of a black-box ML model (overcoming the accuracy vs interpretability tension) is highly useful from a power systems perspective—where traditionally, SOs and Transmission System Owners (TOs) are highly risk-averse, often leading to a reluctance to change existing approaches.

SHAP Mathematical Overview

SHAP [162] has gained traction in ML communities, and recently in power systems [116]. This Chapter proposes using SHAP to gain insights into each locational ML model, which is trained to predict the transient stability margin. In doing so, an understanding of the factors influencing the shape of the entire stability boundary can be obtained.

SHAP is used to attribute an effect to each feature in the training database for a given operational scenario. This can be interpreted as the change in the expected model prediction (if no features are known, taken as the average prediction from the training database) for a feature and is in the units of the target variable. Therefore, in the context of this Chapter, SHAP gives the change in expected CCT of each feature in sec. Local explanations for individual operational scenarios can be analysed—from which global interpretations can be revealed when observing multiple scenarios. Local explanations are "atomic units" of the global interpretations, making them consistent

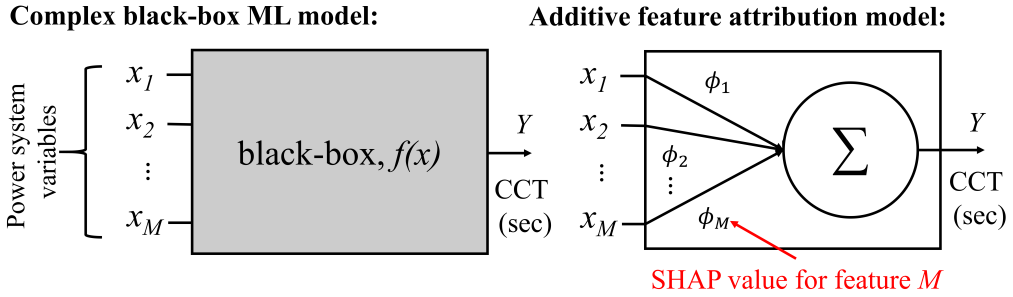

Figure 7.5: Representation of a black-box model using additive feature attribution overview. Left: Original model complex model (black-box). Right: Simple linear explanation model (additive feature attribution model) for a particular prediction (e.g., a single operational scenario).

[162]. This makes SHAP particularly advantageous for explaining single operational scenarios and for more general trend identification across a database of operational scenarios.

The SHAP framework identifies a new class of additive feature attribution methods [162]. Such methods seek to build a simpler explanation model g to explain the complex original model f (which is often black-box), as shown in Figure 7.5. This explanation model is expressed as a linear function of binary variables that enables explanations of a model prediction based on a single input x. Simplified inputs x' are used to map to the original input via some mapping function h_x, where $x = h_x(x')$. The goal is to ensure $g(z^{'}) \approx g(h_x(z^{'}))$, whenever $z^{'} \approx x'$ and where $z^{'} \in \{0,1\}^M$ and M is the number of simplified input features. The method attributes an effect ϕ_i (where $\phi_i \in \mathbb{R}$) to each feature and summing the effects of all feature attributions approximates the output $f(x)$ of the original complex model Equation 7.1. This results in an intuitive feature importance measure.

$$g(z^{'}) = \phi_0 + \sum_{i=1}^{M} \phi_i z_i^{'} \tag{7.1}$$

The SHAP framework demonstrates that for additive feature attribution methods to adhere to three desirable properties Shapley values from cooperative game theory [163] must be used (and thus improves previous methods) [162]:

- *local accuracy*: when approximating the original model f for a specific input x, the explanation model $g(x')$ should at least match the output of $f(x)$ for the simplified input x' (which corresponds to the original input x via $x = h_x(x')$),
- *missingness*: if the simplified inputs represent feature presence, then features missing in the original input should have no impact $x'_i = 0 \Rightarrow \phi_i = 0$,
- *consistency*: if a model changes so that some simplified input's contribution increases or stays the same regardless of the other inputs, that input's attribution should not decrease. Let $f_x(z^{'}) = f(h_x(z^{'}))$ and $z^{'} \setminus i$ represent fixing $z_i^{'} = 0$. For two models f and f', if $f'_x(z^{'}) - f'_x(z^{'} \setminus i) \geq f_x(z^{'}) - f_x(z^{'} \setminus i)$ for all inputs $z^{'}\{0,1\}^M$, then $\phi_i(f', x) \geq \phi_i(f, x)$.

The unified approach proposed by SHAP improves previous methods by preventing unintentional violations of these properties. A Shapley value can be interpreted as the *average marginal contribution* by a feature to all coalitions that contain contributions from this feature. The Shapley value, ϕ_i, of feature i is given by:

$$\phi_i(f, x) = \sum_{z^{'} \subseteq x'} \frac{|z^{'}|!(M - |z^{'}| - 1)!}{M!}[f_x(z^{'}) - f_x(z^{'} \setminus i)] \tag{7.2}$$

where $f_x(z^{'}) = f(h_x(z^{'}))$ and $z^{'} \setminus i$ denotes setting $z_i^{'} = 0$. Note: when $\phi_0 = f_\emptyset(\emptyset)$ then the Shapley values match Equation 7.1 and is hence an additive attribution method. SHAP requires a model comparison which is retrained on the features that are not withheld—which is hard in a ML context. This is overcome by expressing the explanation model as a "conditional expectation function of the original model" [162] (i.e., the explanation model in the SHAP framework is a conditional expectation function of the original model). Therefore, SHAP values are the solution to Equation 7.2, where $f_x(z^{'}) = f(h_x(z^{'})) = E[f(z)|z_S]$ and S is the set of non-zero indexes in $z^{'}$. When conditioning on a feature, SHAP values attribute the change in model prediction to that feature, explaining how to move from the base value $E[f(z)]$ (i.e., the prediction if no features are known (i.e., $\phi_0 = f_\emptyset(\emptyset)$), which is taken to be the average of all predictions in the training database) to the current output $f(x)$. Therefore, in the context of this

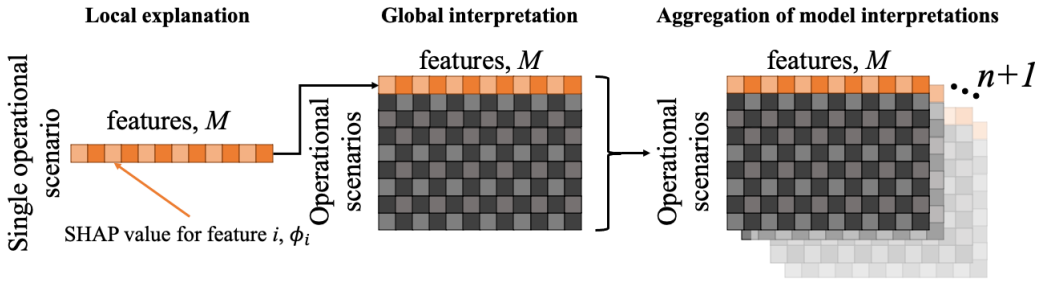

Figure 7.6: Data structure for SHAP local, global and for locational trend identification.

Chapter, a SHAP value gives the average effect—in sec—of a VOI taking a particular value on shifting the CCT from the expected value (average CCT in the training database) to the predicted CCT.

The Shapley value is computationally expensive to compute because of the exponential number of coalitions required to compute a true average and thus becomes intractable. SHAP tackles this by incorporating approximate Shapley value computations (using fewer coalitions of features—see a summary below and complete details of various different methods in [162]).

It is important to note that while SHAP values can reveal associations learned from the data, they do not necessarily guarantee or reflect causal relations. Identified associations can be helpful for system operators and planners but would need further validation based on domain knowledge or other causal inference methods to guarantee causal effects.

SHAP Data Structure

A local explanation gives a 1D matrix of SHAP values of each feature, i. Global interpretations can be obtained by repeating this across the entire training database; resulting in a 2D matrix of SHAP values consisting of one row per operational scenario and one column per feature, i (Figure 7.6). Since in this Chapter, $n+1$ ML models and generates—a 3$^{\text{rd}}$ dimension is added (one per location, as in Figure 7.6). The resultant 3D matrix therefore consists of the SHAP values for all features across all operational scenarios in the training database for each $n+1$ locational ML models. This matrix is later used for stability boundary trend identification in Section 7.2.6.

SHAP Approximation Methods

ML algorithms are often referred to as black-boxes since the decision-making process between the input data set and the output is often opaque. The SHAP framework is compatible with all ML algorithms. However, Shapley values are computationally expensive to calculate [162] (due to exponential time to calculate over all possible subsets of features), therefore various SHAP methods are proposed to either calculate *exact* or *approximate* Shapley values. The SHAP implementation can vary depending on the ML algorithm implemented, which will depend on the accuracy required.

KernelExplainer is a model-agnostic method which approximates Shapley values based on a user-defined background dataset. Note that when using KernelExplainer, the SHAP values are equivalent to using LIME. Several model-specific algorithms also exist that use the inherent model structure to assist in the calculation of Shapley values. Relevant explainers used in this thesis are the TreeExplainer and DeepExplainer, briefly outlined below.

The TreeExplainer method is specific to tree-based methods. It calculates the *exact* Shapley values by taking advantage of the tree structure and is very *fast* to compute [174]). This enables the precise values to be calculated in *polynomial* time. Therefore, SHAP values using the TreeExplainer SHAP implementation are equivalent to Shapley values, but SHAP values in other implementations are approximate Shapley values.

The DeepExplainer (DeepSHAP) algorithm [162] is specific to neural networks and also calculates *approximate* Shapley values. The algorithm calculates SHAP values for small components in the network (e.g., linear layers or non-linear functions with one input) and backpropagates using concepts taken from the DeepLIFT algorithm [162]. In DeepLIFT, the mapping $x = h_x(x')$ converts binary values into the original inputs, where 1 indicates that each input takes its original value, and 0 indicates that it takes some reference value (representing a typical uninformative background feature value). By integrating over many user-defined background samples, DeepExplainer estimates approximate SHAP values such that they sum up to the difference between the expected model output on the passed background samples and the current model output ($f(x)$ - $E[f(x)]$).

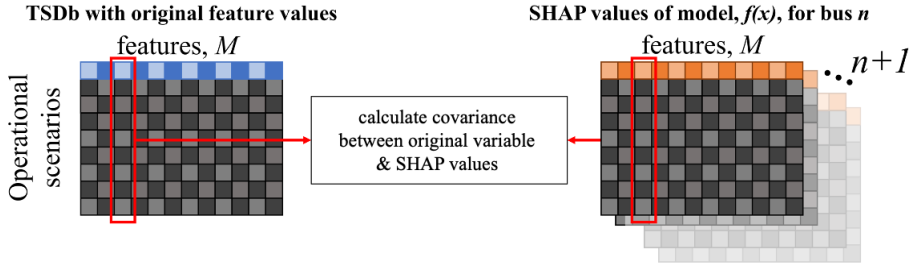

Figure 7.7: Identification of locational trends between actual Variable of Interest (VOI) value and the corresponding SHAP values from each Machine Learning (ML) model.

There is little in the way of analysis into how approximate the SHAP values are for KernelExplainer and DeepExplainer, making this a potential avenue of future research. Since the TreeExplainer calculates exact SHAP values (by taking advantage of the tree structure) and is very *fast* to compute [174] (polynomial time), then this explainer should be used if accuracy of the SHAP values is a particular concern. However, note that this limits the user to tree-based algorithms which may have implications for model accuracy.

7.2.6 Identification in Locational Trends using SHAP Values

This Chapter seeks to identify how a change in a particular power system VOI may impact the stability margin throughout the network. To do so, covariance (a measure of how two variables will change together) between a VOI and the location-specific SHAP values corresponding to that VOI for each ML model is calculated—resulting in n+1 covariance values per VOI. In doing so, the effect of a VOI across the entire network is obtained—capturing locations with *similar* (or *dissimilar*) stability margin behaviour with respect to that VOI.

Figure 7.7 shows how the covariance between the actual feature values from the TSDb for a given VOI and the corresponding column for that VOI in the 3D matrix of SHAP values for each model is calculated. This results in a measure of how the stability boundary will be impacted due to changes in some VOI. Such insights may enhance situational awareness and inform the design and development of stability enhancement measures.

Covariance describes how two variables are related to one another, that is, a measure of how two random variables in a data set change. This is described mathematically as:

$$COV(a,b) = \frac{\sum_{i=1}^{N}(a_i - \bar{a})(b_i - \bar{b}))}{N-1} \tag{7.3}$$

where a is the independent variable (in this case the power system VOI), $\bar{a}$ the mean of a, b the dependent variable (SHAP value for the VOI at a given location), $\bar{b}$ the mean of b, and N represents the number of data points in the sample. This is repeated for each location, resulting in $n+1$ covariance values per VOI. A positive covariance means that the two variables are positively related, moving in the same direction. A negative covariance indicates that the variables are inversely related, moving in opposite directions. Observing covariance between the VOI and SHAP values at each $n+1$ location reveals the impact of a VOI on location-specific SHAP values and thus on the transient stability margin throughout the network.

7.3 Test Network and Case Study Design

7.3.1 IEEE 39-Bus Test Network Overview

In this Chapter, the IEEE 39-bus (Figure 6.8) test network is once again used, the details of which are outlined in Section 6.4.1.

7.3.2 Generator Dispatch via AC Optimal Power Flow

In this Chapter, the same cost functions are allocated to generators as specified in Table 6.2 in Section 6.4.2.

7.3.3 Operational Scenarios

In this Chapter, the same case studies as defined in Section 6.4.3 are used.

Performance Metric	DT	RF	XGBoost	ANN
Average RSQ	0.9731	0.9815	0.9936	0.9932
Average MSE (sec^2)	0.0013	0.0008	0.0003	0.0002
Average RMSE (sec)	0.0288	0.0228	0.0137	0.0110
Max MOE (sec)	0.37	0.29	0.14	0.08
Min MUE (sec)	-0.32	-0.26	-0.13	-0.07
Max MOE <0.3 (sec)	0.14	0.11	0.03	0.01
Min MUE <0.3 (sec)	-0.01	-0.01	-0.01	-0.01

Table 7.2: Impact of Machine Learning (ML) algorithm on accuracy metrics (average for all locations).

7.4 Results

The following section details key results and findings from implementing the proposed methodology on the IEEE 39-bus test network for the same case studies as outlined in Chapter 6. First, in Section 7.4.1 the accuracy of the 26 $(n + 1)$ ML models are compared. Then from Section 7.4.3 onwards, focus turns to the interpretability of the ML models. Insights into a single (local) operational scenario are provided using the SHAP framework before a global analysis is given, including a comparison to insights available through PFI (which was proposed for gaining insights into DT models in Chapter 6). In addition, system-wide stability boundary trends are identified.

7.4.1 Accuracy

The accuracy of three different tree-based algorithms are compared—specifically DT, RF and XGBoost (scikit-learn [175])—and a feedforward ANN (a sequential regressor implemented using Keras, Tensorflow [176]) with 2 hidden layers (Section 7.2.3). Accuracy of each algorithm is reported in Table 7.2 using the metrics outlined in Section 5.2.3. Note that tuning of hyperparameters of ML models that will have a significant impact on the performance. Numerous ways to do this exist (e.g. random search, grid search and bayesian optimization), but ultimately the approach selected depends on the application and results will vary due to the stochastic nature of the algorithm, or indeed differences in numerical precision. Results here show that performance improves as the algorithm becomes increasingly opaque. The high degree of accuracy

achieved by the black-box ANN for locational CCT estimation increases confidence in the interpretation of the model, since the locational models are closely aligned to RMS-TDS results—compared to DT, RF and XGBoost algorithms. In particular, the ability of ANN to reduce outliers is highly advantageous over the other algorithms. This is important for transient stability applications, where the consequences of a large over-estimate of the stability margin could result in a LOS, a cascade and ultimately a blackout. Therefore, the ANN algorithm is used in this case.

The high degree of accuracy achieved by the black-box ANN for locational CCT estimation increases confidence in the interpretation of the model, since the locational models are closely replicating RMS-TDS results—compared to DT, RF and XGBoost algorithms. In particular, the ability of ANN to reduce outliers is highly advantageous over the other algorithms; however rule extraction from an ANN model is impossible due to the black-box nature, particularly when compared to a DT model (as in Chapter 6).

7.4.2 Computational Details

The methodology was conducted on an Intel CoreTM i7- 6700 CPU @3.40GHz with 16 GB installed RAM. An average of 40 sec are required to calculate the CCT for a given contingency using a Python script to automate DIgSILENT PowerFactory. A single ANN can be trained in approximately 60 sec in Python. All the above stages are conducted offline when time is less expensive. CCT estimation in an online setting is , however, time critical, taking approximately 0.2 sec (200-fold time reduction compared to RMS-TDS). SHAP explanations from the training portion of the TSDb are constructed offline (using the Deep Explainer package in Python, taking approximately 30 sec). Note that the ML algorithm (which may vary with accuracy requirements) and SHAP explainer selected will impact computational speed depending on user selections.

7.4.3 Local SHAP Explanation of CCT_{min} Model

This section provides a local explanation of the power system variables that impact the estimation of the $\mathrm{CCT_{min}}$ for a particular operational scenario. Similar analysis of the

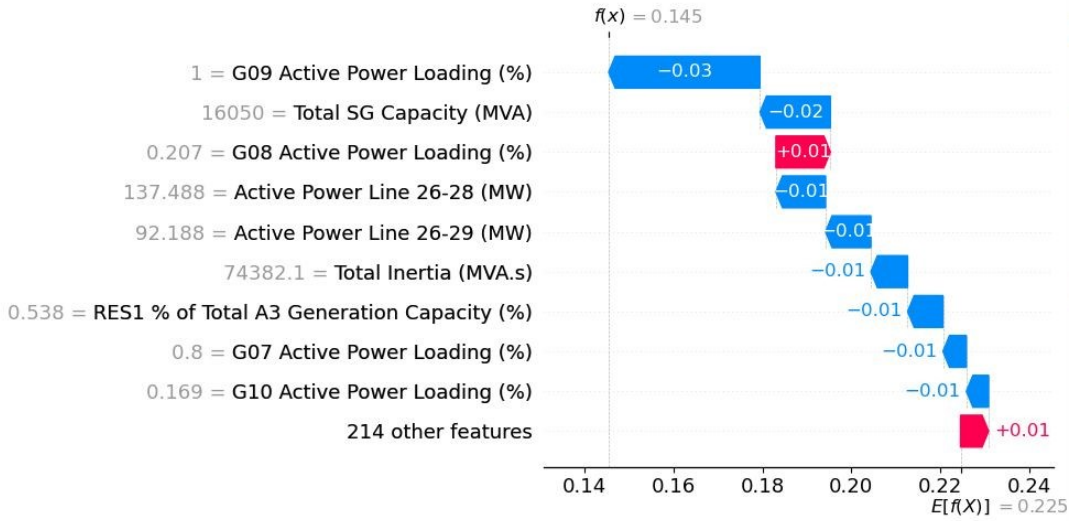

Figure 7.8: Example of a local SHAP explanation of the CCT_{min} model for a single operational scenario.

remaining 25 ML models (that predict the CCT at each bus) can also be conducted are omitted as one example illustrates the point effectively.

In addition to the local interpretability of the model as a whole, the impact of features on individual estimations can also be extracted using SHAP. This provides insights into the unique solutions obtained for a given operational scenario. One such operational scenario example is provided in Figure 7.8, where the base value ($E[f(x)]$) is 0.225 sec (x-axis). All features included in the TSDb are on the y-axis, ranked from top to bottom based on the magnitude of the feature effect (i.e., the magnitude of the SHAP value) for this specific prediction. The actual value of the feature is also given on the y-axis. The impact of each feature taking that value on the prediction is represented by a blue or pink arrow and corresponding SHAP value. This value is the attributed effect on the model prediction of that feature. Moving upwards from the base value ($E[f(x)]$), the impact of each feature shifts the prediction until the actual model prediction $f(x)$ is reached. Here the final prediction of $\mathrm{CCT_{min}}$ for this operational scenario is 0.145 sec. The sum of the SHAP values is equal to the difference between the actual prediction and the expected value, demonstrating the additive nature of SHAP, first introduced in Equation 7.1.

Starting at the base value ($E[f(x)]$) of 0.225 sec, the lowest ranked 214 features only have a combined impact of +0.01 sec on the CCT_{min} prediction. G08 active power loading (3$^{\text{rd}}$ most important feature) in this operational scenario is 20.7%, which consequently increases the model prediction by 0.01 sec. Conversely, the impact of G09 active power loading (the highest-ranked feature) being 100% has a -0.03 sec impact on the CCT_{min} prediction.

These types of insights can be compared to engineering knowledge to enhance confidence in the results from the ML model and indeed SHAP. In an online setting, for example, in a control room, this information could support control room engineers—by highlighting additional power system variables to consider or reinforcing engineering judgements. In addition, similar local explanations for all operational scenarios can be generated, providing a global interpretation of the model.

7.4.4 Global PFI Interpretation of CCT_{min} Model

Global interpretations using PFI (used in the methodology proposed in Chapter 6) are compared to SHAP to illustrate the advantage of SHAP in providing feature effects.

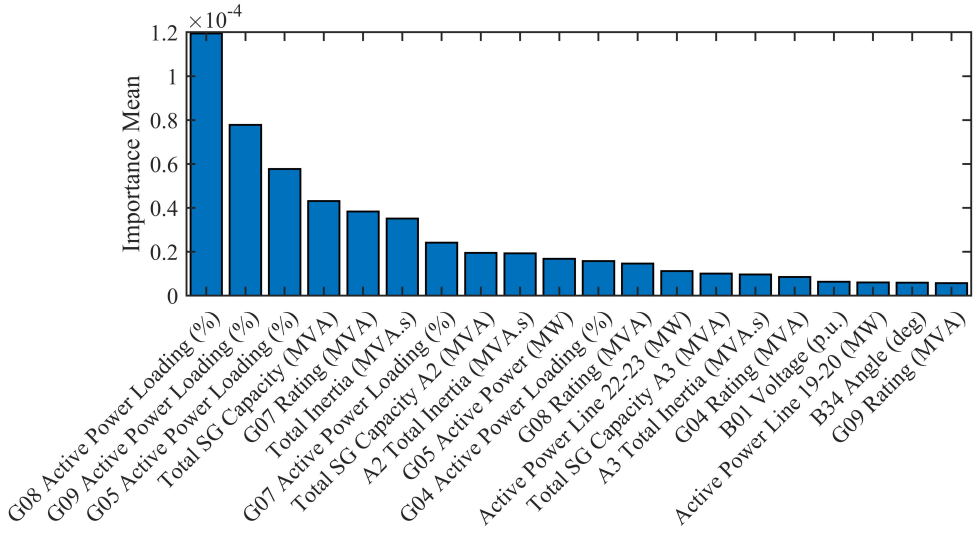

Figure 7.9: Permutation Feature Importance (PFI) for top-20 features of Artificial Neural Network (ANN) model for CCT_{min} estimation.

As previously outlined, the output from PFI is a ranked list of features based on the mean importance based on the decrease in model performance when a feature is permutated (Figure 7.9). Whilst useful for identifying important features, interpreting the meaning of the importance score has no relation to the target variable (here, $\mathrm{CCT_{min}}$), and no additional information is provided relating to feature values or key turning points. While extraction of additional details was possible when using DTs (see Chapter 6), the black-box nature of the ANN implemented here prohibits such analysis—demonstrating the accuracy-interpretability tension.

7.4.5 Global SHAP Interpretation of CCT_{min} Model

As previously outlined, a global interpretation of a model can be achieved by extending local SHAP (such as the one presented above) across all operational scenarios. This results in a matrix of SHAP values (Figure 7.6), with one row per operational scenario and one column per feature. This can be presented in a SHAP summary plot (e.g., Figure 7.10) that provides details relating to the impact of important features (and their magnitude) on the model prediction for all operational scenarios.

The SHAP summary plot for $\mathrm{CCT_{min}}$ (Figure 7.10) provides an indication of the relationship between top-20 important features and their values on the estimation of $\mathrm{CCT_{min}}$. Each point on Figure 7.10 is a SHAP value of a feature for a given operational scenario. The position on the y-axis is determined by the feature importance (mean SHAP value across all scenarios), and on the x-axis, the SHAP value (i.e., the impact of that feature on the model prediction for that particular operational scenario). The colour represents the feature value for that operational scenario from 'low' (blue) to 'high' (pink) based on the original feature value from the training portion of the TSDb. Any point with a positive SHAP value indicates an improvement in the $\mathrm{CCT_{min}}$ prediction from the base value ($E[f(x)]$, which is equal to average $\mathrm{CCT_{min}}$ for all training samples). Conversely, any datapoint with a negative SHAP value indicates a decrease in the estimation of $\mathrm{CCT_{min}}$ from the base value. Overlapping points are distributed in the y-axis direction, providing a sense of the distribution of the SHAP values per feature.

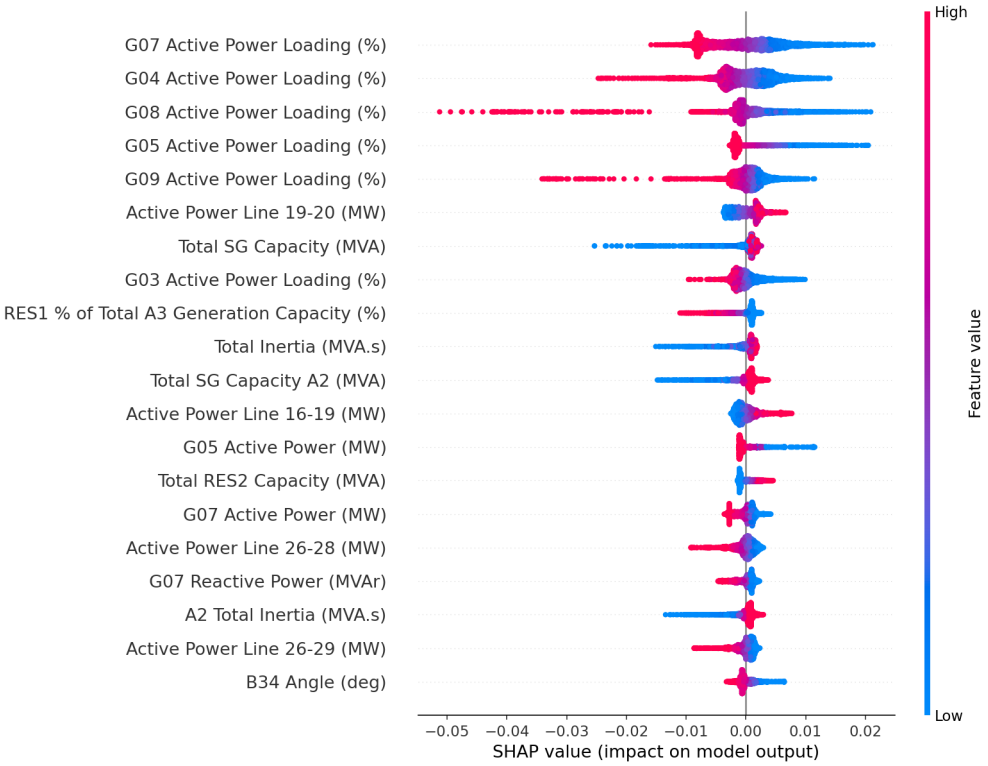

Figure 7.10: Global SHAP summary plot for top-20 features of Artificial Neural Network (ANN) model for CCT_{min} estimation.

There is some degree of consistency between PFI (Figure 7.9) and SHAP (Figure 7.10) feature importance, with 12 out of the 20 top important features appearing in both importance lists. The differences between the ordering of feature importance are caused by differences in the interpretability method used, with SHAP accounting for interaction effects between features whilst PFI only accounting for the impact on the model score with and without that feature. In addition, the level of detail able to be extracted is significantly greater with SHAP since it provides the feature effects and PFI does not. As outlined in Section 7.2.5, SHAP Explainers reduce the computational burden associated with calculating Shapley values by leveraging the attributes that different ML algorithms possess. Shapley values possess certain fairness properties, which is another reason why SHAP is particularly advantageous over methods such as PFI However, while significantly more efficient than calculating Shapley values, the insights available from SHAP still come with an associated time cost. This varies depending

on the explainer used; for example, KernelExplainer computes in exponential time, TreeExplainer in linear time and DeepExplainer scales with the size of the background data used.

The top-5 features in the example provided in Figure 7.9 relate exclusively to the active power loading of specific SGs, which is extensively reported to be important for transient stability in the literature [30]. Whilst this can be considered trivial from a power system dynamics perspective, the fact that important features match up with domain expertise enhances confidence in the ability of the black-box model to accurately represent power system dynamics. In addition, SHAP is useful because specific generators can be pinpointed, and the impact of their setpoints on the CCT prediction can be revealed for a large number of operational scenarios. This cannot be quickly and easily achieved using RMS-TDS alone. For example, Figure 7.9 pinpoints G07 active power loading (%) as the most important variable for CCT_{min} estimation. When G07 active power loading (%) is 'low' (blue), the model estimation for CCT_{min} increases from the expectation by up to 0.02 sec. Conversely when G07 active power loading (%) is 'high' (pink), the CCT_{min} model estimation decreases by up to 0.015 sec. Since a common colour axis is used for all features, the summary plot in Figure 7.9 cannot provide precise details of the actual generator active power loading due to the common colour axis used. The actual feature value can, however, can be plotted independently, as demonstrated below.

The impact of other VOI can also be observed, providing detailed information on the complex dynamics affecting transient stability. For example; 'low' SG capacity results in a reduction in CCT_{min} estimation. Similarly, 'high' RES2 capacity results in an increase in CCT_{min} estimation. The resulting insights depend on the features included in the TSDb, highlighting the importance of careful and considered feature selection.

Detailed Feature Dependence Insights

The SHAP summary plot highlights high-level relationships between power system variables and their impact on the prediction (as described above). Additional insights

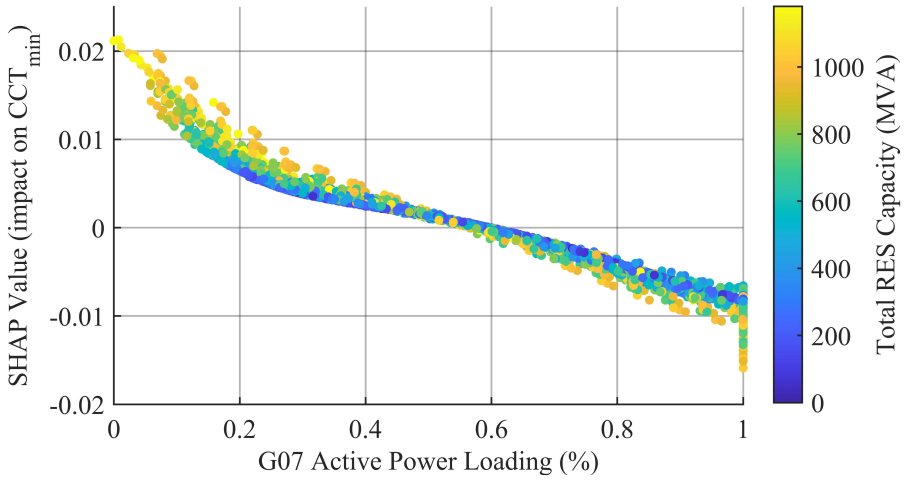

Figure 7.11: Dependence plot for G07 active power loading vs SHAP values with total Wind Farm (WF) capacity colour axis.

can be provided by looking at specific VOI in detail—which can be achieved using a dependence plot (e.g., Figure 7.11) that reveals the effect a single feature has on the predictions made by the model.

In a dependence plot, the SHAP values for a primary VOI can be plotted on the y-axis, with the feature value on the x-axis. An additional secondary VOI can be added to the colour axis, capturing interaction effects between features. In Figure 7.11, G07 active power loading (%) is taken as the primary VOI, since it is found to be the most important variable for CCT_{min} estimation (Figure 7.10). The corresponding SHAP values are given on the y-axis. The secondary VOI—here taken to be the total RES capacity (MVA) installed (since it may be of interest to assess the overall impact of RES on the transient stability margin)—is plotted on the colour axis. When G07 active power loading $< 55\%$, the impact on the model estimation of CCT_{min} is positive (i.e., increases the prediction for CCT_{min}). Inversely, when G07 active power loading $> 55\%$, the impact on the model estimation of CCT_{min} becomes negative (i.e., reduces the estimation for CCT_{min}). Therefore, an operational rule may be: "maintain G07 active power loading (%) below 55%".

In addition to this, the impact of the total RES capacity (MVA) on CCT_{min} estimation with respect to G07 active power loading (%) is revealed. The largest improvement

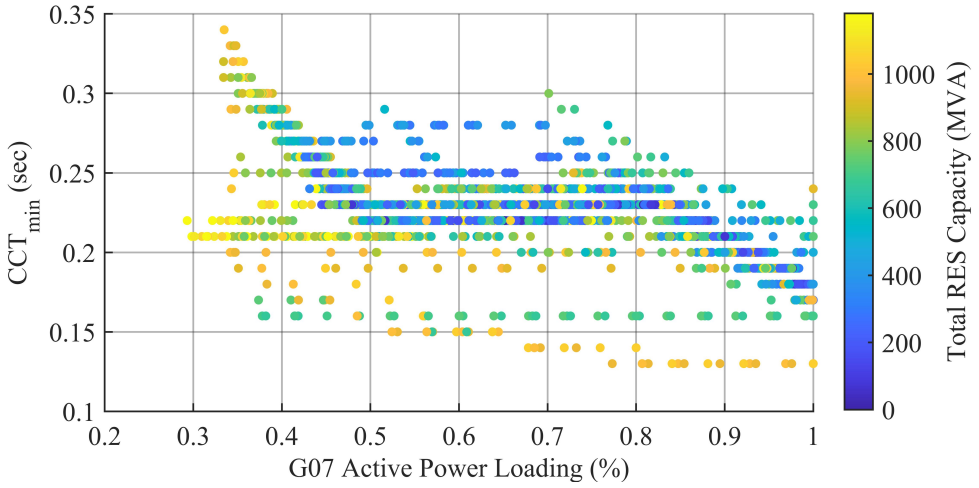

Figure 7.12: G07 Active power loading vs CCT_{min} training data with total RES capacity color axis.

in the CCT_{min} prediction is when G07 active power loading (%) $< 55\%$ and the system has a large RES capacity (MVA) connected. However, this trend reverses when G07 active power loading (%) $> 55\%$—suggesting an interaction effect between the two variables. Since a perfect linear relationship between G07 active power loading and the SHAP values is not observed (i.e., there is vertical dispersion of SHAP values for the same G07 active power loading value), this indicates that there are other parameters impacting CCT_{min}. When G07 loading $< 55\%$, the colour gradient (based on total RES capacity) changes from yellow to blue (top to bottom)—i.e. a higher RES capacity has more of a positive influence on CCT_{min}. Conversely when G07 loading $> 55\%$, the colour gradient goes from blue to yellow (top to bottom)—i.e., a lower RES capacity has a more positive impact on CCT_{min}. Therefore, another layer of complexity can be added to the previously described operational rule: "maintain G07 active power loading (%) below 55%, particularly if there is a high capacity of RES connected to the system". Identifying such relationships between power system variables on the stability margin is a key benefit of using SHAP and can be extended to other VOI.

To highlight the extent of the insights available using SHAP, a plot of the G07 active power loading and CCT_{min} training data is given in Figure 7.12. Whilst there is a negative correlation between G07 loading and CCT_{min}, the level of detail available

in the dependence plot (Figure 7.11) is not replicated when using training data alone as opposed to SHAP values.

7.4.6 Locational Trend Identification

A key aspect of the proposed methodology is the ability to identify trends not only between power system variables and CCT at a particular location but also between locations (refer to Figure 7.6 and 7.7). To achieve this, the covariance between a VOI and the location-specific SHAP values corresponding to that VOI for each ML model is calculated—resulting in $n+1$ covariance values per VOI. This is contingent on training a ML model at each location of interest (in this case, all busbars in the network) and obtaining the SHAP values for each feature across all operational scenarios.

SHAP Global Interpretations for all Location-Specific Models

All location-specific global SHAP summary plots are given in Appendix B, a selection of which are given in Figure 7.13. This provides a high-level system-wide perspective of the factors that impact the entire stability boundary. However, even with this reduction in the dimensions of the stability boundary on a locational basis—the complexity is still too great to identify trends and understand the system-wide impact of a power system VOI. The identification of locational trends using covariance between a particular power system VOI and location-specific SHAP values (e.g., Appendix B) is outlined below using two examples.

Example A: System-wide Impact of SG Active Power Loading

Taking the critical fault (CCT_{min}) once again as an example, a reasonable approach to enhance the stability margin would be to decrease G07 active power loading (the most important feature in Figure 7.10). The impact on CCTs of taking such an action can be assessed by calculating the covariance between G07 active power loading and the SHAP values for G07 active power output at each location, i.e., for the different ML models trained for each location (Figure 7.14). Locations B15, B17, B18 and B21-B24 all have similar (negative) covariance to CCT_{min}, suggesting that a decrease in G07

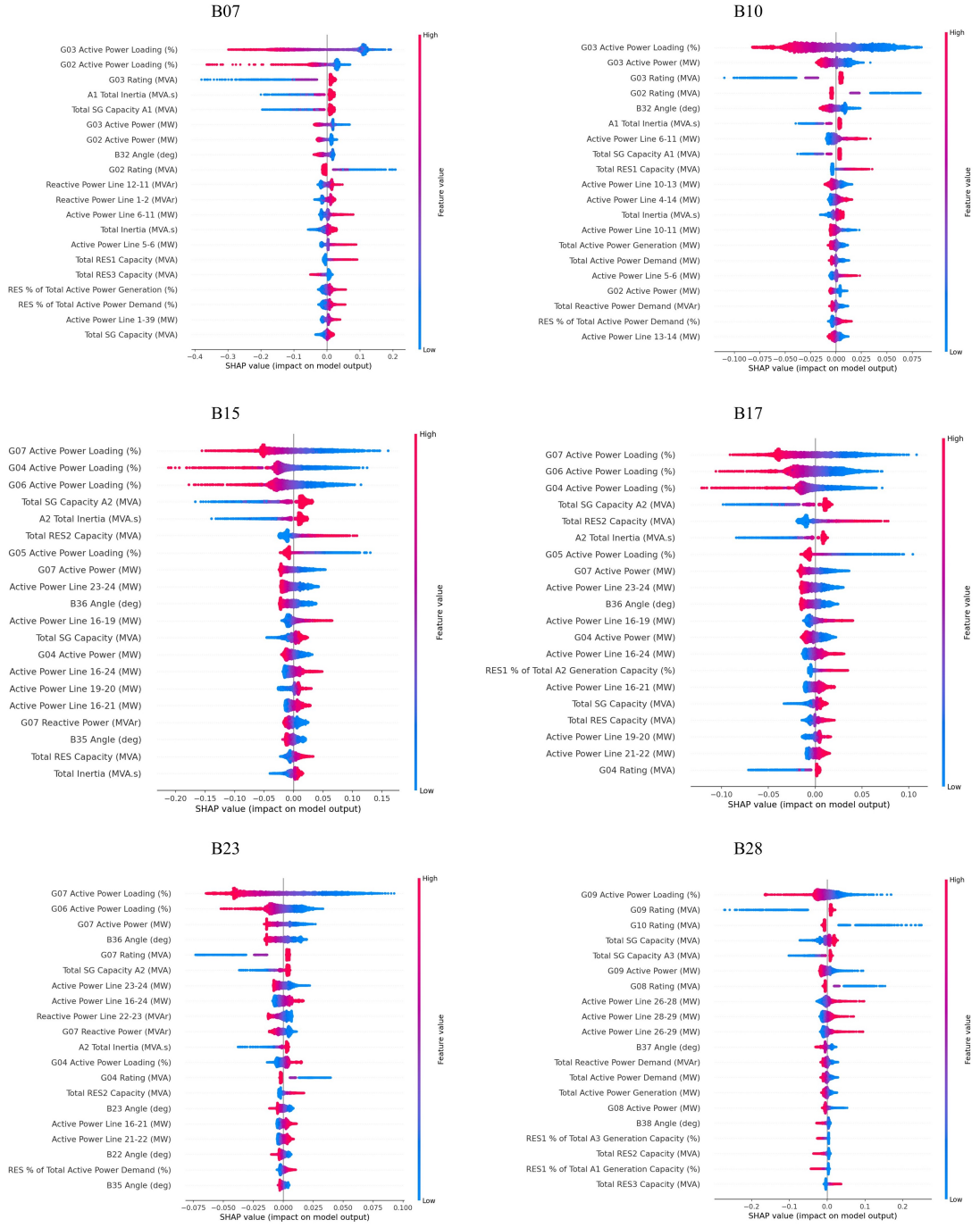

Figure 7.13: Stability boundary representation for six locations using SHAP to interpret locally trained artificial neural networks (ANNs).

active power output will result in stability margin improvement at these locations (i.e., inversely related). On the other hand, B14 has a small positive covariance, indicating CCT at this bus will deteriorate (i.e., shorten).

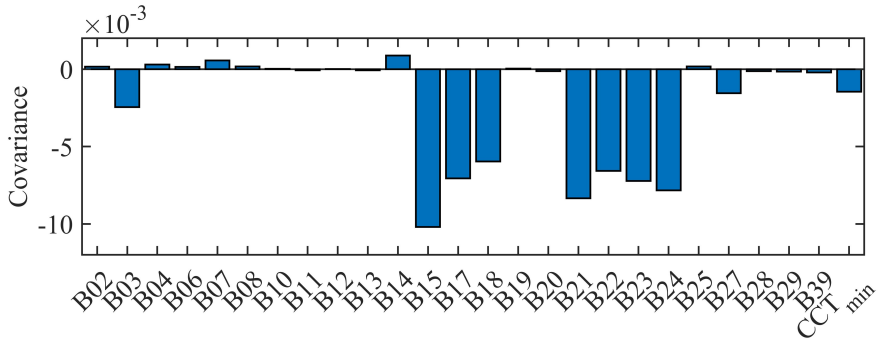

Figure 7.14: Covariance between G07 active power loading and G07 active power loading SHAP values at all locations for all $n+1$ ML models (n=25).

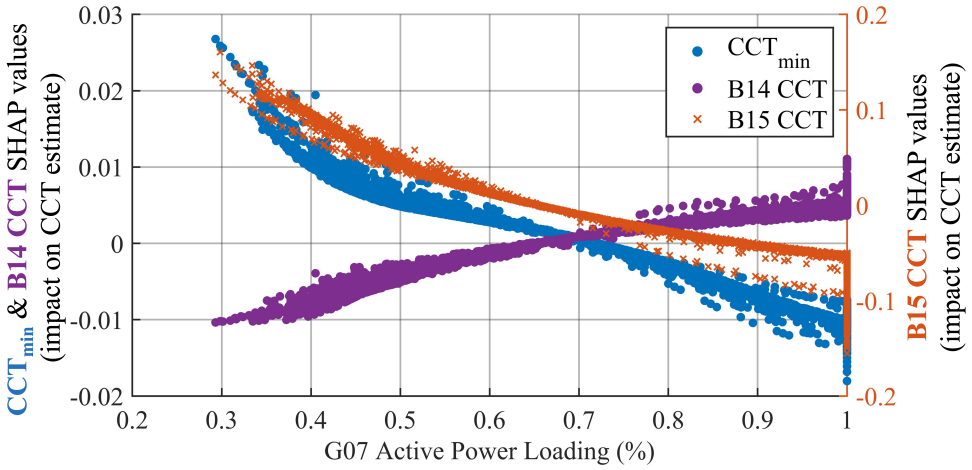

Figure 7.15: Impact of G07 active power loading on SHAP values for CCT_{min}, B15 and B14 models.

Figure 7.15 illustrates this for CCT_{min}, B15 and B14. A reduction in the active power loading of G07 from 100 to 40% may have as much as a 0.04 sec increase in CCT_{min}, 0.25 sec improvement at B15—whilst reducing B14 CCT by 0.02 sec. Since the typical CCT range for CCT_{min} is much shorter (more critical) than the typical CCT range for a B14 fault (Figure 7.16), this local deterioration in stability margin may be deemed acceptable on balance.

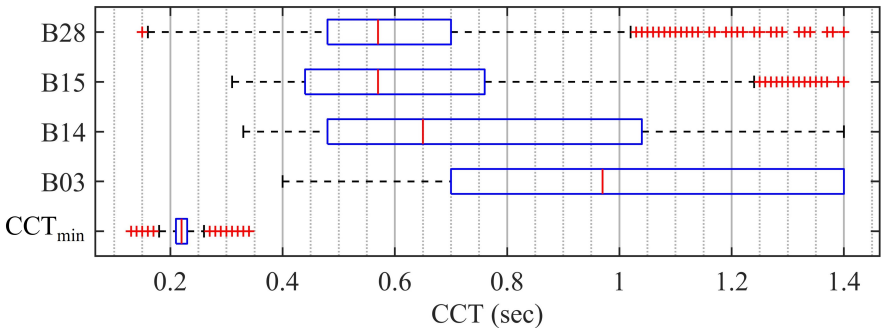

Figure 7.16: Critical Clearing Time (CCT) ranges for key fault locations of interest.

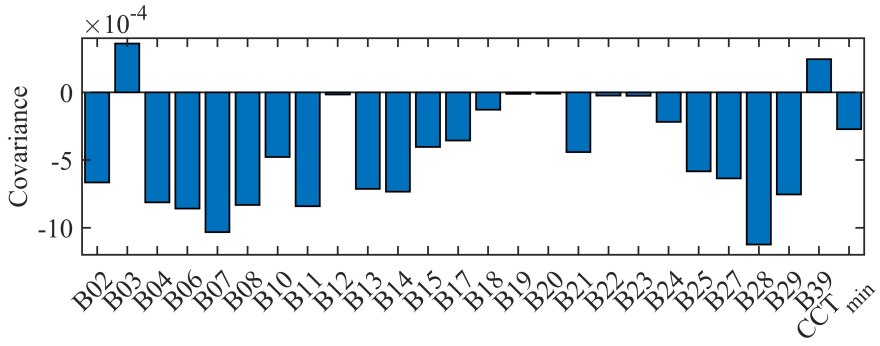

Figure 7.17: Covariance between RES3 percentage of total A3 generation capacity and locational SHAP values for all locations.

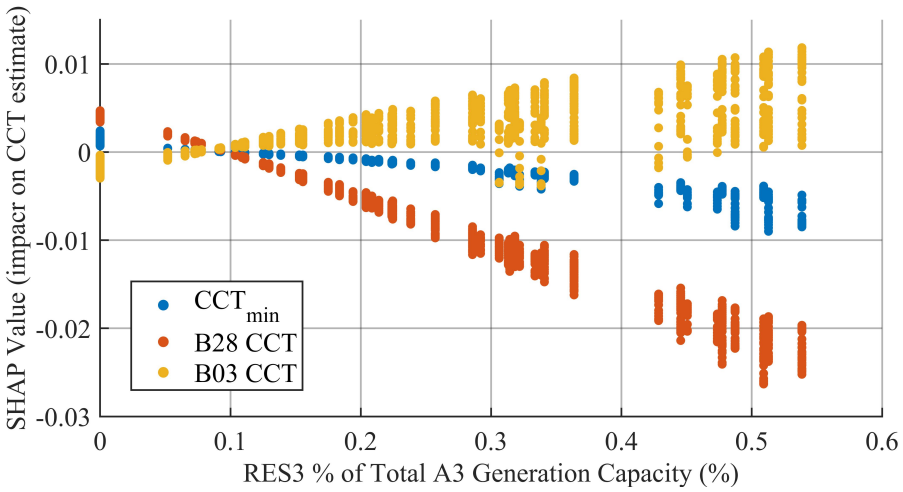

Figure 7.18: Impact of RES3 percentage of total A3 generating capacity on SHAP values for CCT_{min}, B03 and B28 models.

***Example B*: System-wide Impact of RES3 Penetration**

As previously outlined, the impact of SG active power loading on transient stability margin is widely documented in academic literature. However, similar analysis can be conducted for other important power system variables, such as the impact of the connection of RES on the stability margin.

Figure 7.17 shows the covariance between RES3 percentage of total A3 generation capacity and the stability margin at each location. An increase in the share of A3 generating capacity coming from RES3 has a negative impact (i.e., a reduction) on the CCT at almost every location (including the critical fault, CCT_{min}). It should also be noted that small increases are observed at B03 and B39. Figure 7.18 shows how B28 CCT is significantly impacted by an increase in RES3 share of A3 generating capacity, with B28 CCT prediction reducing by up to 0.02 sec. In addition, CCT_{min} reduces by up to 0.005 sec. Whilst this is a relatively small value, this is only one factor influencing CCT_{min} (which tends to be very short (Figure 7.16).

7.5 Conclusions

This Chapter presented a methodology based on SHAP to overcome the challenges previously set out associated with TSA in the context of increased CIG and the desire to understand better factors influencing the transient stability boundary. SHAP computes approximate Shapley values, giving the contribution of features in a model to the prediction for a given instance (i.e., local explanation). Local explanations can be extended across all instances, providing a global interpretation of the entire model. Using the SHAP framework in this manner to perform TSA reveals the contribution of power system variables to the prediction of the stability margin of a ML model—in the units used to measure the stability margin (in this instance, sec). The benefit of these types of insights are twofold:

- increase confidence in ML models in a very risk-averse industry, and
- reveal trends otherwise difficult to understand due to the increasing complexity

and uncertainty of power system operation.

Since transient stability is a locational problem, the methodology centres around a locational framework. Specifically, the proposed method involves training a ML model to predict the CCT at each bus n on a network and for different credible operational scenarios. An additional model is trained to predict the duration of the critical fault (i.e., the CCT_{min} of any bus for an operational scenario), resulting in a total of $n + 1$ ML models. This is identical to the steps outlined in Chapter 6; however, this method differs from the previous in that the SHAP framework is used to gain insights into each of the $n + 1$ location-specific models.

The method is applied to a modified version of the IEEE 39-bus networks with RES. The process of ML algorithm selection is demonstrated by increasing ML algorithm complexity until the desired degree of accuracy is reached—in this case through using ANN. The types of insights that SHAP can extract from individual ML models are then showcased (first locally, then globally) and compared to the results obtained using PFI. SHAP is shown to be capable of more detailed insights compared to PFI by capturing not just feature importances but also feature effects.

This Chapter also proposes a novel use of SHAP values to identify locational trends in the stability boundary. This is achieved by calculating the covariance between some power system VOI and the locational SHAP value for that VOI. In doing so, the system-wide impact on the stability margin of changes to that VOI is revealed. The insights provided could be used to formulate rules for system planners and operators, which are only available when using a locational approach as proposed.

Through the development of this locational methodology that leverages the powerful insights that can be obtained when using the SHAP framework, the three desirable attributes of TSA methods for modern power systems set out in Section 5.1 are met.

Chapter 8

The Impact of Wind Control Parameters and Location on Transient Stability using SHapley Additive exPlanations

8.1 Introduction

The previous two Chapters have focused on developing two methodologies that adhere to the three desirable attributes of modern TSA methods, defined in Section 5.1. Having addressed this in Chapter 6, an improved location-based approach using the SHAP framework to gain detailed insights into power system variables impact on the transient stability margin was proposed in Chapter 7.

Therefore, this Chapter seeks to showcase further the powerful insights that SHAP can provide. In particular, this Chapter aims to understand the specific impact of WTG controller parameters and location on the transient stability margin with respect to other important parameters (which were first introduced in this thesis in Chapter 3 and Appendix A) using aspects of the methodology presented in Chapter 7. Such an analysis is likely most suitable for a planning environment where computational speed

is not a primary concern. Whilst the results presented in this Chapter are specific to the test network used, and the single contingency analysed, the method could be implemented on any network to conduct a similar analysis.

8.1.1 Contributions

The novel contribution from this Chapter is the application of a version of the SHAP method outlined in Chapter 7 to identify important power system variables and quantify their impact on the transient stability margin (specifically the CCT), with a particular focus on understanding the impact of WTG *controller parameters* and *location*.

These aspects are included as *categorical variables*, highlighting the ability of SHAP to identify trends in both continuous and categorical variables. This is important to demonstrate since variables may not always be continuous. For example, a planner may only have a choice between connecting a WF in location A or B. Similarly, a network owner or operator may want to test the impact of a few updated RES control parameter options (e.g., current vs proposed controller settings proposed by a manufacturer). Interdependencies between important variables can also be identified using the proposed method, enabling the extraction of system-specific conclusions from a system agnostic method.

8.2 Methodology

Operational scenarios are designed to illustrate disconnection of SG and connection of RES (specifically WTG). As in previous Chapters, the generator dispatch is determined via an AC-OPF. In doing so, the impact of the market on generator dispatch and, thus, transient stability is realised. RMS-TDS used to determine the stability margin (specifically the CCT) for each dispatch for a specified fault. Power system variables relating to SG, RES and system attributes are selected as features for the TSDb and the CCT is included as the target. In this Chapter, additional categorical features relating to; (a) wind control parameter settings and (b) WF location are also included as features in the TSDb since these are of particular interest in this Chapter. The

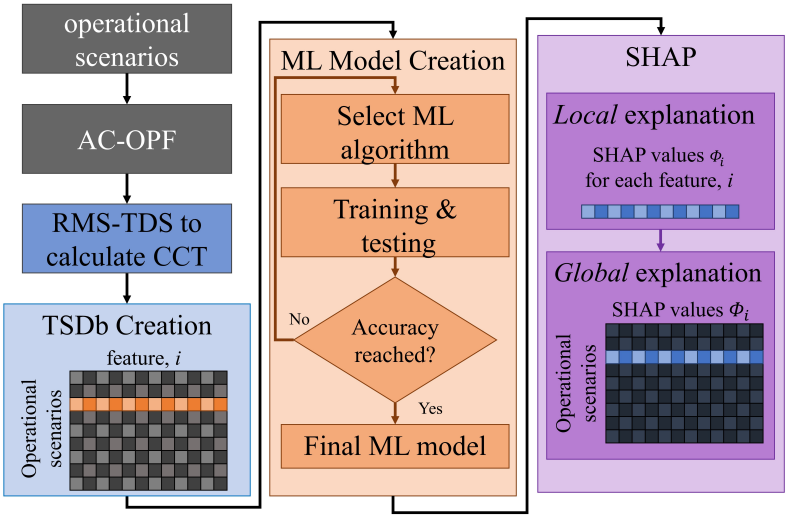

Figure 8.1: Overview of the proposed methodology.

TSDb is divided into a training and testing portion and different ML algorithms tested until the desired level of accuracy is achieved. Finally, SHAP is used to gain detailed insights into the ML model (Figure 8.1).

8.2.1 Generator Dispatch via AC Optimal Power Flow

The procedure used to determine the generator dispatch is described in Section 6.2.1.

8.2.2 Transient Stability and the Critical Clearing Time

The means of determining the stability margin is outlined in Section 2.5.2.

8.2.3 Feature Selection and Transient Stability Database Creation

As outlined in Section 5.2, a TSDb consists of some power system variables (features, X) and the transient stability margin (CCT) of the system for a specified fault (target, Y) (Figure 5.2). This is created using a series of simulated system responses to a short-circuit fault via RMS-TDS in DIgSILENT PowerFactory. A ML algorithm is then trained using the TSDb to identify the relationship between the features and the target.

SG	RES	System
$\mathrm{SG}_{P,v}, SG_{Q,v}, SG_{MVA,v}$, $\mathrm{SG}_{MVA,k,total}, SG_{MVA,total}$, $\mathrm{SG}_{H,v}, SG_{H,k,total}, SG_{H,total}$, $\mathrm{SG}_{P,max,v}, SG_{P,min,v}, SG_{Q,max,v}$, $\mathrm{SG}_{Q,min,v}, SG_{Ploading,v}$.	$\mathrm{RES}_{P,w}, RES_{Q,w}$, $\mathrm{RES}_{MVA,w}$, $\mathrm{RES}_{MVA,total}$, Location, Control Parameter Category.	$\mathrm{P}_{d,l}, Q_{d,l}$, $\mathrm{v}_{bus,n}, v_{bus,\delta,n}$, $\mathrm{P}_{from,n}, P_{to,n}$, $\mathrm{Q}_{from,n}, Q_{to,n}$.

Table 8.1: Power system features used for model training.

Feature Selection

The importance of feature selection in relation to both accuracy and interpretability has been discussed extensively throughout this thesis. Since this Chapter is particularly focused on the impact of RES (specifically location and parameters) in the context of reducing SG capacity, features relating to this are included in the TSDb in Table 8.1. This includes SG attributes (i.e., MVA rating and inertia), RES capacity, generator set points (P, Q and V of SG and RES), network voltages and angles and demand level (both P and Q). Full details are provided in Table 8.1 for a network with k generating areas, v SG units, w RES units, l loads and n busbars.

In addition, RES controller parameters and RES location are each included as separate categorical features. *Categorical* features are encoded using integer encoding, where each unique label is mapped to an integer. Including these features may offer limited additional predictive power to the model; however, insights relating to optimal parameter settings with respect to other important power system variables may be uncovered using SHAP. RES controller categories are encoded using integer encoding, defined in Table 8.2. Similarly, RES location is also included as a categorical feature based on generating area (Figure 8.2).

Target Selection

A single contingency is considered in this study at bus 27, as the locational aspects of transient stability have been addressed in previous Chapters. Therefore the target is the CCT at a single location of interest (i.e., a location where a planner or operator has a particular interest in the stability margin). Should other locations be of interest,

a different busbar can be selected.

8.2.4 Machine Learning Algorithm Selection

In this Chapter, the accuracy of tree-based algorithms is compared using the framework set out in Section 7.2.3. In particular DT, RF and XGBoost.

8.2.5 Desired Accuracy

Section 7.2.3 set out a process for selecting the ML algorithm. The performance metrics used to assess the accuracy of the ML models are defined in Section 5.2.3. In this Chapter RSQ, RMSE and MAPE (Equation 5.2, 5.3 and 6.5 respectively) are used to benchmark performance. Here acceptable model accuracy is defined as a model with a RMSE < 0.05 sec.

The accuracy metric(s) used and desired accuracy threshold can be varied depending on the requirements and proposed use of the method. For example, in Chapter 7 MOE and MUE were of interest in order to minimise maximum errors. However, in this Chapter, to avoid further complexity, MOE and MUE are not deemed necessary since the focus is on understanding trends relating to RES location and control parameters in more of an offline type of analysis. Whilst accuracy is important, it is not as important as an online application—such as the one presented in Chapter 7.

8.3 Test Network and Case Study Details

The proposed method is demonstrated on an adapted version of the IEEE 39-bus, 10-generator test network (Figure 8.2). The RMS-TDS simulations are carried out in DIgSILENT PowerFactory [171] and the AC-OPF is solved in MATPOWER [106]. A set of operational scenarios designed to represent how the generation connected to the system may change as a result of planning or operational decisions (i.e., closure of SG plant and the opening of WFs, which may be as a consequence of government policy), is outlined in below.

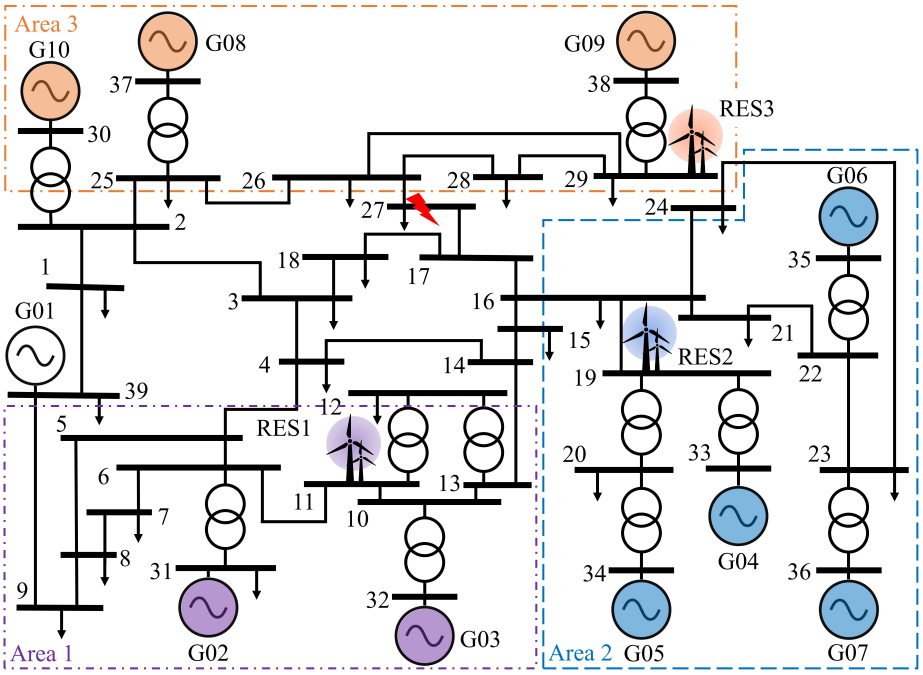

Figure 8.2: Adapted version of IEEE 39-bus, 10-generator test network with wind connected to B29. Fault location at bus 27 indicated.

8.3.1 IEEE 39-Bus Test Network Overview

An adapted version of the IEEE 39-bus network is used for these studies and is described in detail in Chapter 6. However in these studies, the RES connects at different locations (see Figure 8.2) compared to Chapter 6.

IEC Type-4A wind turbines [103] are used to model wind generation in these studies. This means that the dynamic characteristics of wind—including the LVRT capabilities—on the dynamic response of the system is captured in the CCT. The controller operates at unity power factor pre-fault. This may vary between systems and will impact reactive power dispatch and, thus, transient stability. A WF is treated as an aggregate of individual 2 MW turbines connected in parallel, each with its own transformer. As in previous studies, the volume of wind and connection location (which is included as a categorical variable in the TSDb) on the network depends on the operational scenario. Three generation areas are defined (Figure 8.2). The location of RES is encoded using integer encoding in the TSDb based on the area number.

Category (encoding)	K_{qv} (I_n)	I_{qh1} (I_n)	I_{maxdip} (I_n)	dp_{maxp4a} (P_n/sec)
A: default (1)	2	1.05	1.2	1
B: fault-on, **fast** post-fault (2)	10	1.155	1.08	1
C: fault-on, **slow** post-fault (3)	10	1.155	1.08	0.8

Table 8.2: Wind control parameter categories considered. Category A (default), B (fault-on and fast post-fault) and C (fault-on and slow post-fault).

As previously outlined, these studies are interested in developing a method capable of assessing the impact of typical system variables, as well as RES control parameters and RES location. In Appendix A, the impact of RES connecting to a simple SMIB was investigated. In particular, the impact of changes to the fault-on and post-fault parameters were investigated. From this, three RES control parameter categories can be extracted (defined in Table 8.2), which are defined below.

- Category A: Original parameters. The *default* parameters are taken from [171], forming a baseline.
- Category B: *Fault-on* parameters and **fast** *post-fault* recovery. The proposed fault-on parameters (Table A.2) are used, along with the fast active power recovery ramp rate.
- Category C: *Fault-on* parameters and **slow** *post-fault* recovery. The proposed fault-on parameters (Table A.2) are used, however a slow active power recovery ramp rate is adopted.

The impact of each control parameter category (defined in Table 8.2) on the output from the WF in the IEEE 39-bus network is demonstrated by connecting RES3 to B29 with an output 700 MW and applying a zero-impedance three-phase-to-ground fault with a 150 msec duration at B27 (Figure 8.3). Between Category A and B, the fault-on active power is significantly reduced and reactive injection somewhat increased, permitting SGs to export more active power. Category C has the same fault-on behaviour as B; however, category C has a slower rate at which the active power recovers. Note that between category A and B there is no change to the active power recovery ramp

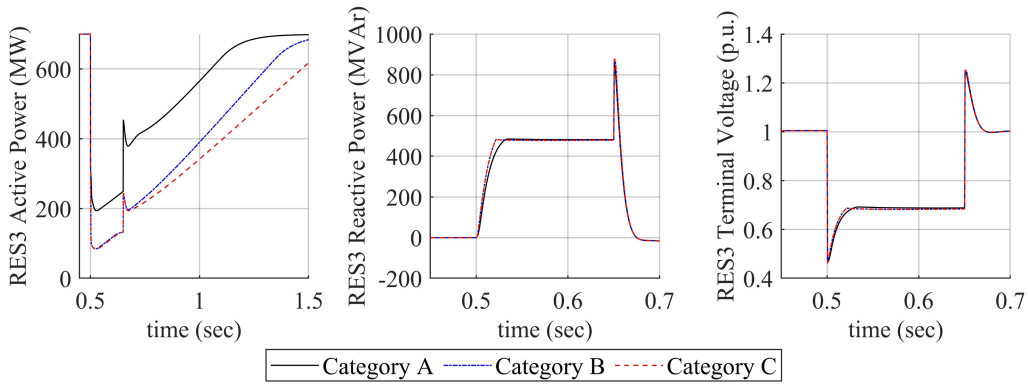

Figure 8.3: Time-series response for RES3 active power, reactive power and terminal voltage for each control parameter category in IEEE 39-bus test network.

rate (dp_{maxp4a}) (Table 8.2), however the recovery rate observed in Figure 8.2 is different. This suggests the reduction in active power output due to changes in the fault-on parameters is also impacting the post-fault period—further adding to the complexity and highlighting the need for methods such as the one proposed to better understand the stability boundary.

8.3.2 Operational Scenarios

The operational scenarios used are detailed in Section 6.4.3; however, the database is expanded to reflect the 3 controller parameter setting categories specified. In total 11,682 operational scenarios are designed based on 18 demand levels, 36 SG disconnection stages (9 SGs, each disconnected in 4 stages), 6 RES levels and 3 controller parameter setting categories (Table 8.2). This results in 11,664 displacement scenarios, plus 18 scenarios with no displacement. From these 11,682 operational scenarios, 954 (that is 8.2%) do not result in a successful convergence of the OPF solution. For the successfully converged scenarios (10,728, that is 91.8%) RMS-TDS are executed using DIgSILENT PowerFactory, for all fault locations. B27 (indicated by the red bolt in Figure 8.2) is selected as the fault location; however, the same approach can be applied to any fault of interest in the same manner.

Performance Metric	DT	RF	XGBoost
RSQ	0.9857	0.9910	0.9945
MSE (sec^2)	0.0042	0.0026	0.0016
RMSE (sec)	0.0645	0.0514	0.0400
MAPE (%)	0.4576	0.4653	0.3341

Table 8.3: Accuracy achieved by different tree-based Machine Learning (ML) algorithms.

8.4 Results

The following section details key results and findings from implementing the proposed methodology on the IEEE 39-bus test network for the case study previously described.

8.4.1 Accuracy

As previously outlined, the accuracy of a ML model is extremely important and typically improves with model complexity. To illustrate this, the accuracy between three different tree-based methods are compared (specifically DT, RF and XGBoost implemented using scikit-learn [175] with no tuning of hyperparameters in this instance. Note that tuning hyperparameters will impact the performance of the models). Accuracy of the method is reported in Table 8.3 using the metrics outlined in Section 8.2. The performance of the XGBoost model exceeds that of both DT and RF across all accuracy metrics considered. The high degree of accuracy achieved by the XGBoost model for B27 CCT prediction increases confidence in any interpretations obtained from the model using the SHAP framework, since the model is closely replicating RMS-TDS results compared to DT and RF algorithms. In this instance, only the XGBoost algorithm satisfies the accuracy condition specified of RMSE < 0.05 sec (set out above).

8.4.2 Interpretability: Wind Control Parameter and Wind Farm Location Insights

The SHAP summary plot (Figure 8.4) provides an indication of the relationship between the value of a feature (power system variables) and the impact on the prediction from the base value ($E[f(x)]$) for each operational scenario in the training data (i.e., the

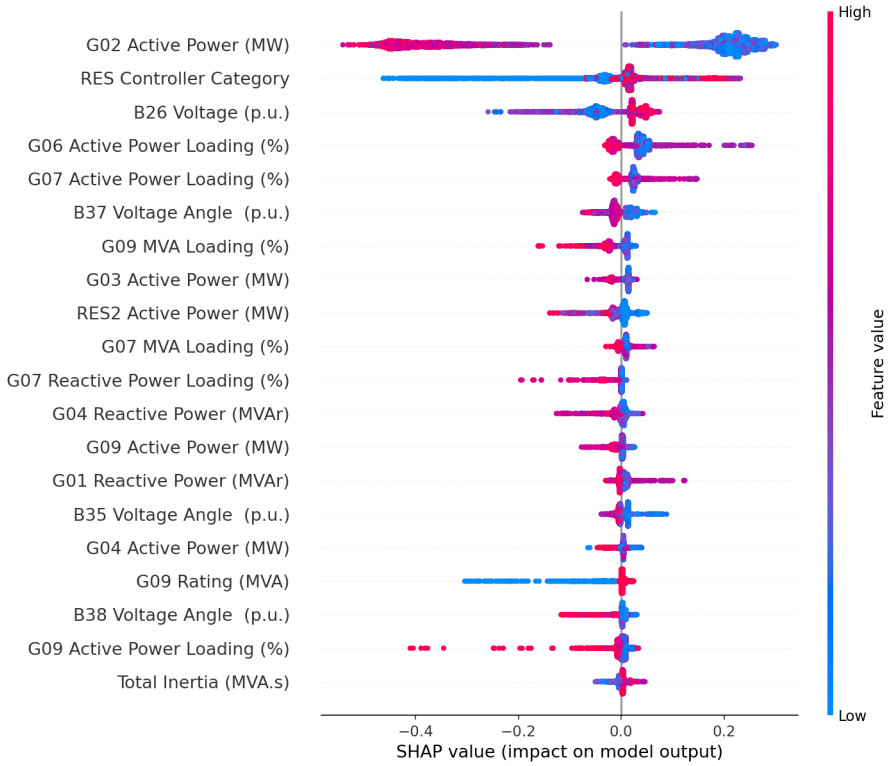

Figure 8.4: Global SHapley Additive exPlanations (SHAP) summary plot highlighting feature importance, SHAP values and feature values for top-20 most important features.

CCT prediction, in sec). The most important feature is G02 active power output, and the SHAP values with respect to MW output are given in Figure 8.5. In doing so, the impact of G02 active power output (in MW) on the model prediction of B27 CCT can be revealed in sec. In this case, there is a clear threshold of 145 MW, above which the model prediction for B27 CCT is negatively impacted by up to -0.4 sec.

Notably, the second most important feature in Figure 8.4 is identified as the RES controller setting category (category encoding given in Table 8.2: A=1, B=2 & C=3). When RES control parameter category A is used, the prediction of B27 CCT is consistently negatively impacted. When categories B or C are used, the model prediction typically improves. Since the RES controller parameters in categories B and C reduce the fault-on active power output from RES, this is a key reason for this trend. There is no observable difference between category B and C, suggesting that in this instance (i.e., for these operational scenarios in this network), changes to the post-fault recovery

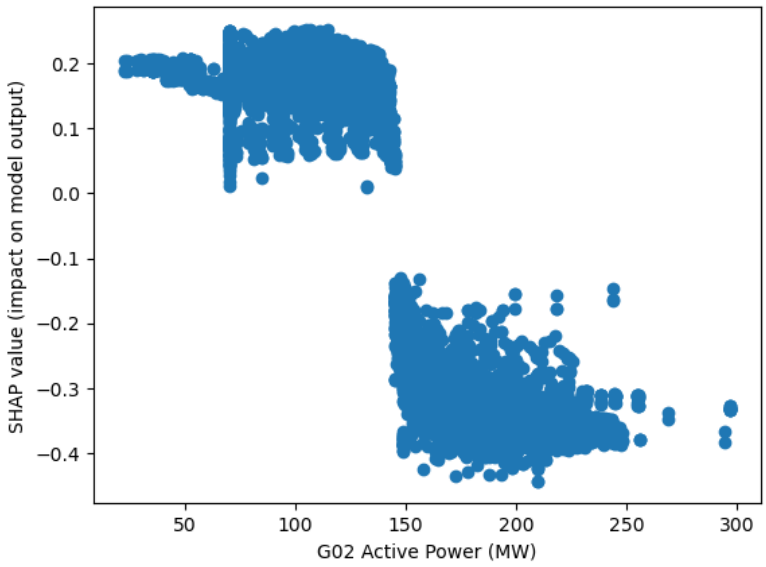

Figure 8.5: G02 active power output vs SHapley Additive exPlanations (SHAP) values.

ramp rate have no impact on the stability margin at B27.

While this offers a high-level overview of the impact of RES control parameters, more details around the interdependencies with other power system features are also desirable. This is achieved using feature dependence plots, where a VOI can be plotted with SHAP values for that feature, and a second feature is plotted on the colour axis. In doing so, the interaction effects between important features and the model prediction can be uncovered.

For example, a system planner may be particularly interested in the impact of decommissioning G09 and connecting RES (due to their position in a radial part of the network (Figure 8.2)) on the transient stability margin at B27. In particular, the system planner may be interested in specifying wind controller settings for a WF connecting to the network to ensure sufficient transient stability margin. Therefore, G09 MVA rating and RES controller category would be selected as VOI (Figure 8.6). The four stages of G09 disconnection are visible on the x-axis. When G09 is not disconnected (G09 = 1000 MVA), the CCT at B27 is positively impacted. Once G09 is disconnected (G09 Rating $<$ 1000 MVA), the prediction for B27 CCT is negatively impacted. This negative impact is most pronounced when the G09 rating is 750 MVA and improves somewhat

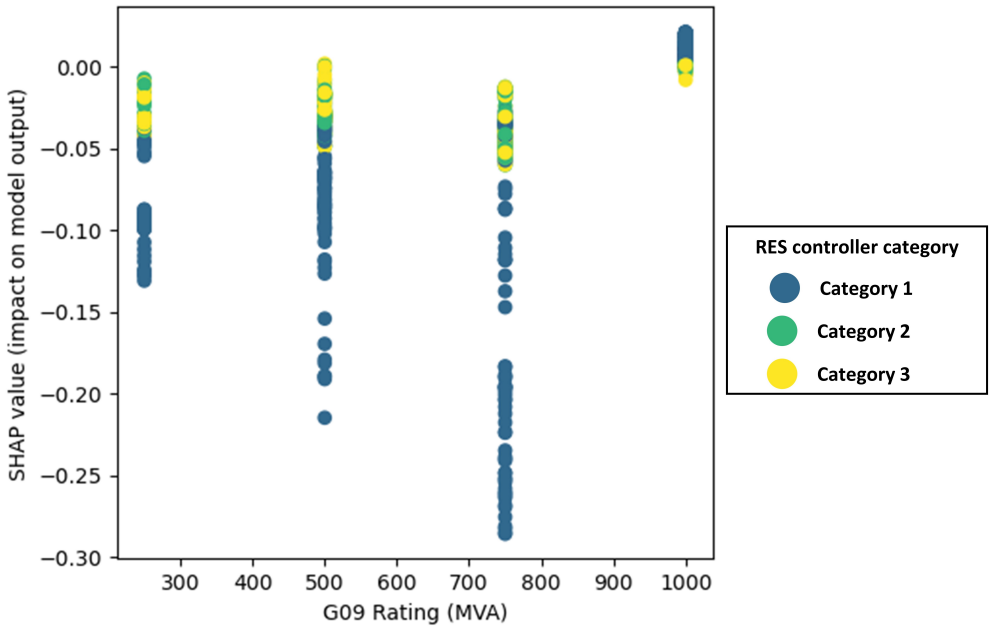

Figure 8.6: G09 rating (MVA) vs SHapley Additive exPlanations (SHAP) value with wind control parameter category.

as G09 is disconnected further. Since RES3 and G09 are connected and disconnected in a similar inverse manner, this is capturing the ability of a larger RES3 to support a smaller G09 through LVRT behaviour (decrease in active power and injection of reactive power). This conclusion is further reinforced when looking at the colour axis. Adopting wind controller settings that further reduce the active power from RES (i.e., category B (green points) and C (yellow points) that enhance the braking resistor effect), the negative impact on B27 CCT prediction is significantly reduced when G09 is disconnected.

As previously outlined, the location of RES with respect to SG has been demonstrated to impact transient stability in academic literature [30]. As such, the impact of RES location on B27 CCT with respect to G06 active power loading (the 4$^{\text{th}}$ most important feature (Figure 8.4)) is given in Figure 8.7. From engineering principles, this makes sense because G06 is electrically close to the fault location. A lower active power loading (%) for G06 increases the B27 CCT prediction; conversely, when G06 active power loading is greater than 70% the model prediction is negatively impacted. The equal area criterion (Figure 2.8) outlines that when a SG has a higher active power

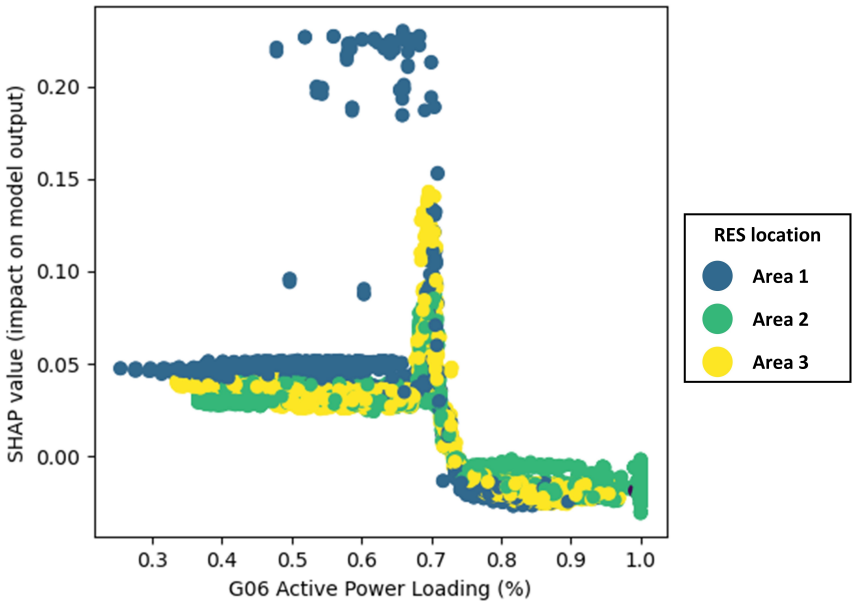

Figure 8.7: G06 active power loading (%) vs SHapley Additive exPlanations (SHAP) value with Wind Farm (WF) location.

loading, it is more susceptible to LOS and thus has a large impact on the overall system transient stability.

The location of the connection of RES is given on the colour axis in Figure 8.7. Specifically, for scenarios where G06 active power loading is $< 70\%$, the largest SHAP values are when RES is connected in area 1 (blue points). Conversely, for scenarios where G06 active power loading is $> 70\%$, the largest SHAP values are when RES is connected in area 2 (green points). This highlights an interdependency between RES location and G06 active power loading. Therefore, when RES is connected in area 2, the favourable LVRT behaviour from RES has a larger influence G06 dynamic response due to the relatively short electrical distance between G06 and RES2 (Figure 8.2). Furthermore, the reduced inertia of G06 in these scenarios means that the machine accumulates less energy during the fault.

Planning and/or operational rules can be extracted from an analysis using the SHAP framework, with a solid theoretical mathematical foundation from Shapley values, unlike other interpretability approaches. The selection of features for rule development could be based on; (a) most important features, (b) controllable features or (c) features

of interest after applying engineering judgement.

8.5 Discussion

Results highlight the impact of RES controller parameters on transient stability and the efficacy of SHAP in identifying favourable settings from a transient stability perspective. The parameter sets selected for these studies sought to further reduce the active power output from RES during the fault-on period compared to the standard LVRT behaviour. In addition, the post-fault active power recovery ramp rate was varied. SHAP (Figure 8.4) assigns high importance to RES controller settings, suggesting that control parameter selection is crucial. In addition to assigning importance scores to features, SHAP can also identify the extent to which features impact the stability margin—including control parameter categories. For example, Figure 8.4 shows that a low RES controller category (i.e., the default RES controller parameter settings category A in Table 8.2) is associated with a reduction in CCT by as much as -0.4 sec. There is no observable difference between categories B and C, suggesting that the fault-on decrease in active power is the main reason for transient stability improvements for these particular case studies in this network. This can be likened to a braking resistor; however, implementing changes to RES control parameters is likely far cheaper and easier to implement than installing braking resistors in a power system. Indeed, changes to RES controller settings could be specified in connection agreements or grid code.

It should be highlighted that RES control parameters are not a problem exclusive to power systems with high-RES penetration. The complex interactions of multiple features can interact in such a manner as to reduce transient stability even with low volumes of RES. The high dimensionality of the transient stability boundary is large, making tools such as SHAP highly effective in developing a detailed understanding of the transient stability boundary, particularly in the context of non-linear dynamics introduced by RES. Insights can be compared to domain expertise and engineering judgement applied to test the robustness and be backed up by subsequent targeted RMS-TDS.

8.6 Conclusion

This Chapter presented a modified use of the core SHAP-based methodology presented in Chapter 7 to specifically reveal the impact of RES control parameters (introduced in Chapter 4 and Appendix A) and location (analysed in Chapter 4).

The SHAP framework [162] was used to gain detailed insights into a ML model trained to predict the stability margin. In order to obtain SHAP values relating to wind control parameter settings and location, and thus their impact on the transient stability margin, they were included in the TSDb as categorical features. A XGBoost model was subsequently trained to predict the stability margin (specifically, the CCT) for a three-phase-to-ground short circuit on bus 27 of the IEEE 39-bus network. XGBoost was found to be the only algorithm tested to reach the desired level of accuracy in the example given, with a RMSE of 0.04 sec.

The ability of the proposed method to effectively identify trends in locational and control parameters was demonstrated. Results show that the RES control parameters are highly important in the case study presented in this Chapter. It was found that the transient stability margin increases when controller settings further reduce the fault-on active power compared to the original LVRT settings. It was also found that the location of RES was not found to have high importance; however, the impact of RES location with respect to SG loading was uncovered. Results showed that whilst an SG with high active power loading reduces the model prediction for CCT, connecting RES closer to that highly loaded SG can mitigate this effect.

Such an analysis could form part of the process for new connection agreements and/or network reinforcement planning processes. Including a SHAP-based methodology as a guiding tool in an offline environment may be the first step in building confidence and understanding in the SHAP framework in power system communities for broader use.

Chapter 9

Conclusions and Further Work

For decades, power systems have been built and operated around conventional thermal SG and the associated characteristics. The drive to decarbonise electrical power generation is driving changes to the mix of generation connected to modern power systems. In particular, this has resulted in conventional thermal SG such as coal and gas plant, being displaced by RES such as WFs and solar PVs. RES often connect in locations remote from demand centres where the natural resource is abundant, leading to changes in network power flows. Moreover, the intermittent nature of RES means that the power output can fluctuate significantly in relatively short timescales. This will lead to changes in the setpoints of the remaining SG, which will impact transient stability. In addition, during 2022, extreme European gas price volatility [5] has led to changes in operational practices across the continent, such as the emergency recommissioning of coal-fired generation in Germany [4]. These fast policy changes in response to market price signals may lead to irregular generator dispatch patterns and changes to the transient stability boundary.

Along with changes to generators connected, their setpoints and resulting network power flows—SG and RES possess significantly different dynamic characteristics. Many RES are connected to power systems via PEC, which decouples any rotational mass that would otherwise help to slow the response of the system to a fault (as is the case with SG). This is further complicated by the non-linear control behaviour of CIG.

The extent of this complexity was showcased in Chapter 3 through a detailed lit-

erature review. The review demonstrates the vast number of variables and parameters that have been shown to impact the transient stability boundary, many of which are often linked in complex non-linear ways. This Chapter addresses research question 1, set out in Section 1.1.2. This is further emphasised by the supplementary studies in Appendix A that use a SMIB with RES added to highlight some mechanisms that impact transient stability. A common drawback with much of the existing literature is that single parameters or variables are frequently isolated to understand their specific impact. What is more, the findings of the studies are frequently specific to the simple systems used in these studies. As such, these studies are often constrained to the academic domain, where they are useful for simplifying the transient stability problem to understand the mechanisms at play better. Therefore, it is concluded that methodologies that can be used for TSA of any power system is advantageous.

Addressing research question 1, Chapter 4 also aimed to demonstrate some key mechanisms that impact transient stability through carefully designed operational scenarios and a simple test network. In particular, this Chapter investigated the impact of generator cost (which consequently determines generator dispatch) and the location of RES on transient stability. Whilst the work was published in 2020, the impact of generator cost on system stability is only now (in 2022, during a period of unprecedented gas price volatility) becoming more apparent. The studies presented in this Chapter showed that (in an adapted version of the IEEE 9-bus network); (a) connecting WFs close to low-cost generators (i.e., that frequently run at full output) could lead to improvements in transient stability for local generators whilst the stability of more distant machines may deteriorate, and (b) the uncertain nature of wind can vary the loading of conventional generation such that the CFL and CSG could change in operational timescales. These trends may differ in larger (and inherently more complex) systems.

Such trends are only able to be captured due to the extensive (and computationally expensive) methodology that specifies that stability margin should be determined at each bus using RMS-TDS. Such changes to the CFL and duration of $\mathrm{CCT}_{\mathrm{min}}$ may go undetected unless TSA is performed with sufficient locational granularity.

The significant and unpredictable changes to the transient stability margin high-

lighted in Chapter 3 and Chapter 4 as a consequence of increasing volumes of RES connecting increases the requirement for detailed TSA. This is also highlighted in the studies in Appendix A. Existing tools for TSA have different limitations. For example, TEF-based methods are computationally inexpensive but cannot represent the dynamic characteristics of RES. Conversely, the more widely used RMS-TDS can capture the full dynamic response of RES but are computationally expensive, leading to a requirement for the development of new tools and methodologies capable of detailed analysis to ensure sufficient stability margins. Moreover, there is also a desire to uncover the predominant factors that influence transient stability, which can then be used to design transient stability enhancement measures. Therefore, addressing research question 2, this thesis sets out *three desirable attributes* that new methods for TSA in modern power systems should possess:

1. reduction of computational expense in operational timescales,
2. enhancement of understanding of the predominant factors influencing the transient stability boundary, and
3. accurate representation of the transient stability boundary.

This thesis proposed the use of ML to accelerate the computationally heavy task of RMS-TDS (which can capture the dynamic response of CIG), thus addressing desirable attributes 1 and 3. In addition, the use of IML—an emerging area of research capable of uncovering how complex ML models make predictions—is proposed to address desirable attribute 2. Indeed, developing such methodologies was the focus of the remaining Chapters.

Chapter 6 presents a methodology centred around DTs, that is capable of fast and accurate estimation of the transient stability margin at each bus of a system—directly addressing research questions 3 and 4. Due to the exhaustive locational nature of the proposed method (as first proposed in Chapter 4), the $\mathrm{CCT}_{\mathrm{min}}$ and CFL can also be predicted. PFI is used to interrogate the location-specific DT models to determine an importance-ranked list of power system parameters—going some way in addressing

research question 5. The proposed method is demonstrated using an adapted version of the IEEE 39-bus test network, achieving high accuracy for all DT models, with some variation. Specifically, MAPE averages 1.27 % across all DTs (ranging 0.34–2.45 % at B19 and B27 respectively). In addition, the RSQ averages 0.9756 across all DTs (ranging 0.9403–0.9975 at B10 and B21) and the average RMSE is 0.0279 sec (ranging 0.0037–0.0689 sec at B19 and B27). Estimation of CCT_{min} is also found to be highly accurate for both CCT_{min} estimation methods proposed. Whilst the methodology technically possesses the three desirable attributes, there are two key limitations. Firstly, the method is constrained to using DTs for extracting key threshold values of the important parameters influencing the stability boundary. In some instances, this may result in poor model accuracy and, thus, inaccurate insights. Second, PFI gives global feature importance and not the more informative feature effect.

Chapter 7 seeks to overcome these limitations and answer research questions 4 and 5 more comprehensively. This is achieved through the model-agnostic SHAP framework, which provides feature effects for local points that can be extended to provide global interpretations of the model. The model-agnostic nature means that accuracy does not need to be sacrificed for interpretability. Indeed, a process is outlined for ML algorithm selection based on a user-defined accuracy threshold. A case study using an adapted version of the IEEE 39-bus test network demonstrated how SHAP can be used to reveal important power system variables in a ML model.

In the case study presented, various ML algorithms are trained to predict the stability margin (the CCT) at each bus with a reduced online computational burden. It is found that an ANN is the only algorithm to surpass the desired accuracy threshold. A single operational scenario can be analysed using the local SHAP insights, which attribute an effect (a SHAP value) of each power system variable on the CCT prediction—explaining how the prediction moves from the base value (if no feature information was known) to the final prediction. This effect is given in the same units as the target (i.e., sec). The model can be analysed as a whole by extending local explanations across multiple operational scenarios, using multiple feature effects to obtain a global feature importance measure. Since a locational approach is again adopted,

the SHAP values from global SHAP explanations can be compared between locations. Specifically, the covariance between a VOI and the SHAP values for that VOI from each location-specific ML model are calculated. This can reveal trends in the transient stability boundary, highlighting locations with similar (or dissimilar) stability boundary behaviour with respect to a VOI—directly addressing research question 5.

Chapter 8 also makes use of the SHAP framework in a manner more suited to a planning environment. In particular, SHAP is used to assess the impact of wind control parameters and location specifically—both of which were highlighted as important in Chapter 3 and indeed Appendix A. The methodology uncovered that transient stability tends to improve when controller settings further reduce the fault-on active power compared to the original LVRT settings in the adapted version of the IEEE 39-bus test network. The location of RES was not found to have high importance. However, the impact of RES location with respect to SG loading was uncovered—showing that whilst SG with high active power loading reduces the model prediction for CCT, connecting RES closer to that machine can minimise this effect.

Along with the increasing connection of PEC; the current global energy environment—which is being most acutely noticed in Europe through energy shortages, changes to generation connected, changing demand patterns and unprecedented market interventions—may lead to significant changes to the transient stability boundary. This is leading to an increasingly urgent requirement for new TSA tools and methodologies to be adopted. The IML-based methodologies presented in this thesis have shown that such methods can reduce the online computational burden and uncover the predominant factors influencing the stability boundary whilst capturing the dynamic response of CIG—i.e., they possess the three desirable attributes of modern TSA methodologies. Such methods could initially be used to direct computational effort for full RMS-TDS in an online environment (i.e., a screening process) until such a time that sufficient confidence is established in such methods for online use. Such methods may also have value in planning environments, enabling the assessment of larger numbers of operational scenarios, thus reducing operationally risky blind spots.

9.1 Further Work

The method(s) developed in this thesis are envisaged as being part of the control room of the future, relaying the transient stability margin on a locational basis back to the SO in near real time—along with communicating the details relating to why a particular prediction of stability margin is given. Such insights may be used by the SO to improve the stability margin, should a particular location be of concern (e.g., the CCT is nearing a protection threshold).

The work presented in this thesis answers the research questions that had been defined, making several contributions to the body of research in the area of TSA of modern power systems (detailed in Section 1.2). Nonetheless, there are several additional research areas where the work presented in this thesis could be extended relating to three key themes (power system modelling, IML and transient stability enhancement measures.

9.1.1 Power System Modelling

- The search space for operational scenarios could be refined using a probabilistic approach to narrow down the search space to more '*credible*' dispatches. For example, probabilistic wind speed data could be used rather than using arbitrary RES capacity values and having the output at 100 %. This can inform a probabilistic measure of the stability margin and help inform CBA of stability enhancement measures. Some of these approaches are detailed in [177].

- Along with assessing the impact of wind generation (both grid-following and grid-forming), other prominent technologies such as solar PV, HVDC, active distribution networks and battery technologies should be included in the test networks used for IML-based studies. Indeed, the impact of so-called active distribution networks is studied in [178], and found to have an impact. Therefore, such an approach will better represent modern power systems that have a blend of technologies connected. These technologies have different characteristics to WTG, which were the focus of this thesis. The use of IML (and in particular SHAP)

can improve understanding of their combined impact on transient stability.

- A larger test network could be used to verify the scalability of the proposed methods. The computational burden increases with network size, and should be tested since this may result in the need for the methodology to be adapted (e.g., less locational granularity). Literature has already demonstrated that the stability of large systems can be accurately predicted (e.g., [179]). Therefore an obvious next step would be to try to better understand the factors influencing transient stability in these larger systems. Questions around how network size impacts the quality of the insights must then be answered.

9.1.2 Interpretable Machine Learning

- A different metric for transient stability could be selected as the target variable for the IML-based methodologies presented. CCT is a metric largely used in academia, so other metrics such as the power flow in a particular line may be of more use in real systems (e.g., when the power flow in a line is approaching or above a certain threshold then transient stability is known to be poor). This may increase the potential use case of the methods in an industrial setting.

- The feature selection process can be further refined. For example, to determine how the method performs with only PMU data and what the impact is if there is a loss of data would be interesting questions to investigate. Perhaps a more interesting avenue of research in relation to this point, is only selecting features that can be directly controlled from a control room (this is likely to be the generator active power and voltage setpoints). If desired accuracy is reached, the interpretations form SHAP can then be used directly to inform actions. This may be extended to controlling demand should the SO possess such capabilities in the control room of the future.

- Further detailed consideration of the ML algorithms used. For example, physics-informed neural networks could be used to improve the interpretability of the method. Such methods use the physical laws that govern the observed data to

improve performance. This can be achieved by adding the known differential equations that govern a dynamic system directly into the loss function when training the neural network. One such example relating to transient stability can be found in [180]. Such a method may assist in the interpretability stages since results will be based on the physics of the system and could be more easily traced.

- The selection of an appropriate IML method could be further refined based on the specific application. This complex process is discussed in [130].

9.1.3 Transient Stability Enhancement

- Robust verification of the accuracy of the interpretations from the methods proposed (i.e., closing the loop). Steps toward this have been taken in Chapter 6—where as a result of the 3D stability boundary representation, an additional transmission line was added to overcome an active power flow constraint. The results (verified using RMS-TDS) demonstrated that the CCT at the location in question is improved as a result. Further such analysis must be undertaken—with a particular focus on SHAP. In particular, do interventions (both local and global) result in changes to the CCT that are consistent with the SHAP values? Such steps are required to enhance trust in the method.

- Adding constraints into the OPF problem based on the important parameters identified to constrain the dispatch to only transiently stable operating points and assess the impact on the transient stability margin and economic operation of the power system. This is widely known in academic literature as TSC-OPF (e.g., [181]), but using SHAP to inform the constraints has not yet been studied at present.

- More detailed designs of potential transient stability enhancement measures based on the important parameters from both a *planning* and *operational* perspective. The goal of the former is to minimise the likelihood of the system operating near to the stability boundary. In regard to the latter, the goal is to move the system away from the stability boundary in near real time. From a planning perspective, SHAP

insights could be used to inform grid codes, connection agreements, ancillary service design and network asset planning (forming part of the CBA). From an operational perspective, operational rules can be developed from global SHAP interpretations—and real time corrections to operating points supported by local SHAP explanations.

- Causal ML approaches to identify causation and not just correlation, which is key in the development of tools that are of practical use in industry. The goal is to understand how a system would react to an intervention. This has been studied in the medical domain [182], but further research for applications relating to power system TSA.

Appendix A

Impact of Type-4 Wind Generation on Transient Stability in a Single-Machine Infinite-Bus System

A.1 Introduction

Chapter 3 highlights some of the key parameters that impact the transient stability boundary as more RES connects to power systems. However, some key mechanisms by which RES may impact transient stability were missing from the academic literature at the time of writing. As such, the studies presented in this Appendix seek explicitly to assess the impact of wind control parameters, location, penetration and loading on transient stability using the maximum rotor angle deviation (a fixed fault-time stability metric).

This analysis is particularly interested in the impact of wind control parameters on transient stability due to the ability of these parameters to be changed with relative ease and at minimal cost in real power systems. Should changes to key parameters result in significant changes in the transient stability of the system, mandating control

parameters as part of a connection agreement would be relatively straightforward to implement. In addition, the impact of Wind Turbine (WT) penetration with respect to WT capacity is assessed. This is a widely studied aspect of transient stability; however, the studies presented in this Appendix aim to identify trends in the stability boundary rather than specify a hard limit for wind penetration. Moreover, these studies seek to assess the impact of the location of WT with respect to SG by varying the length of the line that connects WT to the network. Finally, the impact of WT loading (that is; the active power output with respect to the nameplate rating) on transient stability is analysed.

A SMIB is used to reduce the complexity of the problem, simplify the analysis of results and effectively investigate the above aspects. While this approach is appropriate and offers some interesting insights, the simplicity of the network means that results may not translate directly into larger systems (which are inherently more complex). Therefore, the results presented in should not be generalised to all power systems. This is a common drawback for studies in the transient stability literature—where studies are limited to analysis of a single variable on a specific system (as was the case for many studies in Chapter 3). However, it is still essential to understand the mechanisms responsible for changes to the transient stability boundary, which this analysis goes some way in addressing. This further highlights the need to develop new methodologies capable of uncovering the factors influencing the transient stability margin in any power system.

Findings from the studies presented in this Appendix are built on in various Chapters of this thesis. In particular, locational aspects of transient stability are comprehensively investigated in Chapter 4, 6, 7 and 8 and control parameters are analysed in Chapter 8.

A.1.1 Contribution

The key contribution resulting from the studies presented in this Appendix give an initial overview of some of the mechanisms affecting transient stability in power systems with increased RES, specifically Type-4A wind generation. In particular, a sensitivity

analysis of the following variables is conducted;

- wind *control parameters*,
- *penetration* of wind with respect to SG,
- *location* of wind with respect to SG,
- wind active power output with respect to nameplate rating (i.e., active power *loading*).

A.2 Test Network and Stability Metric

A.2.1 Single-Machine Infinite-Bus Test Network Overview

A SMIB network (Figure A.1) is developed in DIgSILENT PowerFactory. Two 555 MVA SGs, each with an inertia constant of 3.525 sec. One of the SGs is equipped with a IEEE 1968 IEEE Type 1 Excitation System (AVR), IEEE Type 1 Speed-Governing Model (governor) and IEEE Type PSS2A - Dual-Input Stabilizer Model (PSS). A step-up transformer connects the units to the 500 kV HV grid, where two parallel lines (lines 1 and 2) connect to the infinite bus.

Since the studies presented in this Appendix and indeed thesis is particularly focused on transient stability in the context of increased RES, wind generation added to the SMIB. A third line connects a WF, consisting of 250 parallel IEC Type-4A units, each rated at 2 MVA to the network via step-up transformers (i.e., a combined rating of 500 MVA). All lines have a resistance of 0.028 Ohm/km, reactance of 0.325 Ohm/km and susceptance of 5.2 uS/km.

A.2.2 Transient Stability Metric

In the studies presented in this Appendix, a fixed fault-time metric (as introduced in Section 2.5.1) is used for assessing the transient stability of a given scenario. Whilst determining the stability margin (i.e., the CCT using a variable fault-time approach) is more accurate than fixed fault-time metrics, a fixed fault-time metric is sufficient for

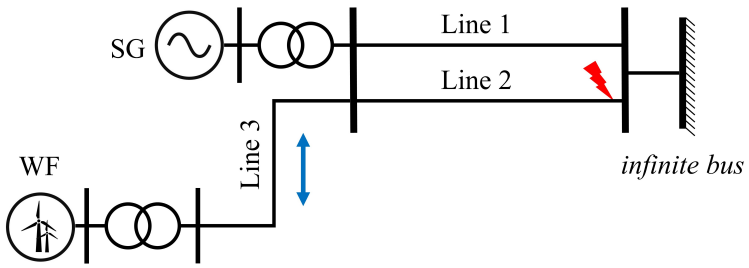

Figure A.1: Single-Machine Infinite-Bus (SMIB) with wind generation added at the end of a transmission line. Fault location indicated by a red lightning bolt.

these simple studies where we seek to identify trends and showcase mechanisms at play. In this instance, the maximum rotor angle deviation (deg) of the SG is considered. This metric gives a sense of how close to instability the SG is to LOS, as defined in Equation 2.11). The fault considered in these studies is a three-phase-to-ground self-clearing fault lasting for 150 msec at 99% along the length of line 2 (as indicated in Figure A.1).

A.3 Results

A.3.1 Impact of Wind Control Parameters

Parameters are grouped based on the time period where they impact the response from the WF; either during the fault-on period or post-fault. Note that pre-fault variables will also have an impact, particularly the mode of operation; constant voltage or reactive power. However, this is not considered in these studies.

Fault-on parameters

Braking resistors are a widely known means of improving the transient stability of a SG [77]—the premise of which is to absorb the accelerating energy of nearby SG. This reduction in accelerating energy typically relates to an improvement in transient stability, as per the EAC (Figure 2.8). However, these resistors may have a high capital cost and only serve a single purpose. Therefore, here we propose controlling WFs so that they behave like braking resistors to enhance transient stability. This behaviour is already mandated by the Grid Code [183] and is termed LVRT—however the premise

of the studies presented in this Appendix is to exaggerate this behaviour in order to improve transient stability with IEC Type-4A WF (modular structure for the control model is given in Figure A.2 and full details in [104]). More specifically, we propose that

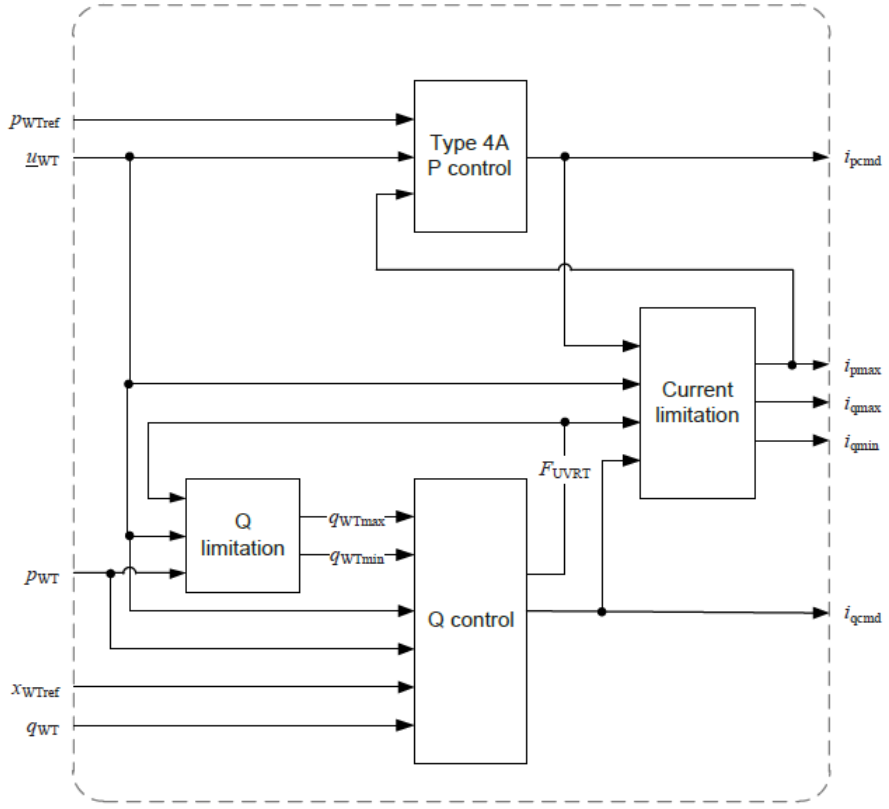

Figure A.2: Modular structure for the Type-4A wind control model [104].

the WF should reduce active power output as far as possible during the fault to enable SG to export more active power. In doing so, a WF may be able to offer additional grid services other than purely energy delivery. To achieve this, the fault-on parameters of the WF (i.e., parameters that impact the LVRT behaviour) are varied such that the active power from the WF during the fault-on period is *suppressed*, enabling the SG to export *more energy*—thus *reducing* the accelerating energy as per the EAC (see Chapter 2).

In addition, supporting voltages (i.e., keeping as near nominal during the fault and restoring quickly post-fault) near the terminals of a SG can also increase power export—as per the power angle equation (Equation 2.3). As such, the reactive power

output of WF close to SG is likely to be able to prop up local voltages during the fault and thus reduce SG accelerating energy. Since each WT converter has limited capacity, either active or reactive current must be prioritised during the short circuit. Based on the above analysis, prioritising reactive power is advantageous—and indeed, this is the premise of LVRT behaviour. Parameters of the Type-4A controller (Figure A.2) are varied to achieve the desired active and reactive power response. In particular, parameters in the Type-4A reactive power controller (Figure A.3) are varied.

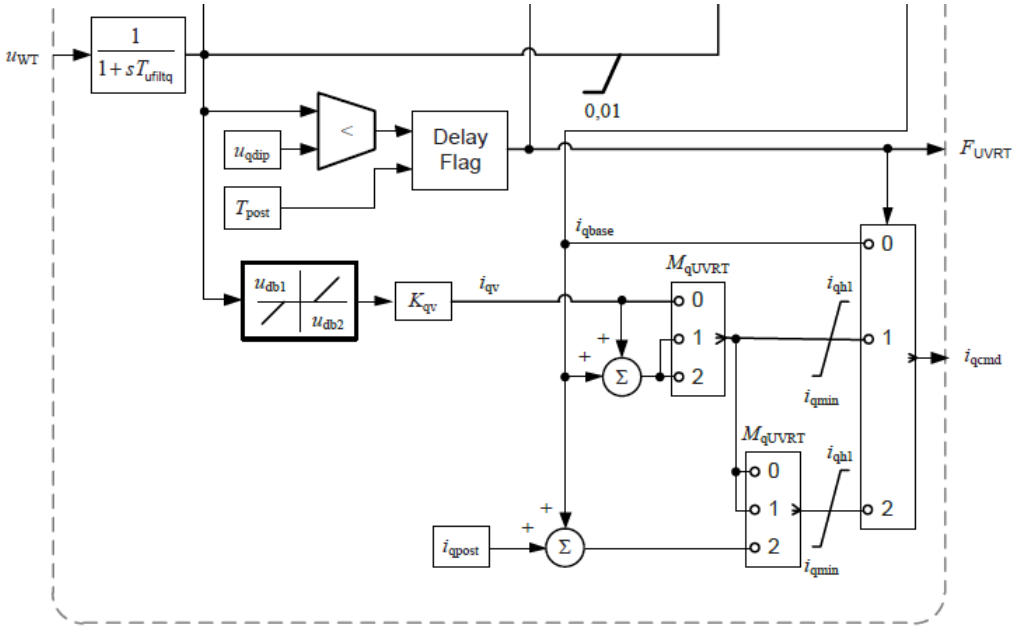

Figure A.3: Section of the modular structure for the Type-4A reactive power control model. Full diagram available in [104].

Increasing the voltage-dependent current constant (K_{qv}) in turn increases the voltage-dependent reactive current signal (i_{qv}) in the IEC Type-4A reactive power control block (Figure A.3). If the limiter for reactive current (i_{qh1}) is also increased, this removes the upper constraint for the reactive current command to the generator system (i_{qcmd}) from the set limit. Since Equation A.1 governs the magnitude of converter current (which is limited by the physical size of the converter); if i_{qcmd} increases, it follows that i_{pcmd} must then decrease (unless the physical size of the converter is increased).

$$I = \sqrt{{i_{qcmd}}^2 + {i_{pcmd}}^2} \tag{A.1}$$

During the voltage dip, the short-term overcurrent magnitude is limited by the current limiter (Figure A.4)—specifically i_{maxdip}, the impact of which is also tested. This is equivalent to increasing the size of the converter, which would have an additional cost component (i.e., it may not just be a software change). The increase in reactive current during the fault may also assist in increasing local voltages and subsequently enable SG to export more active power (based on the power angle equation, Equation 2.3). The extent to which the LVRT behaviour impacts a SG is likely to be dependent on the location of the WF with respect to SG.

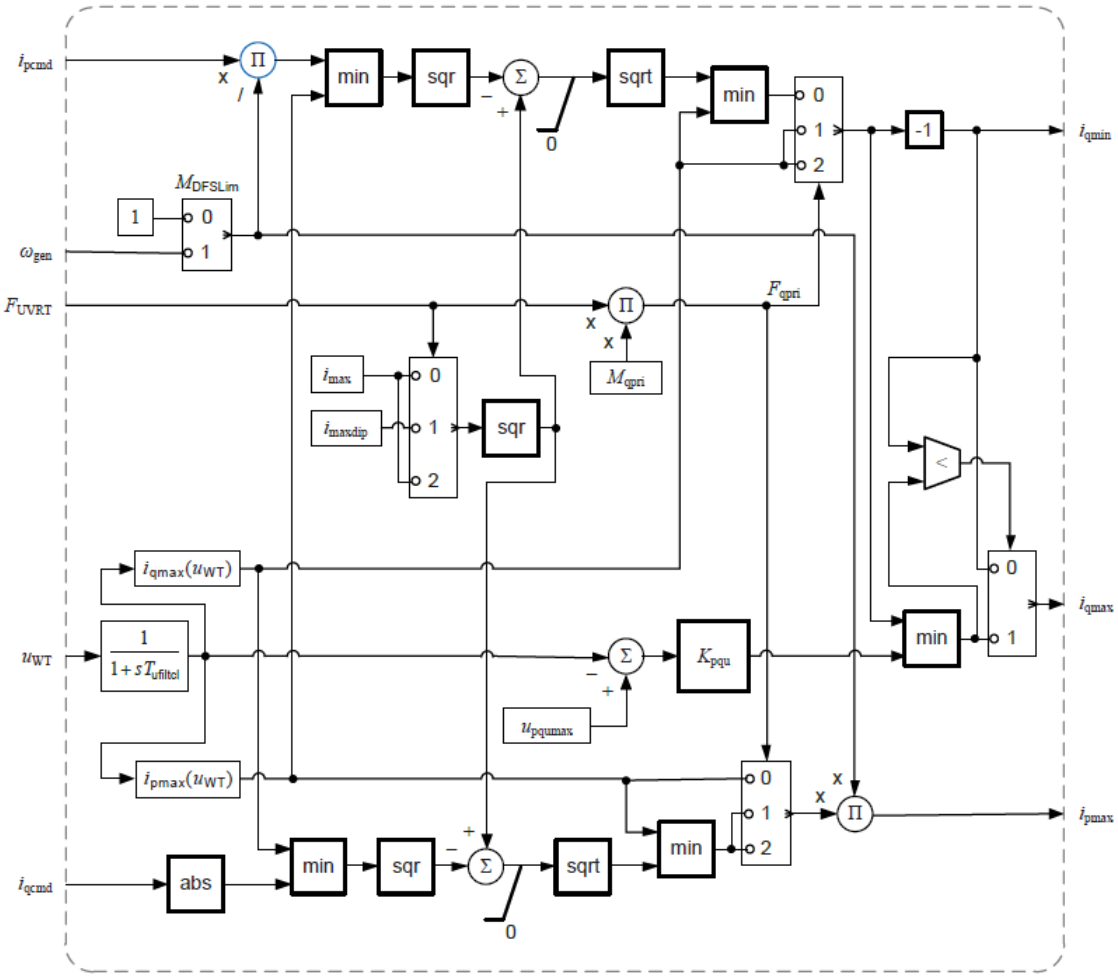

Figure A.4: Block diagram for the Type-4A current limiter [104].

Appendix A. Impact of Type-4 Wind Generation on Transient Stability in a Single-Machine Infinite-Bus System

Parameter	Original Value	Range
$K_{qv}(I_n)$	2	1, 2, ..., 10
$i_{qh1}(I_n)$	1.05	$\pm 5\%, \pm 10\%$
$i_{maxdip}(I_n)$	1.2	$\pm 5\%, \pm 10$

Table A.1: Type-4A controller parameter ranges selected.

The original values and ranges for the fault-on control parameters considered are given in Table A.1. These ranges are selected based on typical values [184], and all possible combinations of the three are considered to identify the 'optimal' combination from a transient stability perspective for this case study. Three parameters are selected for testing due to their impact on the reactive current output of the converter during the fault-on period.

1. **Voltage dependent current constant** (K_{qv}): Impacts (i_{qv}) control signal and ultimately i_{qcmd} (however, the latter is limited by (i_{qh1})).
2. **Reactive current limiter** (i_{qh1}): Limits the i_{qv} and hence the i_{qcmd} signal.
3. **Short-term overcurrent magnitude** (i_{maxdip}): Limits the maximum overcurrent during fault-on period.

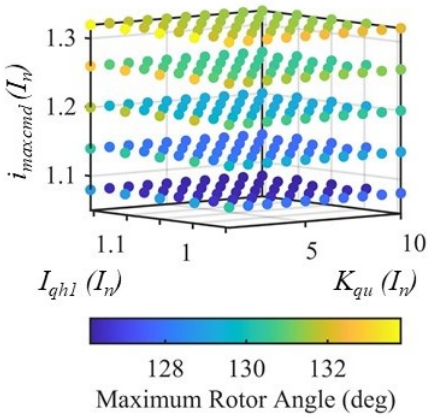

Figure A.5: Impact of Wind Turbine (WT) control parameters on the Synchronous Generator (SG) maximum rotor angle deviation for all combinations of parameters.

Figure A.5 shows the impact of all combinations of the above-described wind control parameters on the maximum rotor angle deviation. The most significant improvement

in transient stability (i.e., the smallest maximum rotor angle deviation) is observed for a reduction in i_{maxcmd}. However, all three parameters have some impact on stability. The 'optimal' parameters—that is, the combination of parameters that results in the best transient stability from the combinations of parameters considered (Table A.2).

Parameter	Original	Proposed
$\mathrm{K}_{qv}(I_n)$	2	10
$\mathrm{i}_{qh1}(I_n)$	1.05	1.05+10% (=1.155)
$\mathrm{i}_{maxdip}(I_n)$	1.2	2-10% (=1.08)

Table A.2: Original vs proposed wind control parameters.

The time series response plot for the SG between the original and proposed parameter sets is given in Figure A.6, showing an increase in active power export during the fault, which leads to a smaller maximum rotor angle deviation. In addition, the time-series response form the WF is given in Figure A.7. During the fault-on period, the active power output from the WF drops lower when the proposed parameter set is adopted compared to the original set (Figure A.2). This in turn means that the SG is able to export more active power during the fault (Figure A.6), limiting the acceleration of the machine (as per the EAC described in Chapter 2). This is a similar mechanism for stability improvement that braking resistors target [77]. However, by implementing such changes to the wind control parameters (a relatively simple change that could be mandated through connection agreements), the need to build a braking resistor (with all the capital costs associated) could be reduced/eliminated.

Post-fault parameters

As per the EAC, the post-fault behaviour of generators (in particular, the active power recovery ramp rate) connected to a system will also impact the transient stability—since this will impact the decelerating energy of SG connected to the system. Indeed, authors in [78] conclude that a lower post-fault active power recovery ramp rate ($\mathrm{d}p_{\mathrm{maxp4a}}$ in the active power control model, Figure A.8) in an exporting region of a power system can lead to improvements in transient stability.

It is highlighted in [78] that the most suitable active power recovery ramp rate

Appendix A. Impact of Type-4 Wind Generation on Transient Stability in a Single-Machine Infinite-Bus System

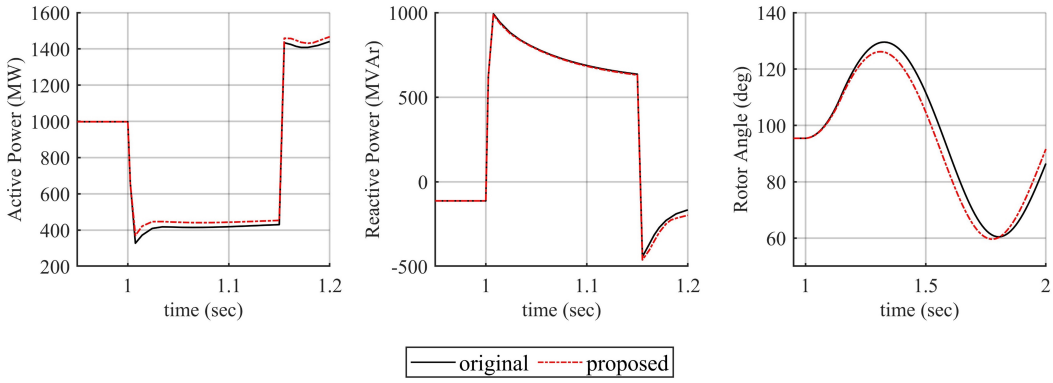

Figure A.6: Synchronous Generator (SG) time series response with original and proposed parameters.

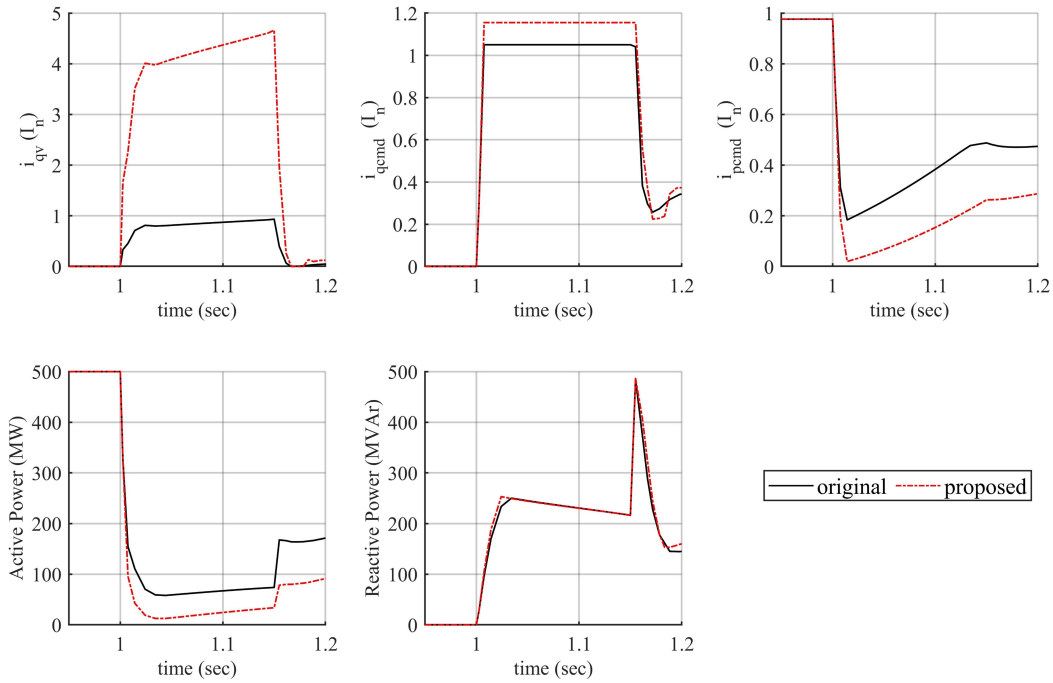

Figure A.7: Wind Turbine (WT) control signals (i_{qv}, i_{qcmd} and i_{pcmd}) and WF time series response with original and proposed parameters.

setting for the WF depends on whether the WF is in an importing or exporting region of the power system. In particular, a *slower* active power recovery ramp rate in *exporting areas* can improve transient stability. However, it should be noted that results were from a single network representation of the GB transmission system. This finding may vary in more complex and meshed networks with varying power flows and parameter

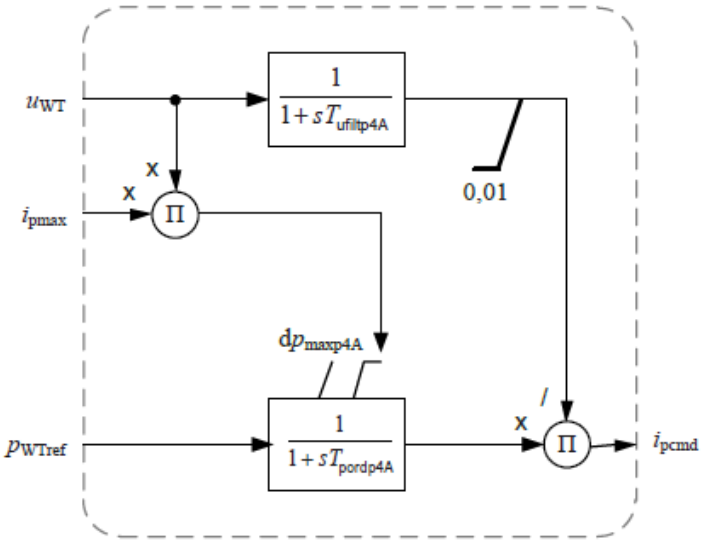

Figure A.8: Modular structure for the Type-4A active power control model [104].

interdependencies. Therefore in the studies presented in this Appendix, the impact of a *high* and *low* (($\mathrm{d}p_{\mathrm{maxp4a}}$) = 1 or 0.8 Pn/sec) setting are considered for these studies.

A.3.2 Impact of Displacement of Synchronous Generation by Wind

Displacement of SG by CIG (that is; the disconnection of SG and connection of CIG) is a widely discussed topic in literature, with various studies reaching different conclusions—as outlined in Chapter 3. Many factors influence transient stability, including network topology, demand level, generator dispatch, system inertia and CIG technology deployed (e.g., Type-3 vs Type-4 WTG vs solar PV). Ultimately, the impact depends on a wide range of system variables that are difficult to track and fully understand to reach a conclusion for a single network, let alone for power systems in general.

The impact of displacement on transient stability is demonstrated by varying the capacity of the SG and WF in the SMIB (Figure A.1) and transient stability assessed for all possible combinations of each. Specifically, the capacity of the two 555 MVA SG units are varied from 555-1665 MVA in steps of 55.5 MVA (i.e., 1110 ±50% in steps of 5%). The WF capacity is varied from 250-750 MVA in steps of 25 MVA (i.e., 500 MVA ±50% in steps of 5%). This results in 441 operational scenarios that reflect the

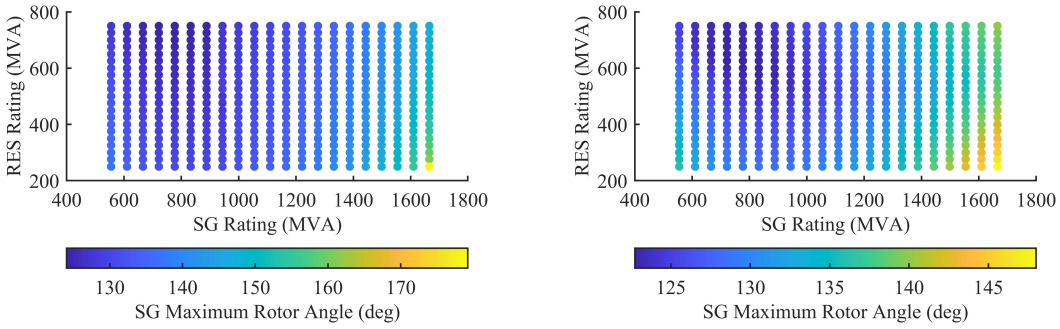

Figure A.9: Impact of displacement of Synchronous Generation (SG) by wind on the maximum rotor angle of the SG for different displacement scenarios. Original parameters (left) vs proposed parameters (right)—note colour axis differences.

decommissioning of conventional SG plant by RES.

The impact of doing so on transient stability is illustrated in the Figure A.9 for both the *original* wind control parameters and the *proposed* wind control parameters. The first aspect to note is the different colour axis between the left and right plots, highlighting a significant benefit of the proposed wind control parameters compared to the original—since the maximum rotor angle deviation is significantly reduced.

It is notable that—for either sets of parameters—the *maximum* rotor angle deviation (i.e., the *worst* transient stability, points highlighted yellow in Figure A.9) occurs when the WF capacity is low and the SG capacity is large. This is because when the relative size of the WF compared to SG is very small (e.g., SG MVA $\gg$ WF MVA), the impact of the LVRT behaviour of the WF is negligible. Conversely when the relative size of the WF and SG are similar, the LVRT behaviour of the WF has a greater impact at limiting the acceleration of the SG (blue points in Figure A.9).

This effect is exaggerated when the wind control parameters are selected to further emphasise the LVRT behaviour of the WF (as in the right plot in Figure A.9). This is because the reduction in active power and improved voltage support enables the SG to export more active power during the fault, thus reducing the accelerating area (as per the EAC).

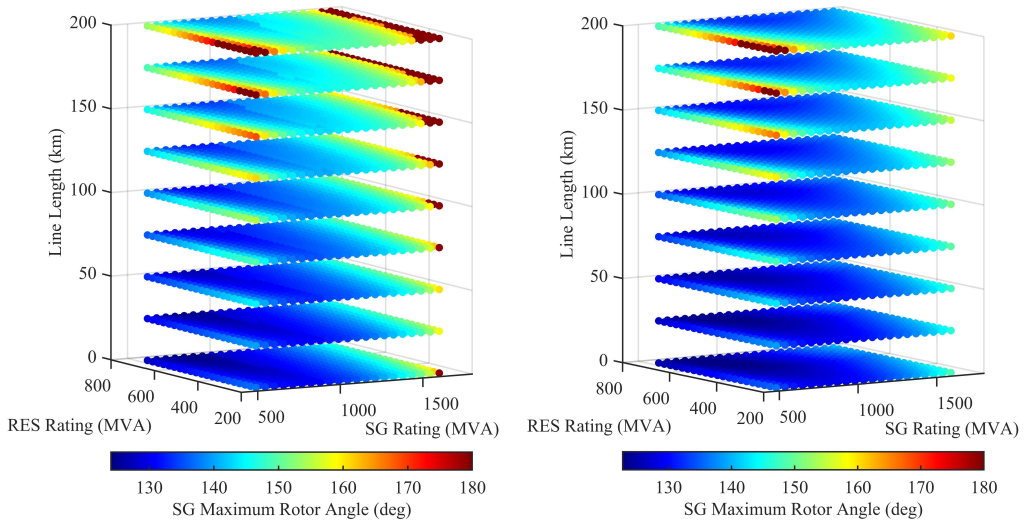

Figure A.10: Impact of the location of wind with respect to Synchronous Generation (SG) on the maximum rotor angle of the SG for different displacement scenarios. Original parameters (left) vs proposed parameters (right).

A.3.3 Impact of Wind Farm Location

In addition to the displacement of SG by wind, the location of the WF with respect to SG also plays a role in transient stability. Whilst this is not a controllable parameter in operational timescales, it should be carefully considered in planning timescales. To test the impact of the location of the WF with respect to SG, the length of line 3 is increased from 25 km to 200 km in increments of 25 km (as indicated by the blue arrow in Figure A.1). Therefore as the line length increases, the electrical distance between WF and the SG increases.

Figure A.10 shows the impact of increasing the length of line 3 on the maximum SG rotor angle deviation using the original (left) and proposed (right) wind control parameters. It is observed that an increase in line length leads to an increase in the maximum rotor angle deviation, highlighting the spatial aspect of the problem.

There is once again a clear difference in the maximum rotor angle deviation between the two sets of wind control parameters, with the proposed set reducing the maximum rotor angle deviation compared to the original set. A similar trend is observable when the proposed wind control parameters are implemented, but to a lesser extent (i.e.,

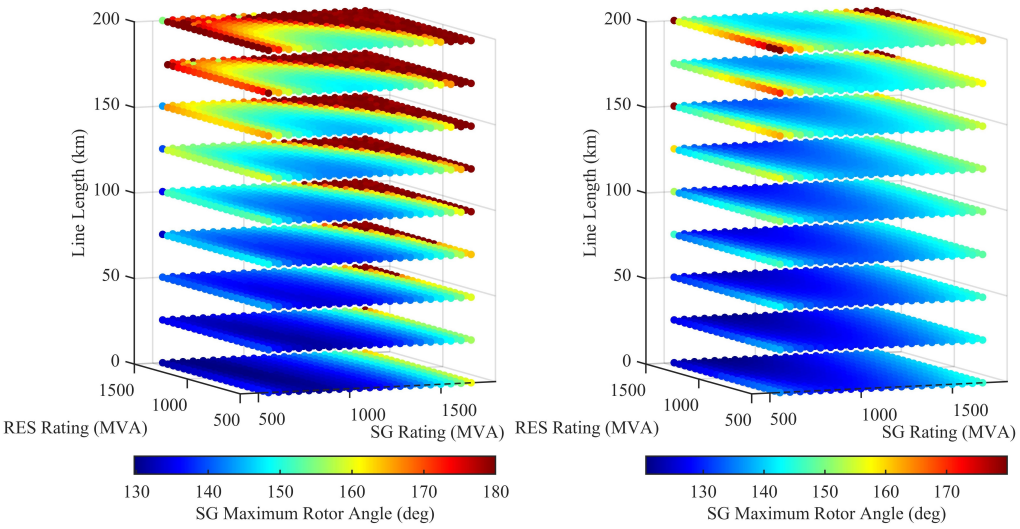

Figure A.11: 50% Wind Farm (WF) loading. Impact of the location of wind with respect to Synchronous Generation (SG) on the maximum rotor angle of the SG for different displacement scenarios. Original parameters (left) vs proposed parameters (right).

stability improves—see Figure A.10). Indeed, smaller angle deviations (dark blue points in Figure A.10) across a broader range of scenarios are observable when the proposed parameters are implemented. It is likely that the extent to which wind can support a SG through LVRT behaviour (through the reduction of active power output and injection of reactive power) decreases as the electrical distance between the two increases.

A.3.4 Impact of Wind Farm Loading

The loading of the WF may have implications for transient stability since a WF operating at a lower output has more converter capacity to provide a larger response. Conversely, a WF operating at capacity has a limited ability to provide a response (i.e., 100 % loading vs 50 % loading). The WF capacity is doubled—whilst maintaining the same dispatch—to test the impact of this.

Figure A.11 shows the maximum rotor angle deviation for the same displacement and line length scenarios described above, with the WF at 50% loading. This can be compared directly to Figure A.10, where the WF loading is 100%. Upon comparison, it can be seen that part loading the WF to 50% results in a deterioration in transient

stability compared to the fully loaded case.

The increase in WF capacity results in an increased ability for the converter to provide both active and reactive current during the fault. With the parameters selected for these studies, this additional capacity enables the WF to provide both an active and reactive current injection during the fault. This is not advantageous for transient stability, where a reduction in active power as far as possible during the fault is desirable due to the braking resistor effect described previously. This is illustrated in the time series plots for the WF and SG provided in Figure A.13 and Figure A.12 respectively. In particular, it can be seen that the WF can export more active power during the fault-on period when 50% loaded (dashed lines in Figure A.13). This results in the SG maximum rotor angle deviation in the 50% wind loading case being greater than the 100% case regardless of the wind control parameters used (Figure A.12).

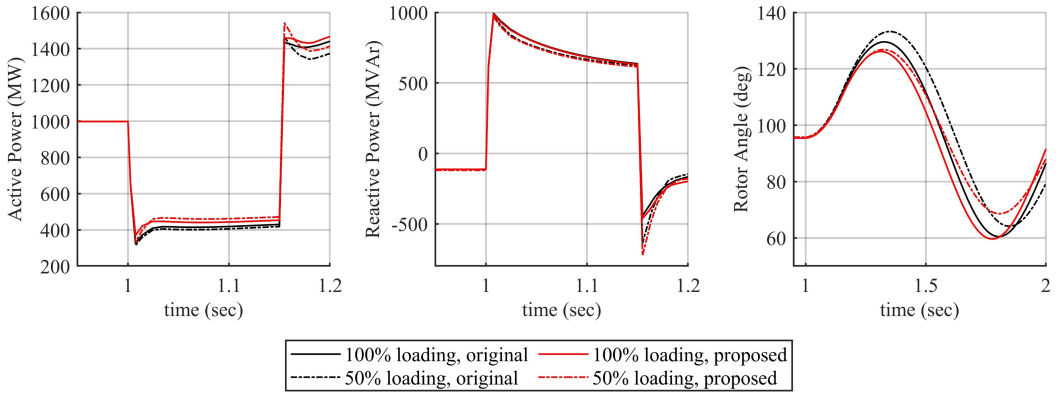

Figure A.12: Synchronous Generator (SG) time series plot with original and proposed parameters w.r.t. wind loading.

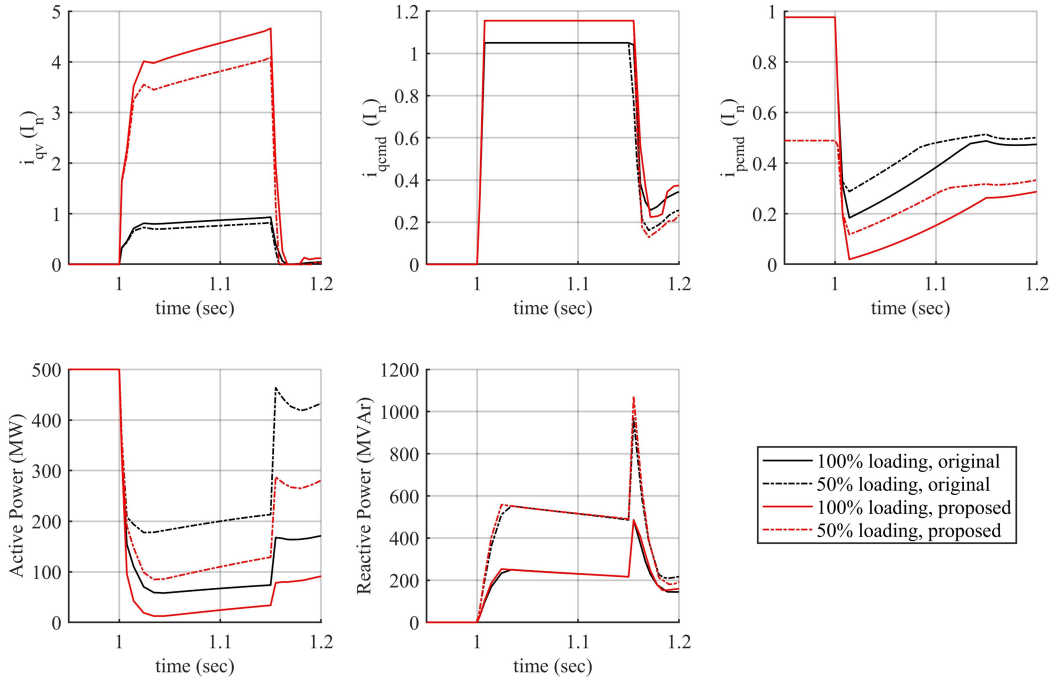

Figure A.13: Wind Turbine (WT) control signals (i_{qv}, i_{qcmd} and i_{pcmd}) and Wind Farm (WF) time series response with original and proposed parameters w.r.t. wind loading.

A.4 Conclusions and Discussion

The studies presented in this Appendix has highlighted some of the complexities that CIG, specifically WTG, adds to the dynamic response of a power system. In particular,

wind control parameters, the location of the WF with respect to SG, displacement of SG by wind and the loading of the WF were analysed. This was achieved using a simple SMIB network with wind added to reduce complexity and simplify analysis results.

The fault-on wind control parameters are found to improve transient stability when set to minimise active power output from the WF during the fault—effectively working in a similar manner to a braking resistor, in terms of enabling the SG to export more power during the fault. Displacement of SG by wind is also shown to impact transient stability. In this simple SMIB test network, the results show that transient stability is improved when the relative capacity of the WF and SG are similar. The impact of the location of the WF with respect to SG is explored by varying the length of the transmission line that connects the WF to the network. As the length of the line increases, the transient stability of the system deteriorates (likely caused by the reduction in the effectiveness of LVRT behaviour of the WF to support the voltage at the SG terminals). Finally, it is found that as the loading of the WF increases, the reduction in spare capacity means that the active power output is constrained, enabling the SG to export more active power and improve transient stability. This may have implications for the real-time operation of WFs since a variation in active power output of a WF may impact transient stability.

However, by using a SMIB to assess the impact of the mechanisms mentioned above on transient stability, the simplicity of the network means that results presented may not translate directly into larger, inherently more complex, systems. The insights and trends identified in the studies presented in this Appendix may or may not hold in different systems—where numerous factors influence the stability boundary. Indeed, this type of simplification of the problem is a key drawback of works reviewed in Chapter 3 and motivates the research presented in Chapter 6 onwards—where methodologies are developed to reduce the complexity of the transient stability problem.

Appendix B

Supplementary Figures

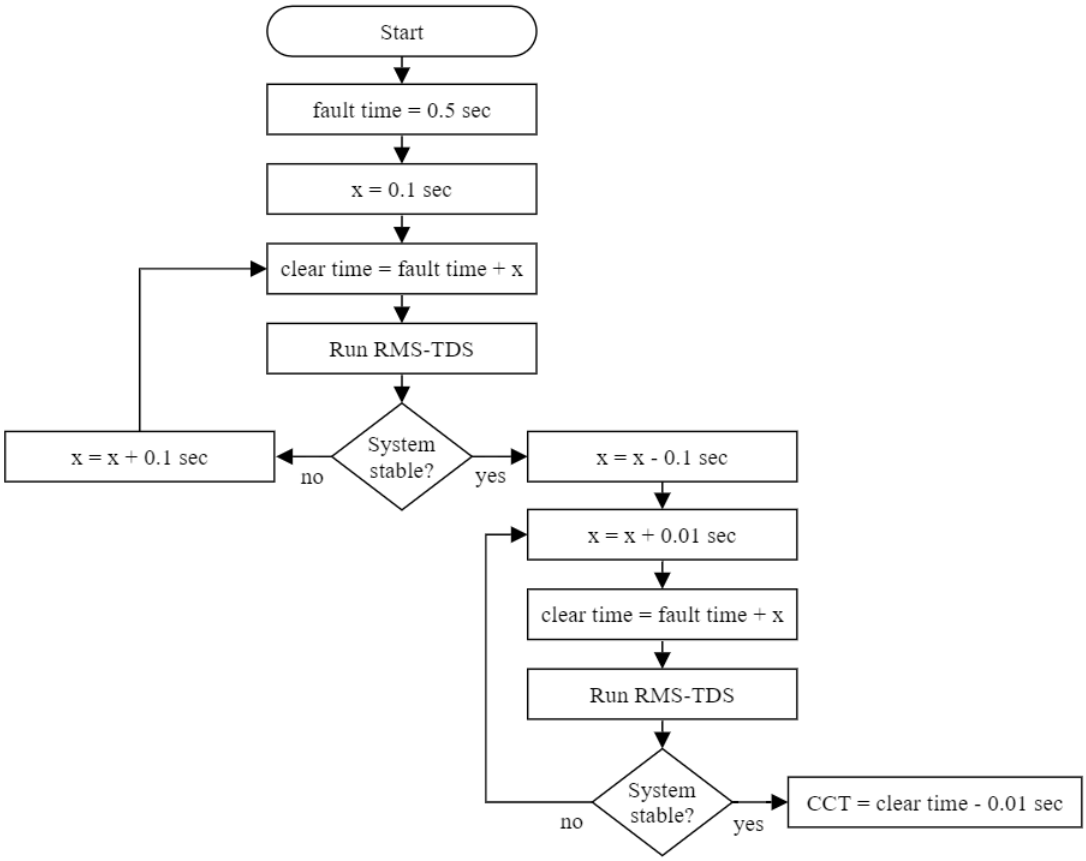

Figure B.1: Algorithm developed and used to find the Critical Clearing Time (CCT) for each fault location and operational scenario.

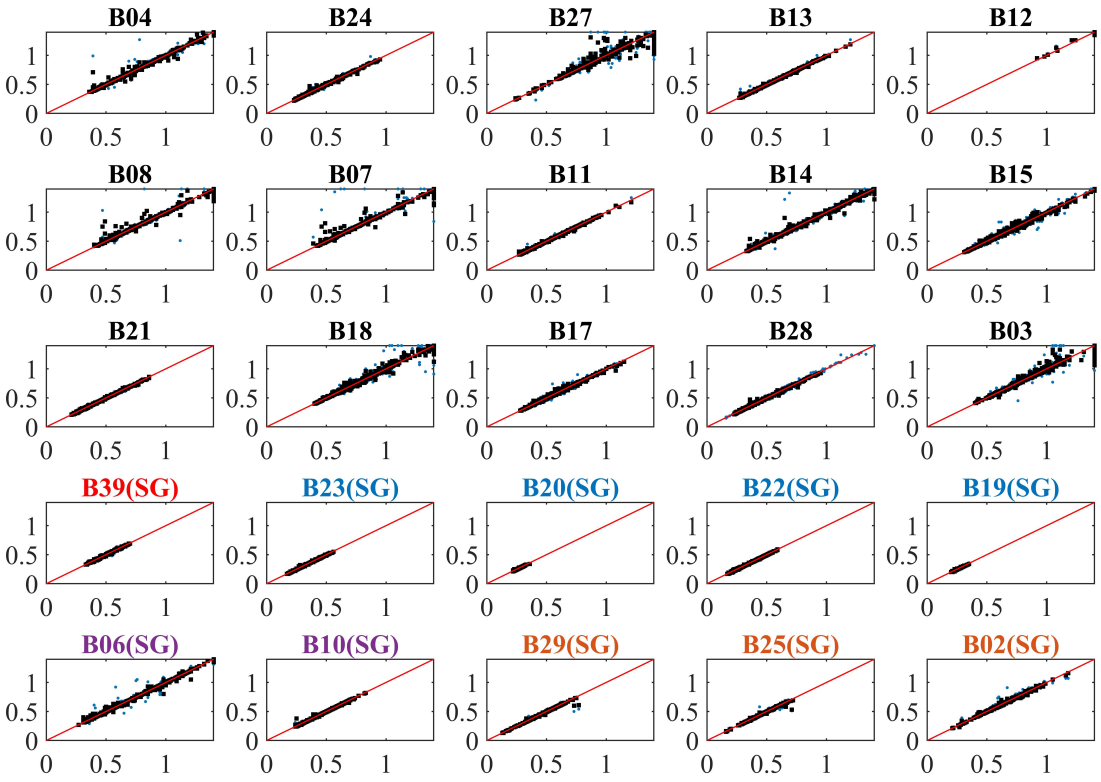

Figure B.2: Comparison between Decision Tree (DT) (blue circles) and Random Forest (RF) (black squares) locational Critical Clearing Time (CCT) estimation accuracy in sec.

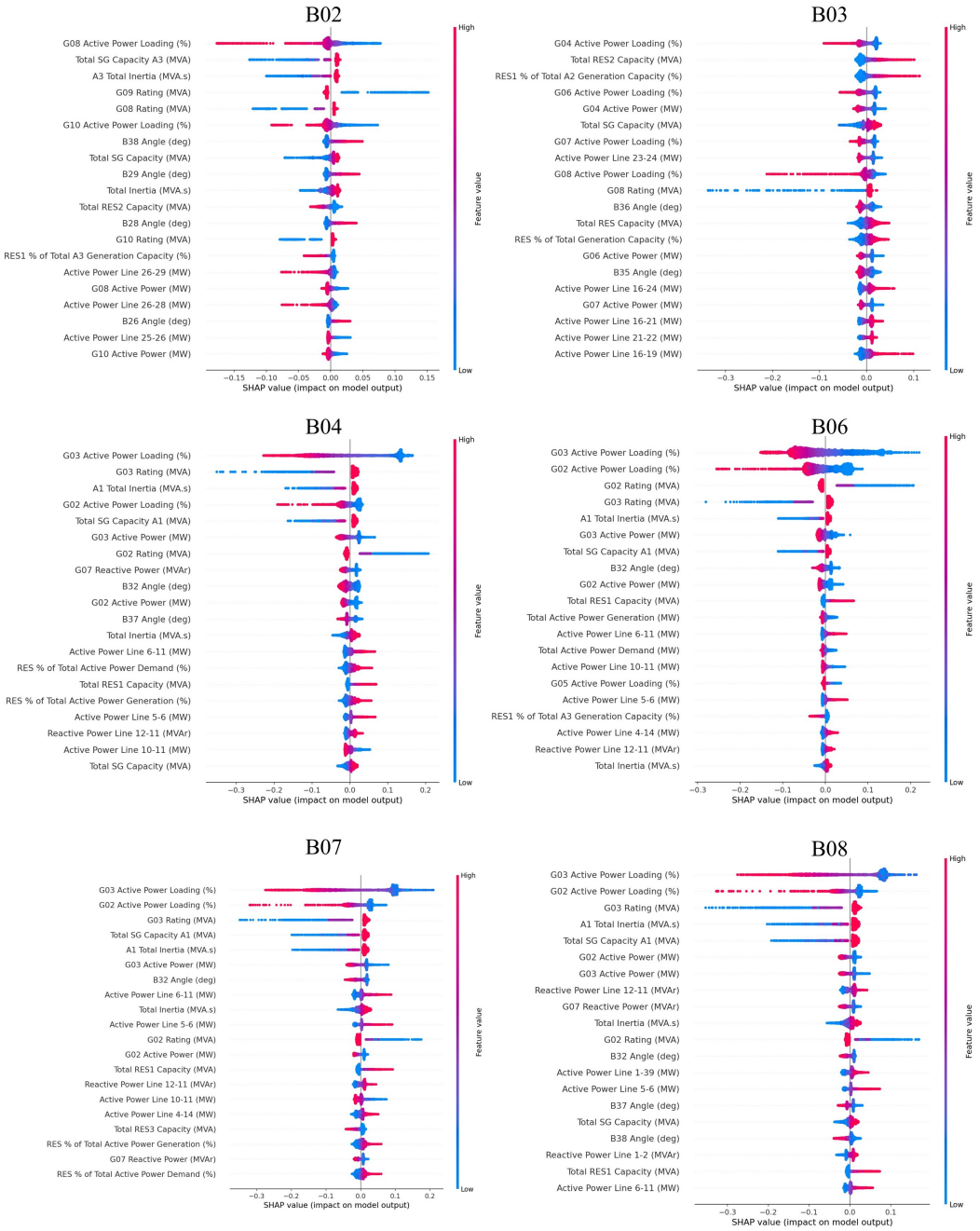

Figure B.3: Stability boundary representation (B02, B03, B04, B06, B07 & B08) using SHAP to interpret locally trained artificial neural networks (ANNs).

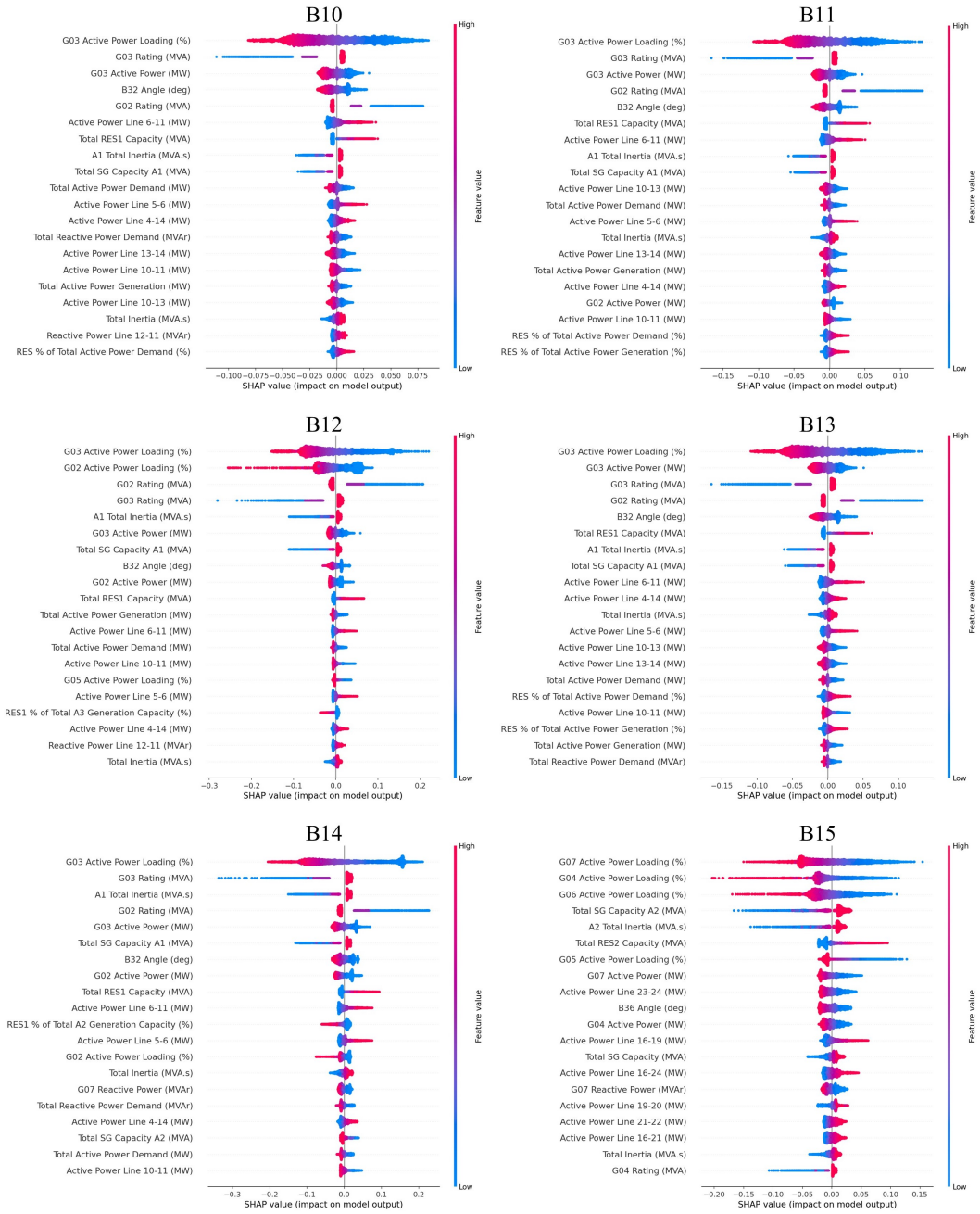

Figure B.4: Stability boundary representation (B10, B11, B12, B13, B14 & B15) using SHAP to interpret locally trained artificial neural networks (ANNs).

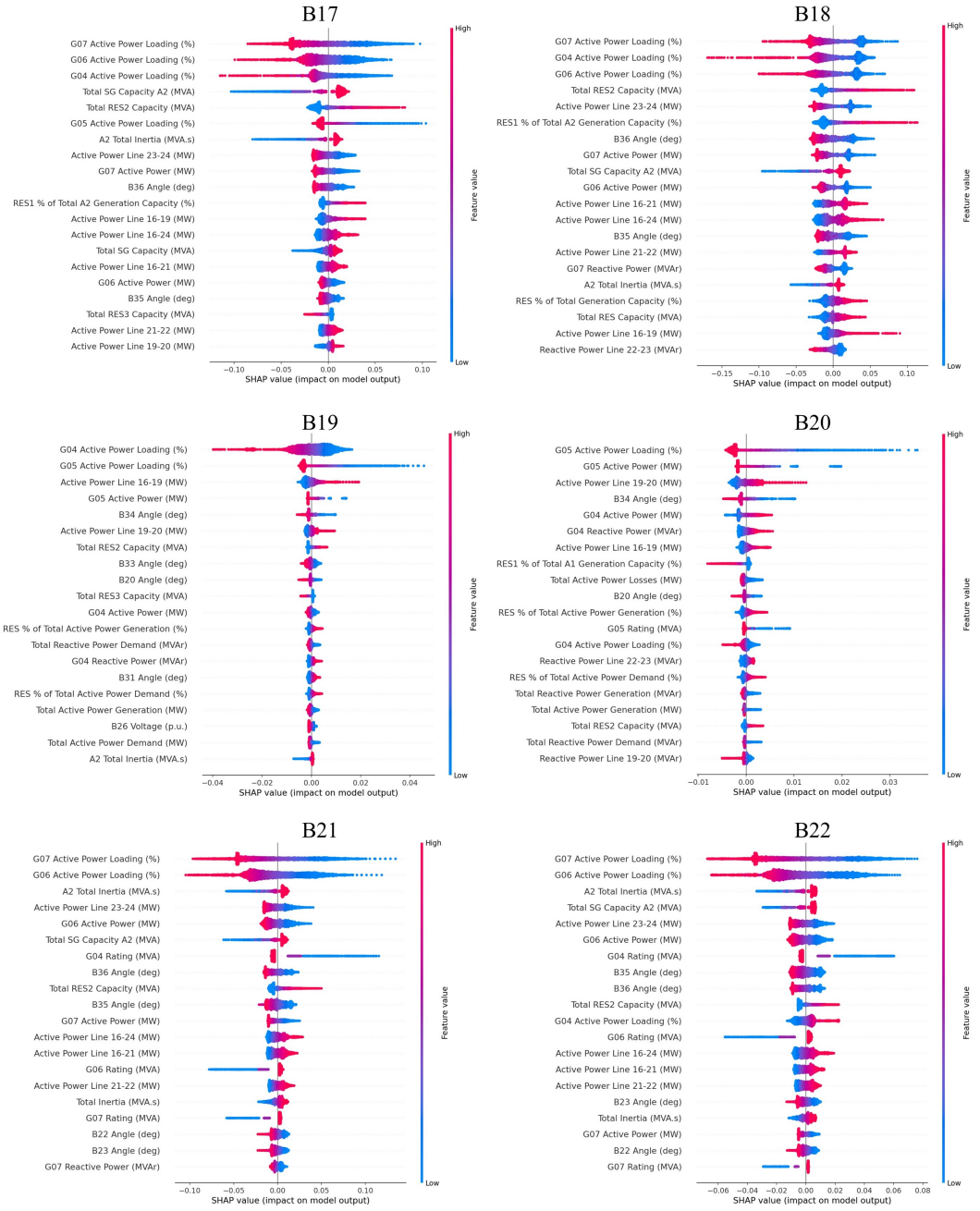

Figure B.5: Stability boundary representation (B17, B18, B19, B20, B21 & B22) using SHAP to interpret locally trained artificial neural networks (ANNs).

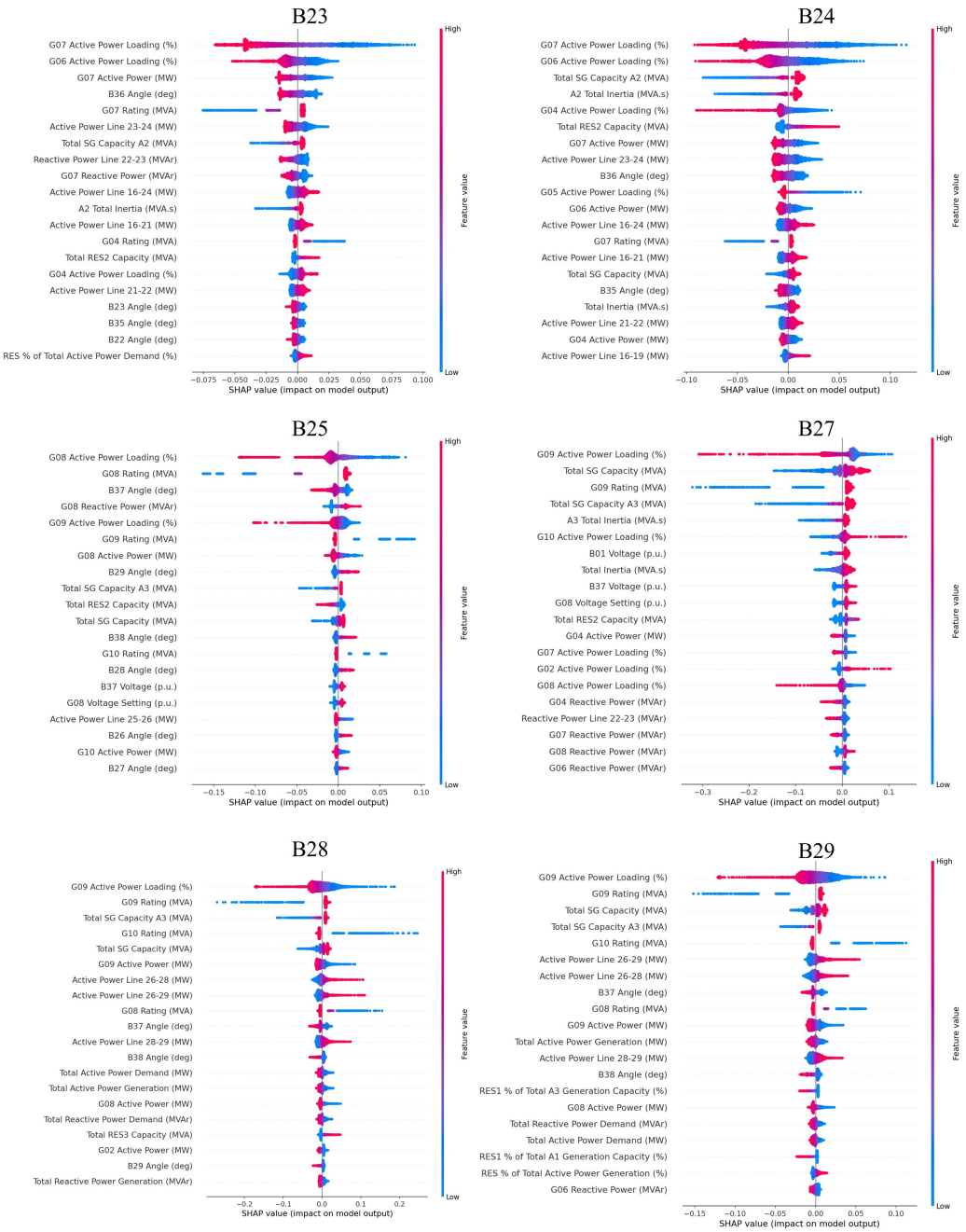

Figure B.6: Stability boundary representation (B23, B24, B25, B27, B28 & B29) using SHAP to interpret locally trained artificial neural networks (ANNs).

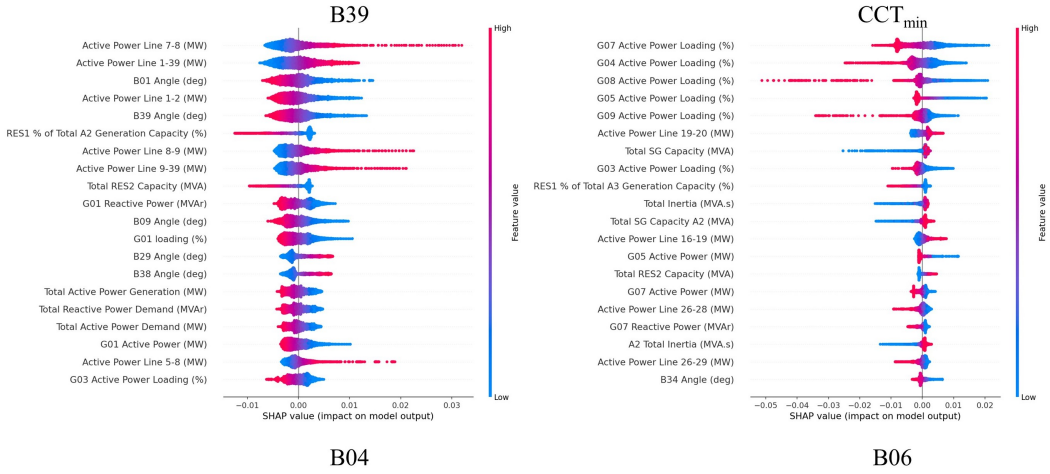

Figure B.7: Stability boundary representation (B39 & CCT_{min}) using SHAP to interpret locally trained artificial neural networks (ANNs).

Bibliography

[1] P. Kundur, J. Paserba, V. Ajjarapu, G. Andersson, A. Bose, C. Canizares, N. Hatziargyriou, D. Hill, A. Stankovic, and C. Taylor, "Definition and classification of power system stability," *IEEE Transactions on Power Systems*, vol. 19, no. 2, pp. 1387–1401, 2004.

[2] N. Hatziargyriou, J. Milanović, C. Rahmann, V. Ajjarapu, C. Cañizares, I. Erlich, D. Hill, I. Hiskens, I. Kamwa, and B. Pal, "Stability definitions and characterization of dynamic behavior in systems with high penetration of power electronic interfaced technologies," IEEE Power and Energy Society, Tech. Rep., 2020. [Online]. Available: https://resourcecenter.ieee-pes.org/publications/technical-reports/PES_TP_TR77_PSDP_STABILITY_051320.html

[3] P. N. Papadopoulos and J. V. Milanović, "Probabilistic framework for transient stability assessment of power systems with high penetration of renewable generation," *IEEE Transactions on Power Systems*, vol. 32, no. 4, pp. 3078–3088, 2016.

[4] K. Connolly, "Germany to reactivate coal power plants as Russia curbs gas flow," 7 2022.

[5] T. Wilson and N. Hume, "European gas prices shoot to new high as energy crunch worsens," 12 2021. [Online]. Available: https://www.ft.com/content/a0bc7996-ab5d-465b-aab4-90472e088af7

[6] D. M. King and B. J. C. Perera, "Morris method of sensitivity analysis applied to assess the importance of input variables on urban water supply yield–a case study," *Journal of hydrology*, vol. 477, pp. 17–32, 2013.

[7] I. A. Hiskens and J. Alseddiqui, "Sensitivity, approximation, and uncertainty in power system dynamic simulation," *IEEE Transactions on Power Systems*, vol. 21, no. 4, pp. 1808–1820, 2006.

[8] A. Saltelli, M. Ratto, T. Andres, F. Campolongo, J. Cariboni, D. Gatelli, M. Saisana, and S. Tarantola, *Global sensitivity analysis: the primer*. John Wiley & Sons, 2008.

[9] K. N. Hasan, R. Preece, and J. V. Milanović, "Efficient identification of critical parameters affecting the small-disturbance stability of power systems with variable uncertainty," in *2016 IEEE Power and Energy Society General Meeting (PESGM)*. IEEE, 2016, pp. 1–5.

[10] B. Iooss and P. Lemaître, "A review on global sensitivity analysis methods," *Uncertainty management in simulation-optimization of complex systems*, pp. 101–122, 2015.

[11] K. N. Hasan, R. Preece, and J. V. Milanović, "Priority ranking of critical uncertainties affecting small-disturbance stability using sensitivity analysis techniques," *IEEE Transactions on Power Systems*, vol. 32, no. 4, pp. 2629–2639, 2016.

[12] R. Preece and J. V. Milanović, "Assessing the applicability of uncertainty importance measures for power system studies," *IEEE Transactions on Power Systems*, vol. 31, no. 3, pp. 2076–2084, 2015.

[13] I. M. Sobol, "Sensitivity estimates for nonlinear mathematical models (English Translation)," *Mathematical Modeling and Computational Experiment*, vol. 1, no. 4, pp. 407–414, 1993.

[14] C. Molnar, *Interpretable machine learning*. Lulu.com, 2020. [Online]. Available: https://christophm.github.io/interpretable-ml-book/

[15] BP, "BP Statistical Review of World Energy ," BP, Tech. Rep., 2021. [Online]. Available: https://www.bp.com/en/global/corporate/energy-economics/statistical-review-of-world-energy/primary-energy.html

[16] C. A. S. Hall and K. Klitgaard, "Energy return on investment," in *Energy and the Wealth of Nations*. Springer, 2018, pp. 387–404.

[17] L. Delannoy, P.-Y. Longaretti, D. J. Murphy, and E. Prados, "Peak oil and the low-carbon energy transition: A net-energy perspective," *Applied Energy*, vol. 304, p. 117843, 2021. [Online]. Available: https://www.sciencedirect.com/science/article/pii/S0306261921011673

[18] National Grid, "Future Energy Scenarios 2021," Tech. Rep., 2021. [Online]. Available: https://www.nationalgrideso.com/future-energy/future-energy-scenarios/fes-2021#fes-reports

[19] "The Paris Agreement." [Online]. Available: https://www.un.org/en/climatechange/paris-agreement

[20] T. Macalister, "Longannet power station closes ending coal power use in Scotland," 2016. [Online]. Available: https://www.theguardian.com/environment/2016/mar/24/longannet-power-station-closes-coal-power-scotland

[21] R. Davies, "Hunterston B nuclear power station retires after 46 years in service," 1 2022.

[22] National Grid, "Electricity Ten Year Statement 2021," National Grid, Tech. Rep., 2021. [Online]. Available: https://www.nationalgrideso.com/research-publications/etys

[23] Stattnett and National Grid, "North Sea Link," 2018. [Online]. Available: http://northsealink.com/

[24] Financial Times, "How does Europe get its gas?" 2021. [Online]. Available: https://ig.ft.com/europes-gas-crisis-pipelines-explainer/

[25] K. Johnstone, R. M. Tumilty, K. R. W. Bell, and C. D. Booth, "Transient stability assessment of the GB transmission system with high penetrations of wind power," in *Proceedings 13th Wind Integration Workshop*. Energynautics GmbH, Darmstadt, Germany., 2014.

[26] F. Milano, F. Dörfler, G. Hug, D. J. Hill, and G. Verbič, "Foundations and challenges of low-inertia systems," in *2018 Power Systems Computation Conference (PSCC)*. IEEE, 2018, pp. 1–25.

[27] T. M. Masaud and R. D. Mistry, "Fault current contribution of Renewable Distributed Generation: An overview and key issues," in *2016 IEEE Conference on Technologies for Sustainability (SusTech)*. IEEE, 2016, pp. 229–234.

[28] National Grid, "System Operability Framework 2016," Tech. Rep., 2016. [Online]. Available: https://www.nationalgrid.com/sites/default/files/documents/8589937803-SOF2016-FullInteractiveDocument.pdf

[29] J. O'Sullivan, A. Rogers, D. Flynn, P. Smith, A. Mullane, and M. O'Malley, "Studying the maximum instantaneous non-synchronous generation in an island system—Frequency stability challenges in Ireland," *IEEE Transactions on Power Systems*, vol. 29, no. 6, pp. 2943–2951, 2014.

[30] P. Kundur, N. N. J. Balu, and M. G. M. Lauby, *Power system stability and control*. McGraw-hill New York, 1994, vol. 7. [Online]. Available: http://www.academia.edu/download/28284657/invitation.pdf

[31] E. H. Camm, M. R. Behnke, O. Bolado, M. Bollen, M. Bradt, C. Brooks, W. Dilling, M. Edds, W. J. Hejdak, D. Houseman, S. Klein, F. Li, J. Li, P. Maibach, T. Nicolai, J. Patino, S. V. Pasupulati, N. Samaan, S. Saylors, T. Siebert, T. Smith, M. Starke, and R. Walling, "Characteristics of wind turbine generators for wind power plants," in *2009 IEEE Power Energy Society General Meeting*, 2009, pp. 1–5.

[32] A. D. Hansen, "Wind turbine technologies," in *Wind Energy Engineering*. Elsevier, 2017, pp. 145–160.

[33] Western Electricity Coordinating Council, "WECC Type 4 Wind Turbine Generator Model - Phase II," Tech. Rep., 2013. [Online]. Available: https://www.wecc.biz/Reliability/WECC-Type-4-Wind-Turbine-Generator-Model-Phase-II-012313.pdf

[34] L. Stoker, "Solar sends GB transmission system demand to historic lows," 2017. [Online]. Available: https://www.solarpowerportal.co.uk/news/solar_sends_gb_transmission_system_demand_to_historic_lows

[35] R. Shah, N. Mithulananthan, R. C. Bansal, and V. K. Ramachandaramurthy, "A review of key power system stability challenges for large-scale PV integration," *Renewable and Sustainable Energy Reviews*, vol. 41, pp. 1423–1436, 2015.

[36] O. E. Oni, I. E. Davidson, and K. N. I. Mbangula, "A review of LCC-HVDC and VSC-HVDC technologies and applications," in *2016 IEEE 16th International Conference on Environment and Electrical Engineering (EEEIC)*. IEEE, 2016, pp. 1–7.

[37] Scottish & Southern Electricity Networks, "Eastern HVDC link," 2012. [Online]. Available: https://www.ssen.co.uk/EasternHVDClink/

[38] A. Ortega and F. Milano, "Generalized model of VSC-based energy storage systems for transient stability analysis," *IEEE Transactions on Power Systems*, vol. 31, no. 5, pp. 3369–3380, 2016.

[39] National Grid, "Enhanced Frequency Response Market Information Report," Tech. Rep., 2016. [Online]. Available: https://www.nationalgrideso.com/sites/eso/files/documents/EFRMarketInformationReportv1.pdf

[40] ScottishPower Renewables, "ScottishPower Renwables Battery Energy Storage System." [Online]. Available: https://www.scottishpowerrenewables.com/pages/bess.aspx

[41] National Grid, "Enhanced Frequency Control Capability (EFCC)," 2018. [Online]. Available: https://www.nationalgrideso.com/innovation/projects/enhanced-frequency-control-capability-efcc

[42] "Analysis and control of power system oscillations," Cigré Task Force, Tech. Rep., 1996.

[43] P. M. Anderson and A. A. Fouad, *Power system control and stability.* John Wiley & Sons, 2008.

[44] M. Chen, D. Zhou, and F. Blaabjerg, "Modelling, implementation, and assessment of virtual synchronous generator in power systems," *Journal of Modern Power Systems and Clean Energy*, vol. 8, no. 3, pp. 399–411, 2020.

[45] D. Ramasubramanian, P. Pourbeik, E. Farantatos, and A. Gaikwad, "Simulation of 100% inverter-based resource grids with positive sequence modeling," *IEEE Electrification Magazine*, vol. 9, no. 2, pp. 62–71, 2021.

[46] Q. Huang and V. Vittal, "Advanced EMT and Phasor-Domain Hybrid Simulation with Simulation Mode Switching Capability for Transmission and Distribution Systems," *IEEE Transactions on Power Systems*, 2018.

[47] J. Lv, M. Pawlak, and U. D. Annakkage, "Prediction of the Transient Stability Boundary Based on Nonparametric Additive Modeling," *IEEE Transactions on Power Systems*, vol. 32, no. 6, pp. 4362–4369, 2017.

[48] M. Bakhtvar, E. Vittal, K. Zheng, and A. Keane, "Synchronizing torque impacts on rotor speed in power systems," *IEEE Transactions on Power Systems*, vol. 32, no. 3, pp. 1927–1935, 5 2017.

[49] L. Shi, S. Dai, Y. Ni, L. Yao, and M. Bazargan, "Transient stability of power systems with high penetration of DFIG based wind farms," in *2009 IEEE Power & Energy Society General Meeting.* IEEE, 2009, pp. 1–6.

[50] C. S. Saunders, M. M. Alamuti, and G. A. Taylor, "Transient stability analysis using potential energy indices for determining critical generator sets," in *2014 IEEE PES General Meeting— Conference & Exposition.* IEEE, 2014, pp. 1–5.

[51] J. G. Slootweg and W. L. Kling, "Impacts of distributed generation on power system transient stability," in *IEEE Power Engineering Society Summer Meeting,*, vol. 2. IEEE, 2002, pp. 862–867.

[52] A. Sajadi, R. Preece, and J. V. Milanovic, "Evaluation of suitability of different transient stability indices for identification of critical system states," in *10th Bulk Power Systems Dynamics and Control Symposium – IREP'2017.* IREP, 2017.

[53] National Grid, "GC0062: Fault Ride Through," 2015. [Online]. Available: https://ngrid.com/2LUETvg

[54] R. Zárate-Miñano, T. Van Cutsem, F. Milano, and A. J. Conejo, "Securing transient stability using time-domain simulations within an optimal power flow," *IEEE Transactions on Power Systems*, vol. 25, no. 1, pp. 243–253, 2010.

[55] R. Shah, N. Mithulananthan, R. C. Bansal, and V. K. Ramachandaramurthy, "A review of key power system stability challenges for large-scale PV integration," *Renewable and Sustainable Energy Reviews*, vol. 41, pp. 1423–1436, 2015.

[56] L. Sigrist, F. Echavarren, L. Rouco, and P. Panciatici, "A fundamental study on the impact of HVDC lines on transient stability of power systems," in *2015 IEEE Eindhoven PowerTech.* IEEE, 2015, pp. 1–6.

[57] W. Du, J. Bi, and H. F. Wang, "Small-signal angular stability of power system as affected by grid-connected variable speed wind generators-A survey of recent representative works," *CSEE Journal of Power and Energy Systems*, vol. 3, no. 3, pp. 223–231, 2017.

[58] Q. Wang, A. Xue, T. Bi, and Y. Zheng, "Impact of DFIG-based wind farm on transient stability of single machine infinite bus system," in *Power and Energy*

Engineering Conference (APPEEC), 2013 IEEE PES Asia-Pacific. IEEE, 2013, pp. 1–5.

[59] M. V. A. Nunes, J. A. P. Lopes, H. H. Zurn, U. H. Bezerra, and R. G. Almeida, "Influence of the variable-speed wind generators in transient stability margin of the conventional generators integrated in electrical grids," *IEEE Transactions on Energy Conversion*, vol. 19, no. 4, pp. 692–701, 2004.

[60] L. Meegahapola, D. Flynn, and T. Littler, "Transient stability analysis of a power system with high wind penetration," in *Universities Power Engineering Conference, 2008. UPEC 2008. 43rd International.* IEEE, 2008, pp. 1–5.

[61] E. Muljadi, C. P. Butterfield, B. Parsons, and A. Ellis, "Effect of variable speed wind turbine generator on stability of a weak grid," *IEEE Transactions on Energy Conversion*, vol. 22, no. 1, pp. 29–36, 2007.

[62] M. Ma, Y. H. Liu, and D. M. Zhao, "Research on the impact of large-scale integrated wind farms on the security and stability of regional power system," in *2010 International Conference on Power System Technology.* IEEE, 2010, pp. 1–6.

[63] E. Vittal, M. O'Malley, and A. Keane, "Rotor Angle Stability With High Penetrations of Wind Generation," *IEEE Transactions on Power Systems*, vol. 27, no. 1, pp. 353–362, 2 2012.

[64] L. Meegahapola and T. Littler, "Characterisation of large disturbance rotor angle and voltage stability in interconnected power networks with distributed wind generation," *IET Renewable Power Generation*, vol. 9, no. 3, pp. 272–283, 4.

[65] C. Yu, G. James, Y. Xue, and F. Xue, "Impacts of large scale wind power on power system transient stability," in *2011 4th International Conference on Electric Utility Deregulation and Restructuring and Power Technologies (DRPT).* IEEE, 2011, pp. 277–283.

[66] C. Wang, L. Shi, L. Yao, L.-m. Wang, and Y.-x. Ni, "Small signal stability analysis of the large-scale wind farm with DFIGs," *Proceedings of the CSEE*, vol. 30, no. 4, pp. 63–70, 2010.

[67] D. Gautam, V. Vittal, and T. Harbour, "Impact of increased penetration of DFIG-based wind turbine generators on transient and small signal stability of power systems," *IEEE Transactions on power systems*, vol. 24, no. 3, pp. 1426–1434, 2009.

[68] K. Elkington, V. Knazkins, and M. Ghandhari, "On the rotor angle stability of power systems with doubly fed induction generators," in *Power Tech, 2007 IEEE Lausanne*. IEEE, 2007, pp. 213–218.

[69] H. Hou, L. Lin, T. Wu, and Y. Miao, "Comparison of Transient Stability between Wind Farm Based on DFIG and Traditional Power Plant in an Actual Grid," in *2010 Asia-Pacific Power and Energy Engineering Conference*, 2010, pp. 1–4.

[70] C. Samarasinghe and G. Ancell, "Effects of large scale wind generation on transient stability of the New Zealand power system," in *2008 IEEE Power and Energy Society General Meeting - Conversion and Delivery of Electrical Energy in the 21st Century*, 2008, pp. 1–8.

[71] L. Meegahapola and D. Flynn, "Impact on transient and frequency stability for a power system at very high wind penetration," in *IEEE PES General Meeting*, 2010, pp. 1–8.

[72] C. Eping, J. Stenzel, H. Muller, and M. Poll, "Impact of large scale wind power on power system stability," in *5th Int. Works. on Large-Scale Integration of Wind Power and Trans. Net. for Offshore Wind Farms*, Glasgow, 2005.

[73] X. Chen, W. Du, and H. F. Wang, "Power system angular stability as affected by the reduced inertia due to wind displacing synchronous generators," in *2017 2nd International Conference on Power and Renewable Energy, ICPRE 2017*. Institute of Electrical and Electronics Engineers Inc., 6 2018, pp. 402–406.

[74] N. R. Ullah and T. Thiringer, "Effect of operational modes of a wind farm on the transient stability of nearby generators and on power oscillations: a Nordic grid study," *Wind Energy: An International Journal for Progress and Applications in Wind Power Conversion Technology*, vol. 11, no. 1, pp. 63–73, 2008.

[75] "All Island TSO Facilitation of Renewables Studies," EirGrid & SONI, Tech. Rep., 2008. [Online]. Available: http://www.eirgridgroup.com/site-files/library/EirGrid/Facilitation-of-Renewables-Report.pdf

[76] M. Edrah, K. L. Lo, and O. Anaya-Lara, "Impacts of high penetration of DFIG wind turbines on rotor angle stability of power systems," *IEEE Transactions on Sustainable Energy*, vol. 6, no. 3, pp. 759–766, 2015.

[77] R. Tumilty, C. G. Bright, G. M. Burt, O. Anaya-Lara, and J. R. McDonald, "Applying series braking resistors to improve the stability of low inertia synchronous generators," *CIRED 2007*, 2007.

[78] K. Johnstone, K. Bell, and C. Booth, "The impact of post-fault active power recovery ramp rates of wind turbines on transient stability in Great Britain," in *EWEA 2015 Annual Event*, 2015.

[79] G. Tsourakis, B. M. Nomikos, and C. D. Vournas, "Contribution of doubly fed wind generators to oscillation damping," *IEEE Transactions on Energy Conversion*, vol. 24, no. 3, pp. 783–791, 2009.

[80] R. V. de Oliveira, J. A. Zamadei, and C. H. Hossi, "Impact of distributed synchronous and doubly-fed induction generators on small-signal stability of a distribution network," in *Power and Energy Society General Meeting, 2011 IEEE*. IEEE, 2011, pp. 1–8.

[81] J. Quintero, V. Vittal, G. T. Heydt, and H. Zhang, "The impact of increased penetration of converter control-based generators on power system modes of oscillation," *IEEE Transactions on Power Systems*, vol. 29, no. 5, pp. 2248–2256, 2014.

[82] J. G. Slootweg and W. L. Kling, "The impact of large scale wind power generation on power system oscillations," *Electric Power Systems Research*, vol. 67, no. 1, pp. 9–20, 2003.

[83] H. Liu, L. Jin, D. Le, and A. A. Chowdhury, "Impact of high penetration of solar photovoltaic generation on power system small signal stability," in *2010 International Conference on Power System Technology*, 2010, pp. 1–7.

[84] T. Knuppel, J. N. Nielsen, K. H. Jensen, A. Dixon, and J. Ostergaard, "Small-signal stability of wind power system with full-load converter interfaced wind turbines," *IET Renewable Power Generation*, vol. 6, no. 2, pp. 79–91, 2012.

[85] A. Mendonca and J. A. P. Lopes, "Impact of large scale wind power integration on small signal stability," in *Future Power Systems, 2005 International Conference on*. IEEE, 2005, pp. 5–pp.

[86] S. Chen, X. Chang, H. Sun, and L. Zeng, "Impact of grid-connected wind farm on damping performance of power system," *Power System Technology*, vol. 37, no. 6, pp. 1570–1577, 2013.

[87] E. Munkhchuluun, L. Meegahapola, and A. Vahidnia, "Impact on rotor angle stability with high solar-PV generation in power networks," in *2017 IEEE PES Innovative Smart Grid Technologies Conference Europe (ISGT-Europe)*. IEEE, 2017, pp. 1–6.

[88] P. K. Olulope, K. A. Folly, and G. K. Venayagamoorthy, "Modeling and simulation of hybrid distributed generation and its impact on transient stability of power system," in *2013 IEEE International Conference on Industrial Technology (ICIT)*, 2013, pp. 1757–1762.

[89] E. Vittal and A. Keane, "Identification of critical wind farm locations for improved stability and system planning," *IEEE Transactions on Power Systems*, vol. 28, no. 3, pp. 2950–2958, 2013.

[90] E. Vittal, P. Cuffe, and A. Keane, "Transient stability impacts from distribution connected wind farms," in *Power and Energy Society General Meeting, 2012 IEEE*. IEEE, 2012, pp. 1–5.

[91] E. Vittal, M. O'Malley, and A. Keane, "Rotor angle stability with high penetrations of wind generation," *IEEE Transactions on Power Systems*, vol. 27, no. 1, pp. 353–362, 2011.

[92] N. Ding, Z. Lu, Y. Qiao, and Y. Min, "Simplified equivalent models of large-scale wind power and their application on small-signal stability," *Journal of Modern Power Systems and Clean Energy*, vol. 1, no. 1, pp. 58–64, 2013.

[93] D. Remon, A. M. Cantarellas, J. M. Mauricio, and P. Rodriguez, "Power system stability analysis under increasing penetration of photovoltaic power plants with synchronous power controllers," *IET Renewable Power Generation*, vol. 11, no. 6, pp. 733–741, 2017.

[94] Y. Xu, X. Xie, Z. Y. Dong, D. J. Hill, and R. Zhang, "Risk-averse multi-objective generation dispatch considering transient stability under load model uncertainty," *IET Generation, Transmission & Distribution*, vol. 10, no. 11, pp. 2785–2791, 2016.

[95] I. A. Calle, P. Ledesma, and E. D. Castronuovo, "Advanced application of transient stability constrained-optimal power flow to a transmission system including an HVDC-LCC link," *IET Generation, Transmission and Distribution*, vol. 9, no. 13, pp. 1765–1772, 10 2015.

[96] "UK Natural Gas NBP Spot Price," ERCE Group, Tech. Rep., 2022. [Online]. Available: https://www.erce.energy/graph/uk-natural-gas-nbp-spot-price/

[97] P. N. Papadopoulos and J. V. Milanović, "Probabilistic Framework for Transient Stability Assessment of Power Systems With High Penetration of Renewable Generation," *IEEE Transactions on Power Systems*, vol. 32, no. 4, pp. 3078–3088, 7 2017.

[98] B. Qi, K. N. Hasan, and J. V. Milanovic, "Identification of Critical Parameters Affecting Voltage and Angular Stability Considering Load-Renewable Generation Correlations," *IEEE Transactions on Power Systems*, vol. 34, no. 4, pp. 2859–2869, 7 2019.

[99] A. Mitra and D. Chatterjee, "A sensitivity based approach to assess the impacts of integration of variable speed wind farms on the transient stability of power systems," *Renewable energy*, vol. 60, pp. 662–671, 2013.

[100] M. Ma, W. Jie, Z. Wang, and M. W. Khan, "Global Geometric Structure of the Transient Stability Regions of Power Systems," *IEEE Transactions on Power Systems*, p. 1, 5 2019.

[101] A. Ortega, F. Milano, Ortega, F. Milano, A. Ortega, and F. Milano, "Stochastic transient stability analysis of transmission systems with inclusion of energy storage devices," *IEEE Transactions on Power Systems*, vol. 33, no. 1, pp. 1077–1079, 1 2017.

[102] Y. Zhang, M. Ding, P. Han, H. Sun, W. Yang, and Z. Chen, "Analysis of the Interactive Influence of the Active Power Recovery Rates of DFIG and UHVDC on the Rotor Angle Stability of the Sending-End System," *IEEE Access*, vol. 7, pp. 79 944–79 958, 2019.

[103] P. Sørensen, B. Andresen, J. Fortmann, and P. Pourbeik, "Modular structure of wind turbine models in IEC 61400-27-1," in *2013 IEEE Power & Energy Society General Meeting*. IEEE, 2013, pp. 1–5.

[104] British Standards Institute, "BSI Standards Publication BS EN 61400-27-1:2015," British Standards Institute, London, Tech. Rep., 2015. [Online]. Available: https://bit.ly/2HDR7v5

[105] H. W. Dommel and W. F. Tinney, "Optimal power flow solutions," *IEEE Transactions on power apparatus and systems*, no. 10, pp. 1866–1876, 1968.

[106] R. D. Zimmerman, C. E. Murillo-Sánchez, and R. J. Thomas, "MATPOWER: Steady-state operations, planning, and analysis tools for power systems research and education," *IEEE Transactions on Power Systems*, vol. 26, no. 1, pp. 12–19, 2010.

[107] A. J. Conejo, E. Castillo, R. Mínguez, and F. Milano, "Locational marginal price sensitivities," *IEEE Transactions on Power Systems*, vol. 20, no. 4, pp. 2026–2033, 2005.

[108] "Electricity Generation Costs," UK Government Department for Business, Energy and Industrial Strategy, Tech. Rep., 2016. [Online]. Available: www.nationalarchives.gov.uk/doc/open-government-licence/

[109] P. S. R. Murty, *Power systems analysis*. Butterworth-Heinemann, 2017.

[110] "Short-Circuit Currents in Three-Phase A.C. Systems," International Electrotechnical Commission, Tech. Rep., 2016. [Online]. Available: https://bit.ly/30dA1se

[111] O. A. Alimi, K. Ouahada, and A. M. Abu-Mahfouz, "A review of machine learning approaches to power system security and stability," *IEEE Access*, vol. 8, pp. 113 512–113 531, 2020.

[112] A. R. Sobbouhi and A. Vahedi, "Transient stability prediction of power system; a review on methods, classification and considerations," *Electric Power Systems Research*, vol. 190, p. 106853, 2021.

[113] S. You, Y. Zhao, M. Mandich, Y. Cui, H. Li, H. Xiao, S. Fabus, Y. Su, Y. Liu, H. Yuan, H. Jiang, J. Tan, and Y. Zhang, "A Review on Artificial Intelligence for Grid Stability Assessment," in *2020 IEEE International Conference on Communications, Control, and Computing Technologies for Smart Grids (SmartGridComm)*, 11 2020, pp. 1–6.

[114] J. Sohoni and S. K. Joshi, "A Survey on Transient Stability Studies for Electrical Power Systems," in *2018 Clemson University Power Systems Conference (PSC)*, 2018, pp. 1–8.

[115] P. Sarajcev, A. Kunac, G. Petrovic, and M. Despalatovic, "Artificial Intelligence Techniques for Power System Transient Stability Assessment," *Energies*, vol. 15, no. 2, p. 507, 2022.

[116] R. Machlev, L. Heistrene, M. Perl, K. Y. Levy, J. Belikov, S. Mannor, and Y. Levron, "Explainable Artificial Intelligence (XAI) techniques for energy and power systems: Review, challenges and opportunities," *Energy and AI*, p. 100169, 2022.

[117] A. D. Rajapakse, F. Gomez, K. Nanayakkara, P. A. Crossley, and V. V. Terzija, "Rotor angle instability prediction using post-disturbance voltage trajectories," *IEEE Transactions on Power Systems*, vol. 25, no. 2, pp. 947–956, 2009.

[118] L. Zhu, D. J. Hill, and C. Lu, "Hierarchical Deep Learning Machine for Power System Online Transient Stability Prediction," *IEEE Transactions on Power Systems*, vol. 35, no. 3, pp. 2399–2411, 5 2020.

[119] M. Rahmatian, W. G. Dunford, A. Palizban, and A. Moshref, "Transient stability assessment of power systems through wide-area monitoring system," in *2015 IEEE Power & Energy Society General Meeting*. IEEE, 2015, pp. 1–5.

[120] T. Liu, Y. Liu, L. Xu, J. Liu, J. Mitra, and Y. Tian, "Non-parametric statistics-based predictor enabling online transient stability assessment," *IET Generation, Transmission & Distribution*, vol. 12, no. 21, pp. 5761–5769, 2018.

[121] M. Rahmatian, Y. C. Chen, A. Palizban, A. Moshref, and W. G. Dunford, "Transient stability assessment via decision trees and multivariate adaptive regression splines," *Electric power systems research*, vol. 142, pp. 320–328, 2017.

[122] Y. Zhang, Y. Xu, Z. Y. Dong, Z. Xu, and K. P. Wong, "Intelligent Early Warning of Power System Dynamic Insecurity Risk: Toward Optimal Accuracy-Earliness

Tradeoff," *IEEE Transactions on Industrial Informatics*, vol. 13, no. 5, pp. 2544–2554, 10 2017.

[123] A. K. Ozcanli, F. Yaprakdal, and M. Baysal, "Deep learning methods and applications for electrical power systems: A comprehensive review," *International Journal of Energy Research*, vol. 44, no. 9, pp. 7136–7157, 2020.

[124] G. Baryannis, S. Dani, and G. Antoniou, "Predicting supply chain risks using machine learning: The trade-off between performance and interpretability," *Future Generation Computer Systems*, vol. 101, pp. 993–1004, 2019.

[125] M. He, J. Zhang, and V. Vittal, "Robust online dynamic security assessment using adaptive ensemble decision-tree learning," *IEEE Transactions on Power Systems*, vol. 28, no. 4, pp. 4089–4098, 2013.

[126] T. Guo and J. V. Milanović, "Probabilistic framework for assessing the accuracy of data mining tool for online prediction of transient stability," *IEEE Transactions on Power Systems*, vol. 29, no. 1, pp. 377–385, 2013.

[127] N. Amjady and S. F. Majedi, "Transient stability prediction by a hybrid intelligent system," *IEEE Transactions on Power Systems*, vol. 22, no. 3, pp. 1275–1283, 2007.

[128] F. Hashiesh, H. E. Mostafa, A.-R. Khatib, I. Helal, and M. M. Mansour, "An intelligent wide area synchrophasor based system for predicting and mitigating transient instabilities," *IEEE Transactions on Smart Grid*, vol. 3, no. 2, pp. 645–652, 2012.

[129] C. Molnar, G. Casalicchio, and B. Bischl, "Interpretable Machine Learning – A Brief History, State-of-the-Art and Challenges," 10 2020. [Online]. Available: https://arxiv.org/abs/2010.09337

[130] C. Molnar, G. König, J. Herbinger, T. Freiesleben, S. Dandl, C. A. Scholbeck, G. Casalicchio, M. Grosse-Wentrup, and B. Bischl, "General pitfalls of model-

agnostic interpretation methods for machine learning models," *arXiv preprint arXiv:2007.04131*, 2020.

[131] L. Wehenkel, T. Van Cutsem, and M. Ribbens-Pavella, "Artificial intelligence applied to on-line transient stability assessment of electric power systems," *IFAC Proceedings Volumes*, vol. 20, no. 5, pp. 311–316, 1987.

[132] ——, "Decision trees applied to on-line transient stability assessment of power systems," in *IEEE International Symposium on Circuits and Systems*. IEEE, 1988, pp. 1887–1890.

[133] F. R. Gomez, A. D. Rajapakse, U. D. Annakkage, and I. T. Fernando, "Support vector machine-based algorithm for post-fault transient stability status prediction using synchronized measurements," *IEEE Transactions on Power Systems*, vol. 26, no. 3, pp. 1474–1483, 2010.

[134] L. Wehenkel, T. Van Cutsem, and M. Ribbens-Pavella, "An artificial intelligence framework for online transient stability assessment of power systems," *IEEE Transactions on Power Systems*, vol. 4, no. 2, pp. 789–800, 1989.

[135] L. Wehenkel, M. Pavella, E. Euxibie, and B. Heilbronn, "Decision tree based transient stability method a case study," *IEEE Transactions on Power Systems*, vol. 9, no. 1, pp. 459–469, 1994.

[136] T. Amraee and S. Ranjbar, "Transient instability prediction using decision tree technique," *IEEE Transactions on Power Systems*, vol. 28, no. 3, pp. 3028–3037, 2013.

[137] Y. Chen, S. M. Mazhari, C. Y. Chung, S. O. Faried, and B. C. Pal, "Rotor Angle Stability Prediction of Power Systems With High Wind Power Penetration Using a Stability Index Vector," *IEEE Transactions on Power Systems*, vol. 35, no. 6, pp. 4632–4643, 11 2020.

[138] B. Li, J. Wu, L. Hao, M. Shao, R. Zhang, and W. Zhao, "Anti-Jitter and Refined Power System Transient Stability Assessment Based on Long-Short Term Memory Network," *IEEE Access*, vol. 8, pp. 35 231–35 244, 2020.

[139] I. Kamwa, S. R. Samantaray, and G. Joos, "Development of rule-based classifiers for rapid stability assessment of wide-area post-disturbance records," *IEEE Transactions on Power Systems*, vol. 24, no. 1, pp. 258–270, 2009.

[140] T. Liu, Y. Liu, J. Liu, Y. Yang, G. A. Taylor, and Z. Huang, "Multi-indicator inference scheme for fuzzy assessment of power system transient stability," *CSEE Journal of Power and Energy Systems*, vol. 2, no. 3, pp. 1–9, 2016.

[141] S. Kretsinger, S. Rovnyak, D. Brown, and J. Thorp, "Parallel decision trees for predicting groups of unstable generators from synchronized phasor measurements," in *Precise Measurements in Power Systems Conference*, 1993.

[142] S. Rovnyak, S. Kretsinger, J. Thorp, and D. Brown, "Decision trees for real-time transient stability prediction," *IEEE Transactions on Power Systems*, vol. 9, no. 3, pp. 1417–1426, 1994.

[143] N. Senroy, G. T. Heydt, and V. Vittal, "Decision tree assisted controlled islanding," *IEEE Transactions on Power Systems*, vol. 21, no. 4, pp. 1790–1797, 2006.

[144] Q. Gao and S. M. Rovnyak, "Decision trees using synchronized phasor measurements for wide-area response-based control," *IEEE Transactions on Power Systems*, vol. 26, no. 2, pp. 855–861, 2010.

[145] K. Mei and S. M. Rovnyak, "Response-based decision trees to trigger one-shot stabilizing control," *IEEE Transactions on Power Systems*, vol. 19, no. 1, pp. 531–537, 2004.

[146] T. Guo and J. V. Milanović, "Online identification of power system dynamic signature using PMU measurements and data mining," *IEEE Transactions on Power Systems*, vol. 31, no. 3, pp. 1760–1768, 2015.

[147] P. N. Papadopoulos, T. Guo, and J. V. Milanović, "Probabilistic framework for online identification of dynamic behavior of power systems with renewable generation," *IEEE Transactions on Power Systems*, vol. 33, no. 1, pp. 45–54, 2017.

[148] J. An, G. Mu, Z. Li, and D. Liu, "Power system transient stability margin assessment using steady-state information," in *2019 IEEE Innovative Smart Grid Technologies - Asia (ISGT Asia)*, 5 2019, pp. 642–647.

[149] R. Diao, V. Vittal, and N. Logic, "Design of a real-time security assessment tool for situational awareness enhancement in modern power systems," *IEEE Transactions on Power Systems*, vol. 25, no. 2, pp. 957–965, 2009.

[150] J. Machowski, J. W. Bialek, and J. R. Bumby, *Power System Dynamics: Stability and Control*. New York: Wiley, 2008.

[151] W. Phootrakornchai and S. Jiriwibhakorn, "Online critical clearing time estimation using an adaptive neuro-fuzzy inference system (ANFIS)," *International Journal of Electrical Power & Energy Systems*, vol. 73, pp. 170–181, 2015.

[152] Z. Chen, X. Han, C. Fan, H. Zhang, and C. Liu, "Prediction of Critical Clearing Time for Transient Stability Based on Ensemble Extreme Learning Machine Regression Model," in *2019 IEEE Innovative Smart Grid Technologies-Asia (ISGT Asia)*. IEEE, 2019, pp. 3601–3606.

[153] X. Liu, Y. Min, L. Chen, X. Zhang, and C. Feng, "Data-driven transient stability assessment based on kernel regression and distance metric learning," *Journal of Modern Power Systems and Clean Energy*, 2020.

[154] J. Q. James, D. J. Hill, A. Y. S. Lam, J. Gu, and V. O. K. Li, "Intelligent time-adaptive transient stability assessment system," *IEEE Transactions on Power Systems*, vol. 33, no. 1, pp. 1049–1058, 2017.

[155] T. Dimitrovska, U. Rudež, and R. Mihalič, "Real-time application of an indirect power-system contingency screening method based on adaptive pca," *IEEE Transactions on Power Systems*, vol. 34, no. 6, pp. 4665–4673, 2019.

[156] D. Wang, J. L. Rueda Torres, E. Rakhshani, and M. Van der Meijden, "MVMO-based identification of key input variables and design of decision trees for transient stability assessment in power systems with high penetration levels of wind power," *Frontiers in Energy Research*, vol. 8, p. 41, 2020.

[157] C. Ren, Y. Xu, and R. Zhang, "An Interpretable Deep Learning Method for Power System Transient Stability Assessment via Tree Regularization," *IEEE Transactions on Power Systems*, vol. 37, no. 5, p. 3359, 2022.

[158] M. T. Ribeiro, S. Singh, and C. Guestrin, "Why should I trust you? Explaining the predictions of any classifier," in *Proceedings of the 22nd ACM SIGKDD international conference on knowledge discovery and data mining*, 2016, pp. 1135–1144.

[159] M. Chen, Q. Liu, S. Chen, Y. Liu, C. Zhang, and R. Liu, "XGBoost-Based Algorithm Interpretation and Application on Post-Fault Transient Stability Status Prediction of Power System," *IEEE Access*, vol. 7, pp. 13 149–13 158, 2019.

[160] J. Ren, B. Li, M. Zhao, H. Shi, H. You, and J. Chen, "A fast sequential transient stability preventive control approach driven by model interpretation," *Electric Power Systems Research*, vol. 213, p. 108214, 2022.

[161] S. Asvapoositkul and R. Preece, "Decision tree-based prediction model for small signal stability and generation-rescheduling preventive control," *Electric Power Systems Research*, vol. 196, p. 107200, 2021.

[162] S. M. Lundberg and S.-I. Lee, "A unified approach to interpreting model predictions," *Advances in neural information processing systems*, vol. 30, 2017.

[163] L. S. Shapley, "Stochastic Games." *Proceedings of the National Academy of Sciences of the United States of America*, vol. 39, no. 10, pp. 1095–100, 10 1953. [Online]. Available: http://www.ncbi.nlm.nih.gov/pubmed/16589380http://www.pubmedcentral.nih.gov/articlerender.fcgi?artid=PMC1063912

[164] J. Kruse, B. Schäfer, and D. Witthaut, "Revealing drivers and risks for power grid frequency stability with explainable AI," *Patterns*, vol. 2, no. 11, p. 100365, 2021.

[165] W. Yi and D. J. Hill, "Topological Stability Analysis of High Renewable Penetrated Systems using Graph Metrics," in *2021 IEEE Madrid PowerTech*. IEEE, 2021, pp. 1–6.

[166] J. Ren, L. Wang, S. Zhang, Y. Cai, and J. Chen, "Online Critical Unit Detection and Power System Security Control: An Instance-Level Feature Importance Analysis Approach," *Applied Sciences*, vol. 11, no. 12, 2021. [Online]. Available: https://www.mdpi.com/2076-3417/11/12/5460

[167] B. Tan, J. Zhao, T. Su, Q. Huang, Y. Zhang, and H. Zhang, "Explainable Bayesian Neural Network for Probabilistic Transient Stability Analysis Considering Wind Energy."

[168] F. Pedregosa, G. Varoquaux, A. Gramfort, V. Michel, B. Thirion, O. Grisel, M. Blondel, P. Prettenhofer, R. Weiss, and V. Dubourg, "Scikit-learn: Machine learning in Python," *the Journal of Machine Learning Research*, vol. 12, pp. 2825–2830, 2011.

[169] L. Breiman, J. Friedman, R. Olshen, and C. Stone, *Classification and Regression Trees*. Routledge, 1984.

[170] L. Breiman, "Random forests," *Machine learning*, vol. 45, no. 1, pp. 5–32, 2001.

[171] "DIgSILENT PowerFactory User Manual," DIgSILENT GmbH, Tech. Rep., 2019.

[172] M. A. Pai, *Energy function analysis for power system stability*. Kluwer Academic Publishers, 1989.

[173] L. Breiman, "Random Forests," *Machine Learning*, vol. 45, no. 1, pp. 5–32, 2001. [Online]. Available: https://doi.org/10.1023/A:1010933404324

[174] S. M. Lundberg, G. Erion, H. Chen, A. DeGrave, J. M. Prutkin, B. Nair, R. Katz, J. Himmelfarb, N. Bansal, and S.-I. Lee, "From local explanations to global understanding with explainable AI for trees," *Nature machine intelligence*, vol. 2, no. 1, pp. 56–67, 2020.

[175] F. Pedregosa, G. Varoquaux, A. Gramfort, V. Michel, B. Thirion, O. Grisel, M. Blondel, P. Prettenhofer, R. Weiss, and V. Dubourg, "Scikit-learn: Machine learning in Python," *the Journal of machine Learning research*, vol. 12, pp. 2825–2830, 2011.

[176] F. Chollet *et al.*, "Keras," 2015. [Online]. Available: https://keras.io

[177] K. N. Hasan, R. Preece, and J. V. Milanović, "Existing approaches and trends in uncertainty modelling and probabilistic stability analysis of power systems with renewable generation," *Renewable and Sustainable Energy Reviews*, vol. 101, pp. 168–180, 2019.

[178] A. Fuchs, T. Demiray, and M. Larsson, "Aggregated models of active distribution networks for stability studies of large transmission systems," *Electric Power Systems Research*, vol. 212, p. 108607, 2022.

[179] S. Cheng, Z. Yu, Y. Liu, and X. Zuo, "Power system transient stability assessment based on the multiple paralleled convolutional neural network and gated recurrent unit," *Protection and Control of Modern Power Systems*, vol. 7, no. 1, pp. 1–16, 2022.

[180] J. Stiasny, G. S. Misyris, and S. Chatzivasileiadis, "Transient stability analysis with physics-informed neural networks," *arXiv preprint arXiv:2106.13638*, 2021.

[181] H. R. Cai, C. Y. Chung, and K. P. Wong, "Application of differential evolution algorithm for transient stability constrained optimal power flow," *IEEE Transactions on Power Systems*, vol. 23, no. 2, pp. 719–728, 2008.

[182] P. Sanchez, J. P. Voisey, T. Xia, H. I. Watson, A. Q. O'Neil, and S. A. Tsaftaris, "Causal machine learning for healthcare and precision medicine," *Royal Society Open Science*, vol. 9, no. 8, p. 220638, 2022.

[183] C. Sourkounis and P. Tourou, "Grid code requirements for wind power integration in Europe," in *Conference Papers in Science*, vol. 2013. Hindawi, 2013.

[184] "Model user guide for generic renewable energy system models," EPRI, Tech. Rep., 2015. [Online]. Available: https://www.epri.com/research/products/000000003002014083